Ecology and Development Series No. 20, 2004

Joseph D. Intsiful

Upscaling of land surface parameters through inverse-SVAT modeling

Cuvillier Verlag Göttingen

ABSTRACT

Accounting for subgrid scale effects in climate modeling is crucial for accurate representation of surface energy fluxes and moisture indicators on the grid scale. Existing Soil-Vegetation-Atmosphere Transfer (SVAT) models most often do not adequately account for subgrid scale effects. Although the effects of spatial variability on estimation of surface energy fluxes are well established, the representation and analysis of subgrid scale variability has been an issue of considerable debate. The main controversy comes from the fact that assumptions based on different parameterization approaches for the same physical process, can lead to very different results.

To contribute to this debate, a solution is formulated in this work for which upscaling laws are derived to map the mean and standard deviation of some given heterogeneous land surface parameters (at the subgrid scale) to their corresponding effective parameter (at the grid scale). This is subject to the condition that the relative change in output response (e.g. surface energy fluxes and moisture indicators) between the aggregated (subgrid scale) output and the effective parameter output (grid scale) is less than 10% (i.e. scale invariant).

A numerical experimentation was set up using inverse-SVAT modeling to estimate optimal effective parameters which adequately yield scale invariant outputs for surface temperature, incoming solar radiation, Bowen ratio, evaporative fraction, sensible and latent heat fluxes. The tunable effective parameters of interest are surface albedo, surface emissivity, roughness length, minimum stomatal resistance, leave area index, vapor pressure deficit factor, solar insolation factor and Clapp-Hornberger soil parameter, b. In this numerical experimentation, a validated public domain 1D SVAT model, the OSU LSM (Oregon State University Land Surface Model), is coupled to an existing advanced nonlinear Parameter Estimation Tool (PEST). The SVAT model is driven by 1998 observation forcing data (4 days subset, January 1- 4) from the Meyer's measurement site in Champaign, Illinois. Initial parameter estimates obtained from existing parameter aggregation methods are used to drive the parameter estimation process. The parameters of interest are iteratively adjusted until the difference between the observation and the model-generated output is below some tolerance value. The setup is extended to the full 3D mesoscale case by coupling the Penn State University Mesoscale Model MM5 (which includes the same SVAT model as lower boundary) to PEST. MM5 was applied in one-way nesting mode to five domains within the Volta Basin for the duration December 2 – 5, 1998.

Upscaling laws were developed for both the 1D SVAT case and the fully 3D coupled MM5 model system, that map the mean and standard deviation of the distributed land surface parameters at the subgrid scale to their corresponding effective parameter at the grid scale. For the stand-alone SVAT mode, both linear and parabolic upscaling laws were obtained for the roughness length. The parabolic upscaling law fitted best for the remaining land surface parameters, except surface albedo and emissivity, which were best fitted with linear upscaling laws. For the full 3D mode, linear upscaling laws were obtained for surface albedo and emissivity as in the 1D SVAT mode, whereas, parabolic upscaling laws were obtained for the remaining land surface parameters. The performance of the proposed method was verified by comparing the results obtained from this work to that of other existing methods. More importantly, simple aggregation rules of harmonic, geometric and arithmetic means gave comparable results at small subgrid scale variability. However, at higher levels of heterogeneity, the proposed method gives better results compared to the other methods. The geometric mean values approximate very well to the values obtained from the proposed method.

Upscaling von Landoberflächenparametern durch inverse SVAT-Modellierung

ZUSAMMENFASSUNG

Die Berücksichtigung der Wirkung subskaliger Prozesse in der Klimamodellierung ist entscheidend für die genaue Darstellung der Energieflüsse an der Erdoberfläche und den Feuchteindikatoren im skaligen Bereich. Bestehende SVAT(Boden-Vegetation-Atmosphären-Transfer)-Modelle berücksichtigen die Effekte im subskaligen Bereich nicht ausreichend. Obwohl die Auswirkungen der räumlichen Variabilität bei der Abschätzung von Energieflüssen an der Erdoberfläche unzweifelhaft sind, bleiben die Darstellung und die Analyse der subksaligen Variabilität noch Inhalt von Diskussionen. Der wesentliche Diskussionspunkt hierbei ist die Tatsache, dass Annahmen, welche auf verschiedenen Methoden der Parameterisierung für einen identischen physikalischen Prozess beruhen, zu äußerst verschiedenen Ergebnissen führen können.
Um einen Beitrag für diese Diskussion zu leisten, wird in dieser Arbeit folgende Lösung entworfen: Es werden Gesetzmäßigkeiten für das Upscaling abgeleitet, um das arithmetische Mittel sowie die Standardabweichung von gegebenen Parametern der Landoberfläche (im subskaligen Bereich) auf deren entsprechende effektive Parameter (im skaligen Bereich) abzubilden. Dies unterliegt der Bedingung, dass der relative Unterschied im Ergebnis (beispielsweise Energieflüsse an der Erdoberfläche und Feuchteindikatoren) zwischen dem des gesamten subskaligen Outputs und dem Output der effektiven Parameter im skaligen Bereich weniger als zehn Prozent beträgt (d.h. invariant in Bezug auf den Maßstab).
Unter Verwendung eines SVAT-Modells zur inversen Modellierung wird ein Versuch unternommen, die optimalen effektiven Parameter zu berechnen. Diese Parameter führen zu maßstabsinvarianten Ergebnissen für die Oberflächentemperatur, die einfallende Solarstrahlung, das Bowen-Verhältnis, den Anteil der Verdunstung, den fühlbaren und den latenten Wärmestrom. Folgende effektive Parameter können angepasst werden: Die Albedo und das Emissionsvermögen der Erdoberfläche, die Rauhigkeitslänge, der minimale Stomata-Widerstand, der Blattflächenindex (LAI), der Sättigungsdampfdruckdefizitfaktor, die Solarstrahlung und der Clapp-Hornberger-Parameter b. In diesem numerischen Versuch wird das validierte, lizenzfreie eindimensionale SVAT-Modell OSU LSM (Oregon State University Land Surface Modell) mit dem erweiterten nicht linearen Tool zur Schätzung von Parametern PEST (Parameter-Estimation) gekoppelt. Das SVAT-Modell wird von Beobachtungsdaten aus dem Jahr 1998 (vier ausgewählte Tage, 1. bis 4. Januar) des Meyer-Meßgeländes in Champaign, Illinois angetrieben. Um den Vorgang der Schätzung der Parameter zu ermöglichen, werden initiale Parameterwerte, welche von bereits vorhandenen Verfahren der Parameter-Schätzung übernommen werden, verwendet. Die gewünschten Parameter werden solange schrittweise angepasst, bis der Unterschied zwischen dem beobachteten und dem vom Modell erzeugten Ergebnisses unterhalb eines bestimmten Toleranzwertes liegt. Der Aufbau wird zu einem komplett dreidimensionalen, mesoskaligen Prozess erweitert, indem das mesoskalige Modell der Penn State University MM5, welches das gleiche SVAT-Modell wie das subskalige Modell beinhaltet, mit PEST gekoppelt wird. MM5 wird im Verfahren eines Ein-Wege-

Nestings für fünf Domains innerhalb des Volta-Beckens im Zeitraum vom 2. bis 5. Dezember des Jahres 1998 angewandt.
Gesetzmäßigkeiten für das Upscaling werden sowohl für das eindimensionale SVAT-Modell sowie für das gekoppelte dreidimensionale MM5 entwickelt. Letzteres Modell bildet die mittlere- und die Standardabweichung der auf der Erdoberfläche verteilten Parameter im subskaligen Bereich auf deren entsprechende effektive Parameter im skaligen Bereich ab. Für das stand-alone SVAT-Modell werden sowohl lineare als auch parabolische Gesetzmäßigkeiten des Upscalings für die Rauhigkeitslänge ermittelt. Die parabolische Gesetzmäßigkeit des Upscalings liefert das beste Ergebnis für die verbleibenden Parameter der Erdoberfläche mit Ausnahmen der Albedo und des Emissionsvermögens, welche beide mit der linearen Gesetzmäßigkeit für das Upscalings optimal angepasst werden. Bei der komplett dreidimensionalen Methode werden die Regeln des linearen Upscalings für die Albedo und des Emissionsvermögen auf dieselbe Art und Weise ermittelt wie in der eindimensionalen SVAT-Methode. Zudem werden parabolische Gesetzmäßigkeiten für das Upscaling für die verbleibenden Parameter der Erdoberfläche ermittelt. Die Güte der ermittelten Methode wird überprüft, indem die in dieser Arbeit ermittelten Ergebnisse mit denen anderer bereits bestehender Methoden verglichen werden. Von größerer Bedeutung ist die Tatsache, dass einfache Regeln für die Zusammenfassung von harmonischem, geometrischem und arithmetrischem Mittel vergleichbare Ergebnisse bei einer kleinen subskaligen Variabilität liefern. Bei einer ausgeprägteren Heterogenität jedoch erbringt die vorgeschlagene Methode bessere Ergebnisse als andere Methoden. Das geometrische Mittel entspricht in hohem Maße den Werten der vorgeschlagenen Methode.

TABLE OF CONTENTS

LIST OF SYMBOLS

Symbol	Meaning	Section
z_{blend}	Blending height (m)	2.2.1
L_x	Horizontal length scale of surface heterogeneity (m)	2.2.1
u_*	Friction veleocity (ms^{-1})	2.2.1
H^D	Distributed/subgrid sensible heat flux (Wm^{-2})	2.3.2
G_s^D	Distributed/subgrid ground heat flux (Wm^{-2})	2.3.2
R_s^D	Distributed/subgrid incoming solar radiation (Wm^{-2})	2.3.2
R_{down}^D	Distributed/subgrid incoming longwave radiation (Wm^{-2})	2.3.2
R_{up}^D	Distributed/subgrid outgoing longwave radiation (Wm^{-2})	2.3.2
G_s^L	Grid scale ground heat flux (Wm^{-2})	2.3.2
R_{down}^L	Grid scale incoming longwave radiation (Wm^{-2})	2.3.2
R_{up}^L	Grid scale outgoing longwave radiation (Wm^{-2})	2.3.2
$Rcmin_{eff}$	Effective canopy resistance (sm^{-1})	2.3.2
Rgl_{eff}	Effective solar insolation factor (Wm^{-2})	2.3.2
ε_{eff}	Effective surface emissivity [-]	2.3.2
α_{eff}	Effective surface albedo [-]	2.3.2
$z_{o,eff}$	Effective roughness length (m)	2.3.2
LAI_{eff}	Effective leaf area index [-]	2.3.2
Hs_{eff}	Effective vapor pressure deficit factor (kg/kg)	2.3.2
R_s	Incoming solar radiation (Wm^{-2})	2.3.2
R_n	Net surface radiation (Wm^{-2})	2.3.2
λ	Latent heat of vaporization (Jg^{-1})	2.3.2
ρ	Density of air (kg/m^3)	2.3.2
G_s	Ground heat flux (Wm^{-2})	2.3.2
σ	Stefan-Boltzmann constant ($KJ^{-4}m^{-2}s^{-1}$)	2.3.2
c_p	Specific heat capacity ($Jkg^{-1}K^{-1}$)	2.3.2
r_a	Aerodynamic resistance (sm^{-1})	2.3.2
r_s	Stomatal resistance (sm^{-1})	2.3.2

$r_{s,i}$	Stomatal resistance of the *i*-th subgrid (sm^{-1})	2.3.2
$r_{a,i}$	Aerodynamic resistance of the *i*-th subgrid (sm^{-1})	2.3.2
$\varepsilon_{s,i}$	Emissivity of the *i*-th subgrid [-]	2.3.2
α_i	Albedo of the *i*-th subgrid [-]	2.3.2
θ_{ov}	Virtual potential temperature at the earth's surface (K)	3.2.1
θ	Potential temperature (K)	3.2.1
γ_o	Counter-gradient to atmospheric flow [-]	3.2.1
T_s	Surface temperature (^oC)	3.2.3
T_a	Air temperature (^oC)	3.2.3
K_s	Saturated soil hydraulic conductivity (sm^{-1})	3.2.4
K	Soil hydraulic conductivity (sm^{-1})	3.2.4
D	Soil hydraulic diffusivity (m^2s^{-1})	3.2.4
D_s	Saturated soil hydraulic diffusivity (m^2s^{-1})	3.2.4
b	Clapp-Hornberger parameter [-]	3.2.4
Θ	Volumetric soil moisture content (kg/kg)	3.2.4
Θ_s	Saturated volumetric soil moisture content (kg/kg)	3.2.4
Ψ	Soil matric potential (m)	3.2.4
Ψ_s	Soil matric potential at bubbling pressure (m)	3.2.4
d_{zi}	Root depth of the *i*-th soil layer (m)	3.2.6
Rc	Canopy resistance (sm^{-1})	3.2.6
χ	Objective function [-]	3.3.2
$C(\boldsymbol{p})$	Covariance matrix [-]	3.3.2
$\boldsymbol{p}$	Parameter vector [-]	3.3.2
$M'(\boldsymbol{p})$	Transformation matrix from state space to parameter space [-]	3.3.2
α	Albedo [-]	4.2
ε	Emissivity [-]	4.2
LAI	Leaf area index [-]	4.2
Rgl	Plant insolation factor (Wm^{-2})	4.2
z_o	Roughness length (m)	4.2
Hs	Vapor pressure deficit factor (kg/kg)	4.2
$Rcmin$	Minimum stomatal resistance (sm^{-1})	4.2
H	Sensible heat flux (Wm^{-2})	4.2

λE	Latent heat flux (Wm^{-2})	4.2
AE	Available surface energy (Wm^{-2})	4.2
β	Bowen ratio [-]	4.2
Λ	Evaporative fraction [-]	4.2
G	General representation for SVAT model output	5.2.1
f	Distributed map or functional	5.2.1
p	Land surface parameter [-]	5.2.2
$p_{i,k}$	The land surface parameter of the prescribed distribution for the i-th subgrid.	6.2.1
$p_{i,j}$	The i-th random field of the j-th realization (for the i-th subgrid)	6.2.1
$p_{i,jo}$	The i-th random field of the optimal realization	6.2.1
μ_k	The mean of the prescribed distribution	6.2.1
σ_k	The standard deviation of the prescribed distribution	6.2.1
μ_j	The mean of the j-th realization	6.2.1
σ_j	The standard distribution of the j-th realization	6.2.1
k	The index of the prescribed distribution	6.2.1
n	The number of parameters or subgrids	6.2.1
j	The index for the number of a given realization or iteration	6.2.1
μ_{jo}	The mean of the optimal realization	6.2.1
σ_{jo}	The standard distribution of the optimal realization	6.2.1
$p_{eff,k}$	The effective parameter of a given prescribed distribution.	6.2.1
g	Random number generator function	6.2.1

1 INTRODUCTION

1.1 Background

Over 70% of the population in West Africa depends primarily on rainfed agriculture for its livelihood. Moreover, the main source of power for socio-economic development is hydro-based and depends heavily on availability of rainfall and its distribution. Therefore, water resources are the life-blood of the economies of West African countries, and changes in amount and distribution of rainfall can significantly impact socio-economic activities in the region.

In an attempt to address the problem of efficient utilization of the scarce water resources in the Volta Basin of West Africa, the German government and its partner countries within the Volta Basin (Ghana & Burkina Faso) have set up a multidisciplinary research project on Global Change in the Hydrological Cycle, called the GLOWA-Volta project. The principal objective of the project is to develop a scientifically sound decision support system for the assessment, sustainable use and development of water resources in the Volta Basin.

A critical component of this multidisciplinary research involves regional climate modeling of the Volta Basin to identify and characterize the dynamics of the energy and hydrological cycles in the Basin. However, the location of the Volta Basin in the tropics, coupled with the complex nature of the landuse characteristics of the region demands a new approach for representing the relevant physics in climate models to accurately account for subgrid scale heterogeneity effects.

As the GLOWA-Volta project is multi-disciplinary in nature, the different subprojects made up of different disciplines must be optimally integrated across different scales to ensure the harmonious functioning of the project as a whole. The issue of scaling land surface characteristics is therefore a critical issue for scientific enquiry.

1.2 Motivation

Ongoing intensification of agriculture in West Africa has led to changes in land surface and subsurface characteristics, which directly affect evapotranspiration rates. If these changed evapotranspiration rates in turn affect regional precipitation patterns, rainfed and irrigated agriculture in West Africa may face changed boundary conditions because of the complex feedback mechanisms between the surface and atmosphere. The investigation of these feedback effects requires the application of regional climate models that accurately account for soil and vegetation states through SVAT schemes.

The land surface characteristics of the Volta Basin is characterized by mosaics of small patches made up of agricultural fields, fallows, villages and forest (savannah mosaic). The surface heterogeneity introduced by the composing surface elements of the savannah mosaic lead to complicated conditions affecting both local and regional climates. Depending on the horizontal scale of these surface heterogeneities, the planetary boundary layer (PBL) could be affected, and in effect, influence the regional climatic conditions. Three scales of surface heterogeneity have been identified and, depending on the horizontal scale, they can be classified as microscale or organized heterogeneity, mesoscale or disorganized heterogeneity, and macroscale or large scale heterogeneity respectively (Shuttleworth, 1988; Raupach, 1991; Mahrt, 2000).

For the microscale heterogeneity, the surface changes are disorganized at scales less than 10 km (Shuttleworth, 1988) such that the atmospheric boundary layer responds to only the composite structure. The influence of the local advection on the surface flux profiles becomes appreciable and a characteristic height called the blending height can be found where the fluxes are close to its surface values (Claussen and Klassen, 1992; Klassen and Claussen, 1995; Mahrt, 2000). For the mesoscale or organized heterogeneity, the atmospheric boundary layer responds independently over each patch of the surface and occurs on scales greater than 10 km (André et al., 1986; Chehbouni et al., 1995; Raupach, 1991). The blending height extends sufficiently high such that no level exists where the Monin-Obukhov similarity theory is applicable for estimating surface fluxes close to the surface value. In the case of the macroscale heterogeneity, the boundary layer establishes equilibrium with the local surface type, and the entire boundary layer is controlled by the local surface structure. At low wind speeds, macroscale heterogeneity can occur at the mesoscale scale length(Mahrt, 2000).

Regional climate models use landuse data in resolutions of 10-100 km because of the limitation of computing resources required for fine resolution runs over the domain of interest. However, information on land surface parameters is usually available at much finer resolution such that their implementation in the coarse resolution climate models do not properly account for the subgrid scale effects associated with the surface heterogeneity. More importantly, the scales at which most of these subgrid scale processes occur are far too fine to be captured by the coarse scale resolution at which climate runs are undertaken.

Although the relevance of parameterizing subgrid scale processes in climate modeling is well established, the question of how to represent and analyze the effects of spatial variability on the scaling of land surface parameterization has been an issue of great controversy. The main contention comes from the fact that assumptions related to different parameterization for the same physical process often lead to different inferences. As a result, several studies based on different approaches have recently focused on how to fully represent and parameterize this land surface heterogeneity so as to enhance model efficiency and accuracy. Therefore, a fundamental and not yet satisfactorily solved problem in hydrological research is how subgrid scale variability can be accounted for at coarse resolutions.

1.3 Objectives

The main objective of this work is to derive effective soil and vegetation parameters to account for subgrid scale variability in 1D SVAT and full 3D regional climate models.

The specific objectives of this research are:

- To undertake sensitivity analysis of SVAT model parameters with respect to surface energy fluxes (latent and sensible heat fluxes) and moisture indicators (Bowen ratio and evaporative fraction) to identify sensitive SVAT parameters.
- To develop a parameter estimation environment for SVAT models (stand-alone and full 3D).
- To identify suitable objective functions for the estimation of selected soil and vegetation parameters.

- To derive upscaling laws (an equivalent for lookup tables) for soil and vegetation parameters in SVAT models, with particular emphasis on the Volta Basin.
- To compare the developed method to existing aggregation/upscaling schemes.
- To investigate differences between derived effective parameters for SVAT models in stand-alone mode (1D) and fully 3D mode.
- To investigate the uniqueness of the estimated parameters.

1.4 Problem definition

The problem of representing subgrid scale effects can be formulated in several ways, based on the nature of the solution strategy adopted (Chehbouni et al., 1995; Hu et al., 1999; Shuttleworth et al., 1999). For this study, the subgrid scale problem is posed as an inverse problem and considered ill-posed.

The subgrid scale problem is posed as follows:

- Given a distributed heterogeneous land surface (characterized by land surface parameters of mean μ_p and standard deviation σ_p) at the subgrid scale, can we find an effective parameter p_{eff} at the grid scale such that the relative change in output response (e.g. surface energy fluxes and moisture indicators) is less than 10% (Hu et al., 1997)?
- If such an effective parameter p_{eff} exists, can we find a functional relation that maps the mean μ_p and standard deviation σ_p of the distributed land surface parameters at the subgrid scale to their corresponding effective parameter p_{eff} at the gridscale?

The first question addresses the problem of scale invariance in that it seeks an effective parameter for which the surface energy fluxes would be accurately partitioned. The second problem seeks an upscaling law that would enable the estimation of the effective parameter at the grid scale based on the mean and standard deviation of the distributed subgrid scale parameters. The problem is generally of highly nonlinear nature.

1.5 Overview

In this work, the estimation of optimal effective land surface parameters through inverse modeling is adopted. The subgrid scale effects are accounted for by the upscaling of land surface parameters through inverse-SVAT modeling. The solution strategy is based on the premise that solutions of existing methods are sub-optimal and hence parameter estimates obtained from these techniques can be used as initial parameters for driving the parameter estimation process. In effect, if good initial parameter estimates can be found such that they are within the neighborhood of the true solution, it is possible to iteratively adjust these parameters for the solution to converge to the optimal solution.

As the inverse problem is ill-posed, it is transformed into an almost well-posed problem via an approximate technique. Using prior information about the subgrid scale processes as a regularization constraint, the parameter estimation process is constrained to converge to the true solution. An exact algebraic solution does not exist, hence an approximate numerical solution using the Gauss-Levenberg-Marquardt algorithm is adopted.

To realize this, the SVAT model (OSU LSM) (Ek and Mahrt, 1991) was coupled to the nonlinear parameter estimation tool PEST (Doherty, 2002), which is able to iteratively adjust the SVAT parameters such that scale invariant outputs of heat fluxes are achieved. The SVAT model was driven by 1998 observation forcing data (4 days subset, January, 1- 4) obtained from the Meyer measurement site in Champaign (Meyers & Ek, 1999), which is characterized by the vegetation type “groundcover only” and soil type “silty loam”. A Monte Carlo random number generator was used to provide parameter inputs to the SVAT model. Initial parameter estimates derived from approximate methods of Hu et al. (1999) and related methods were used to initialize the nonlinear parameter estimation process. To verify, if the proposed method was independent of atmospheric forcing, extended runs ranging from 1 to 30 days were undertaken, and the results obtained do not differ significantly from the usual 4 day episode runs used in this exercise.

The experiment was extended to cover the full 3D mesoscale meteorological model MM5 to account for the lateral interactions between adjacent cells. The MM5 runs are initialized and run with National Center for Environmental Predictions (NCEP) reanalysis data. A one-way nested approach was applied for five domains, where the

outer boundaries provide boundary conditions to drive the inner domain. Here, an area in the Volta Basin (West Africa) was chosen for the investigations (4 days subset December, 2 - 5 1998).

The thesis provides a simple and effective method for accounting for the subgrid scale effects through inverse-SVAT modeling. Beyond accounting for subgrid scale effects, it also provides a framework for the automatic calibration of distributed models.

1.6 Organization of the thesis

The earlier sections of this chapter gave a brief outline of the thesis. The remaining chapters provide the conceptual and technical details applied in this thesis for the solution of the subgrid scale heterogeneity problem.

In Chapter 2, a detailed literature review of existing methodologies is given. The nature of the planetary boundary layer processes and their parameterization is presented. Other relevant information for the conceptual design of the upscaling method and its numerical implementation is also discussed.

Chapter 3 gives a brief description of the theoretical formulation of the models used in this study. The theoretical formulation of the upscaling of land surface parameters as an inverse-SVAT problem and its approximate solution is discussed. The theoretical formulation of SVAT modeling as a forward problem is also discussed.

A sensitivity analysis of surface energy fluxes and moisture indicators with respect to key vegetation parameters is given in Chapter 4. The analysis covers the whole Volta Basin. The result of the sensitivity analysis provides relevant information on critical land surface parameters and hence helps to improve the parameter estimation process.

Chapter 5 gives a detailed description of the upscaling methodology. It uses the theoretical formulations outlined in chapters 2 and 3 to develop a solution strategy for addressing the problem of subgrid scale effects as an inverse problem.

Chapter 6 gives a description of the numerical implementation of the proposed upscaling method developed in Chapter 5. A numerical experimentation is carried out to access the performance of the model with other existing techniques. The generation of the distributed land surface parameters by a Monte Carlo simulation and its coupling to

both the 1D SVAT and 3D SVAT (MM5) models is discussed. Initialization and coupling of PEST to the 1D SVAT model and its extension to the fully coupled 3D SVAT model (MM5) are also discussed.

A detailed analysis of the results of the numerical experimentation presented in chapter 6 is discussed in Chapter 7. This includes the representation of the various forms of upscaling laws for the coupled 1D SVAT-PEST (stand-alone), where lateral interactions between adjacent cells are ignored, and its extension to the fully coupled 3D SVAT-PEST (MM5; accounting for full interaction between adjacent cells). A unified framework for assessing the performance of the proposed method and other existing techniques is presented. Pertinent issues related to the enhancement of the performance of the inverse-SVAT modeling process are also discussed.

In Chapter 8, a summary and conclusion of the thesis is presented followed by an outlook for future research.

2 LITERATURE SURVEY

2.1 General survey of existing strategies for representing subgrid scale effects

The parameterization of subgrid scale processes in climate modeling has generated a great deal of controversy over the years. This has come about mainly because there is no unified theory from which subgrid scale heterogeneity can be modeled. As a result, several studies based on different approaches have recently focused on how to fully represent and parameterize the land surface heterogeneity so as to enhance model efficiency and accuracy.

Some methods propose the increase of the resolution of model grid at the ground surface, break the domain into finer subgrids and then estimate surface energy fluxes at the subgrid scale (e.g. Dickenson et al.,1989; Hu et al., 1997; Koster and Suarez,1992). Dickenson et al. (1989) used General Circulation Model (GCM) horizontal boundary conditions to drive a Regional Circulation Model (RCM) and observed that intragrid topography and land surface properties strongly influence the distribution of precipitation at the mesoscale. They also observed that a nested GCM-RCM model produces more realistic results than the original GCM. Other studies (Koster and Suarez, 1992) assume weak lateral interactions between subgrids such that each subgrid interacts independently with the atmosphere, making it possible to apply the same atmospheric forcing to all subgrids within the grid. The land surface model is applied to each subgrid to estimate surface energy fluxes, humidity, temperature and other variables of interest. The grid output is then obtained by a weighted average of the relevant variables of interest over all subgrids in the domain.

Another approach that has attracted much attention is the use of effective roughness length to account for the effect of surface heterogeneity. One very popular approach is the blending height concept developed by Wieringa (1986). He reasoned that at a certain characteristic height above a heterogeneous surface, the atmospheric flow does not depend on the characteristics of the underlying heterogeneous surface. Hence it is possible to derive an effective parameter for the heterogeneous surface. Several studies (Mason 1988; Wood and Claussen 1990; Grotzner et al., 1996) have used this concept to estimate the horizontal scale length of surface heterogeneity. The limitation of this model is that it is only applicable to small-scale heterogeneity and

requires a stable lower atmosphere. Grotzner et al. (1996) argue that when the scale of heterogeneity becomes large and the lower atmosphere is unstable, the blending height lies beyond the convective layer, and hence the similarity law for the flux estimation would not be applicable. It has been shown recently that there is no general approach to defining effective land surface parameters (McNaughton, 1994; Lhomme et al., 1994; Shuttleworth et al., 1999).

The energy matching method is a form of energy conservation approach where the terms in the energy balance equation at the grid scale are matched to the area-weighted sum of the corresponding terms at the subgrid scale (Braden, 1995; Chehbouni et al., 1995; Hu et al., 1999; Lhomme, 1992; Raupach, 1991). Using appropriate physics assumptions, a set of relationships are derived between the grid scale and subgrid scale parameters.

The problem with the energy matching method is that most versions use crude assumptions in minimizing the residual errors associated with the difference between the grid scale and subgrid scale terms. Hu et al. (1999), argue that the linearization of the surface energy balance equation can lead to energy partitioning problems for the available energy (difference between net radiation flux and ground heat flux), sensible and latent heat fluxes. For instance, the use of the linearized Stefan-Boltzmann equation and vapor pressure dependence on temperature has been found to be problematic in some cases. Lhomme et al. (1994) observed that three different aggregated surface temperatures can be derived depending on whether available energy, sensible or latent heat flux is preserved. Additionally, effective parameters derived from schemes based on these crude physics assumptions can lead to parameters with no physical meaning (Braden, 1995).

Several statistical approaches have also being proposed for representing subgrid scale effects. In these statistical formulations, land surface processes are characterized by relevant statistical measures of heterogeneity. A common example is the statistical-dynamic approach in which statistical probability distributions are used to characterize the subgrid scale spatial heterogeneity of certain variables of interest from which probability density functions for an aggregated response are derived (Entekhabi and Eagleson, 1989; Famiglietti and Wood, 1991). Several variations of the statistical dynamic approach exist. Collins and Avissar (1994) used a derivative of the statistical-

dynamic approach that incorporates the Fourier Amplitude Sensitivity Test (FAST) to identify critical parameters that influence surface flux heterogeneity. This technique is attractive, because it eliminates the computational burden introduced by representing the covariances between the various PDFs used in the normal statistical-dynamic approach.

Mixed conclusions have been made by different researchers. Whereas Wood and Lakshmi (1993) found the latent heat flux not to be particularly sensitive, Li and Avissar (1994) found the land surface characteristics to be important for the grid level sensible and latent heat fluxes. Hu et al. (1997), and Li and Avissar (1994) established that in general the latent heat flux is the most sensitive, whereas the radiative flux from the surface is the least sensitive to spatial variability. The problem with this approach is that the probability distribution functions for the parameters are very difficult to formulate, mostly due to lack of data. Also, most experiments involve statistical simulations (e.g. Monte Carlo runs) that require multiple model runs (over a million runs) and intensive CPU utilization.

Shuttleworth (Chehbouni et al., 1995) suggest that an appropriate aggregation scheme would be to define the effective area-average value of a land surface parameter as the weighted average of the subgrid scale parameters through the function containing the parameter that most succinctly expresses its relation with the associated surface flux. Chehbouni (1995) argues that such an approach may not satisfy the energy conservation law. Additionally, it can lead to different results for the same physical parameter depending on which energy flux is applied.

Scale invariance methods determine the effect of land surface heterogeneity on the surface and other state variables by using scale invariant land surface parameterization. An effective parameter is estimated such that the percentage change in a given output response is less than some tolerance (often 10%). Another approach is to estimate an effective parameter such that output response obtained at a local or point scale is applicable at a larger scale. Hu et al. (1997) developed an analytical scheme for analyzing scale-invariance of atmospheric variables using distributed maps and Taylor series expansion of the relevant physical functions. They deduced that there are two conditions under which a scale-invariant assumption would be applicable: (i) If the parameters are homogeneous over the grid, and (ii) if the map is a linear combination of

inputs and parameters. They observed that correlation between the drag coefficients for heat and moisture, and also temperature and humidity, can lead to appreciable errors. Analysis from the FIFE experiment (Sellers et al., 1992; Hall, 1992) show that land surface energy fluxes are almost scale invariant.

The approach chosen in this work for resolving the controversy surrounding the representation of subgrid scale effects is the optimal parameter estimation method through inverse-SVAT modeling. This approach involves the minimization of the sum of the objective function (e.g. square of the error between some observation and model output) by iteratively adjusting model parameters until the minimum of the objective function is obtained. Although this approach shows much promise, the formulation of the inverse problem and its solution is not trivial. A major reason for this is the fact that in an attempt to represent in detail the mechanisms governing the interactions between soil, vegetation and the atmosphere, current physically-based land surface schemes have become increasingly complex, resulting in the specification of a large number of parameters. Even the simple patch scale SVAT model still permits too many degrees of freedom in terms of fitting model predictions or data validation. The result is high parameter correlations and singular covariance matrices, a condition that makes the parameter estimation process a very formidable task. The success of this method is based primarily on the formulation of the inverse problem and the closeness of the initial parameter estimates to the true solution. Existing methods use either trial and error or Monte Carlo methods to obtain initial parameter estimates to drive the parameter estimation process. This approach is, however, a very expensive exercise as the model has to be run several times (mostly over a million times) to derive a good initial parameter set.

The main objective of this chapter is to review existing aggregation schemes that have relevance to this thesis. A brief review of the general problem of parameterizing the planetary boundary layer in climate models and types of land surface surface heterogeneity are also discussed. Basic principles for developing methods of particular interest to this work are discussed in detail in section 2.3.

2.2 General problem of parameterizing the Planetary Boundary Layer (PBL)

Numerical climate simulations are performed by the numerical integration of the governing equations of atmospheric motions using finite difference approximation methods. Application of the finite difference approximations to discrete volumes constituting the earth's geometry implying only processes occurring at scales larger than twice the grid length can be captured by the grid-point model. However, due to practical limitations on computing resources, the model length (in the case of a GCM) cannot be reduced far below 100 km (Tiedtke, 2001) because it would be very expensive computationally. But subgrid scale processes occurring at scales far less than 100 km are responsible for the transport of a considerable amount of moisture, sensible heat and momentum into the PBL by turbulent and convective motions.

To account for subgrid scale effects in climate models, the statistical contributions of the various (unresolved) subgrid scale processes are expressed in terms of the large-scale (mean) flow. More importantly, many of the subgrid scale processes are too complicated to the extent that derivation of parameterization from first principle is not practicable. For this reason, empirical relationships are derived from experimental data using the similarity theory.

In general, a realistic representation of the PBL in climate models is crucial because:

- The large-scale budgets of heat, momentum and moisture are considerably affected by the surface fluxes on time scales of a few days.
- The model variables in the boundary layer are important products, because they serve as input and verification for atmospheric wave models, air pollution models and climate models.
- The boundary layer interacts with other processes and greatly influences their dynamics, e.g. soil moisture, clouds and convection.

The relevance of surface fluxes can be further illustrated by the recycling time of different quantities on the basis of typical values of surface fluxes as given in Table 2.1.

Table 2.1: Global energy budget (order of magnitude estimates)

Budget	***Total***	***Surface flux***	***Recycling time***
Water	$7x10^{7}$ Jm^{-2}	80 Wm^{-2}	10 days
Internal + potential energy	$4x10^{9}$ Jm^{-2} (0.5% available)	30 Wm^{-2}	8 days
Kinetic energy	$2x10^{6}$ Jms^{-2}	2 Wm^{-2}	10 days
Momentum	$2x10^{5}$ $kgms^{-1}$	0.1 Nm^{-2}	25 days (Eckman spin down time 4 days)

Courtesy ECMWF Met. Training course lecture series, 2001.

A detailed discussion on the parameterization of subgrid scale processes can be found in Avissar (1992), Beljaars (2001), Mahrt (2000), Peixoto and Oort (1992), Tiedtke (1984) and Viterbo (1996).

2.2.1 Description of the PBL

The discussion presented in this section closely follows Bastiaanssen (1995) and Beljaars et al. (2001). The PBL constitutes the lower part of the atmosphere where the influence of land surface flux densities on atmospheric motion is felt. In this layer, the coriolis force, which determines the rotation of the earth, is negligible compared to the influence of the land surface processes. The atmospheric flow in the PBL is characterized by turbulence generated by wind shear and thermal convection. Figure 2.1 shows a hybrid PBL for a dry, well-mixed ideal case consisting of different sub-layers.

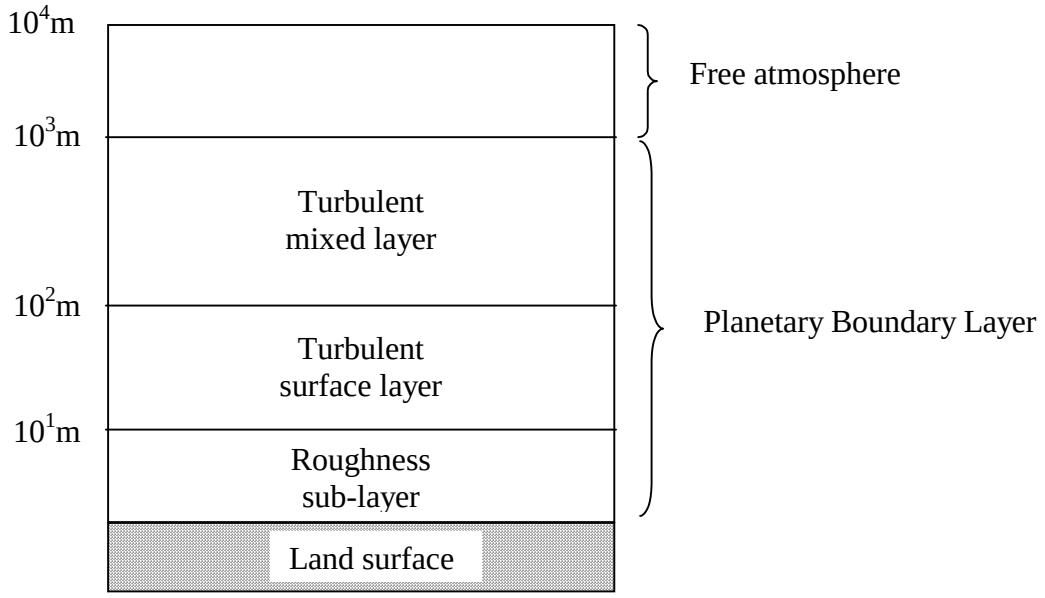

Figure 2.1: Schematic representation of the hybrid Planetary Boundary Layer (PBL) into sub-layers with typical heights. Source: Bastiaanssen (1995).

A roughness sub-layer lies above the land surface. It consists of elements with variable surface roughness including canopy-like structures and other rough surfaces. The turbulent surface layer is the lowest part of the PBL constituting 10% of the PBL height (Holtslag and Nieustadt, 1986). In this region, the Monin-Obukhov (1954) similarity theory is applicable. Studies by Holtslag (1984) using Cabauw (Netherlands) data show that the Monin-Obukhov similarity is valid up to a height of about 100 m. In the mixed layer, potential temperature and humidity vary almost constant with height. The top of the PBL is limited by the free atmosphere. The region where the laminar process of the free atmosphere interacts with the turbulent eddies (mixing processes of air parcels) leaving the PBL is called the entrainment layer.

The maximum spatial variability in sensible and latent heat fluxes over composite terrains are found close to the land surface in the turbulent surface layer. The vertical transport of fluxes of heat, momentum and vapor exhibit spatial non-uniformity resulting in horizontal advection. At some critical height, called the blending height, the momentum flux becomes almost independent of the influence of the surface heterogeneities (Wieringa, 1986). It is assumed that below this height, the wind profiles primarily respond to local roughness elements. More importantly, multiple blending heights at different levels and horizontal scales may arise under the appropriate

conditions (Arain et al., 1997; Chehbouni et al., 1995; Hu et al., 1999; Mahrt, 2000). The blending height concept constitutes a very powerful tool for establishing scaling relationships for the momentum flux density (Claussen, 1990;Mason, 1988; Wieringa, 1986).

Following Mason (1988), the relation for the blending height and surface conditions can be represented as

$$z_{blend} = \left(\frac{u_*}{U}\right)^2 L_x \qquad 2.1$$

where L_x is the characteristic length scale for horizontal distances between obstacles and u_* and U are the friction velocity and average wind speed at the blending height respectively. A detailed description of the blending height approach will be presented in section 2.3.

2.3 Detail review of selected land surface parameter upscaling approaches

A detailed description of some selected land surface parameter upscaling approaches that have relevance to this work is presented below. These are: 1) the blending height method, 2) the energy matching method, 3) the simple averaging method, and 4) the inverse modeling method. The three main types of land surface heterogeneities (i.e. microscale, mesoscale and macroscale) defined based on the blending height concept are briefly described.

2.3.1 The blending height approach

Horizontal scales of surface heterogeneity

Section 2.2 gave a brief description of the blending height concept in relation to the PBL. It is one of the key theories required for a better understanding of land surface heterogeneity. For this reason, the blending height assumptions are invoked in almost all land surface parameter aggregation schemes in formulating the relevant parameter aggregation relations. Several formulations of the blending height approach exist (Claussen , 1990; Mahrt, 2000; Mason, 1988; Schmid and Bünzli, 1995; Wieringa, 1986; Wood and Mason, 1991). Following Mahrt (2000), it is assumed to be the height where the influence of surface heterogeneity gradually decreases below some threshold value. It has been shown to increase linearly with horizontal scale of the surface

heterogeneity (see equation 2.1) so that the influence of larger scale surface features extends farther into the boundary layer (Marht, 2000; Wood and Mason, 1991). Figure 2.2 shows the planetary boundary layer and the different scaling regimes of surface heterogeneity. Below the blending height, the turbulence may not be in equilibrium with the local vertical gradient, in which case the Monin-Obukhov similarity theory (MOST) is not applicable. MOST can be successfully applied to heights above the blending height, if the blending height is low compared to the boundary layer depth (Mahrt, 2000). This is a basic requirement that ensures that the flux immediately above the blending height is close to the spatially-averaged value and that the boundary-layer depth does not influence the flux-gradient relationship.

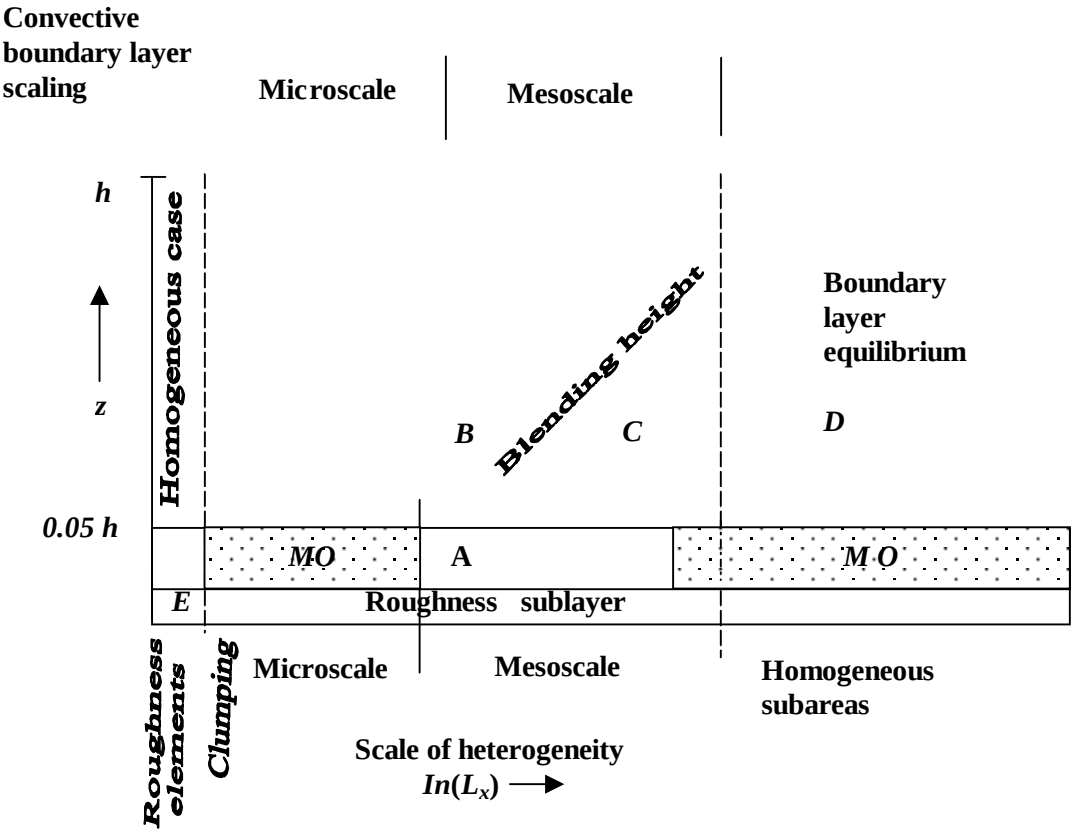

Figure 2.2: Scaling regimes based on the blending height concept (lower main part) and convective boundary layer scaling (upper part). *Courtesy Mahrt (2000).*

The formulation of the blending height approach described above is based on a shear-driven mixing where the transport of momentum is localized and diffused. However, in the convective boundary layer, large boundary layer eddies can transport

surface information on time scales of few tens of minutes to the top of the deep boundary layer, making the blending height concept invalid. For this scenario, Raupach and Finningan (1995) derived expressions for the influence of surface heterogeneity on the basic time scales of the convective boundary layer. A basic conclusion from the analysis is that the horizontal influence of the surface heterogeneity is modulated by the large convective boundary layer eddies to the point that it does not affect the bulk of the boundary layer. An elegant description of the boundary layer convective scaling is also given in Mahrt (2000).

Additionally, the thermodynamic processes in the PBL can induce a thermal scaling length depending on its influence on the stability of the PBL. The horizontal scale length of surface heterogeneity has been found to decrease with increasing instability (Mahrt, 2000). However, when the surface heating is appreciable, this weak dependence on instability becomes irrelevant and leads to underestimation of instability, and a more explicit formulation of stability dependence is required. A thermal blending height based on a linearized thermodynamic budget has been developed by Wood and Mason (1991).

In general, three horizontal scales of surface heterogeneity can be defined as discussed previously:

- The blending height based on local diffusive mixing by shear-generated turbulence, which is applicable in near neutral or stable conditions.
- The thermal blending height based on the buoyancy modification of the turbulence.
- The boundary layer convective scaling, which describes the extent of nonlocal bulk mixing due to buoyancy-driven eddies on the scale of the boundary layer.

These three length scales give an estimate of the minimum horizontal scale of surface heterogeneity that significantly influences the flow at a given height or, in the case of the thermal blending height, the entire boundary layer. Additionally, they are all proportional to the wind speed and inversely proportional to some measure of the strength of the prevailing turbulence.

Scale regimes based on the blending height concept

Following the arguments advanced in formulating the different horizontal length scales (section 2.3.1), different scaling regimes are possible depending on the organization of the planetary boundary layer processes. Following Mahrt (2000), three main scaling regimes have been identified: 1) microscale or disorganized heterogeneity, 2) mesoscale or organized heterogeneity and 3) macroscale heterogeneity.

Disorganized or microscale heterogeneity occurs when the length scales of surface heterogeneity is small enough (<10 km) for the PBL to respond only to the composite surface structure. In this case, the scale of surface heterogeneity is smaller than the integral mixing length (Chehbouni et al., 1995). The blending height based on local diffusive mixing by shear-generated turbulence, as discussed in section 2.3.1, is applicable and valid under near neutral or stable conditions. It is assumed that it is a necessary condition for the Monin-Obukhov similarity theory to be applicable (Mahrt, 2000).

These arguments form the basis of many surface flux and parameter aggregation methods. For instance, they can be used to assess the suitability of the energy matching, mosaic or flux aggregation approach to partition subgrid surfaces in numerical models (Avissar and Pileke, 1989; Chehbouni et al., 1995; Hu et al., 1997; Hu et al., 1999; Mahrt, 1996). Taylor (1987) applied this approach for momentum transfer over heterogeneous surfaces to estimate the effective roughness length. In his approach, each grid is divided into subgrids representing different land surface types, while the variables at the first model level (presumably in the surface layer) are assumed equal to their grid-averaged values and unaffected by subgrid scale heterogeneity. Mahrt (2000) argues that such an assumption can only be valid as a rough approximation if the blending height is below the first model level, which in turn must be below the top of the surface layer. Such arguments break down for large scales of surface heterogeneity (> 10 km) or higher blending heights.

Mesoscale or organized heterogeneity occurs where the PBL behaves independently over each patch of the surface (> 10 km). This occurs when the surface heterogeneity extends upward to a significant fraction of the boundary layer depth (region C of Figure 2.2), and where there is no longer a model level above the blending height where the flux-gradient relationship depends on the ratio of vertical height to the

Monin-Obukhov length alone. More importantly, the flow immediately above the blending height is too high so that the spatially-averaged flux is very different from the surface value. The similarity theory is not applicable in the entire PBL. Several controversies have resulted from the failure of the similarity theory to provide a uniform framework for analyzing the scales of surface heterogeneity (Chehbouni et al., 1995; Hu et al. 1997; Mahrt, 2000). Up till now, no rigorous treatment of organized heterogeneity exists, but recent studies have shown varying successes in addressing the issue (Pielke, 1997).

In the macroscale or large scale heterogeneity, the local features control the entire boundary layer. A blending height can be found where the boundary layer establishes equilibrium with the local land surface and the similarity theory is applicable. This scenario is illustrated in region D of Figure 2.2.

2.3.2 The energy matching method

General formulation of the energy matching method

A brief survey of the energy matching method was given in section 2.1. The objective of this approach is to find functional relationships for land surface parameters such that the aggregation of surface fluxes at the subgrid scale match that of the effective parameter at gridscale. This is subject to the condition that the residual errors associated with the matching process are minimal. In this formulation, the flux-resistance model for surface heat fluxes (sensible (H), latent (λE), and net radiation (R_n)) are given respectively as

$$H = \frac{\rho c_p (T_s - T_a)}{r_a} \qquad 2.2$$

$$\lambda E = \frac{\rho c_p \left(e^*(T_s) - e(T_a)\right)}{r_a + r_s} \qquad 2.3$$

and

$$R_n = H + \lambda E + G_s = (1-\alpha)R_s + \varepsilon_s (R_l - \sigma T_s^4) \qquad 2.4$$

where

G_s = Ground heat flux (Wm^{-2})

σ = Stefan-Boltzmann constant ($Wm^{-2}K^{-4}$)

R_s = Downward shortwave (Wm^{-2})

R_l = Downward longwave (Wm^{-2})

T_s = Surface temperature (K)

T_a = Air temperature (K)

H = Sensible heat flux (Wm^{-2})

λE = Latent heat flux (Wm^{-2})

α = Surface albedo [-]

ε_s = Surface emissivity [-]

c_p = Specific heat capacity ($Jg^{-1}K^{-1}$)

r_a = Surface roughness length (m)

r_s = Stomatal resistance (sm^{-1})

e = Vapour pressure (mb)

e^* = Saturated vapour pressure (mb)

The grid is divided into i subgrids, each assumed to be homogeneous with respect to land surface characteristics. Aggregated (area-weighted) subgrid output responses (denoted by superscript D) are obtained as

$$H^D = \sum_i a_i \frac{\rho c_p (T_{s,i} - T_a)}{r_{ai}} \qquad 2.5$$

$$\lambda E^D = \sum_i a_i \frac{\rho c_p \left(e^*(T_{s,i}) - e(T_a)\right)}{r_{a,i} + r_{s,i}} \qquad 2.6$$

$$G_s^D = \sum_i a_i G_{s,i} \qquad 2.7$$

$$R_s^D = \sum_i a_i (1 - \alpha_i) R_s \qquad 2.8$$

$$R_{down}^D = \sum_i a_i \varepsilon_{s,i} R_l \qquad 2.9$$

$$R_{up}^{D} = \sum_{i} a_i \varepsilon_{s,i} \sigma T_{s,i}^{4} \qquad 2.10$$

The associated surface energy balance is given by

$$H^{D} + \lambda E^{D} + G_s^{D} = R_s^{D} + R_{down}^{D} - R_{up}^{D} \qquad 2.11$$

where a_i is the fractional area weight of the $i-th$ subgrid.

For the lumped or effective parameter output response (denoted by superscript L), the corresponding surface energy fluxes are given as

$$H^{L} = \frac{\rho c_p (T_s - T_a)}{r_a} \qquad 2.12$$

$$\lambda E^{L} = \frac{\rho c_p \left(e^{*}(T_s) - e(T_a) \right)}{r_a + r_s} \qquad 2.13$$

$$G_s^{L} = G_s \qquad 2.14$$

$$R^{L} = (1-\alpha) R_s \qquad 2.15$$

$$R_{down}^{L} = \varepsilon_s R_l \qquad 2.16$$

$$R_{up}^{L} = \varepsilon_s \sigma T_s^{4} \qquad 2.17$$

Similarly, the energy balance should be valid over the grid (lumped parameter) giving

$$H^{L} + \lambda E^{L} + G_s^{L} = R_s^{L} + R_{down}^{L} - R_{up}^{L} \qquad 2.18$$

A set of land surface parameters is obtained via some physics assumptions that would conserve energy and partition the energy fluxes within reasonable accuracy.

The method of Hu et al. (1999): Use of nonlinearized (complete) energy terms

Hu et al. (1999) used the above energy matching technique to derive effective parameters for estimating grid scale fluxes. Their approach provides forcing-independent effective parameters similar to those obtained from the proposed method described in Chapter 5 of this thesis. More importantly, a comparison between the proposed method and that of Hu et al. (1999) is presented in Chapter 6.

For their approach, Hu et al. (1999) obtained effective parameter estimates through the minimization of the objective function

$$\begin{aligned} \chi^2 = & (H^{L} - H^{D})^2 + (\lambda E^{L} - \lambda E^{D})^2 + (G_s^{L} - G_s^{D})^2 \\ & + (R_s^{L} - R_s^{D})^2 + (R_{down}^{L} - R_{down}^{D})^2 + (R_{up}^{L} - R_{up}^{D})^2 \end{aligned} \qquad 2.19$$

by taking derivatives of χ^2 with respect to $G_s, \alpha, r_s, r_a, T_s, \varepsilon_s$ and setting the derivatives to zero. This gives the following energy conservation relations:

$$G_s^L = G_s^D \quad \text{2. 20}$$

$$H^L = H^D \quad \text{2. 21}$$

$$\lambda E^L = \lambda E^D \quad \text{2. 22}$$

$$R_s^L = R_s^D \quad \text{2. 23}$$

$$R_{up}^L = R_{up}^D \quad \text{2. 24}$$

$$R_{down}^L = R_{down}^D \quad \text{2. 25}$$

The above relations (Equations 2.20 – 2.25) represent the law of conservation of energy fluxes and are equivalent to the following:

$$\frac{T_s - T_a}{r_a} = \sum_i a_i \frac{T_{s,i} - T_a}{r_{a,i}} \quad \text{2. 26}$$

$$\frac{e^*(T_s) - e(T_a)}{r_a + r_s} = \sum_i a_i \frac{e^*(T_{s,i}) - e(T_a)}{r_{a,i} + r_{s,i}} \quad \text{2. 27}$$

$$G_s = \sum_i a_i G_{s,i} \quad \text{2. 28}$$

$$\varepsilon_s = \sum_i a_i \varepsilon_{s,i} \quad \text{2. 29}$$

$$\alpha = \sum_i a_i \alpha_i \quad \text{2. 30}$$

$$\varepsilon_s T_s^4 = \sum_i a_i \varepsilon_{s,i} \sigma T_{s,i}^4 \quad \text{2. 31}$$

The following aggregation schemes are obtained as estimates of the effective parameters and output response of interest:

$$G_s = \sum_i a_i G_{s,i} \quad \text{2. 32}$$

$$\alpha = \sum_i a_i \alpha_i \quad \text{2. 33}$$

$$\varepsilon_s = \sum_i a_i \varepsilon_{s,i} \quad \text{2. 34}$$

$$T_s^4 = \sum_i a_i \left\{ \frac{\varepsilon_{s,i}}{\varepsilon_s} \right\} T_{s,i}^4 \quad \text{2. 35}$$

$$\frac{1}{r_a} = \sum_i \frac{a_i}{r_{a,i}} \left\{ \frac{T_{s,i} - T_a}{T_s - T_a} \right\} \quad 2.\ 36$$

$$\frac{1}{r_a + r_s} = \sum_i \frac{a_i}{r_{a,i} + r_{s,i}} \left\{ \frac{e^*(T_{s,i}) - e(T_a)}{e^*(T_s) - e(T_a)} \right\} \quad 2.\ 37$$

These aggregation rules, although elegant, are not suitable for SVAT models in forecasting schemes due to their dependence on forcing data. To obtain forcing-independent effective parameters, assumptions similar to those applied in the blending height approach are invoked (Hu et al., 1999). It is further assumed that the surface forcing is not too heterogeneous such that

$$\frac{e^*(T_{s,i}) - e(T_a)}{e^*(T_s) - e(T_a)} \cong 1, \frac{T_{s,i} - T_a}{T_s - T_a} \cong 1, \frac{\varepsilon_{s,i}}{\varepsilon_s} \cong 1. \quad 2.\ 38$$

Incorporating these simplifying assumptions yields the following:

$$T_s^4 \cong \sum_i a_i T_{s,i}^4 \quad 2.\ 39$$

$$\frac{1}{r_a} = \sum_i \frac{a_i}{r_{a,i}} \quad 2.\ 40$$

$$\frac{1}{r_a + r_s} = \sum_i \frac{a_i}{r_{a,i} + r_{s,i}} \quad 2.\ 41$$

The crude simplification assumptions of equation 2.38 are made without the provision for error corrections, because they are to formulate without forcing information or additional information. This results in the overestimation of surface heat fluxes at higher levels of surface heterogeneity (Hu et al., 1999). A better method is, therefore, sought for in this thesis.

Approaches based on the linearization of the thermodynamic terms

Chehbouni et al. (1995) used similar arguments to derive effective land surface parameters. In their formulation, they respectively linearized the saturated vapor pressure and surface temperature relations

$$e^*(T_s) - e_a = s(T_s - T_a) + D_a \quad 2.\ 42$$

$$T_s^4 = T_a^4 + 4T_a^3(T_s - T_a). \quad 2.\ 43$$

where s and D_a are the respective slope of the saturated vapor pressure curve and vapor pressure deficit at air temperature. The results of Chehbouni et al. (1995) are summarized below as:

$$T_s = \sum_i \frac{a_i T_{s,i}}{\omega_i} \qquad 2.44$$

$$\frac{1}{r_a} = \sum_i \frac{a_i}{r_{a,i}} \qquad 2.45$$

$$\frac{1}{r_a + r_s} = \sum_i \frac{a_i}{r_{a,i} + r_{s,i}} \qquad 2.46$$

$$\frac{1}{\omega} = \sum_i \frac{a_i}{\omega_i} \qquad 2.47$$

$$\frac{1}{\omega_i} = \frac{1}{r_{a,i}} + \frac{1}{r_{o,i}} + \frac{s}{\gamma_o (r_{a,i} + r_{s,i})} \qquad 2.48$$

$$\frac{1}{r_{o,i}} = \frac{4\sigma T_a^3}{\rho c_p} a_i \varepsilon_i \qquad 2.49$$

where γ_o is the psychometric constant.

In addition to equations 2.47 to 2.52, Chehbouni et al. (1995) obtained equivalent relations of equations 2.28, 2.30 and 2.34 obtained by Hu et al. (1999). The linearization assumptions made on the thermodynamic equations can lead to inconsistent results as discussed in section 2.2 (Hu et al., 1997; Hu et al., 1999). Also, too many parameters need to be specified to derive other parameters. Lhomme (1992) observed errors in the order of 30% with this approach.

Other energy matching techniques use the latent heat fluxes obtained from the combination equations to derive effective parameters (Arain et al., 1999; Nakaegawa et al., 2001; Shuttleworth et al., 1997; Shuttleworth et al., 1999). Most of these methods provide parameters with either no physical meaning or require surface information in their formulation (Braden, 1995). More importantly, they are not suitable for SVAT models in forecasting models where surface variables are to be predicted.

2.3.3 Simple averaging methods

The simple averaging methods provide valuable initial parameter estimates for iterative procedures such as the proposed method discussed in Chapter 5 of this thesis. Research on the use of simple averaging techniques has been the topic of many enquiries on land surface parameter aggregation (Arain et al., 1993; Blyth et al., 1993; Mohanty et al., 2002). More importantly, most parameter aggregation schemes simplify to simple aggregation schemes (Chehbouni et al., 1995; Hu et al., 1999). Mohanty et al. (2002) used simple averaging methods (arithmetic, harmonic and geometric means) to investigate the effective and average hydraulic properties of the footprints of a remote sensor consisting of soils of different textures. They found that simple averaging methods can give good results. Arain et al. (1996) and Blyth et al. (1993) applied simple averaging techniques (arithmetic and harmonic means) to study the effective parameters of some selected vegetation parameters using measured data. They found the results to be very promising at low scale surface heterogeneity. Lhomme (1992) observed errors of the order of 186% of the sensible heat fluxes with this approach.

The limitation of this method is that its derivation is purely from statistical arguments with no physics assumptions of the problem. A lot of innovation is required for identifying which of the simple averaging methods is appropriate for a given land surface parameter. However, this method provides a quick and easy way for obtaining effective parameters. More importantly, it serves as an excellent means for obtaining good initial parameter estimates for driving the parameter estimation process of iterative methods, such as the Inverse-SVAT method studied in this research. A discussion on simple averaging schemes is given in Chapter 7, including a comparison with the proposed method.

2.3.4 Inverse modeling approach

The use of optimal parameter estimation techniques in estimating system parameters has gained much acceptance in many branches of geosciences over the years. However, their application has not been extensively explored in the estimation of effective land surface parameters. Quite recently, the approach has been applied successfully for the estimation of 1D SVAT model parameters (Gupta et al., 1999).

Inverse modeling is a form of regression analysis where an attempt is made to minimize the difference between two quantities by iteratively adjusting a tunable parameter in one of the quantities. The formulation is similar to the energy matching method of section 2.3.2 (see equation 2.19) where an objective function is minimized. In the forward problem, the parameters are prescribed and the state variables are computed based on the model parameters. In inverse modeling, the state variables are known or given and the parameters which gave rise to the state variables are solved for.

The upscaling of land surface parameters can be posed as an inverse problem where the aggregated distributed output from the subgrids represent the observation or prescribed state variables. The system parameters that gave rise to these observations are then solved for by iteratively adjusting the SVAT model parameters of interest.

Omer et al. (2000) applied a multicriteria parameter estimation methodology to study the impact of field-calibrated vegetation parameters on GCM output. Gupta (1999) applied this methodology to the calibration of a land surface model, where he described a framework for the application of multi-criteria theory to the calibration of a conceptual, physically-based model. Because most inverse problems are ill-posed, usually no exact algebraic solution exists and hence an approximate solution consisting of the optimal parameter set that best satisfies the objective function is considered the best solution. It is quite simple to implement even in multi-parameter and highly complex environment where automatic calibration of distributed models is required. Its main strength is that it is model-independent and hence does not make crude physics assumptions about the model except for prior knowledge about the systems dynamics which is crucial for its operation.

An emerging thinking in optimal parameter estimation is the concept of equifinality (Aronica et al., 1998; Beven, 2000; Diekkrüger, 2003; Lamb et al., 1998). Equifinality is the concept where more than one model or set of parameters is assumed to give an equivalent good fit. The idea is to give up the notion that only one optimal parameter set or model can fit a given problem and then instead build a probabilistic framework for the predicted value. To this end, a procedure is required that uses the concept of equifinality to derive the collection of equiprobable optimal parameter sets or models. One of such attempts is the generalized likelihood uncertainty estimation (GLUE) procedure, which consists of steps involving the generation of likelihood

surfaces over parameter spaces to produce uncertainty estimates in the predicted model response. To realize this, multiple runs are made with a Monte Carlo simulation of selected parameter set. A selection criteria is then designed to reject all models or parameter sets that do not meet a minimum selection criteria for the goodness of fit. The parameter sets that meet the minimum criteria are assigned higher probabilities.

Table 2.2: Selected schemes for deriving parameter estimates relevant to this thesis.

Land surface parameter	***Formulation of effective parameter***	***Dependence of surface flux on parameter***
Leaf Area Index (LAI)	$LAI_{eff} = \frac{1}{n}\sum_{i=1}^{n} LAI_i$	Linear effect of radiation and evaporation (Arain et al., 1996).
Minimum stomatal resistance (Rcmin)	1. $Rcmin_{eff} = \frac{1}{n}\sum_{i=1}^{n} Rcmin_i$ 2. $\frac{1}{Rcmin_{eff}} = \frac{1}{n}\sum_{i=1}^{n} \frac{1}{Rcmin_i}$	1. Linear effect of evaporation (Arain et al., 1996). 2. Reciprocal effect of evaporation (Arain et al., 1996).
Surface albedo (α)	$\alpha_{eff} = \frac{1}{n}\sum_{i=1}^{n} \alpha_i$	Linear effect of radiation (Chehbouni et al., 1995 and Hu et al., 1999).
Surface emissivity (ε)	$\varepsilon_{eff} = \frac{1}{n}\sum_{i=1}^{n} \varepsilon_i$	Linear effect of radiation (Chehbouni et al., 1995 and Hu et al., 1999).
Roughness length (z_o)	$\frac{1}{z_{o,eff}} = \frac{1}{n}\sum_{i=1}^{n} \frac{1}{z_{o,i}}$	Reciprocal effect of sensible and latent heat fluxes (Chehbouni et al., 1995 and Hu et al., 1999).
Vapor pressure deficit factor (Hs)	$Hs_{eff} = \frac{1}{n}\sum_{i=1}^{n} Hs_i$	Linear effect of evaporation (personal deduction).
Plant insolation factor (Rgl)	1. $Rgl_{eff} = \frac{1}{n}\sum_{i=1}^{n} Rgl_i$ 2. $\frac{1}{Rgl_{eff}} = \frac{1}{n}\sum_{i=1}^{n} \frac{1}{Rgl_i}$	1. Linear effect of evaporation (personal deduction). 2.Reciprocal effect of evaporation (personal deduction).

The main limitation of an inverse problem solution is that it requires a good set of initial parameter estimates to start the parameter estimation process, which can be

very difficult to obtain when the model is highly nonlinear. More importantly, with its gradient-based variants, it requires that the objective function be continuously differentiable on the parameters of interest. Also, correlation of parameters can be a formidable problem when the covariance matrix is nearly singular. The existence of multiple local minima in the parameter space can pose a major problem for the location of the global minimum. However, these problems can be minimized with relevant prior information about the systems dynamics, which allow the use of regularization constraints to guide the parameter search process towards the optimal solution.

2.3.5 Concluding remarks

A number of alternative methods have been considered for deriving effective land surface parameters. Research studies have shown that there is no unique procedure for defining effective parameters (Lhomme et al., 1994; McNaughton, 1994). There is, therefore, a general consensus that averaging schemes should be designed to serve specific purposes. For this reason, the motivation for the thesis is focused on the development of an efficient model-independent approach in which the problematic crude physics assumptions invoked in most models reviewed in this chapter are avoided.

The proposed inverse-SVAT method presented in this work provides a model-independent framework from which any SVAT model can be optimized by iteratively adjusting the SVAT model parameters of interest. The parameter estimates deduced from the surveyed methods that have relevance to this research are summarized in Table 2.2.

In conclusion, a review of the planetary boundary layer and its parameterization has been outlined. Additionally, a concise discussion on the fundamental concepts used in developing existing aggregation schemes has been presented, outlining their relative strengths and weaknesses. These ideas present a theoretical framework from which the proposed upscaling methodology is developed in Chapter 5. Comparison of the proposed methods to selected existing methods is presented in Chapter 7 for accessing the performance of the proposed method. The next chapter gives a theoretical formulation of the models and related ideas used in this work.

3 THEORY AND MODEL DESCRIPTION OF THE INVERSE-SVAT METHOD

3.1 Introduction

The relevance of the accurate representation of the surface energy budget for the simulation of atmospheric flow over various temporal and spatial scales was discussed in Chapter 2. The diurnal variations in the thermal structure and the depth of the atmospheric boundary layer, depends strongly on the exchange of the sensible and latent heat fluxes with the underlying surfaces.

More importantly, characterizing the spatial and temporal variability in land surface processes over regional scales is a difficult task and considerable effort has been put into deriving appropriate models to deal with this challenge. One approach to determine land surface fluxes at a variety of scales is through the application of Soil-Vegetation-Atmosphere-Transfer (SVAT) models. A land surface parameterization model (LSM) or SVAT model, consists of an algorithm for determining the exchanges of energy, mass and momentum between the atmosphere and the land surface. These exchanges are complex functions of a number of processes (physical, chemical and biological) that have a range of temporal and spatial scales. The number and variety of models available to achieve this is substantial, but all require the specification of numerous land surface parameters.

Because there is no unified approach in representing land surface processes, the various SVAT models adopt different parameterization schemes. Depending on their simplifications, land surface schemes in today's atmospheric models exhibit a wide range of complexity from classic "bucket" models (e.g., Manabe 1969) to detailed soil-vegetation-atmosphere transfer schemes (SVATs) (e.g., Dickinson et al*.,* 1993; Sellers et al*.,* 1996). A subset of SVATs takes into account the sub-grid scale variations of surface characteristics and/or atmospheric conditions (e.g. Avissar, 1992; Famiglietti and Wood, 1995; Entekhabi and Eagleson, 1989) to deal with the usually nonlinear relationships among the surface processes/variables. Third generation of SVATs combine the physical processes with the biophysical exchanges needed to represent photosynthesis, respiration and, in some schemes, decay (e.g. Xiao et al*.,* 1998; Tian et al*.,* 1999).

Several methods exist for determining SVAT model parameters (e.g. remote sensing methods and field measurements) as discussed in Chapter 2. The use of inverse methods in determining SVAT model parameters has gained much popularity in recent times, because it provides a model-independent environment where any SVAT model can be optimized based on its physics parameterization. More importantly, it provides an excellent environment for automatic calibration and coupling of distributed models of any complexity (Doherty, 2002; Gupta et al., 1999, and Omer et al., 2000).

In this chapter, the theory of the inverse-SVAT method is presented. Figure 3.1 gives the schematic diagram of the inverse-SVAT method presented in this chapter. The theory of the SVAT model is presented following Chen and Dudhia (2001), and EK and Mahrt (1991). The formulation of the inverse-SVAT problem and its solution is presented following Sun (1994), Cooley and Naff (1990), and Doherty (2002). Because synthetic SVAT model parameters are used to mimic real-life heterogeneous land surface parameters, a brief discussion on the Monte Carlo random number generator for normally-distributed fields is presented following Press et al. (1992).

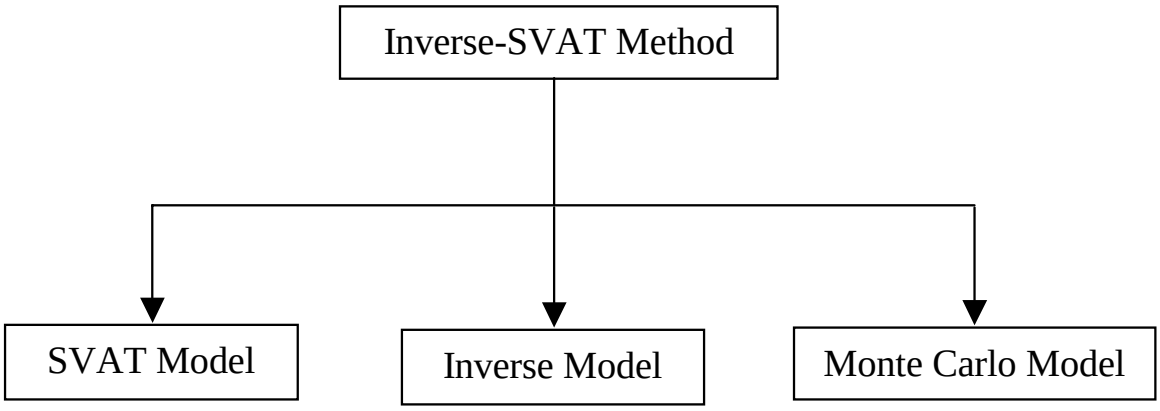

Figure 3.1: Schematic diagram of the Inverse-SVAT Method

3.2 The SVAT model

The SVAT model used in this thesis is the three-layer version of the soil-canopy model developed at the Oregon State University (Chen and Dudhia, 2001; Ek and Mahrt, 1991; Mahrt and Pan, 1984; Meyers, 2002; Pan and Mahrt, 1987). The model has four prognostic variables: soil temperature, volumetric soil water content, canopy water

content and equivalent snow depth. Since snow was not considered in this study, formulation for snow processes would not be discussed but will be mentioned when appropriate. The following subsections give a detailed discussion of the SVAT model.

3.2.1 The boundary layer model

The formulation of the governing equations for climate dynamics is well established (Brutsaert, W., 1982; Stull, R. B., 1988; Oke, T. R., 1978). Following Ek and Mahrt (1991), the tendencies for the 1D climate scheme due to the turbulent mixing of potential temperature (θ), specific humidity (q) and the horizontal components of the wind (V_h, *or u and v*) are given by the set of prognostic equations:

$$\frac{\partial V_h}{\partial t} = \frac{\partial}{\partial z}\left(K_m \frac{\partial V_h}{\partial z} \right) - w\left(\frac{\partial V_h}{\partial z} \right) \quad 3.1$$

$$\frac{\partial \theta}{\partial t} = \frac{\partial}{\partial z}\left(K_h \left(\frac{\partial \theta}{\partial z} - \gamma_\theta \right) \right) - w\left(\frac{\partial V_h}{\partial z} \right) \quad 3.2$$

$$\frac{\partial q}{\partial t} = \frac{\partial}{\partial z}\left(K_h \frac{\partial q}{\partial z} \right) - w\left(\frac{\partial q}{\partial z} \right) \quad 3.3$$

where z is the vertical distance from the surface, w is the vertical wind component, K_m and K_h are the eddy diffusivities for momentum and heat, respectively. The counter gradient correction term (γ_θ) for potential temperature in equation 3.2 is defined following parameterization of Troen and Mahrt (1986). The 3D representation for equations 3.1 to 3.3 can be found in Brutsaert (1982), Dudhia et al. (2000), Oke (1978) and Stull (1988).

3.2.2 The surface layer model

The surface fluxes are parameterized following Mahrt (1987) for the stable case; the unstable case follows Lois et al. (1982), with modification by Holtslag and Beljaars (1989). The fluxes of momentum, heat and moisture are formulated as

$$u_*^2 = C_m |V_o| \quad 3.4$$

$$H = C_h(\theta_s - \theta_o) \quad 3.5$$

$$\lambda E = C_q(q_s - q_o) \quad 3.6$$

where C_m (ms^{-1}), C_q (ms^{-1}) and C_h (ms^{-1}) are the surface exchange coefficients for momentum, moisture and heat, respectively. C_q and C_h are assumed equal. C_h and C_m are defined to incorporate the wind speed factor. $|V_o|$ is the wind speed (ms^{-1}) evaluated at the first model level above the surface. The potential temperature, θ_o (K), and specific humidity q_o are taken at the first model level above the surface, while the surface potential temperature θ_s (K) and the specific humidity q_s are obtained from the surface. H and λE are defined to be positive upwards.

The exchange co-efficients depend nonlinearly on a set of surface parameters and are defined by

$$C_m = k^2 |V_o| \frac{F1(z, z_{om}, Ri_B)}{\left[ln(\frac{z}{z_{om}}) \right]^2} \qquad 3.7$$

$$C_h = \frac{k^2}{R} |V_o| \frac{F2(z, z_{om}, z_{oh}, Ri_B)}{ln(\frac{z}{z_{om}}) ln(\frac{z}{z_{oh}})} \qquad 3.8$$

where k is the nondimensional von Karman constant (0.40). R (estimated as 1.0) is the ratio of the drag co-efficient for momentum and heat in the neutral limit computed following Businger et al. (1971) with modification by Holtslag and Beljaars (1989). Ri_B is the bulk Richardson's number, which defines the stability of the atmosphere. z_{om} is the roughness length for momentum. It gives a measure of the vertical turbulence that occurs when the wind flows over a rough surface. It is one of the key parameters responsible for momentum transfer from the surface into the PBL. z_{oh} is the roughness length for heat/moisture and gives a measure of the resistance to heat and moisture transfer from the surface into the PBL. z_{oh} is often prescribed in SVAT models as one-tenth of z_{om}.

F_1 and F_2 are the respective component stability functions of the exchange co-efficients for momentum and heat and are parameterized as

$$F_1 = \begin{cases} e^{-aRi_B} & , Stable \\ 1 - \dfrac{10 Ri_B}{1 + 7.5 \left[\dfrac{10 k^2}{\left(ln\left(\dfrac{z}{z_{om}} \right) \right)^2} \right] \left(- Ri_B \dfrac{z}{z_{om}} \right)^{1/2}} & , Unstable \end{cases} \qquad 3.9$$

$$F_2 = \begin{cases} e^{-aRi_B} & , Stable \\ 1 - \dfrac{15 Ri_B}{1 + 7.5 \left[\dfrac{10 k^2}{ln\left(\dfrac{z}{z_{om}} \right) ln\left(\dfrac{z}{z_{oh}} \right)} \right] \left(- Ri_B \dfrac{z}{z_{om}} \right)^{1/2}} & , Unstable \end{cases} \qquad 3.10$$

where a is a constant equal to 1.0. The above formulations show the extent of nonlinearity that exists between the surface roughness elements and the surface energy fluxes. As z_{om} and z_{oh} are the critical surface parameters that determine the distribution of turbulent energy fluxes, their accurate estimation and parameterization in SVAT models is crucial for the accurate prediction of the earth's climate system. More importantly, they are the primary agents responsible for the types of surface heterogeneity discussed in Chapter 2.

A compact representation of the surface energy fluxes is the flux-resistance formulation, where the exchange co-efficients, C_q and C_h, are expressed in terms of the aerodynamic resistance, r_a, as

$$C_h = C_q = \frac{1}{r_a} \qquad 3.11$$

The above relation allows the surface energy fluxes to be written in an electrical resistance form (using Ohm's law analogy). Surface fluxes from different subgrids can be then be subjected to a form of electrical resistance network analysis from which relevant climate information can be derived.

3.2.3 The soil thermodynamics model

Neglecting the horizontal exchanges of heat, the tendency equation governing the heat transfer for a soil at temperature, T, can be formulated as

$$C(\Theta)\frac{\partial T}{\partial t} = \frac{\partial}{\partial z}\left[K_T(\Theta)\frac{\partial T}{\partial z}\right] \qquad 3.12$$

where C ($Jm^{-3}K$) is the volumetric heat capacity and K_T ($Wm^{-1}K^{-1}$) is thermal conductivity. C and K_T are formulated as functions of the volumetric soil water content, Θ (m^3m^{-3}), following Pan and Mahrt (1987). The volumetric heat capacity is estimated as a weighted sum of the heat capacity of its various phases (i.e., water, soil and air). This is formulated as

$$C = \Theta C_{water} + (1-\Theta_s)C_{soil} + (\Theta_s - \Theta)C_{air} \qquad 3.13$$

where C_{water}, C_{soil} and C_{air} are the volumetric heat capacity for water, soil and air, respectively.

The thermal heat capacity is parameterized as

$$K_t(\Theta) = \begin{cases} 420\exp\left[-(2.7+P_f)\right], & P_f \le 5.1 \\ 0.1744, & P_f > 5.1 \end{cases} \qquad 3.14$$

where

$$P_f = \log\left[\Psi_s\left(\frac{\Theta_s}{\Theta}\right)^b\right]. \qquad 3.15$$

Θ_s and Ψ_s are the saturated volumetric soil water content and matric potential (bubbling pressure), respectively, and depend on soil texture (Cosby et al., 1984).

The soil consist of layers so that the soil heat transfer equation can be formulated in a layer-integrated form for which the governing equation for the *i*-th soil layer are given by

$$\Delta z_i C_i \frac{\partial T_i}{\partial t} = \left(K_T\frac{\partial T}{\partial z}\right)_{z_i+1} - \left(K_T\frac{\partial T}{\partial z}\right)_{z_i} \qquad 3.16$$

The boundary conditions at the top of the soil model are given as

$$\left[K_T(\Theta)\frac{\partial T}{\partial z}\right]_{z=s} = -G_s \qquad 3.17$$

where G_s is the ground heat flux at the surface ($s=0$ cm). The bottom temperature is assumed to be at 3 m below the surface for the implementation of the OSU LSM in

MM5. In the current version of the OSU LSM, it is assumed to be at 8 m below the surface (Meyers, 2000).

3.2.4 The soil moisture dynamics model

Neglecting the horizontal exchange of soil water, the soil water dynamics in the unsaturated zone is governed by the prognostic equation

$$\frac{\partial \Theta}{\partial t} = \frac{\partial}{\partial z}\left(D(\Theta)\frac{\partial \Theta}{\partial z} \right) + \frac{\partial K(\Theta)}{\partial z} + F_{\Theta} \qquad 3.18$$

based on the diffusive form of Richard's equation derived from Darcy's law under the assumption of a rigid, isotropic, homogeneous, and one dimensional vertical flow domain (Hanks and Ahscroft, 1986). F_{Θ} represents the sources and sinks for soil water (i.e. precipitation, evaporation and runoff).

The soil water diffusivity, D (m^2s^{-1}), hydraulic conductivity, K (ms^{-1}), and matric potential, Ψ (m), are respectively formulated following Cosby et al. (1984) as

$$D(\Theta) = K(\Theta)\frac{\partial \Psi}{\partial \Theta} \qquad 3.19$$

$$K(\Theta) = K_s\left(\frac{\Theta}{\Theta_s} \right)^{2b+3} \qquad 3.20$$

$$\Psi(\Theta) = \Psi_s\left(\frac{\Theta}{\Theta_s} \right)^{-b} \qquad 3.21$$

where K_s and b are the respective saturated hydraulic conductivity and Clapp-Hornberger parameter (a curve-fitting parameter that depends on soil type). The soil hydraulic diffusivity, hydraulic conductivity and matric potential depend nonlinearly on b to the extent that slight changes in b can produce significant changes in their respective values. Additionally, they depend nonlinearly on the soil water content such that they can change several orders of magnitude with slight variations in soil water content, particularly when the soil is dry (Chen and Dudhia, 2001). Figure 3.2 shows the influence of the Clapp-Hornberger exponent, *b*, on soil hydraulic and thermodynamic properties.

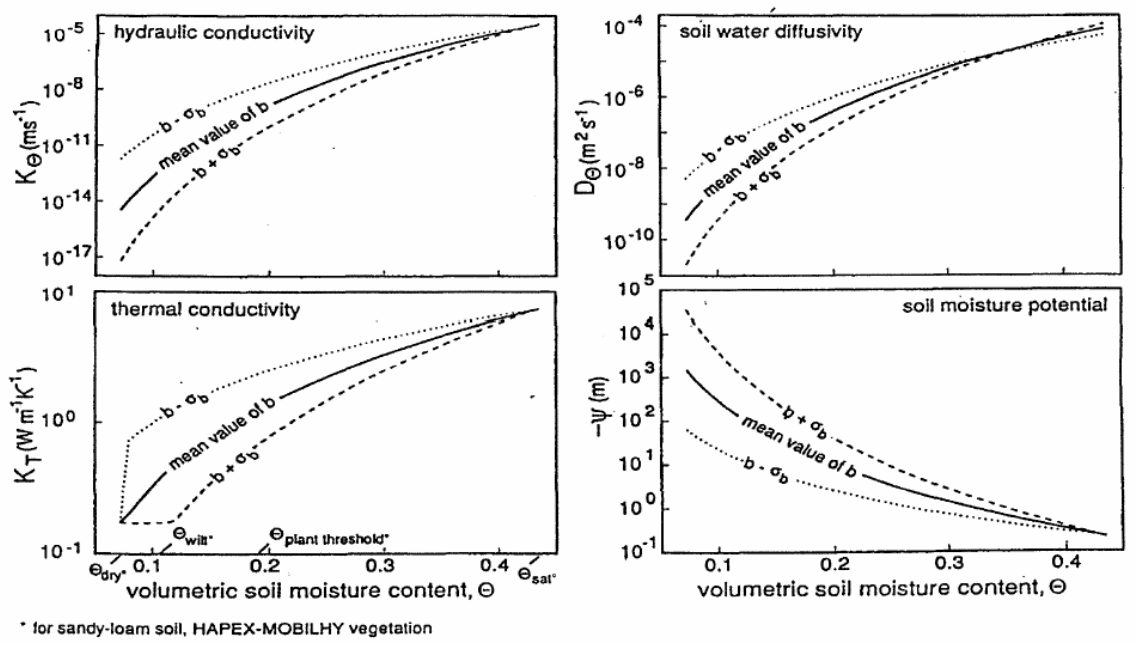

Figure 3.2: Sensitivity of soil hydraulic and thermodynamic properties to variations in Clapp-Hornberger exponent b and soil moiture. *Source: Ek and Cuenca (1994).*

To accurately model the soil moisture dynamics, the soil is divided into four homogeneous layers. Integrating equation 3.18, layered soil hydrology equation over four soil layers and expanding F_Θ to incorporate the relevant components gives

$$d_{z1}\frac{\partial \Theta_1}{\partial t} = D\left(\frac{\partial \Theta}{\partial z}\right)_{z1} - K_{z1} + P_d - R - E_{dir} - E_{t1} \qquad 3.22$$

$$d_{z2}\frac{\partial \Theta_2}{\partial t} = D\left(\frac{\partial \Theta}{\partial z}\right)_{z1} - D\left(\frac{\partial \Theta}{\partial z}\right)_{z2} + K_{z1} - K_{z2} - E_{t2} \qquad 3.23$$

$$d_{z3}\frac{\partial \Theta_3}{\partial t} = D\left(\frac{\partial \Theta}{\partial z}\right)_{z2} - D\left(\frac{\partial \Theta}{\partial z}\right)_{z3} + K_{z2} - K_{z3} - E_{t3} \qquad 3.24$$

and

$$d_{z4}\frac{\partial \Theta_4}{\partial t} = D\left(\frac{\partial \Theta}{\partial z}\right)_{z3} + K_{z3} - K_{z4} \qquad 3.25$$

where d_{zi} and K_{zi} are the respective thickness and hydraulic conductivity of the *i*-th soil layer, P_d is the precipitation not intercepted by the canopy, E_{dir} is the direct soil evaporation, and E_{ti} is the canopy transpiration taken by the canopy root in *i*-th layer within the root zone layers. There are three root layers in the OSU LSM implementation

in MM5. The hydraulic conductivity is assumed to be zero at the bottom so that soil water movement is possible only through gravitational percolation term K_{z4} (drainage).

The direct evaporation from the bare soil surface is assumed to occur at the potential rate, E_p, when the near-surface soil moisture exceeds the field capacity. Otherwise, it is regulated by the rate of transfer of soil moisture to soil surface according to the relation

$$\left(1-\sigma_f\right) Min\left[\left(D(\Theta)\frac{\partial\Theta}{\partial z}+K(\Theta)\right)_{z=s}, E_p\right]_{z=s}$$

The boundary condition at the top of the model soil layer is given by

$$\left(1-\sigma_f\right)\left[D(\Theta)\frac{\partial\Theta}{\partial z}+K(\Theta)\right]_{z=s} = E_{dir} + \left(1-\sigma_f\right)I_n$$

where I_n is the infiltration rate of precipitation and σ_f is the fraction of the surface covered by plant canopy.

3.2.5 The surface runoff and infiltration model

The formulation of the runoff and infiltration dynamics of the soil water follows Schaake et al. (1996) for the version of OSU LSM implemented in MM5. They are parameterized respectively as

$$Runoff = P_d - I_{max} \qquad 3.26$$

where the maximum infiltration is given by

$$I_{\max} = P_d \frac{D_x\left[1-\exp(-kdt\delta_i)\right]}{P_d + D_x\left[1-\exp(-kdt\delta_i)\right]}. \qquad 3.27$$

$$D_x = \sum_{i=1}^{4} \Delta z_i (\Theta_s - \Theta_i) \qquad 3.28$$

and

$$kdt = kdt_{ref}\frac{K_s}{K_{ref}} \qquad 3.29$$

δ_i is the conversion of the current model time step δ_t into daily values, kdt_{ref} and K_{ref} are specified constants based on experimental observations.

In the current stand-alone version of the OSU LSM, infiltration, runoff and maximum infiltration are parameterized respectively following Chang et al. (1999) as

$$I_n = PR_{ref} - Runoff \tag{3.30}$$

$$Runoff = \begin{cases} 0, & PR_{ref} \le I_{max} \\ PR_{ref} - I_{max}, & PR_{ref} > I_{max} \end{cases} \tag{3.31}$$

$$I_{max} = \begin{cases} D(\Theta_s)\dfrac{\Theta_s - \Theta_1}{h_1} + K(\Theta_s), & \Theta_1 \le \Theta_s \\ K(\Theta_s), & \Theta_1 > \Theta_s \end{cases} \tag{3.32}$$

The effective precipitation, PR_{ref}, is formulated as

$$PR_{ref} = (1-\sigma_f)PR_{total} + \sigma_f DRIP \tag{3.33}$$

for the case where there is no snow. In the presence of snow it is given by

$$PR_{ref} = S_m \tag{3.34}$$

where S_m represents snowmelt, σ_f is the vegetation cover, $DRIP$ is the water drip rate from the canopy, and PR_{total} is the total precipitation.

3.2.6 The evapotranspiration model

The total evapotranspiration is formulated as the sum of 1) direct soil evaporation, E_{dir}, 2) evaporation from canopy intercepted precipitation, E_c, and 3) transpiration from canopy and the roots system, E_t:

$$E = E_{dir} + E_c + E_t \tag{3.35}$$

The direct soil evaporation is parameterized based on sensitivity test of Betts et al. (1997) and a simple linear approach following Mahfouf and Noilhan (1991) as

$$E_{dir} = (1-\sigma_f)\beta_{dir}E_p \tag{3.36}$$

where

$$\beta_{dir} = \frac{\Theta_1 - \Theta_w}{\Theta_{ref} - \Theta_w} \tag{3.37}$$

is a linear function of the instantaneous soil moisture content of the first layer. Θ_w is the wilting point; it represents the point where the soil water adjacent to the vegetation roots drops to –200 m with respect to the ground surface (Cosby et al., 1984; Wetzel and Chang, 1987). Θ_w is the field capacity; it is the presumed water content at which the

internal drainage allegedly ceases (Cosby et al., 1984). The wilting soil reference and wilting points are computed respectively as

$$\Theta_{ref} = \Theta_s \left[\frac{1}{3} + \frac{2}{3} \left(\frac{5.76 \, \boldsymbol{x} \, 10^{-9}}{K_s} \right)^{1/(2b+3)} \right] \qquad 3.38$$

$$\Theta_w = 0.5\Theta_s \left(\frac{200}{\Psi_s} \right)^{-1/b} \qquad 3.39$$

The potential evaporation, E_p, is derived from a Penman-based energy balance approach

$$R_n - G_s = H + \lambda E_p \qquad 3.40$$

which incorporates a stability-dependent aerodynamic resistance formulation following Mahrt and Ek (1984). λ (6.25 x 106 Jkg^{-1}) is the latent heat of vaporization and R_n is the net solar radiation at the surface given by equation 2.4 in Chapter 2. It depends linearly on the surface albedo and emissivity. Equation 3.40 is the available energy for turbulent surface energy fluxes and is partitioned between the sensible and latent heat fluxes based on the surface properties and surface wetness.

The wet canopy evaporation is parameterized following Noilhan and Planton (1989) and Jacquemin and Planton (1990) as

$$E_c = \sigma_f E_p \left(\frac{W_c}{S} \right)^n \qquad 3.41$$

where W_c is the intercepted canopy water content, S is the maximum canopy capacity (set to 0.5mm), and n is an empirical constant of value 5.

The formulation of the intercepted canopy water follow the water transport equation

$$\frac{\partial W_c}{\partial t} = \sigma_f P - D - E_c \qquad 3.42$$

where P represents the input total precipitation. The formulation requires that the excess precipitation or drip reaches the ground when W_c exceeds S.

The canopy transpiration is formulated as

$$E_t = \sigma_f E_p B_c \left(1 - \frac{W_c}{S} \right)^n . \qquad 3.43$$

B_c is a function of the canopy resistance and parameterized as

$$B_c = \frac{1 + \frac{\Delta_r}{R_r}}{1 + R_c C_h + \frac{\Delta_r}{R_r}} \qquad 3.44$$

where Δ_r depends on the slope of the saturation specific humidity curve, R_r is a function of air temperature and surface pressure, and R_c is the canopy resistance. In an alternative treatment of transpiration following Pan and Mahrt (1987), and Ek and Mahrt (1991), B_c is replaced by the plant co-efficient defined as

$$P_c = \frac{1}{1 + R_c C_h} \qquad 3.45$$

The formulation of the canopy resistance follows Jacquemin and Noilhan (1990) and Noilhan and Planton (1989). They parameterized the plant resistance as four nonlinear functions of solar insolation, (F_1), atmospheric humidity/vapor pressure, (F_2), atmospheric temperature, (F_3), and soil moisture content, (F_4) as

$$R_c = \frac{R\text{cmin}}{LAI\, F_1 F_2 F_3 F_4} \qquad 3.46$$

$$F_1 = \frac{\frac{Rcmin}{Rcmax} + f}{1 + f} \qquad 3.47$$

where $f = 0.55 \frac{R_s}{Rgl} \frac{2}{LAI}$ 3.48

$$F_2 = \frac{1}{1 + Hs\left[q_s(T_a) - q_a\right]} \qquad 3.49$$

$$F_3 = 1 - 0.0016\left[T_{ref} - T_a\right]^2 \qquad 3.50$$

and

$$F_4 = \sum_{i=1}^{3} \frac{(\Theta_i - \Theta_w) d_{zi}}{(\Theta_{ref} - \Theta_w)(d_{z1} + d_{z2})} \qquad 3.51$$

The functions F_1, F_2, F_3 *and* F_4 lie between *0* and *1*. *Rcmin* is the minimum stomatal resistance, LAI is the leaf area index, and *Rcmax* is the cuticular resistance of the leaves (set to 5000 sm^{-1}; Dickinson et al., 1993). T_{ref} is set to 298 *K* according to Noilhan and Planton (1989). d_{zi} is the depth of the *i*-th root layer. *Rgl* is the solar insolation factor, R_s is the instantaneous solar insolation, and *Hs* is the vapor pressure

deficit factor. The parameters depend nonlinearly on the canopy resistance and hence also nonlinearly on transpiration. $\Theta_{ref} - \Theta_w$ is the soil moisture available to the plant system and represents the range of soil moisture content that influences transpiration. When the soil moisture content exceeds Θ_{ref}, transpiration is not regulated by soil moisture deficit; when the soil moisture content is less than Θ_w, soil water deficit would prevent transpiration within the soil layer. The nonlinear dependence of transpiration on vegetation parameters poses formidable problems even for the 1D SVAT case. Their spatial representation in SVAT models requires a great deal of innovation and computational effort as discussed in Chapter 2.

3.2.7 Soil moisture initialization

The initialization of soil moisture in the stand-alone version of the OSU LSM is implemented with point estimates or site-specific soil moisture data. However, in the implementation of the OSU LSM in MM5 (3D coupled mode), the spatial variability of soil moisture must be incorporated in the initialization process. In the 3D coupled mode, the soil moisture initialization is determined empirically from reanalysis and data assimilation data. The soil moisture fields are adjusted for biases based on the seasons. For the NCEP-NCAR reanalysis system, two regimes have been chosen to represent annual soil moisture initialization. For January to June, the formulation is given by

$$SM_{MM5} = \begin{cases} min(0.75 SM_g + 0.0084, 0.35), & SM_g \geq 0.28 \\ SM_g, & Otherwise \end{cases} \qquad 3.52$$

For July to December, the following formulation is used

$$SM_{MM5} = \begin{cases} 0.429 SM_g + 0.16, & 0.21 \leq SM_g \leq 0.28 \\ 0.19 SM_g, & SM_g \leq 0.21 \end{cases} \qquad 3.53$$

where SM_g is the soil moisture from NCEP-NCAR reanalysis and SM_{MM5} is the initial soil moisture in the MM5 model.

3.3 The inverse-SVAT problem

A discussion on SVAT models was presented in the previous section. This section gives a discussion of an efficient and robust method for parameterizing subgrid processes. The formulation of the inverse-SVAT problem and its numerical solution is presented closely following Sun (1994) and Doherty (2002).

3.3.1 Formulation of the inverse-SVAT problem

The representation of subgrid scale processes can be formulated as a dynamical system governed by differential equations and subject to planetary boundary conditions. The SVAT model output (state variables) is represented in terms of the SVAT model $\boldsymbol{u_D}$ parameter set $\boldsymbol{p}$ by the relation

$$\boldsymbol{u}_D = M'(\boldsymbol{p}) \qquad 3.54$$

where M' is a transformation with dimension m that maps each parameter set $\boldsymbol{p}$ to a unique SVAT model output $\boldsymbol{u_D}$; $\boldsymbol{u_D}$ and $\boldsymbol{p}$ have dimensions of m and n respectively.

A formal discussion on forward and inverse problems was presented in section 2.3.4. Equation 3.54 defines the forward SVAT problem such that for a given SVAT parameter set $\boldsymbol{p}$, the transformation M' produces the SVAT model output $\boldsymbol{u_D}$ (e.g. area-weighted average of surface energy fluxes over a heterogeneous surface). The inverse SVAT problem is the reverse operation where we seek for the parameter set $\boldsymbol{p}$ that produces the same SVAT model output $\boldsymbol{u_D}$. The solution to the inverse-SVAT problem is given by the relation

$$\boldsymbol{p} = (M'^{-1})\boldsymbol{u}_D \qquad 3.55$$

where M'^{-1} is an inverse mapping of M', which maps the SVAT model parameter set $\boldsymbol{p}$ to the SVAT model output $\boldsymbol{u_D}$ (Sun, 1994). The inverse mapping M'^{-1} contains information about the upscaling relationships between the effective parameter at the grid scale and its corresponding subgrid scale parameters as defined in section 1.3.

For equation 3.55 to be solvable, the following conditions must be met:

- The solution must exist, i.e., the SVAT model parameters must be real.
- The solution must be unique, i.e., each SVAT model output $\boldsymbol{u_D}$ must uniquely correspond to a specific parameter set $\boldsymbol{p}$; i.e., a one-to-one mapping exists between SVAT model output and parameters.
- The solution must be stable, i.e., small changes in SVAT model parameters should induce only negligible changes in SVAT model output.

These requirements are very difficult to meet in real-life situations. For this reason, physical inverse problems are generally ill-posed (not well-defined), and hence an exact algebraic solution does not exist. Approximate methods exist for transforming an ill-posed problem to a well-posed one (Sun, 1994; Tikhonov, 1963). More importantly, as SVAT processes are highly nonlinear and parameterized by the similarity theory, the inverse-SVAT problem defined by equation 3.55 is generally ill-posed. Treatment is therefore possible via approximate iterative solutions, since the exact algebraic solution does not exist.

Several techniques have been developed to solve optimization problems, with each technique being suitable for a particular class of problems (Bates et al., 1988; Fletcher, 1987; Sun, 1994; Marquardt, 1963; Tarantola, 1987). In recent studies, hybrid forms of the optimization techniques have gained much attention because of their robustness. In this work, the Gauss-Marquardt-Levenberg hybrid technique implemented in PEST (Doherty, 2000) for the optimal parameter estimation solution is adopted.

3.3.2 The Gauss-Levenberg-Marquardt method

The discussion for the Gauss-Levenberg-Marquardt Method closely follows Doherty (2002) and Cooley and Naff (1990). To formulate an approximate solution to the nonlinear inverse-SVAT problem, the SVAT model representation of equation 3.54 must be reformulated to incorporate model and other errors. This representation is given by

$$\boldsymbol{u_D} = M'(\boldsymbol{p}) + \boldsymbol{e} \qquad 3.56$$

where $\boldsymbol{e}$ is the model error. The regression solution in the least square sense is obtained by minimizing the objective function (weighted sum of square errors)

$$\begin{aligned}\chi^2(\boldsymbol{p}) &= \boldsymbol{e}^T \boldsymbol{Q}\, \boldsymbol{e} \\ &= (\boldsymbol{u_D} - M'(\boldsymbol{p}))^T \boldsymbol{Q}(\boldsymbol{u_D} - M'(\boldsymbol{p}))\end{aligned} \qquad 3.57$$

where $\boldsymbol{Q}$ is the weighting function (Doherty, 2002). Since the problem is generally nonlinear, the solution can be obtained by the linearization of equation 3.56 around an initial parameter estimate, $\boldsymbol{p_o}$, which gives a new set of parameters that minimizes equation 3.57. Expanding $\boldsymbol{u_D}$ about the initial parameter set $\boldsymbol{p_o}$ by Taylor expansion yields

$$\boldsymbol{u_D} = \boldsymbol{u_o} + \boldsymbol{J}(\boldsymbol{p} - \boldsymbol{p_o}) + \boldsymbol{e} \qquad 3.58$$

where

$$\boldsymbol{J} = \frac{\partial M'}{\partial \boldsymbol{p}}\Big|_{p=p_o} \qquad 3.59$$

is the Jacobian matrix of M' calculated at the *i*-th model output point and

$$\boldsymbol{u_o} = M'(\boldsymbol{p_o}) + \boldsymbol{e}\,. \qquad 3.60$$

Equivalently, equations 3.58 can be rewritten in terms of the error term

$$\boldsymbol{e} = \boldsymbol{u_D} - \boldsymbol{u_o} - \boldsymbol{J}(\boldsymbol{p} - \boldsymbol{p_o}) \qquad 3.61$$

and then substituted into equations 3.57 to obtain an appropriate form of the objective function.

The optimal solution for $\boldsymbol{p}$ can be obtained by minimizing

$$\begin{aligned}\chi^2(\boldsymbol{p}) &= \boldsymbol{e}^T \boldsymbol{Q}\, \boldsymbol{e} \\ &\cong (\boldsymbol{u_D} - \boldsymbol{u_o} - \boldsymbol{J}(\boldsymbol{p} - \boldsymbol{p_o}))^T \boldsymbol{Q}(\boldsymbol{u_D} - \boldsymbol{u_o} - \boldsymbol{J}(\boldsymbol{p} - \boldsymbol{p_o}))\end{aligned} \qquad 3.62$$

with respect to $\boldsymbol{p}$. This yields the set of normal equations

$$\boldsymbol{J}^T \boldsymbol{Q} \boldsymbol{J} \boldsymbol{d}_1 = \boldsymbol{J}^T \boldsymbol{Q}(\boldsymbol{u_D} - \boldsymbol{u_o}) \qquad 3.63$$

from which the parameter upgrade vector

$$\boldsymbol{d}_1 = \boldsymbol{p} - \boldsymbol{p_o} \qquad 3.64$$

is computed as

$$\boldsymbol{d}_1 = (\boldsymbol{J}^T \boldsymbol{Q} \boldsymbol{J})^{-1} \boldsymbol{J} \boldsymbol{Q}(\boldsymbol{u_D} - \boldsymbol{u_o})\,. \qquad 3.65$$

The parameter upgrade vector $(\boldsymbol{p} - \boldsymbol{p_o})$ is based on the residual vector

$$\boldsymbol{r} = \boldsymbol{u_D} - \boldsymbol{u_o} \qquad 3.66$$

which defines the discrepancy between the SVAT model output $\boldsymbol{u_o}$ and the numerical observation $\boldsymbol{u_D}$ (e.g. aggregated surface energy fluxes from a heterogeneous surface).

The relevant information about the estimated parameter are contained in the covariance matrix defined as

$$\boldsymbol{C(p)} = \sigma^2 (\boldsymbol{J^T Q J})^{-1} \qquad 3.67$$

where

$$\sigma^2 = \frac{\chi^2(\boldsymbol{p})}{m-n} \qquad 3.68$$

is the variance of the elements of $\boldsymbol{u_D}$. *m-n* is the degree of freedom of the parameter estimation process. A brief discussion will be given later in this section.

The Marquardt parameter

The parameter upgrade vector defined by

$$\boldsymbol{d_1} = (\boldsymbol{J^T Q J})^{-1} \boldsymbol{J^T Q r} \qquad 3.69$$

is the basis of nonlinear weighted least squares parameter estimation. The minimization of the objective function is carried out via a gradient search procedure. The gradient of the

objective function, $\boldsymbol{g}$, defined by

$$\boldsymbol{g} = \frac{\partial \chi^2(\boldsymbol{p})}{\partial \boldsymbol{p}} \qquad 3.70$$

constitutes a critical entity in the search for the optimal parameter set, as it determines the direction in which the optimal solution is located in parameter space. When the angle between $\boldsymbol{d_1}$ and $-\boldsymbol{g}$ is greater than 90^o, the objective function (equation 3.62) will increase.

Although $-\boldsymbol{g}$ defines the direction of steepest descent of the objective function, $\boldsymbol{d_1}$ is considered a better parameter upgrade direction, especially in cases where the parameters are correlated (Doherty, 2002). In such instances, iteratively following the direction of steepest descent leads to hemstitching, where the parameter set jumps from side to side in a valley in $\chi^2(\boldsymbol{p})$ during the parameter upgrade process.

However, the gradient search procedure can be improved by adjusting $\boldsymbol{d}_1$ such that it is closer to the direction of $-\boldsymbol{g}$ in the initial stages of the parameter estimation process.

This is achieved by the introduction of a factor α, called the Marquardt parameter, to $\boldsymbol{d}_1$ (equations 3.69) such that

$$\boldsymbol{d}_1 = (\boldsymbol{J}^T\boldsymbol{Q}\boldsymbol{J} + \alpha\boldsymbol{I})^{-1}\boldsymbol{J}^T\boldsymbol{Q}\boldsymbol{r} \qquad 3.71$$

and $\boldsymbol{I}$ is the $n\,x\,n$ identity matrix.

The gradient vector $\boldsymbol{g}$ (equations 3.70) can be rewritten to incorporate the residual vector $\boldsymbol{r}$ (equations 3.66) as

$$\boldsymbol{g} = -2\boldsymbol{J}^T\boldsymbol{Q}\boldsymbol{r} \qquad 3.72$$

It can be deduced from equations 3.71 and equation 3.72 that, for high values of α, the direction of $\boldsymbol{d}_1$ approaches that of $-\boldsymbol{g}$; when α is zero, equation 3.71 is the same as equation 3.69. Therefore, a high initial α value is preferred.

To reduce round-off errors and the problem of stiffness associated with the observations and parameter values of vastly different magnitudes, the scaling of the normal equations is required. This is achieved by the introduction of a scaling matrix (Doherty, 2002; Cooley et al., 1990). More importantly, an optimal length of the parameter upgrade vector ($\beta\boldsymbol{d}_1$) is required to ensure that the parameter upgrade vector does not overshoot or jump over the location of the optimal solution. A detailed treatment of the determination of the optimal length of the parameter upgrade vector is presented in Doherty (2002).

The upgraded parameter vector $\boldsymbol{p}$ is finally given by

$$\boldsymbol{p} = \boldsymbol{p}_o + \beta\boldsymbol{d}_1 \qquad 3.73$$

Measures of Goodness-of-Fit

Parameter correlation

As mentioned previously, $C(\boldsymbol{p})$ and σ^2 contain very useful information about the quality of the parameter estimation process. In particular, σ^2 is directly proportional to the objective function and hence inversely proportional to the Goodness-of-Fit of the parameter estimation process.

For a successful parameter estimation process, $C(\mathbf{p})$ must be diagonal (nonsingular). However, in most physical problems, the parameters of interest are strongly correlated, so that $C(\mathbf{p})$ becomes almost singular. In this case, one parameter can be better estimated or a number of linear combinations of parameters instead of the individual parameters themselves. For instance, where the parameter correlation is extreme, $C(\mathbf{p})$ becomes singular and parameter estimation is impossible.

Two very useful information on parameter correlations can be obtained from $C(\mathbf{p})$.

- The correlation co-efficient, ρ, between parameters with values ranging from –1 to 1. The closer ρ is to –1 or 1, the stronger the correlation between the parameters.
- The normalized eigenvectors of $C(\mathbf{p})$. If each eigenvector is dominated by one element, individual parameter values may be well resolved by the parameter estimation process. However, if the predominance within each eigenvector is shared between a number of elements (with largest eigenvalues), the corresponding parameters are highly correlated.

Correlation co-efficient between observations and model output

Beyond obtaining information about the estimated parameters, another measure of Goodness-of-Fit is the measure of the correlation between the observations and the model output (Cooley and Naff, 1990; Doherty, 2002). Unlike the objective function, the correlation co-efficient, R, is independent of the number of observations and the uncertainty associated with the observations. Hence, R provides a direct independent measure for comparing the results of different parameter estimation runs. Generally, for an acceptable fit between observations and model output, R, must be above 0.9 (Hill, 1998; Doherty, 2002).

Procedures for improving the parameter estimation process

Beyond the measures incorporated in the PEST algorithm, to ensure successful parameter estimation, additional measures are required to facilitate convergence of the parameter estimation process. As the inverse-SVAT method is a model-independent approach, the parameter estimation process must be constrained by physical information about the problem under investigation. In this way, the problem is customized to meet

the specific requirements of the problem. For example, parameter bounds can be provided so that the search process is constrained within the feasible region of the parameter search space.

Transformation of model parameters and model output from highly nonlinear functions to linear functions greatly facilitates the convergence of the search process to the optimal solution. The essence of such transformations is to ensure that the requirements for well-posedness are met (Tikhonov, 1963; Bates and Watts, 1988; Sun, 1994; Doherty, 2002). Widely used transformations functions are the logarithmic and power laws (Bates and Watts, 1988).

Additionally, provision of good initial parameter estimates is crucial for a successful parameter estimation process. It has been shown (Cooley and Naff, 1990; Sun, 1994) that when an initial parameter estimate can be found within a close neighborhood of the optimal parameter set, convergence to the optimal solution is immensely facilitated. More importantly, when there are several local minima in the parameter space, a good initial parameter is a strict requirement for successfully locating the global minimum.

3.4 The Monte Carlo random number generator for normally distributed fields

The Monte Carlo random number generator is developed based on the Box-Muller transformation following Press et al. (1992). The Box-Muller transformation is a transformation that transforms a two-dimensional continuous uniform distribution to a two-dimensional bivariate normal distribution.

To transform a uniform distribution into a standard normal distribution:

- Start with two independent random variables that are uniformly distributed between 0 and 1.
- The transformation function required is that for which the sum of the squares of the two uniformly distributed variables chosen above is less than 1 (i.e. within the unit circle).
- The derived random variables satisfying the condition above will each be independently distributed according to the standard normal distribution (with zero mean and a standard deviation of 1).

By using different seeds in a uniformly distributed random number generator, different realizations of the standard normally distributed random fields can be obtained from the above procedure. The normally distributed random fields can be used to generate a distribution with a specified mean and standard deviation through a linear transformation. The implementation of the above method is presented in Chapter 5, where distributions of specified means and standard deviations are used to represent land surface parameters. A detailed treatment can be found in Press et al. (1992).

3.5 Concluding remarks

The complexity involved in representing the SVAT processes with respect to the highly nonlinear dependence of surface energy fluxes on most land surface parameters implies that aggregating these parameters spatially presents a formidable challenge. However, these formidable challenges present an opportunity for the development of innovative strategies for resolving the problem of representing subgrid scale processes in SVAT models.

The relevant theoretical formulations for upscaling land surface parameters using inverse -SVAT modeling has been presented. The salient points for enhancing convergence of the parameter estimation process to the optimal solution have been discussed. The subsequent chapters use the formulations discussed in this chapter to development of concepts and methodologies for numerical experimentation on upscaling land surface parameters. In particular, Chapter 5 gives a conceptual design and numerical implementation of the inverse-SVAT method. The following chapter gives the sensitivity analysis of surface energy fluxes and moisture indicators for six land surface parameters.

4 SENSITIVITY OF SURFACE ENERGY FLUXES AND MOISTURE INDICATORS TO CHANGES IN LAND SURFACE PARAMETERS IN THE VOLTA BASIN

4.1 Introduction

Several studies have shown that changes in landuse in West Africa are closely correlated with interannual fluctuations in rainfall (Brubaker et al., 1993; Kunstmann et al., 2003; Mohr et al., 2002; Nicholson et al., 1998). Brukaber et al. (1993) have shown that precipitation recycling approaches 50% in West Africa in summer, implying an important role of landuse in the development of rainfall.

To properly quantify the extent of the impact of vegetation on rainfall and climate in the Volta Basin, the land surface parameters that control evapotranspiration must be accurately determined. However, the functions that govern evapotranspiration are highly nonlinear and too complicated for very detailed analysis. More importantly, the computational effort and computing resources required for a detailed analysis at the regional level is very prohibitive for regional climate modeling. Hence, there is the need for a sensitivity analysis to aid in the identification of the land surface parameters that greatly influence evapotranspiration.

The complex feedback mechanisms between highly nonlinear functions that govern the soil, vegetation and atmospheric interactions make it difficult to generalize the findings obtained from such an analysis in that different initial conditions will drive the climate system differently. However, such an analysis affords one the ability to identify possible states and responses of the climate system to changes in land surface parameters and initial conditions. The results of such an analysis also enables one to identify the most sensitive land surface parameters that greatly influence the dynamics of the earth's climate system and to focus the analysis on these critical parameters. This information is crucial in parameter estimation studies where reducing the number of parameters to be estimated greatly improves the performance of the parameter estimation process. Additionally, one would also like to know which of the parameters are correlated, so that the relevant parameter transformations and prior information can be introduced as regularization constraints to guide the parameter estimation process to the optimal parameter set.

Recent studies have shown that roughness length, plant insolation factor, vapor pressure deficit factor, leaf area index, surface albedo, surface emissivity, fractional vegetation coverage, soil field capacity, wilting point and minimum stomatal resistance are the most important land surface parameters (Avissar et al., 1989; Bastiaanssen, 1995; Collins et al., 1994; Deardoff, 1978; Noilhan et al., 1989). However, due to limitations in computing resources and information obtained from related studies on the relative importance of the land surface parameters for model output, the following six land surface parameters are identified for the sensitivity analysis in this work:

Surface roughness length, z_o.

Surface albedo, α.

Surface emissivity, ε.

Minimum stomatal resistance, ***Rcmin***.

Radiation stress factor, ***Rgl.***

Vapor pressure deficit factor, ***Hs***.

To evaluate the impact of land surface parameters on soil-vegetation-atmosphere interactions in the Volta Basin, a sensitivity analysis on each of the six land surface parameters was done to aid in characterizing and estimating their relative importance on model simulations and to gain deeper understanding of how these parameters interact. These interactions are captured by analyzing how the hydrologically-controlled partitioning of the available surface energy between the sensible and latent heat fluxes is effected. The extent of the energy partitioning is measured via moisture indicators, which express the magnitude between zero evaporation and potential evaporation and hence reveal the surface energy partitioning for an appreciable length of time. Bastiaanssen (1995) recommends the evaporative fraction and Bowen ratio as appropriate moisture indicators as they can be easily computed from surface energy fluxes. Additionally, their diurnal variations are relatively stable and hence reliable moisture indicators.

The sensitivity analysis constitutes model responses to increases in control parameters of the six land surface parameters. For reasons of limitation on computing resources, only 20% increase in the selected land surface parameters are considered. For instances where the 20% increase in a vegetation parameter would lead to violation of the physical limits of that parameter, the maximum possible physical value is used (e.g.

maximum surface emissivity is set to 1). The parameter increases were done exclusively for each parameter type. Two parameter perturbation scenarios were considered. For Case I, an increase of 20% in parameter values was applied to the dominant vegetation (savanna) only. In Case II, the 20% increase in parameter values was applied to all vegetation types in the Volta Basin.

The Pennsylvania State University Mesoscale Meterological Model (MM5) (Grell et al., 1994) coupled to the Oregon-State-University Land-Surface-Model (OSU LSM) (Chen & Dudhia, 2001) was used. In the analysis, the percentage change (ratio of the difference in model output for the perturbed and control runs to the control model output) of a model output was used as a sensitivity index to investigate the relative importance of each vegetation parameter on the energy dynamics of the land-atmosphere interactions in the Volta Basin. A percentage change equal to or greater than 10% is considered significant (Hu et al., 1997). Also, negative values imply that the model output for a given perturbed parameter run is less than that of the control run while a positive value indicates otherwise.

4.2 The numerical experimentation

To investigate the sensitivity of surface energy fluxes and moisture indicators to changes in land surface parameters, MM5 was applied in a non-hydrostatic two-way nesting mode using three domains with horizontal resolutions of 81 × 81 km^2 (61 × 61 gridpoints), 27 × 27 km^2 (61 × 61), and 9 × 9 km^2 (121 × 67) and 26 vertical layers extending up to 30 mbar at the model top (Figure 4.1). The global reanalysis fields obtained from NCEP (National Centres for Environmental Prediction) are used. The outer and middle domains provide boundary conditions for the inner domain (domain 3), which constitutes the experimental domain over which the sensitivity experiment was undertaken.

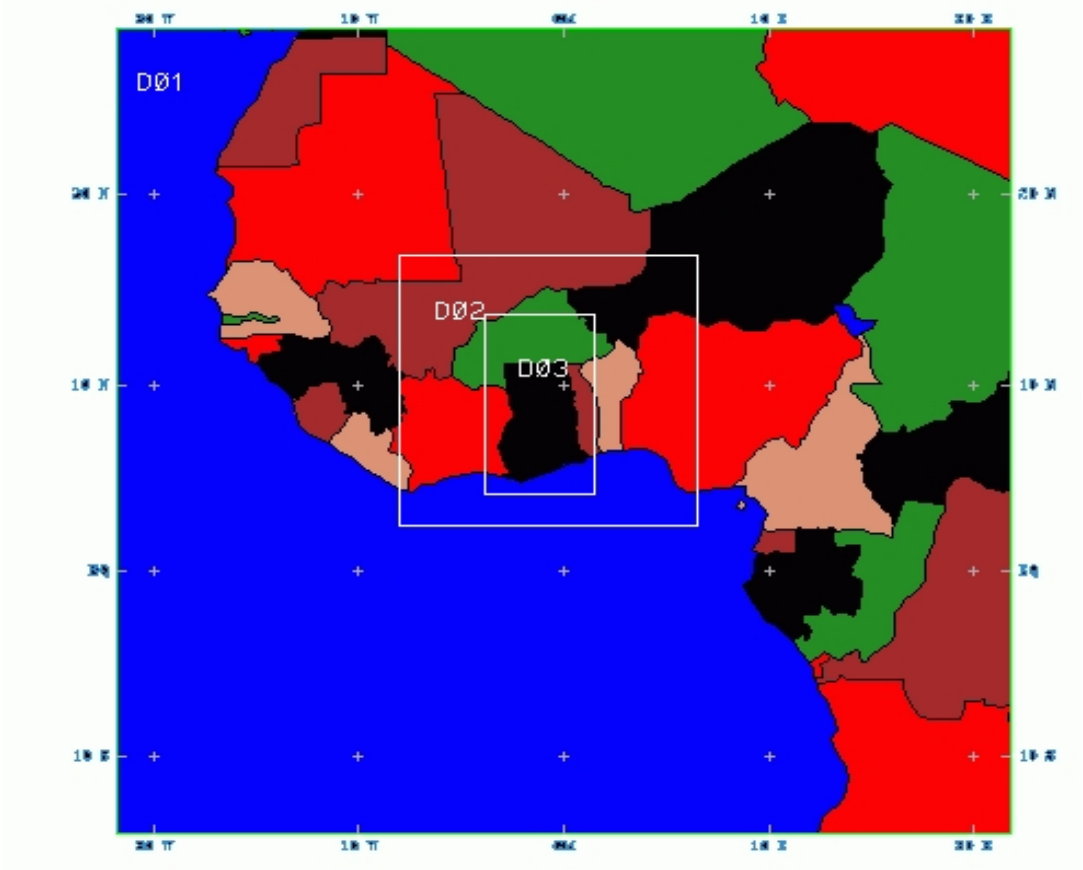

Figure 4.1: The experimental domain configuration for the sensitivity analysis. The outer domains provide boundary and initial conditions for the experimental domain (domain 3; Volta Basin) by dynamically downscaling the global reanalysis data down to 9 × 9 km^2 using a two-way nesting approach.

Additionally, MM5 was coupled to the Oregon State University Land Surface Model (OSU–LSM) (Chen & Dudhia, 2001) to account for the feedback mechanisms between soil, vegetation and the planetary boundary layer. Elevation, landuse and soil data are taken from NCAR data archives, as well as from data sets compiled by the landuse cluster of the GLOWA-Volta project. Figure 4.2 shows the landuse types in the Volta Basin.

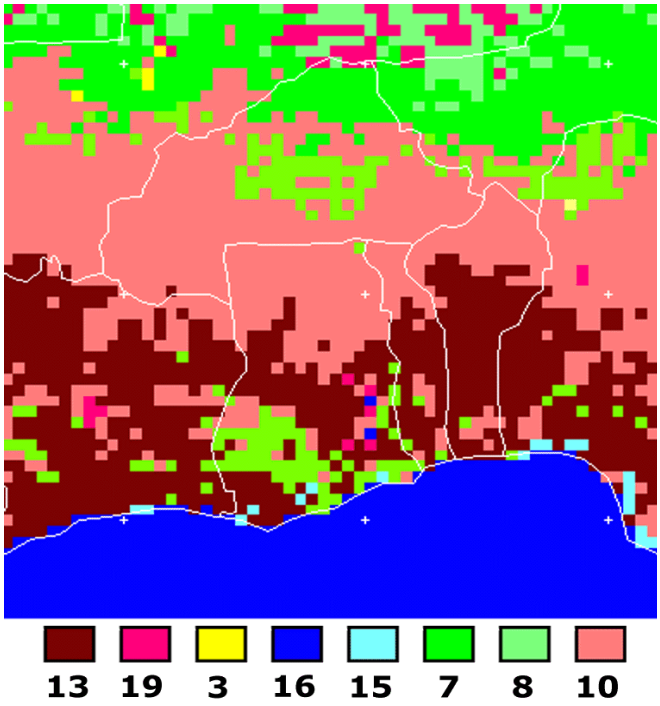

Class	*Landuse type*
3	Irrigated crop/pasture
7	Grassland
8	Shrubland
10	Savanna
13	Evergreen broadleaf
15	Mixed forest
16	Water bodies
19	Sparsely vegetated

Figure 4.2: Landuse types in the Volta Basin based on USGS category 24. Source: NCAR.

The third domain covers an area of 660,000 km^2 of which 400,000 km^2 constitute the Volta Basin. The period July 15, 1998 to August 14, 1998 constitute the first maximum of the bimodal rainy season to the intermediate minimum of the 'Little-Dry-Season' in August. For purposes of capturing the response of surface energy fluxes and moisture indicators to changes in land surface parameters, the period August 15 – 18, 1998 was chosen because there is appreciable amount of soil moisture in the Volta Basin and the rains are not too severe to cause flooding and other climatic events that could complicate the sensitivity experiment.

The model sensitivity analysis was applied to investigate the sensitivity of the surface energy fluxes (available surface energy, sensible and latent heat fluxes) and moisture indicators (evaporative fraction and Bowen ratio) to six USGS category 24 land surface parameters. The parameters were perturbed by 20% increase in the control parameter and simulation runs made for 72 hours at 3-hour intervals (from August 15 – 18, 1998). The surface energy fluxes and moisture indicators were computed for the inner domain by taking the spatio-temporal averages over domain 3 (7920 data points and 72-hour period).

The relevant model outputs were computed as follows:

$$\lambda E = \frac{1}{T}\sum_{j=0}^{T-1}\left\{\frac{1}{N}\sum_{i=1}^{N}\lambda E_{ij}(A_i, t_j)\right\} \quad 4.1$$

$$H = \frac{1}{T}\sum_{i=1}^{T-1}\left\{\frac{1}{N}\sum_{i=i}^{N}H_{ij}(A_i, t_j)\right\} \quad 4.2$$

$$\Lambda = \frac{\lambda E}{\lambda E + H} \quad 4.3$$

$$\beta = \frac{H}{\lambda E} \quad 4.4$$

where λE, H, Λ and β are the spatio-temporal averages over the domain and period of simulation for the latent heat flux, sensible heat flux, evaporative fraction and Bowen ratio respectively. $\lambda E_{ij}(A_i, t_j)$ and $H_{ij}(A_i, t_j)$ are the instantaneous values of latent and sensible heat fluxes in the domain, A_i is the $i-th$ data point (grid) in the model domain, and t_j the $j-th$ time at 3 hour intervals. N=7920 (grids) and T=72 (hours). The percentage changes (SI) in the surface heat fluxes and moisture indicators are estimated and used as sensitivity indices to investigate the relative significance of each vegetation parameter on the model output following Bastiaanssen (1995).

The percentage changes were computed for the surface energy fluxes and moisture indicators as:

$$SI_{H,p_k} = \frac{H(120\%\,x\,Control) - H\ (Control)}{H(Control)} \quad 4.5$$

$$SI_{\lambda E,p_k} = \frac{\lambda E(120\%\,x\,Control) - \lambda E(Control)}{\lambda E(Control)} \quad 4.6$$

$$SI_{\Lambda,p_k} = \frac{\Lambda(120\%\,x\,Control) - \Lambda(Control)}{\Lambda(Control)} \quad 4.7$$

$$SI_{\beta,p_k} = \frac{\beta(120\%\,x\,Control) - \beta(Control)}{\beta(Control)} \quad 4.8$$

Additionally, parameter sensitivities based on the Jacobian formulation (Doherty, 2002) were computed as:

$$S_{H,p_k} = \frac{H(120\% \, x\, Control) - H(Control)}{0.2\, Control} \quad 4.9$$

$$S_{\lambda E,p_k} = \frac{\lambda E(120\% \, x\, Control) - \lambda E(Control)}{0.2\, Control} \quad 4.10$$

$$S_{\Lambda,p_k} = \frac{\Lambda(120\% \, x\, Control) - \Lambda(Control)}{0.2\, Control} \quad 4.11$$

$$S_{\beta,p_k} = \frac{\beta(120\% \, x\, Control) - \beta(Control)}{0.2\, Control} \quad 4.12$$

where p_k is the *k-th* vegetation parameter (other symbols as above). Control is the original/default parameter in the MM5 scheme. The land surface parameters used in the experiment (control/default) are given in Table 4.1.

Table 4.1: Control/default landuse parameters based on the USGS category 24 classification.

Parameter	**Type 3**	**Type 7**	**Type 8**	**Type 10**	**Type 13**	**Type 15**	**Type 16**	**Type 19**
α[-]	0.18	0.20	0.22	0.20	0.12	0.13	0.08	0.25
ε [-]	0.92	0.93	0.88	0.92	0.95	0.94	0.98	0.85
***z_o* (cm)**	0.15	0.16	0.10	0.15	0.50	0.50	0.0001	0.10
Rcmin(sm^{-1})	40.00	40.00	300.00	70.00	150.00	125.00	100.00	999.00
Rgl (Wms^{-2})	100.00	100.00	100.00	65.00	30.00	30.00	30.00	999.00
Hs (kg/kg)	36.25	36.35	42.00	54.53	41.69	51.93	51.75	999.00

The above experimentation was applied under two parameter perturbation scenarios. For Case I, an increase of 20% in parameter values was applied to the dominant vegetation (savanna) only. In Case II, the 20% increase in parameter values was applied to all vegetation types in the Volta Basin. The following section gives the analysis of the results for the two Cases considered.

4.3 Analysis of sensitivity results

4.3.1 Response of surface energy fluxes and moisture indicators to changes in land surface parameters in the Volta Basin

The Volta Basin consists of very heterogeneous land surfaces characterized by water bodies, savanna mosaic, tropical rain forest, cities, irrigated crops, transition landcover zones, bare surfaces and mountains. These highly heterogeneous surfaces greatly influence the near surface atmospheric flow variables and energy distribution. Therefore, changes in land surface characteristics (e.g. albedo, roughness length, emissivity and stomatal resistance) affect the evolution of the atmosphere in a highly nonlinear way.

The available surface energy given by the energy balance relation

$$AE = R_n - G_s = \lambda E + H \qquad 4.13$$

determines the energy available for land surface processes. The net radiation defined by

$$R_n = (1-\alpha)R_s + \varepsilon_s(R_l - \sigma T_s^4) \qquad 4.14$$

in turn determines the magnitude of the available surface energy and is dependent on land surface characteristics (albedo and emissivity). Since the energy dynamics are hydrologically-controlled, the initial (soil) water content plays a very important role in the energy partitioning (balance) processes. Therefore, the interaction of the landcover with the radiation from the sun determines the prevailing climatic conditions in the Volta Basin.

In the afternoon when the available energy is maximum, the vegetated surfaces produce higher latent heat fluxes than the bare soil surfaces. In particular, since a sizable area within the Volta Basin is covered by water (River Volta/Lake Volta), evaporation is at potential rate in these areas. At the same time, the bare soil surfaces heat up faster and produce more sensible heat fluxes than the water and vegetated surfaces. This creates both moisture and temperature gradients between the contrasting surfaces, and hence the climate system is driven in a way that reduces these gradients by redistributing the moisture and temperature profiles. As the atmospheric moisture and temperature profiles move towards establishing equilibrium with the underlying heterogeneous surfaces, the micrometeorological conditions (near surface wind, temperature and moisture profiles) are modified by the fluxes whenever moving air parcels experience changes in the underlying surface. After going over several different

land surfaces, the air parcels modify the meteorological conditions with the differences growing with time and distance from the first change in the underlying surface. These modified micrometeorological properties in effect modify the sensible and latent heat fluxes.

Because the initial meteorological forcing and landuse types are identical in both scenarios (Case I and Case II) considered in the sensitivity experiment, the distribution patterns of the surface energy fluxes differ primarily due to the changes in the landuse parameters. For instance, changes in albedo would lead to differences in the net radiation and available surface energy. Hence, the available surface energy fluxes will be partitioned differently into sensible and latent fluxes. Secondary differences result from the modified micrometeorological conditions that affect the heat fluxes. As time evolves, further differences may arise from the modification of the thermal stratification, cloud formation, net surface radiation and hence modified evapotranspiration. Additionally, differences may occur due to advection of momentum, heat and moisture. The orographic effect of mountains also modifies the climate of the Volta Basin. Studies by Kunstmann and Jung (2003) have shown that changing the landuse type and soil moisture content can create feedbacks in moisture and thermal gradients resulting in different precipitation events. For the short simulation period used in this investigation, the initial water content plays a very important role in the energy budget.

The analysis of the results of the sensitivity experiment is presented in the following sections. Section 4.3.2 gives the response of the surface energy fluxes and moisture indicators to changes in land surface parameters for only the dominant vegetation type (Case I). Section 4.3.2 gives the scenario where the parameter changes are applied to all vegetation types (Case II).

Case I: Response of surface energy fluxes and moisture indicators to 20% increase in parameter values for the dominant vegetation type (savanna)

a. Surface energy fluxes

Figure 4.3 shows the response of the respective average surface energy fluxes to changes in the parameters of the dominant vegetation. Figure 4.4 shows the

corresponding percentage changes in the surface energy fluxes with respect to the corresponding control values.

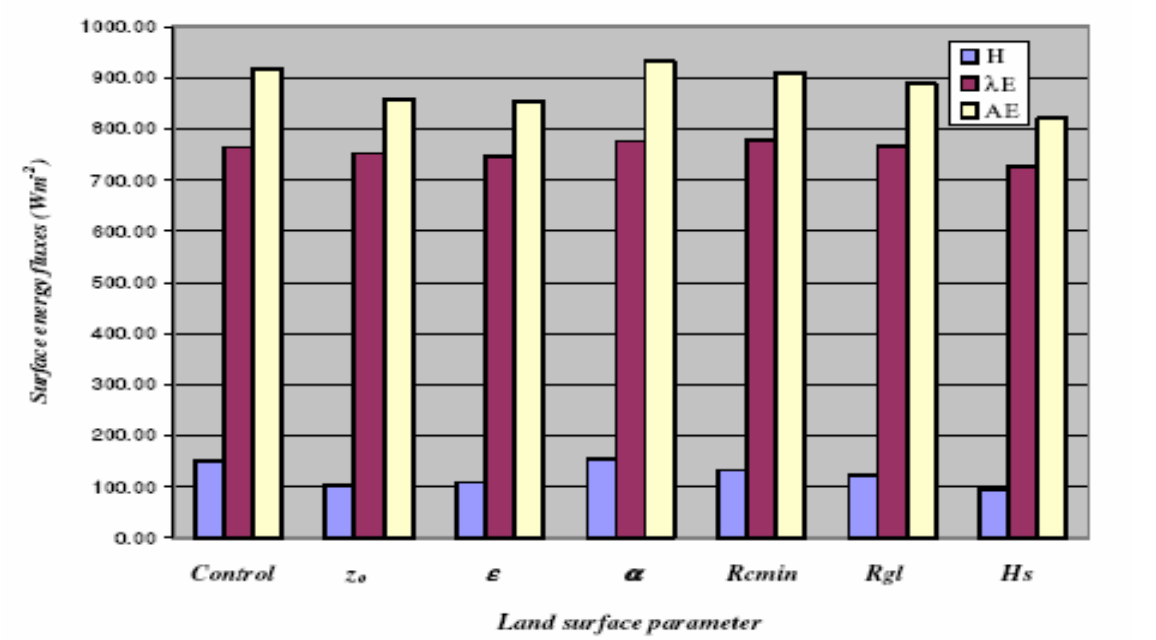

Figure 4.3: Comparison of the response of the surface energy fluxes to changes in land surface parameters based on 20% increase in the dominant vegetation parameters.

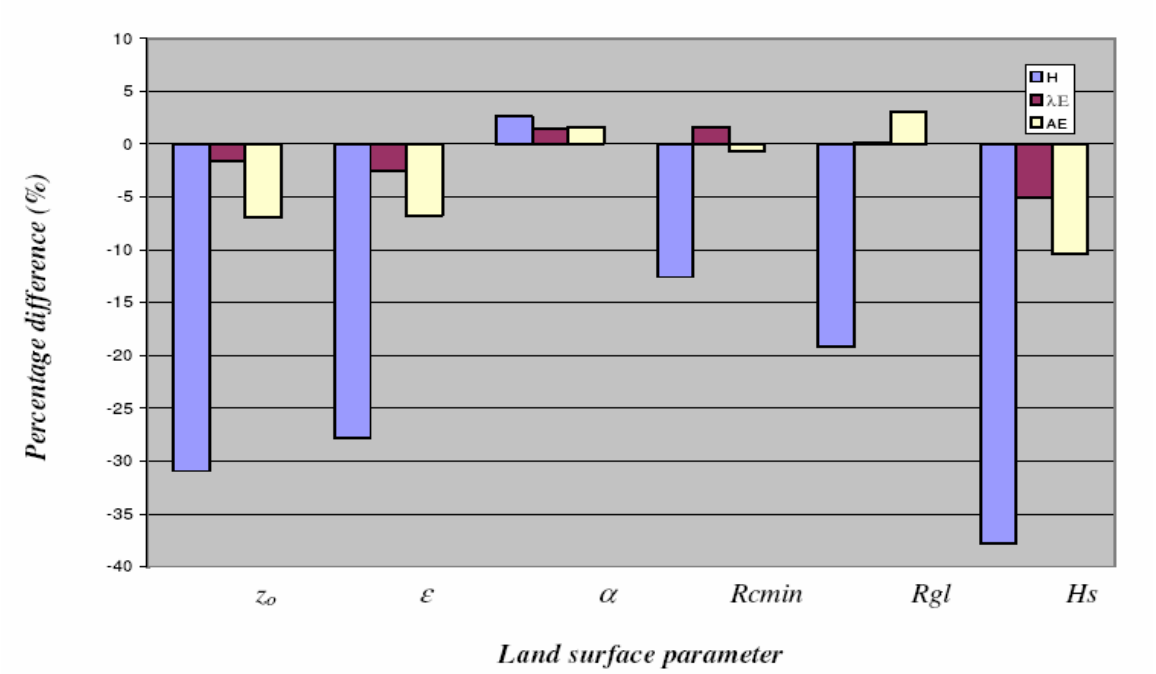

Figure 4.4: Comparison of the percentage changes in the response of the surface energy fluxes to changes in land surface parameters based on 20% increase in the dominant vegetation parameters.

Tables 4.2-4.3 give detailed information on the above plots. The values are based on the spatio-temporal averages over the experimental domain (Domain 3).

Table 4.2: Response of surface energy fluxes to 20% increase in land surface parameters of the dominant vegetation.

	Control	z_o	ε	α	***Rcmin***	***Rgl***	***Hs***
H (Wm^{-2})	151.70	104.81	109.57	155.69	132.66	122.64	94.37
λE (Wm^{-2})	765.39	753.14	745.71	776.52	777.94	766.33	727.10
AE (Wm^{-2})	917.09	857.95	855.28	932.20	910.60	888.96	821.46

Table 4.3: Percentage difference in surface energy fluxes in response to 20% increase in dominant vegetation parameters.

	z_o	ε	α	***Rcmin***	***Rgl***	***Hs***
H (Wm^{-2})	-30.91	-27.77	2.63	-12.55	-19.16	-37.79
λE (Wm^{-2})	-1.60	-2.57	1.45	1.64	0.12	-5.00
AE (Wm^{-2})	-6.89	-6.74	1.65	-0.71	3.07	-10.43

The available surface energy flux (***AE***) has a maximum of 932.20 Wm^{-2} (α) and a minimum of 821.46 Wm^{-2} (***Hs***), and corresponding maximum percentage change of –10.43 % (***Hs***) and minimum of –0.71% (***Rcmin***). The percentage changes in ***AE*** are insignificant (<10%) for all the land surface parameters except for ***Hs*** (-10.43).

The maximum latent heat flux (λE) is 777.94 Wm^{-2} (***Rcmin***) and minimum of 727.10 Wm^{-2} (***Hs***). This indicates a rather wet condition as would be expected due to the fact that the period of the investigation is within the rainy season. The corresponding maximum percentage change is –6.89% (z_o) with a minimum of 0.12% (***Rgl***). The percentage changes in λE are insignificant (<10%) for all parameters. The latent heat fluxes are relatively higher (about 6-fold) than the sensible heat fluxes. This implies that a larger fraction of the available energy is used in evaporating water and a smaller fraction is used in warming the earth's surface in the form of sensible heat fluxes.

The sensible heat flux (***H***) has a maximum percentage change of –37.79% (***Hs***) and a minimum of 2.63% (α). The percentage changes in ***H*** are significant (>10%) for all parameters except for α (2.63%). The ***H*** follows the same trend as ***AE***. The ***AE*** has the highest variability whereas the variability in λE is smaller than that of ***H***.

Albedo produced the highest increase in surface energy fluxes, whereas ***Hs*** had the least decrease in surface energy fluxes. The available energy and sensible heat fluxes show an increase for only albedo, whereas there was a decrease for the remaining parameters. Percentage changes in ***AE*** for ***Rcmin*** and ***Rgl*** are insignificant. The minimum stomatal resistance has the highest latent heat fluxes (somewhat higher than that of albedo, 1.52 Wm^{-2}). This indicates that an increase in albedo results in an increase in the available surface energy for driving the climate system in the Volta Basin. For the latent heat flux, ***Rgl,*** α and ***Rcmin*** show increases.

b. Moisture indicators

Figures 4.5 and 4.6 show the response of the evaporative fraction and Bowen ratio to changes in the dominant land surface parameters. The details of these responses are given in Tables 4.4 and 4.5. The values are based on the spatio-temporal averages over the experimental domain (Domain 3).

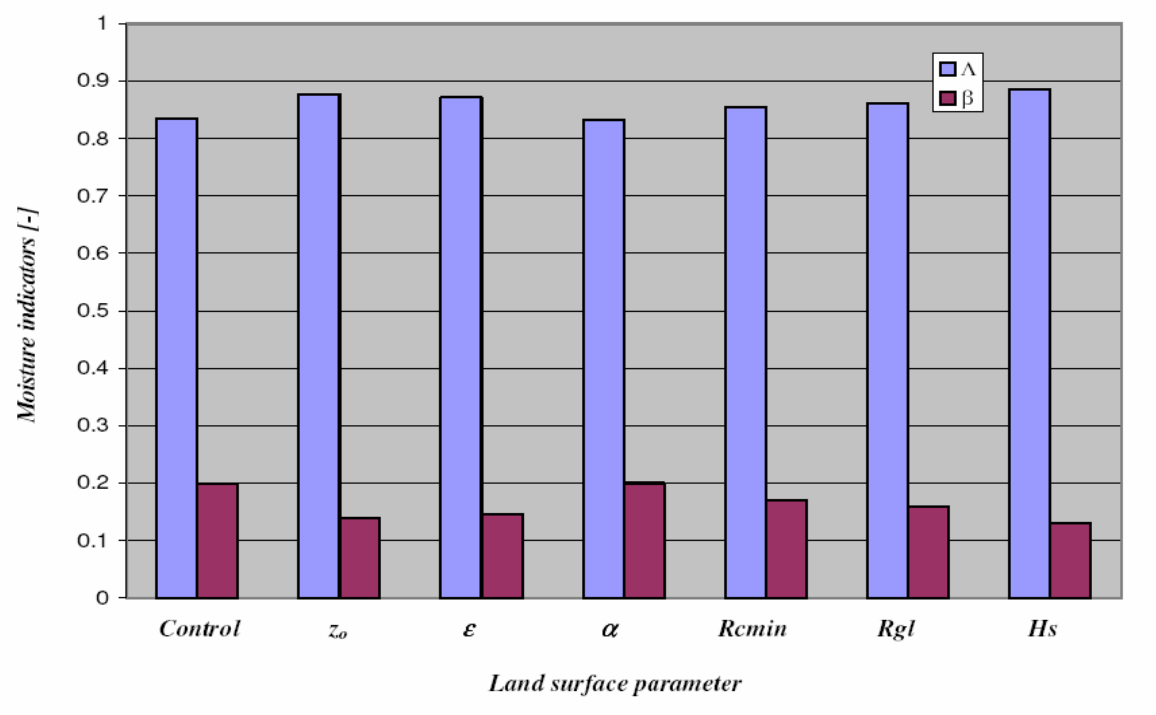

Figure 4.5: Comparison of the response of the moisture indicators to changes in land surface parameters based on 20% increase in the dominant vegetation parameters. The values are based on the spatio-temporal averages over Domain 3.

Table 4.4: Response of moisture indicators to 20% increase in land surface parameters of the dominant vegetation.

	Control	z_o	ε	α	***Rcmin***	***Rgl***	***Hs***
Λ [-]	0.83	0.88	0.87	0.83	0.85	0.86	0.89
β [-]	0.20	0.14	0.15	0.20	0.17	0.16	0.13

Table 4.5: Percentage difference in moisture indicators in response to 20% increase in dominant vegetation parameters.

	z_o	ε	α	***Rcmin***	***Rgl***	***Hs***
Λ [-]	5.18	4.47	-0.19	2.36	3.29	3.29
β [-]	6.74	-25.87	1.16	-13.96	19.26	-19.26

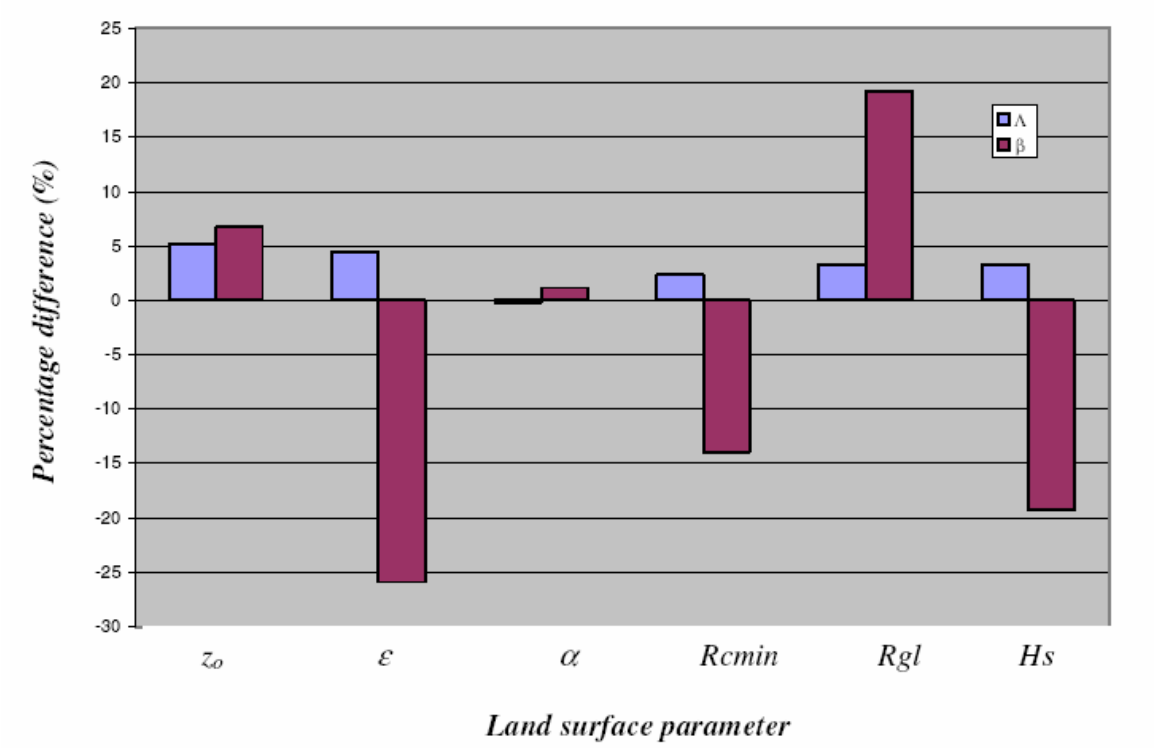

Figure 4.6: Comparison of the percentage changes in the response moisture indicators to changes in land surface parameters based on 20% increase in the dominant vegetation parameters.

The evaporative fraction (Λ) has the lowest variability with a maximum of 0.89 (***Hs***) and minimum of 0.83 (α) and an average of 0.85. The Λ has a maximum percentage change of 5.18% (z_o) and a minimum of –0.19% (α). However, the percentage changes in Λ are insignificant (<10%) for all the land surface parameters.

The Bowen ratio (β) however shows marked sensitivities to the changes in the land surface parameters. It has an average of 0.16, maximum of 0.2 (α) and a minimum of 0.13 (***Hs***). The β has a maximum percentage change of –25.87% (ε) and a minimum of 1.16% (α). The percentage changes in β are significant for all parameters except α, which has a value less than 10%.

Generally, β follows the same trend as ***H*** and ***AE***. The Λ follows a trend similar to that of the latent heat fluxes, but the correlation is not as strong as in the Case of β with respect to ***AE*** and H. The Λ is very high compared to the Bowen ratio as a result of the high λE and small ***H*** values. This again shows the correlation between Λ and λE and β and ***H*** (following the observed pattern for the sensible and latent heat fluxes). More importantly, the evaporative fraction shows lesser variability compared to the Bowen ratio, indicating that the evaporative fraction is a better or reliable moisture indicator than the Bowen ratio.

Case II: Response of surface energy fluxes and moisture indicators to 20% increase in parameter values for all vegetation types

a. Surface energy fluxes

Figures 4.7 to 4.8 show the average surface energy fluxes and their corresponding percentage changes in response to changes in vegetation parameter values for all vegetation types in the Volta Basin. The detailed information associated with the response of surface energy fluxes are shown in Tables 4.6 to 4.7. The highest and lowest average ***AE*** are 988.87 Wm^{-2} (z_o) and 845.38 Wm^{-2} (ε), respectively.

The maximum average λE for changes in all the parameters is less than that of the control (765.39 Wm^{-2}). The second highest is 759.64 Wm^{-2} (***Rgl***). The least and most significant change in λE is 737.56 Wm^{-2} (α). The z_o has the highest percentage change for both ***H*** (53.77%) and ***AE*** (7.83%). The minimum average ***H*** is 102.54 Wm^{-2} (ε). The percentage changes in ***H*** are significant (>10%) for all parameters. However, the percentage changes in all parameters are insignificant for λE and ***AE*** (<10%). The ***Rgl***, ***Hs*** and ***Rcmin*** have the least changes (<1.2%) in λE. The ***AE*** has the highest variability, whereas λE has the lowest variability.

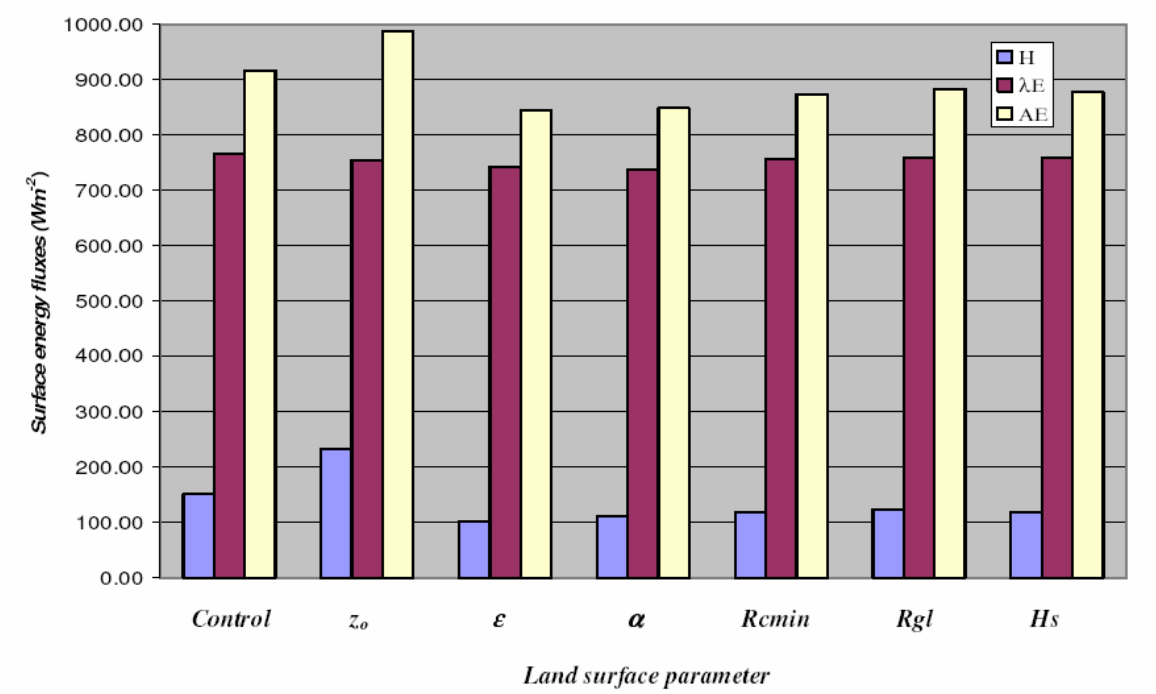

Figure 4.7: Comparison of the response of the surface energy fluxes to changes in land surface parameters based on 20% increase in vegetation parameters for all vegetation types in the Volta Basin. The values are based on the spatio-temporal averages over the experimental domain (Domain 3).

Table 4.6: Response of surface energy fluxes to 20% increase in land surface parameters of vegetation types in the Volta Basin.

	Control	z_o	ε	α	***Rcmin***	***Rgl***	***Hs***
H (Wm^{-2})	151.70	233.26	102.54	111.39	117.93	123.58	119.18
λE (Wm^{-2})	765.39	755.61	742.84	737.56	756.85	759.64	758.76
AE (Wm^{-2})	917.09	988.87	845.38	848.95	874.79	883.22	877.94

Table 4.7: Percentage difference in surface energy fluxes in response to 20% increase in vegetation parameters for all vegetation types in the Volta Basin.

	z_o	ε	α	***Rcmin***	***Rgl***	***Hs***
H (Wm^{-2})	53.77	-32.40	-26.57	-22.26	-18.53	-21.43
λE (Wm^{-2})	-1.28	-2.95	-3.64	-1.11	-0.75	-0.87
AE (Wm^{-2})	7.83	-7.82	-7.43	-4.61	-3.69	-4.27

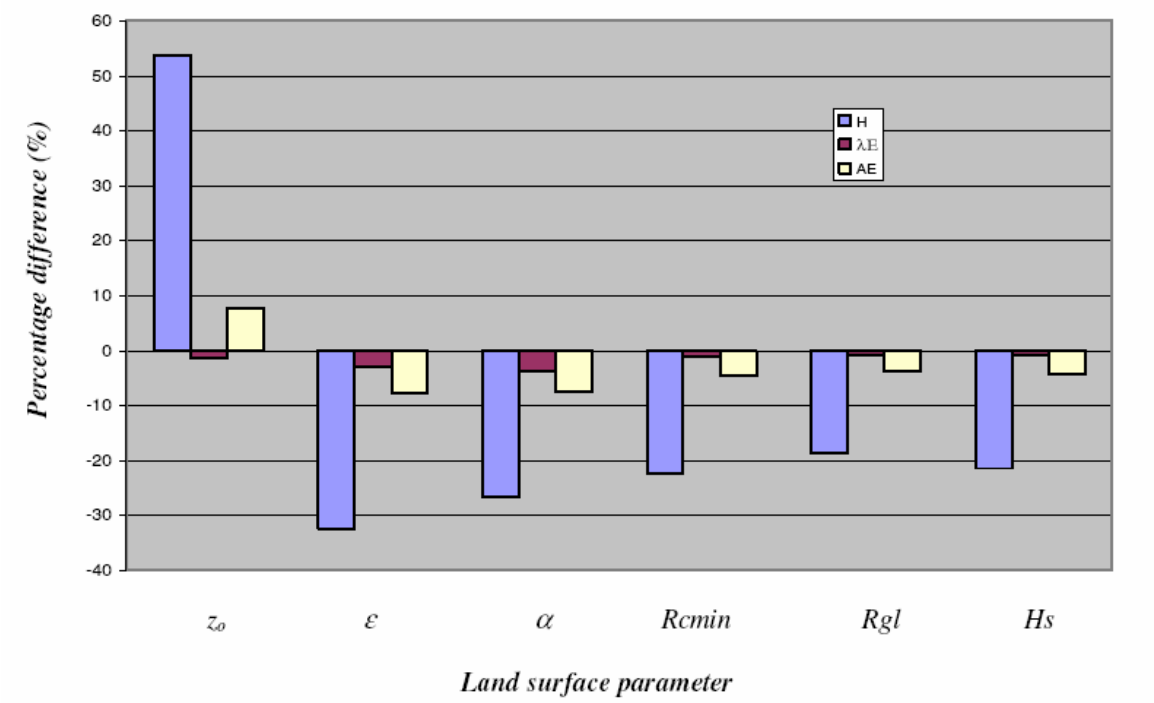

Figure 4.8: Comparison of the percentage changes in the response of the surface energy fluxes to changes in land surface parameters based on 20% increase in vegetation parameters for all vegetation types in the Volta Basin. The values are based on the spatio-temporal averages over the experimental domain (Domain 3).

b. Moisture indicators

The response of the evaporative fraction and Bowen ratio to changes in all the land surface parameters in the Volta Basin is shown in figures 4.9 to 4.10. Tables 4.8 to 4.9 show the corresponding detailed information for the moisture indicators. The moisture indicators do not show any significant deviations from that of Case I. This is an indication that the partitioning of the total available energy into sensible and latent heat fluxes remained fairly constant in both Cases under the applied forcing information.

However, there was quite an appreciable change in the β for z_o (about 56%). Percentage changes in Λ are insignificant (<10%) for all parameters with a maximum percentage change of -8.44% (z_o) and a minimum of 3.05% (***Rgl***). The β has a maximum percentage difference of 55.76% (z_o) and a minimum of –17.92% (***Rgl***). Percentage changes in β are significant (>10%) for all parameters. In general, the β shows marked variability and an inverse relation to the evaporative fraction as observed also in Case I.

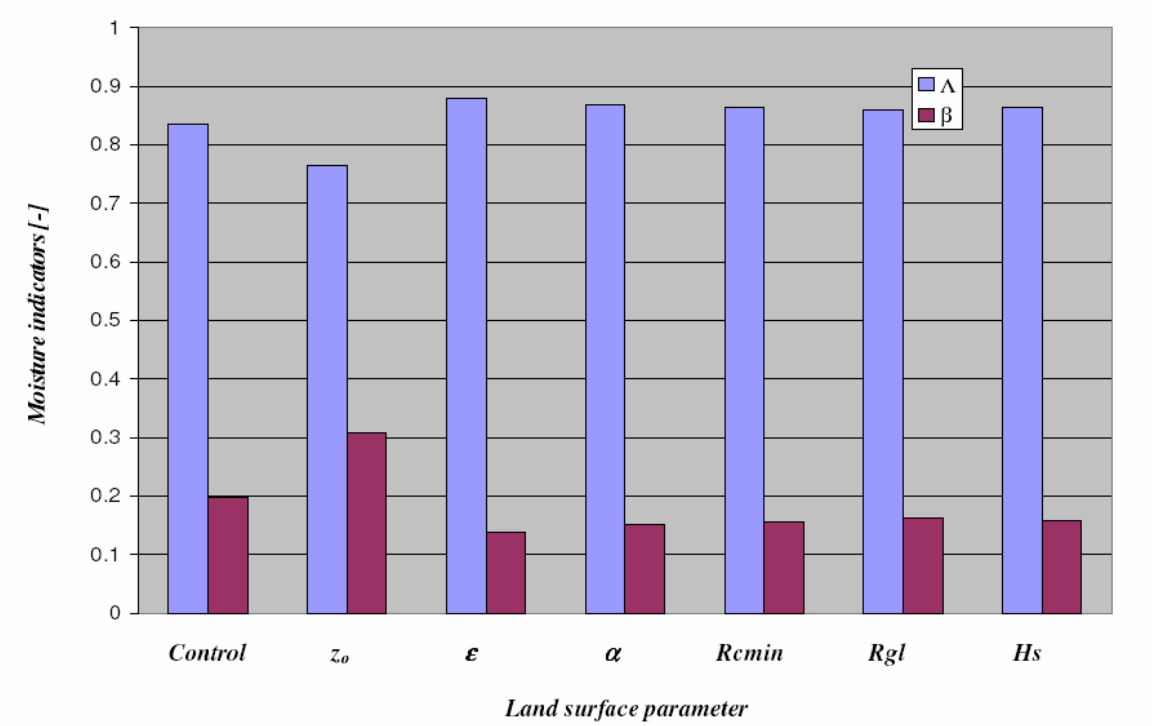

Figure 4.9: Comparison of the response of the moisture indicators to changes in land surface parameters based on 20% increase in the vegetation parameters applied to all vegetation types in the Volta Basin. The values are based on the spatio-temporal averages over the experimental domain (Domain 3).

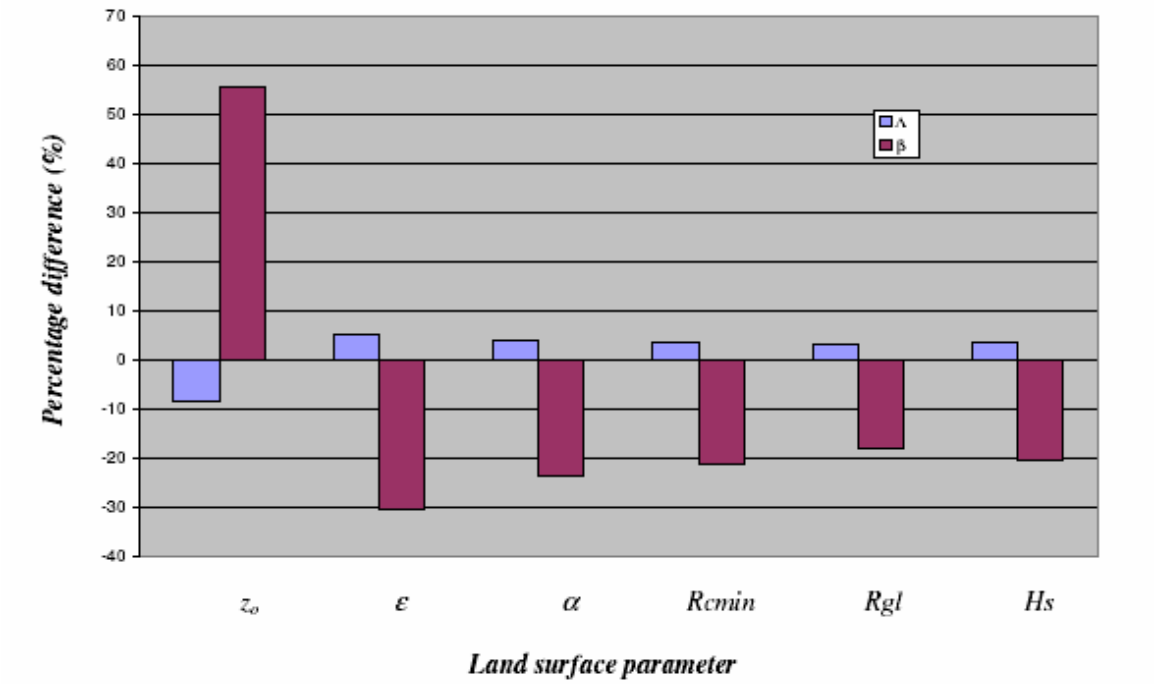

Figure 4.10: Comparison of the percentage changes in the response moisture indicators to changes in land surface parameters based on 20% increase in vegetation parameters applied to all vegetation types in the Volta Basin.

Table 4.8: Response of moisture indicators to 20% increase in land surface parameters applied to all vegetation types in the Volta Basin.

	Control	z_o	ε	α	***Rcmin***	***Rgl***	***Hs***
Λ [-]	0.83	0.76	0.88	0.87	0.87	0.86	0.86
β [-]	0.20	0.31	0.14	0.15	0.16	0.16	0.16

Table 4.9: Percentage difference in moisture indicators in response to 20% increase vegetation parameters applied to all vegetation types in the Volta Basin.

	z_o	ε	α	***Rcmin***	***Rgl***	***Hs***
Λ [-]	-8.44	5.29	4.10	3.67	3.05	3.55
β [-]	55.76	-30.35	-23.80	-21.38	-17.92	-20.75

4.4 Parameter sensitivities based on the Jacobian matrix formulation

Parameter sensitivities give a measure of the rate at which a given model output (e.g. surface energy fluxes or moisture indicator) is changing with respect to changes in a given parameter. The formulation of parameter sensitivities in the context of inverse modeling, was given by the Jacobian matrix (equation 3.59) in Chapter 3.

Figures 4.11 and 4.12 show the respective parameter sensitivity plots for the surface and vegetation parameters investigated. Table 4.10 gives the corresponding data for figures 4.11 and 4.12. For the sensible heat fluxes and available energy, the parameter sensitivities follow the same trend, which is given in ascending order of parameter sensitivity as z_o, ε, α, ***Hs***, ***Rgl*** and ***Rcmin***. In the Case of the latent heat fluxes, the ascending order of parameter sensitivities is z_o, ε, α, ***Hs***, ***Rcmin*** and ***Rgl***. Generally, it can be observed that the surface parameters are (several orders of magnitude) more sensitive than the vegetation parameters.

Table 4.10: Parameter sensitivities based on the Jacobian matrix investigated for Case I. The model outputs are the surface energy fluxes.

	z_o	ε	α	***Rcmin***	***Rgl***	***Hs***
$H(Wm^{-2})$	-1562.92	-870.578	99.67708	-1.35992	-2.23559	-5.25683
$\lambda E(Wm^{-2})$	-408.38	-406.702	278.2083	0.896703	0.07234	-3.51103
$AE(Wm^{-2})$	-1971.3	-1277.28	377.8854	-0.46322	-2.16325	-8.76786

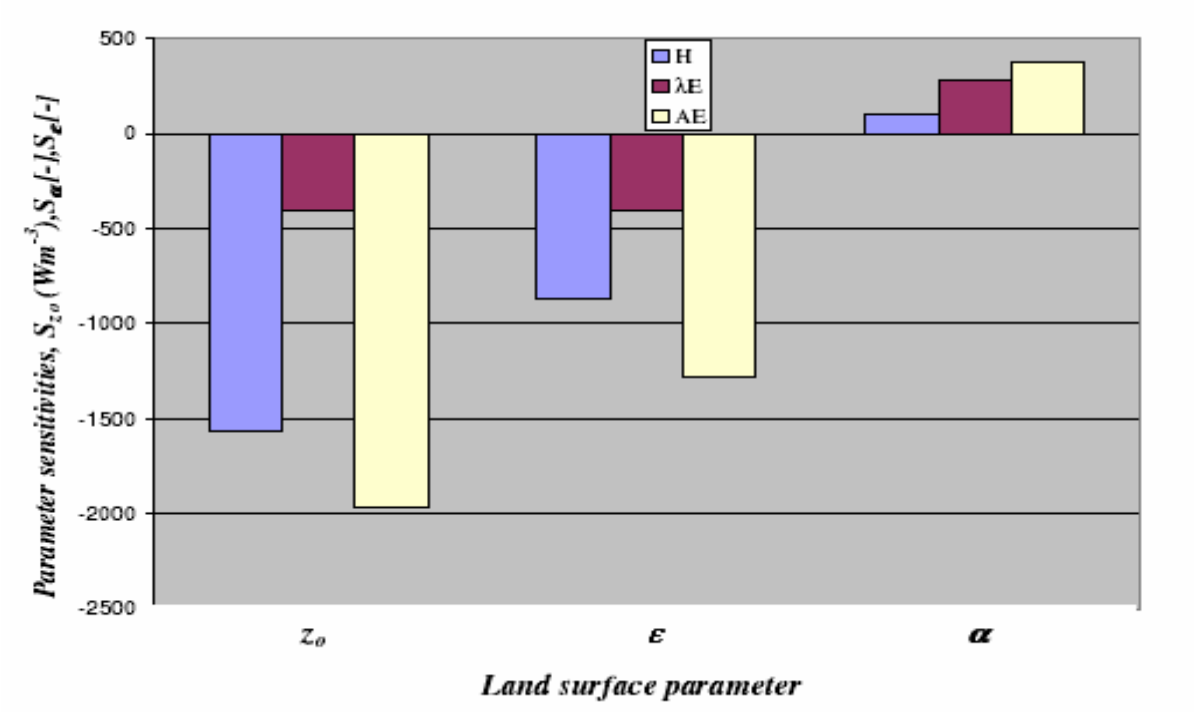

Figure 4.11: Parameter sensitivity plot based on the Jacobian formulation. The land surface parameters are the surface parameters and surface energy fluxes are used as model output (Case I).

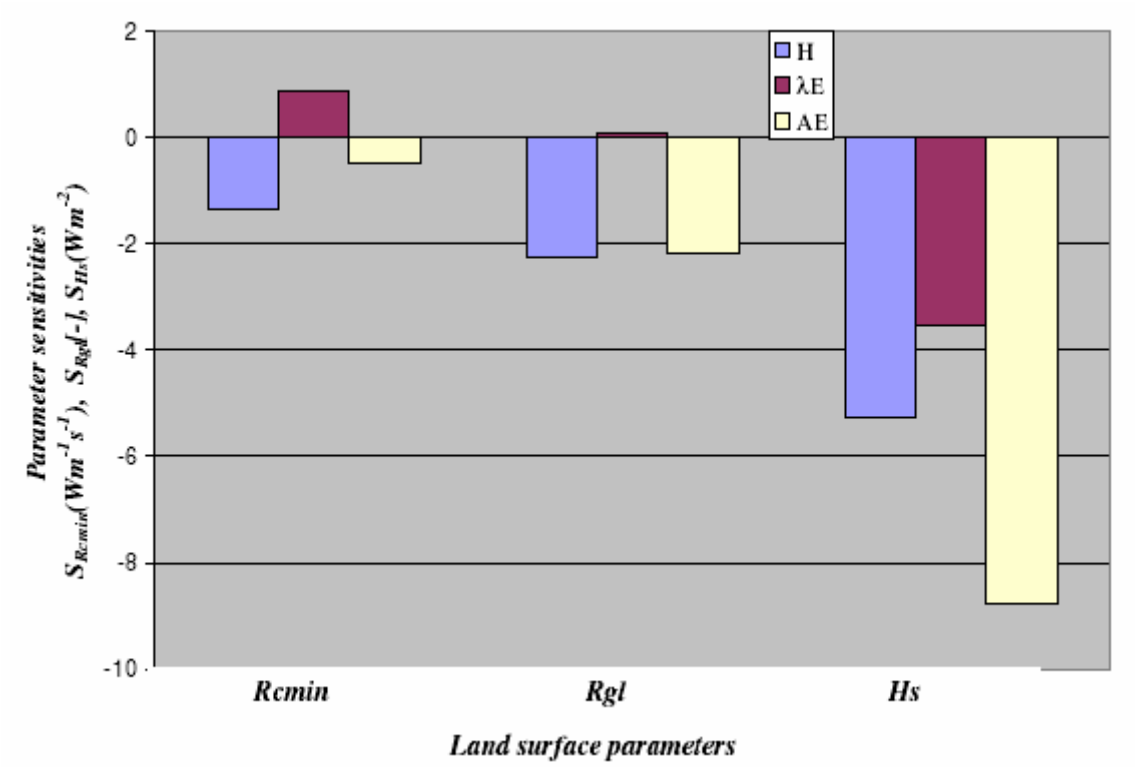

Figure 4.12: Parameter sensitivity plot based on the Jacobian formulation. The land surface parameters are the vegetation parameters and surface energy fluxes are used as model output (Case I).

4.5 General discussion: Comparison between Case I and Case II.

The pattern of the changes in Case II is generally different from that in Case I with respect to the influence of each of the six parameters. However, the relative magnitudes of the surface energy fluxes in each scenario did not change much. This is due to the fact that the effective response of surface energy fluxes and moisture indicators to the moisture and temperature gradients induced by changes in the land surface parameters in each Case is different. Hence the climate dynamics move to different equilibrium levels in both Cases as the moisture and temperature profiles are redistributed. More importantly, as the energy dynamics is hydrologically-controlled, the initial water content (especially of the soil) will have a significant impact on the results.

Details of the variability and average of the surface energy fluxes and moisture indicators are given in Tables 4.11 to 4.16. In general, the changes are more pronounced in Case II. The difference in maximum available energy between Case I and Case II was 56.67 Wm^{-2}. The corresponding difference in minimum available energy is 23.92 Wm^{-2}.

Table 4.11: Statistics on surface energy fluxes (Case II).

	Average	***Max***	***Min***	***Spread***
H (Wm^{-2})	137.08	233.26	102.54	130.72
λE (Wm^{-2})	753.81	765.39	737.56	27.83
AE (Wm^{-2})	890.89	988.87	845.38	143.49

Table 4.12: Statistics on surface energy flux (Case I).

	Average	**Max**	**Min**	***Spread***
H (Wm^{-2})	124.49	155.69	94.37	61.32
λE (Wm^{-2})	758.87	777.94	727.10	50.85
AE (Wm^{-2})	883.36	932.20	821.46	110.74

However, the average available energy between the two Cases was 7.53 Wm^{-2}, which is not very significant. A similar trend exists in the Case of sensible heat fluxes. The difference in maximum, minimum and average sensible heat fluxes is 77.57 Wm^{-2}, 8.17 Wm^{-2} and 12.59 Wm^{-2}, respectively. For the latent heat fluxes, the average and maximum values are higher in Case II than in Case I. Their respective differences in average and maximum values are 18.30 Wm^{-2} and 5.06 Wm^{-2}. The minimum of Case II is higher than that of Case I, and the difference is 10.46 Wm^{-2}.

Figures 4.13 and 4.14 show the deviations of the surface energy fluxes from the control values for Case I and Case II, respectively. The variability in ***H*** for Case II is 130.72 Wm^{-2} as against 61.32 Wm^{-2} for Case I, which is a ratio of about 2:1. The variability in the available surface energy fluxes shows a similar trend to that of the sensible heat fluxes with 143.49 Wm^{-2} in Case II as against 110.74 Wm-2 in Case I. However, the latent heat fluxes show a reverse trend with 27.83 Wm^{-2} in Case II and 50.85 Wm^{-2} in Case I.

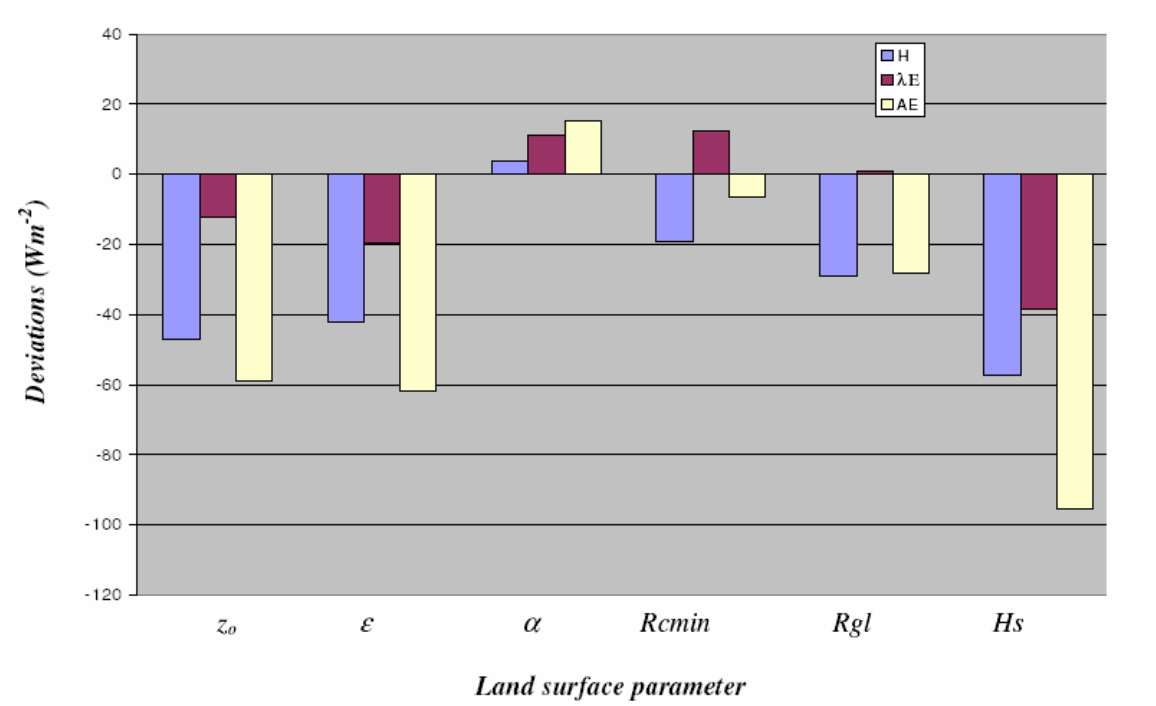

Figure 4.13: Deviations of surface energy fluxes from control run values (Case I).

Table 4.13: Deviations of surface energy fluxes from control run values (Case I).

	z_o	ε	α	Rcmin	Rgl	Hs
H (Wm^{-2})	-46.89	-42.13	3.99	-19.04	-29.06	-57.33
λE (Wm^{-2})	-12.25	-19.68	11.13	12.55	0.94	-38.29
AE (Wm^{-2})	-59.14	-61.81	15.12	-6.49	-28.12	-95.62

Table 4.14: Deviations of surface energy fluxes from control run values (Case II).

	z_o	ε	α	Rcmin	Rgl	Hs
H (Wm^{-2})	81.57	-49.16	-40.31	-33.77	-28.11	-32.52
λE (Wm^{-2})	-9.78	-22.55	-27.83	-8.53	-5.75	-6.63
AE (Wm^{-2})	71.79	-71.70	-68.14	-42.30	-33.86	-39.15

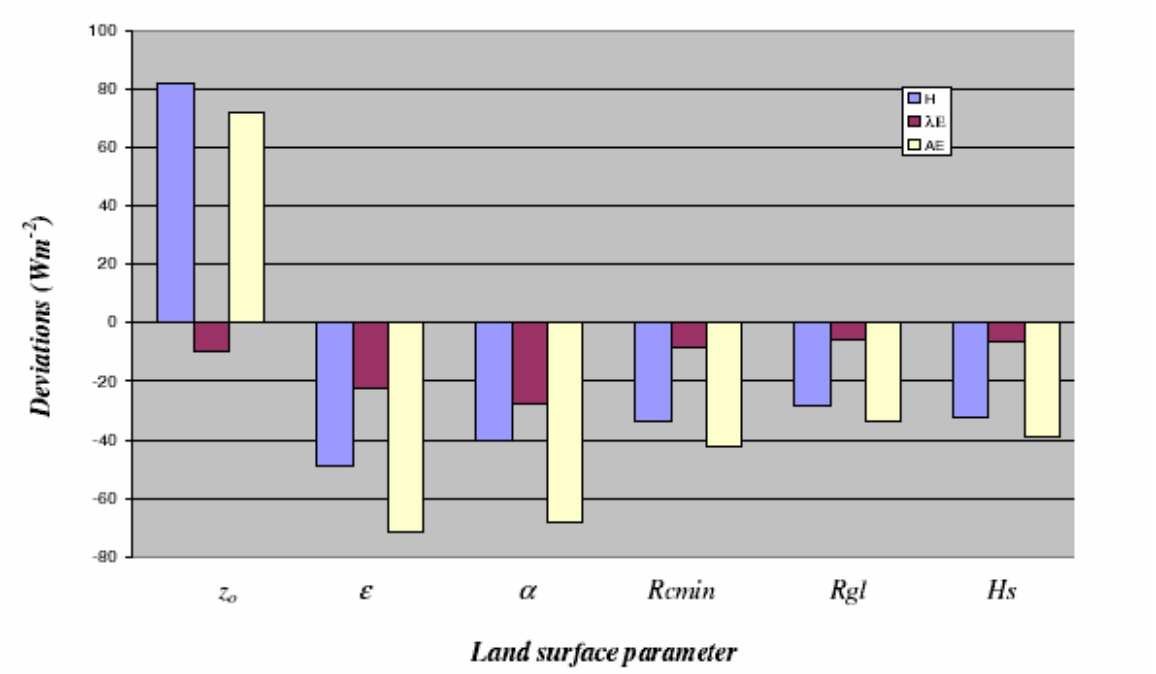

Figure 4.14: Deviations of surface energy fluxes from control run values (Case II).

For the moisture indicators, the Bowen ratio in Case II has a higher percentage change (55.76%) than Case I (-25.87%). The changes are significant (>10%) for all parameters in Case II but significant only for ***ε***, ***Rcmin***, ***Rgl*** and ***Hs*** in Case I. Also, Case II has higher minimum than in Case I. For the evaporative fraction, changes in both Cases I and II are insignificant for all the parameters. A statistical description of the moisture indicators for the both Case I and Case II are summarized in Tables 4.15 and 4.16.

Table 4.15: Statistics on moisture indicators (Case I).

	Average	***Maximum***	***Minimum***	***Spread***
Λ [-]	0.86	0.89	0.83	0.05
β [-]	0.16	0.20	0.13	0.07

Table 4.16: Statistics on Moisture indicators (Case II).

	Average	***Maximum***	***Minimum***	***Spread***
Λ [-]	0.85	0.88	0.76	0.11
β [-]	0.18	0.31	0.14	0.17

4.6 Concluding remarks

In conclusion, the sensitivity analysis shows that the responses of surface energy fluxes and moisture indicators to changes in the six land surface parameters are generally important. However, the sensible heat fluxes and Bowen ratio show significant changes (>10%) for all land surface parameters in both Case I and Case II. The evaporative fraction and latent heat fluxes are not sensitive enough to changes in the six land surface parameters investigated. The available energy is moderately sensitive. A possible explanation for the observed marked differences in sensitivities may be due to the fact that the latent heat fluxes are relatively higher (about 5-fold) than the sensible heat fluxes in both Cases so that the equilibrium state of the energy balance will shift in way that will reduce the energy difference between the latent and sensible heat fluxes. In this Case, the sensible heat fluxes with lower energy fluxes will show more sensitivity. A similar argument can be made for the moisture indicators where the evaporation fraction is also far higher (about 5-fold) than the Bowen ratio. However, these deductions can not be generalized, because under different forcing conditions the results may show otherwise. For instance, Diekkrüger (2003) argues that nonlinear systems (such as investigated in this research) are sensitive to their initial and boundary conditions and that an extreme state of any distribution (dynamical system) may be most important in controlling the observed response. In particularly, the processes in soils depend nonlinearly on boundary and initial conditions, and problems in determining these boundary conditions may significantly influence simulation results (Diekkrüger et al., 1995).

The results show that the sensible heat fluxes and Bowen ratio are very sensitive to the land surface parameters investigated. The order of sensitivity for the land surface parameters investigated in Case I is given in Table 4.17 below.

Table 4.17: Ascending order of parameter sensitivity based on the dominant vegetation

H(Wm^{-2})	***z_o***	***ε***	***α***	***Hs***	***Rgl***	***Rcmin***
λE(Wm^{-2})	***z_o***	***ε***	***α***	***Hs***	***Rcmin***	***Rgl***
AE(Wm^{-2})	***z_o***	***ε***	***α***	***Hs***	***Rgl***	***Rcmin***

In general, the surface energy fluxes were more sensitive to changes in the surface parameters than the vegetation parameters investigated. Although the parameter sensitivity analysis based on the Jacobian model was not applied in Case II, the simple sensitivity analysis (equations 4.5 – 4.8) show that the roughness length was the most sensitive parameter followed by the vapor pressure deficit factor, albedo, emissivity and minimum stomatal resistance. Similar results have been reported in other studies (Lakshmi, 1993). However, results from such sensitivity studies are mixed (Hu et al., 1997), and hence these findings cannot be generalized as the meteorological and soil conditions determine which biophysical processes are dominant under a given set of conditions. For example, Avissar et al. (1989) applied the Fourier Amplitude Sensitivity Test (FAST) with Land-Atmosphere-Interactions Dynamics (LAID) to study the response of surface energy fluxes to changes in land surface parameters and observed that for vegetated land surfaces, stomatal resistance and surface roughness are the two most important land surface characteristics for forcing the atmosphere. For bare land surfaces, they concluded that soil surface wetness and surface roughness are the most important parameters. The leaf area index (LAI) was also found to be important as it gives a measure of the relative abundance of vegetation and bare ground. In some circumstances, albedo can play a very significant role. The relative sensitivity of the model output to each vegetation parameter depends on the extent of the spatial organization of the land cover types within the domain of interest and the prevailing atmospheric conditions.

In Chapter 5 the conceptual design of the upscaling method is presented. Chapter 6 applies the knowledge obtained from the sensitivity analysis presented in this chapter to the numerical implementation of the proposed methodology.

5 THE INVERSE-SVAT TECHNIQUE PART I: DESCRIPTION OF THE UPSCALING METHOD

5.1 Introduction

Methods for upscaling land surface properties have been an issue of many enquiries over the past 20 years. Theoretical studies by McNaughton (1994), Raupach (1995), and Raupach and Finnigan (1995) have shown that the 1D SVAT equations which describe the homogeneous point scale subgrid processes (e.g. surface energy balance) are applicable for describing the area-average (spatial) behavior of heterogeneous land surface characteristics at the coarse scale. More importantly, most methods include the use of surface and meteorological variables at each time step for computing the effective parameters and are therefore not applicable in free-running predictive (forecasting) models where the future meteorological variables are unknown (Arain et al., 1999). However, upscaling relationships are most often required such that they are independent of meteorological forcing (Arain et al., 1996; Chehbouni et al., 1995; Hu et al., 1999).

Chapter 2 gave a survey of existing parameter upscaling techniques. The intense debate surrounding the representation of subgrid scale processes demands that efforts be made towards the development of a unified framework for representing subgrid scale effects. Since the solution for a unified theory has proved evasive, the possibility for developing a model-independent parameter upscaling method seems a more pragmatic approach to resolving the subgrid scale controversy. Therefore, a significant step is made in this thesis towards the development of a model-independent parameter upscaling method via inverse-SVAT modeling. Use is made of the theoretical formulations developed in chapters 2 and 3 to formulate a conceptual design of the inverse-SVAT method and its numerical implementation. The formulation follows closely the energy matching method of Hu et al. (1999) (see section 2.3.2 of Chapter 2), but the optimization of the objective function for the energy residual terms is done through nonlinear parameter optimization (see section 3.3 of Chapter 3).

5.2 Description of upscaling method

5.2.1 Problem definition

The parameterization of subgrid scale effects has been defined in many ways based on the adopted solution strategy. Recent studies have shown that there is no unique procedure for defining effective land surface parameters, and that averaging schemes should be designed to serve specific purposes (Lhomme et. al., 1994; McNaughton 1994).

Therefore, a model-independent formulation of the solution would be a significant step towards resolving the subgrid scale controversy. The problem of aggregating land surface parameters is formulated in this thesis as an inverse problem, and a solution is sought via nonlinear parameter estimation (see section 3.3 of Chapter 3). The subgrid scale problem for this enquiry can be posed as follows:

- Given a distributed heterogeneous land surface (characterized by land surface parameters of mean μ_k and standard deviation σ_k) at the subgrid scale, can we find an effective parameter $p_{eff,k}$ at the grid scale such that the relative change in output response (e.g. surface energy fluxes and moisture indicators) is less than 10% (at least quasi scale invariant)?
- If such an effective parameter $p_{eff,k}$ exists, can we find a functional relation that maps the mean μ_k and standard deviation σ_k of the distributed land surface parameters at the subgrid scale to their corresponding effective parameter $p_{eff,k}$ at the gridscale?

The first question to be addressed is the scale invariant problem that must be addressed. A scale invariant land surface map means that the empirical relationship developed from point observations can be used for large areas. A quasi-scale invariant map means that the resulting error from using an effective parameter (map) to estimate grid scale fluxes will be small (less than 10%). A scale-invariant transformation (or map) must satisfy two conditions (Hu et al., 1997): (i) the parameters of a distributed land surface must be homogeneous over the grid and (ii) the map must be a linear combination of inputs and parameters.

The second question is the determination of the upscaling law that links the heterogeneity of the distributed land surface parameters to their corresponding effective parameter. The implementation of such a scheme would be a significant step towards improving climate model performance. Additionally, it would drastically reduce the intensive utilization of computing resources and CPU time consumed by current high resolution climate models.

5.2.2 Conceptual design of the methodology

The general observation made from the survey of existing methods in Chapter 2 is that these methods are formulated based on some physics assumptions about the subgrid scale processes, which define the type of surface heterogeneity these methods are valid.

To develop the proposed methodology, some basic assumptions about the heterogeneity of the land surface must be made. A common assumption used in developing aggregation schemes for land surface parameters is that at some characteristic height (blending height), the atmospheric flow over a heterogeneous land surface can be considered homogeneous (Blyth et al., 1993; Claussen, 1991; Grotzner et al., 1996; Mason, 1988; Wieringa, 1986). An implication of this assumption is the fact that land surface heterogeneity is disorganized rather than organized. Otherwise due to mesoscale circulations induced by the land surface heterogeneity, the atmospheric boundary layer will behave differently (Hu et al., 1999). However, Claussen (1995) has shown that the limits of the blending height can be stretched to include mesoscale or organized heterogeneity. Additionally, it is assumed that the effect of lateral advection is relatively weak and the classical resistance formulations for the sensible and latent heat fluxes are valid for each relative homogeneous subgrid (Bunzli and Smith, 1998). The similarity law (Raupach and Finnigan, 1995) for surface flux estimation is also assumed to be applicable.

For this work, a heterogeneous land surface within a grid cell is viewed as a collection of land surface elements, referred to as subgrids, patches or tiles. A subgrid represents a small area that can be assumed to be homogeneous. An approach using a distributed map calculates the grid level output by first dividing the grid into a number of subgrids that can be assumed to be homogeneous. Then the response of each subgrid is aggregated by a suitable kernel (e.g. the areal weighted average) to get the grid scale

output (Hu et al., 1997). A distributed model accounts for the spatial variability of inputs, parameters, and outputs within the grid.

Using the concept of the distributed map discussed above, the grid is divided into subgrids with parameters $p_i\,(i=1,..,n)$ characterized by a mean parameter μ_k and standard deviation σ_k as illustrated in figure 5.1 (Hu et al., 1997).

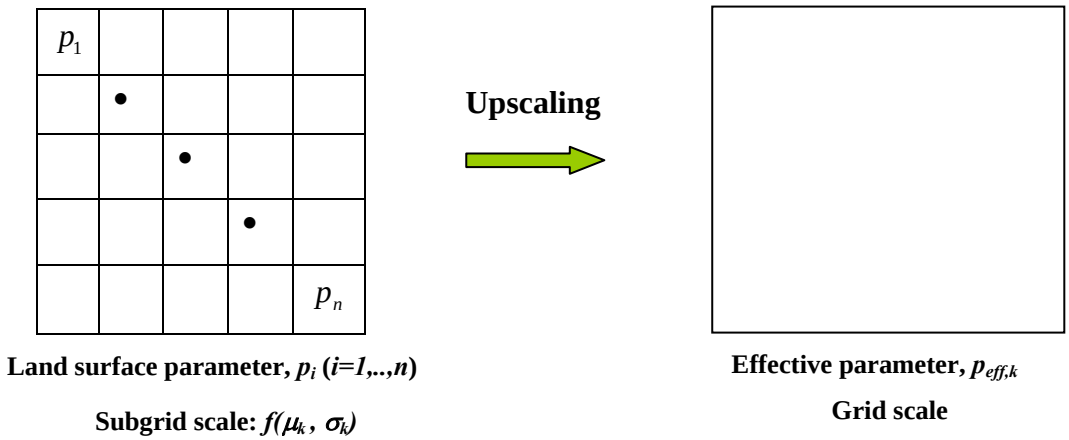

Figure. 5.1: Upscaling of land surface parameters.

The subgrid-scale variability at the fine resolution is resolved by the distributed map at the grid scale. The coupled climate-parameter estimation algorithm (SVAT-PEST) is used to derive a distributed map for estimating an effective parameter $p_{eff,k}$ such that the grid scale $G(p_{eff,k})$ output (e.g. G: sensible heat flux) is almost (less than 10%) equal to that of the subgrid scale aggregated output $\frac{1}{n}\sum_{i=1}^{n} G_i(p_i) = G(\mu_k, \sigma_k)$. This procedure is illustrated in figure 5.2.

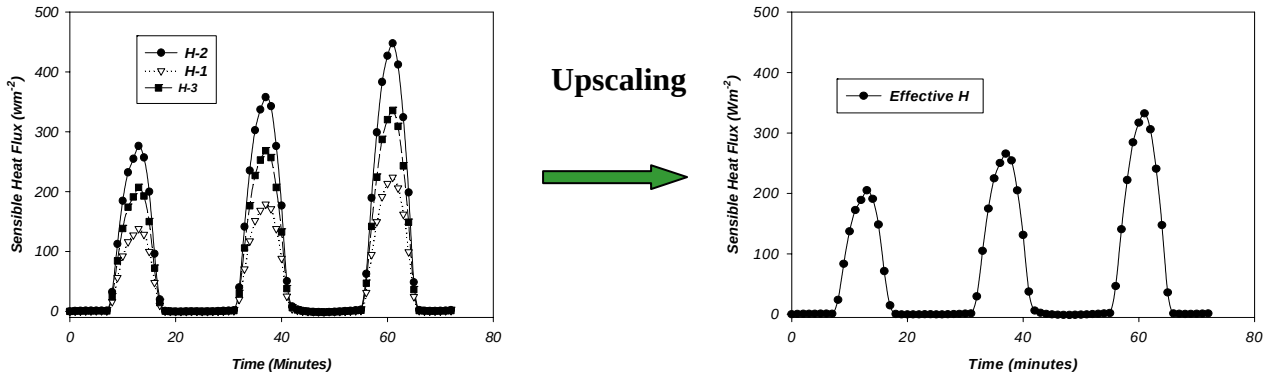

Subgrid scale fluxes: G_i (p_i)

Grid scale fluxes: G($p_{eff,k}$)

Figure. 5.2: Aggregation of surface energy fluxes: *H-1*, *H-2* and *H-3* are subgrid scale sensible heat fluxes.

The problem reduces to an inverse (root finding) problem for $p_{eff,k}$, according to the relation:

$$\frac{1}{n}\sum_{i=1}^{n} G_i(p_i) = G(\mu_k, \sigma_k) \quad \overset{!}{\cong} \quad G(p_{eff,k}) \qquad 5.1$$

Fine scale ⟹ Coarse scale

One then proceeds to derive an upscaling law $f(\mu_k, \sigma_k)$ that maps the mean μ_k and standard deviation σ_k of the distributed parameters at the subgrid scale to their corresponding effective parameter $p_{eff,k}$ at the grid scale. The solution of the inverse problem given by Equation 5.1 ($p_{eff,k}$), is applied to its corresponding sets of (μ_k, σ_k) as

$$p_{eff,k} = f(\mu_k, \sigma_k) \qquad 5.2$$

Equation 5.2 is the required upscaling law that describes the relationship between the land surface heterogeneity (parameters) at the subgrid scale and the corresponding effective parameter at the grid scale.

The solution to the inverse problem of equation 5.1 is to find the coarse scale parameter p_{coarse} for which the chi square objective function

$$\chi^2(p_{coarse}) = \sum_{i=1}^{n}\left[\frac{1}{n}\sum_{i=1}^{n}G_i(p_i) - G(p_{coarse})\right]^2 \qquad 5.3$$

is a minimum. This is equivalent to finding p_{coarse} (= $p_{eff,k}$) such that

$$\left.\frac{\partial \chi^2}{\partial p_{coarse}}\right|_{p_{coarse} = p_{eff,k}} \overset{!}{\cong} 0 \qquad 5.4$$

Since this is a nonlinear problem, the exact algebraic solution does not exist, and hence only approximate solutions via iterative methods are possible. The search process is done along the direction where the chi square function is decreasing. This occurs when the angle between the negative of the Jacobian vector (the derivative of the chi square function with respect to the coarse scale parameter) and the parameter upgrade vector is less than 90^o (Doherty, 2000). The approximate solution of the inverse problem of equation 5.1 is not trivial. The problem is further complicated by the fact that the search process can be trapped in a valley containing a local minimum, making the global minimum evasive as illustrated in figure 5.3.

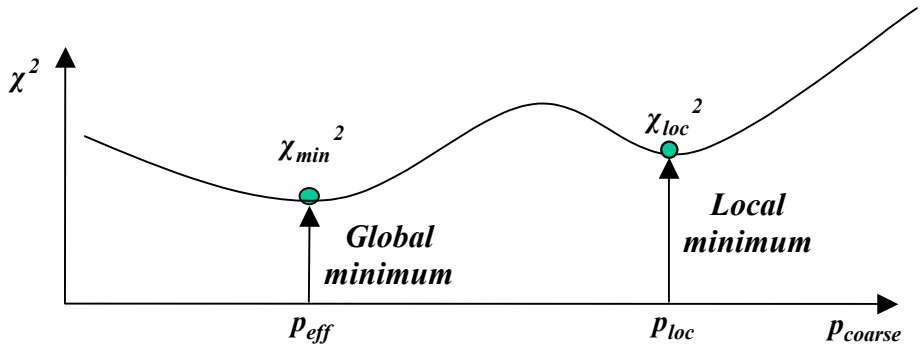

Figure 5.3: Parameter space in relation to the chi square and existence of both local and global minima.

More importantly, when the objective function is granular, the computation of derivatives becomes very problematic and can render the search process impossible. Therefore, for an approximate solution to exist, the following conditions (extended well-posedness in the Tikhonov sense) (Sun, 1994; Tikhonov, 1963) must be met:

- The parameter must exist.
- The parameter must be unique.
- The objective function must be well behaved (stable) and continuously differentiable with respect to the parameter of interest.

Additionally, the solution will converge to the global chi square minimum if an initial parameter estimate can be found such that it lies within a parameter region bounded by the parameter set containing the optimal parameter (Cooley et al., 1990; Doherty, 2002). A good choice of initial parameters helps to resolve the problem of the local minimum. A common approach is the use of Monte Carlo (repeated) runs with variable parameters. A review of the various methods was given in section 3.3 of Chapter 3.

5.3 Concluding remarks

The upscaling methodology presented in this chapter gives a conceptual framework upon which a numerical solution can be developed to calculate effective parameter land surface parameters. A numerical experimentation was setup to test the methodology in both the 1D SVAT mode and the 3D SVAT mode. Chapter 6 gives a description of the numerical experimentation using the OSU LSM as the 1D SVAT mode; the mesoscale model MM5 was applied as the 3D SVAT mode. For the optimal parameter estimation, the highly efficient nonlinear parameter estimation tool PEST (Doherty, 2002) was applied. Synthetic land surface parameters were produced using a Monte Carlo simulation to drive the SVAT models and PEST.

6 THE INVERSE-SVAT TECHNIQUE PART II: NUMERICAL IMPLEMENTATION OF THE UPSCALING METHOD

6.1 Introduction

In chapter 5, a conceptual design of the upscaling method was presented. A numerical experimentation is presented in this chapter to investigate the performance of the proposed methodology. To undertake a numerical implementation of the proposed upscaling methodology presented in the previous chapter, an existing, validated public domain SVAT model (OSU LSM) was coupled to the nonlinear parameter estimation tool PEST. Approximate solutions based on existing methods were used as initial parameters to drive the parameter estimation process. The experiment was extended to include the full 3D mesoscale case by coupling MM5 (which includes the same OSU LSM model as lower boundary) to PEST where the influence of lateral interactions between adjacent grids are accounted for in the analysis. A random number generator was used to provide synthetic normally distributed land surface parameters to drive the models.

The implementation of the scheme consists two parts: 1) the preprocessing of the component models and relevant initialization information, and 2) the coupling of the component models to PEST. For discussion on the preprocessing of the model components, the following procedures are presented:

- The Monte Carlo random number generator
- Initialization of the experimental domains
- Generation of observation data sets
- Computation of initial parameter estimates

For the second part on the coupling of the component models, a description is presented on the coupling and relevant internal interactions between PEST and the component models (Monte Carlo random number generator, 1D and 3D SVAT models). Because, the Monte Carlo random number generator and the coupling procedure are repeated in both 1D and 3D SVAT modes, a single presentation would be given and reference made to them when appropriate.

6.2 Materials and Methods

The choice of the experimental model domains and site locations was based primarily on availability of data and computing resources. For the 1D SVAT upscaling experiments, data on the Meyer/NOAA measurement site was readily available. Additionally, the forcing data had been tested with the current OSU LSM version and good results had been obtained. More importantly, a review of relevant literature helped in identifying the possible (and relevant) experiments to be undertaken and the other appropriate methods for comparison.

Similar arguments follow for the 3D SVAT upscaling experiment. Modeling data and facilities were available from the GLOWA-Volta project. The selected location is within the Volta Basin of West Africa (Northern Ghana). Therefore, an optimal mix of these opportunities and constraints defined the limits of these experiments.

6.2.1 The Monte Carlo experiment

Model setup

The objective of the experiment is to generate random fields to represent land surface parameters that serve as input to the MM5, OSU LSM and PEST models. The Box-Muller transformation method for generating normally-distributed random fields was used because it is a widely proven method (Press et al., 1992). A brief review of the Box-Muller method was presented in chapter 3.

To make sure the random fields are positive (consistent with model physics), the standard normal distribution (with a population mean of zero and standard deviation of one) was first generated. The random fields of the standard normal distribution were then transformed to a prescribed mean and standard deviation (truncated normal distribution). The standard deviation was carefully selected to ensure that the random fields are positive. Additionally, the appropriate random fields of the standard normal distribution must satisfy the following selection criteria:

- The sample mean of the random fields must be close to zero and their corresponding standard deviation close to one.
- The random fields must have enough heterogeneity that is representative of naturally occurring land surface parameters.

The above conditions are difficult to satisfy without the use of advanced tools. To be able to identify the appropriate random fields for the parameter estimation process, the properties of the random fields must be analyzed. To this end, a Monte Carlo experiment was setup to analyze the properties of the random fields and to provide a selection criterion for identifying the appropriate distribution (optimal realization). The schematic of the Monte Carlo random number generation experiment is given in fig.6.1.

The Box-Muller transformation method incorporates a random uniform deviate generator. A number of random number generators were tested with different seeds (initialization numbers), with each seed giving unique random fields. Based on experiment and literature review, a general-purpose robust uniform random deviate generator was applied (Press et al., 1992). The number of realizations needed to produce the required properties was between 30 and 100 but 100 was considered appropriate.

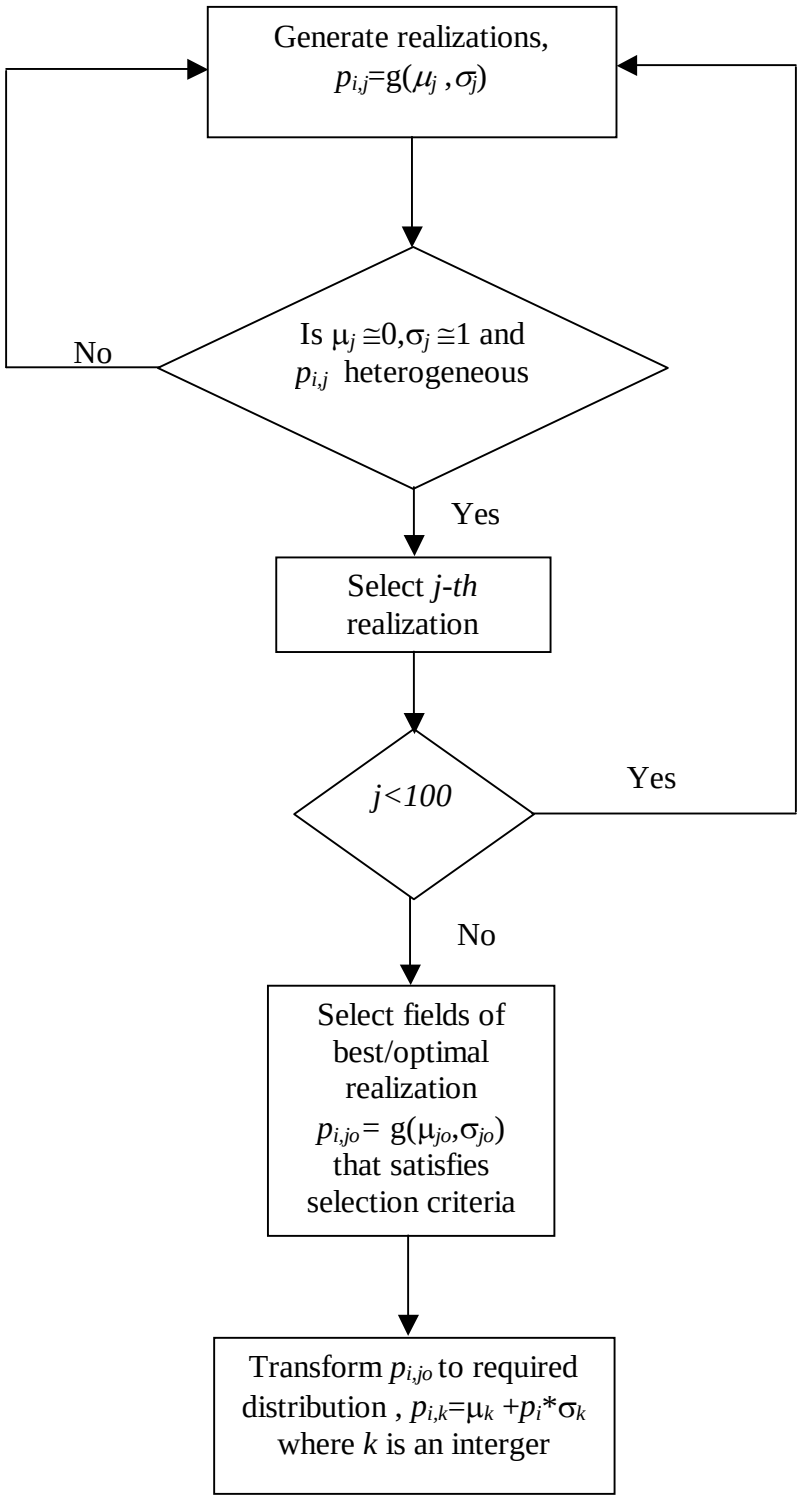

Figure 6.1: Schematic of the Monte Carlo experiment.

The procedure for the analysis is given as follows:

- Generation of large number of realizations (order of 100) of the standard normal distribution ($p_{i,j} = g(\mu_j, \sigma_j)$,*j=1,..,100*).
- Identification of the realization (with optimal properties) that best satisfy the selection criteria $p_{i,jo} = g(\mu_{jo}, \sigma_{jo})$.
- Transformation of the random fields of the optimal realization to a distribution with a prescribed mean and standard deviation through the transformation

$$p_{i,k} = \mu_k + \sigma_k * p_{i,jo}$$

where

$p_{i,k}$ = The distributed land surface parameter of the transformed or prescribed distribution for the i-th subgrid.

$p_{i,j}$ = The *i*-th random field of the standard normal distribution of the *j*-th realization (for the *i*-th subgrid).

$p_{i,jo}$ = The *i*-th random field of the standard normal distribution of the optimal realization.

μ_k = The mean of the prescribed distribution.

σ_k = The standard deviation of the prescribed distribution.

μ_j = The mean of the *j-th* realization.

σ_j = The standard distribution of the *j*-th realization.

k = The index of the prescribed distribution.

n = The number of parameters or subgrids.

j = The index for the number of a given realization.

μ_{jo} = The mean of the optimal realization.

σ_{jo} = The standard distribution of the optimal realization.

For the implementation of the above procedure, the standard normal distribution scheme (Box-Muller transformation method) in Numerical Recipes (Press et al., 1992) was adopted, as it is easy to implement in the parameter estimation process (i.e. easily incorporated into the MM5, NOAH LSM and initial parameter estimation codes). Also, the random number used in this implementation is robust and does not suffer from known limitations of other random number generators (Press et al., 1992).

6.2.2 Initialization of the experimental domains

The 1D SVAT experiment (OSU LSM)

Model setup

In this experiment, the current version of the OSU LSM (Ek & Mahrt, 1991,Mitchell, 2000) was applied with 1998 observation forcing data (4 days subset, Jan. 1^{st}- 4^{th}) from the Meyers/NOAA measurement site in Champaign, Illinois. The measurement site is located at longitude 88.37^{o} W and latitude 40.01^{o} N (Meyers & Ek, 1999). The site is characterized by vegetation type "groundcover only" (for the period of this exercise) and soil type "silty loam". A detail description of the measurement site can be found in Mitchell (2000).

A model description for the OSU LSM can be found in appendix A.1. The model was initialized with an albedo of 0.15 and green vegetation fraction of 0.01. The maximum albedo was set to 0.75 (snow albedo) and the annual constant bottom boundary soil temperature set to 285 K. The initial skin temperature and canopy moisture content are given as 263.95 K and 0.47mm respectively. The soil consists of four layers. The initial actual snow depth and water equivalent snow depth are respectively set to zero. Additional initial soil state variables are given in table 6.1 below.

Table 6.1: The soil initial state variables for the 1D SVAT experiment.

Soil thickness (cm)	***Temperature (K)***	***Liquid Total moist (m^3/m^3)***	***Liquid moist (m^3/m^3)***
10.00	266.0	0.325	0.166
30.00	273.9	0.319	0.282
60.00	276.6	0.317	0.317
100.00	280.1	0.307	0.307

The time step for the model simulations was 30 minutes. The forcing data was available at 30 minutes interval (or interpolated to 30-minute time interval from about 1- 6 hour interval observations). For observation intervals longer than 1-hour, the incoming surface solar insolation was interpolated with a solar zenith angle weighting, in order to capture the full amplitude of the diurnal solar insolation. The required forcing data are: 1) air temperature at 3m above ground, 2) air humidity at 3m above ground, 3) surface pressure 4) wind speed at 10m above ground, 5) surface downward longwave radiation, 6) surface downward solar radiation and 7) precipitation. The OSU LSM computes surface energy fluxes based on the input data and model configuration. A review of the model physics of the OSU LSM was presented in chapter 3.

Generation of observation data

The procedure for generating area-weighted fluxes from a distributed heterogeneous land surface (at the subgrid scale) was discussed in section 5.2.2 of chapter 5. Fig 5.2 shows the flux aggregation over a heterogeneous land surface with distributed (subgrid) parameters.

The current OSU LSM version used in this study has a Fortran namelist construct that allows for the external supply of land surface parameters to the physics routine without recompilation of the whole code. This is a significant improvement because it provides enough flexibility for automating the numerical experimentation. Fig. 6.2 shows the configuration for this experiment. The Monte Carlo random number generator was used to supply nine synthetic land surface parameters of specified mean (μ_k) and standard deviation (σ_k) to the relevant physics routine. Each synthetic parameter represents the land surface parameter of a homogeneous subgrid.

For each mean, four simulations were carried out, each with a specified standard deviation (i.e.10%, 25%, 37.5% and 50% of the mean). Each synthetic land surface parameter was used by the model to compute surface fluxes and the area-weighted average of the subgrid fluxes computed as the observation data set for the parameter estimation process. The observation data set is computed as

$$G(\mu_k, \sigma_k) = \frac{1}{n}\sum_{i=1}^{n} G_i(p_i) \qquad 6.1$$

where n is the number of subgrids. The observation data set is used by PEST in the parameter estimation process. The specific surface energy fluxes used as observation depend on the type of parameter to be estimated. The model output that is chosen as observation is the one that succinctly expresses its relationship with the parameter of interest (Chehbouni et al., 1995). Additionally, a number of model outputs that meet the above condition can be combined into a well-behaved function that satisfies the well-posedness condition (see section 3.3 of Chapter 3).

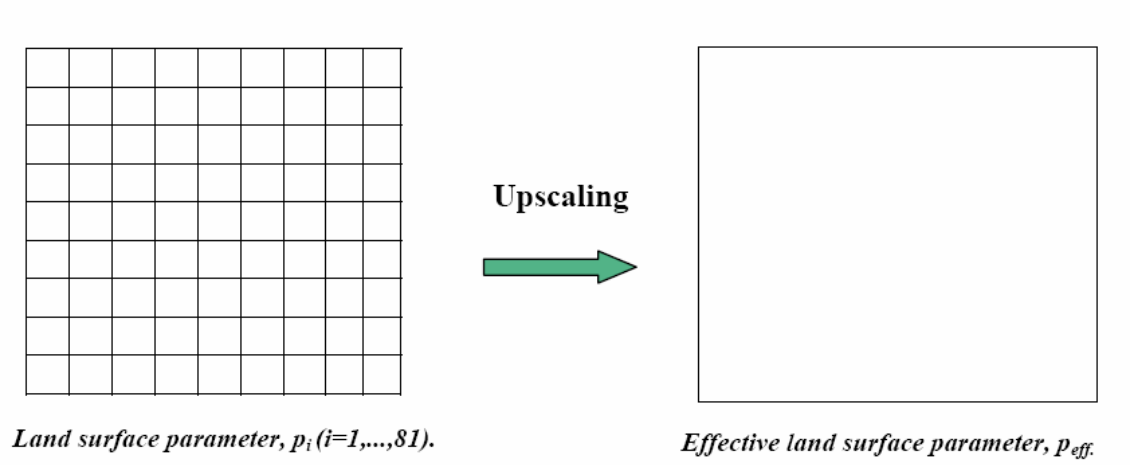

Figure 6.2: Schematic diagram of the upscaling of land surface parameters for 1D SVAT model.

The 3D SVAT experiment (MM5)

Model setup

In this study, MM5 was applied coupled to the OSU LSM in the one-way nesting mode to account for interaction between the soil, vegetation and the atmosphere. The one-way nesting approach was chosen because of the advantage of producing a higher resolution domain from a coarse grid domain. This ensures that: 1) the lateral boundary conditions of the fine grid use consistent physics to those of the coarse grid model, 2) the lateral boundary conditions are available at a relatively high temporal frequency, and 3) the vertical structure of the atmosphere is not significantly modified through vertical interpolation (Dudhia et al., 2000).

An area in the Volta Basin (West Africa) was chosen for the investigations (4 days subset 2 - 5 December, 1998). The one-way nesting model configuration consists

(121x67), 3x3 km^2 (55x49) and 3x3 km^2 (10x10 grid points), and 26 vertical layers extending up to 30mbar at the model top. The nested domains have central latitude at 7.5^o N and central longitude at 0.0^o. The Mercator map projection was used considering the region of interest. Each larger domain provides the lateral and initial boundary conditions for the next smaller domain. The domain resolutions are chosen as powers of three to be consistent with the GLOWA-Volta project specifications for climate modeling. An experimental domain (domain 5) with 9x9 grid cells, each with a resolution of 3x3 km^2 was chosen within domain 4. The experimental domain is chosen to be homogeneous as possible with respect to land surface characteristics. The resolution of the experimental domain was chosen to be the same as domain 4 so that the boundary and initial conditions are consistent. Additionally, this ensures that the same subgrid scale processes are captured in both domains and parameterized with equal precision. Fig. 6.3 shows the domains of interest.

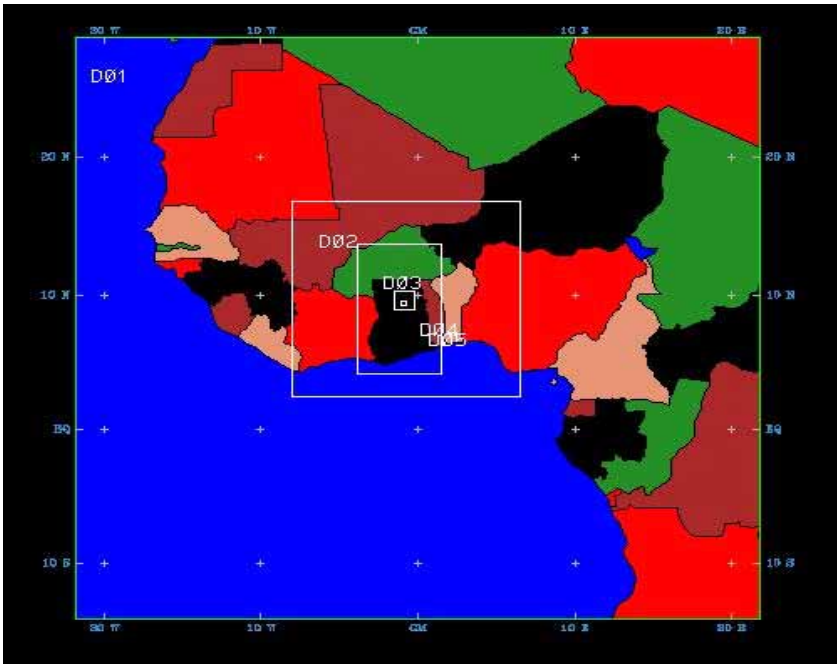

Figure 6.3: Schematic of the five domains for the one-way nesting approach in West Africa. Domain 3 is the Volta Basin and Domain 5 is the experimental domain.

The terrain information was horizontally interpolated from the regular latitude-longitude terrain elevation and vegetation data onto the specified coarse and fine domains. Additional interpolation of soil and vegetation data was incorporated using data from NCAR and other data compilation developed by the land use group of the

GLOWA-Volta project. The terrain and land surface information were produced for each domain. First guess surface and pressure information from a global analysis (e.g. NCAR archived reanalysis data) was used to produce model initial and boundary conditions for the coarsest domain. The MM5 climate model numerically solves the prognostic equations of the atmospheric motions using the OSU LSM output as lower surface boundary condition. The output of the MM5 run for the coarsest domain is used as initial and boundary conditions to drive the next coarsest domain. The process is repeated till the finest (experimental) domain is fully initialized. A detailed description of the one-way nesting approach can be found in appendix A.2.

Generation of the observation data

The procedure for this study is similar to that used for the 1D SVAT case discussed in section 6.2.3. Fig 6.4 shows the configuration for the study. Here, there are 81 subgrids. To generate observation data, the MM5 routine that supplies land surface parameters to the MM5 physics routines was modified to incorporate the Monte Carlo random number routine described in section 6.2.1. The purpose of the Monte Carlo routine is to generate random fields of a specified mean and standard deviation to replace the original land surface parameters in the physics routine. Each field represents a unique land surface parameter of a subgrid within the experimental domain, and has the same physical characteristics as the real-life land surface parameters. The model is run with the modified land surface parameter routines using the physics configuration of the initialized experimental domain to generate surface heat fluxes. Each grid cell generates surface heat fluxes based on the assigned synthetic parameter. The output is then aggregated as an area-weighted average of the surface fluxes. These aggregated fluxes are obtained as synthetic observations for the parameter estimation process.

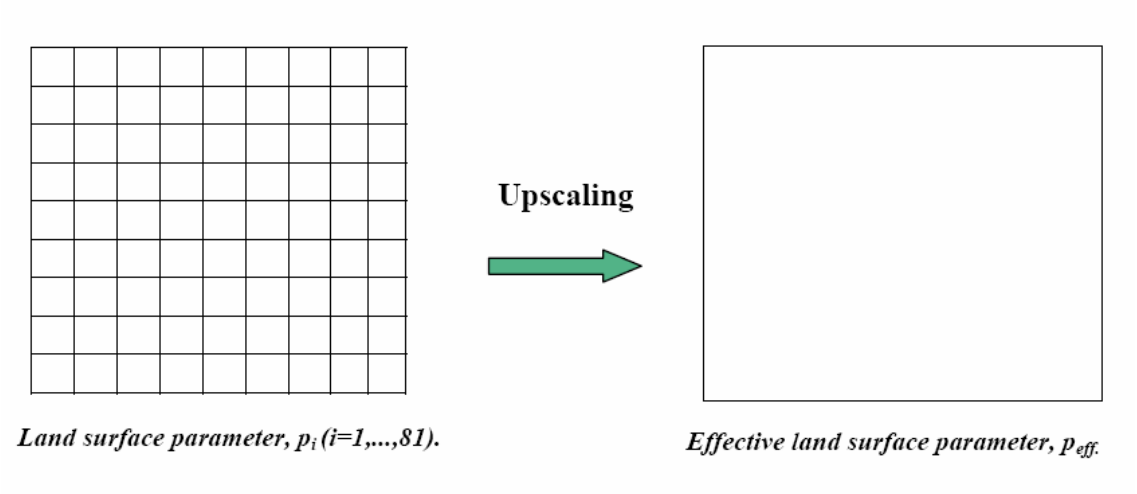

Figure 6.4: Upscaling of land surface parameters for the 3D SVAT Model.

Initial parameter estimation

The approximate method applied in solving the inverse problem is an iterative method that requires an initial parameter set. Several studies have shown that the initial parameter sets are very crucial for a successful parameter estimation process, in particular when the problem is highly nonlinear or ill-posed. To drive the parameter estimation process, PEST must be supplied with good initial parameter estimates. The Gauss-Marquardt-Levenberg algorithm has been shown to converge to the optimal parameter set provided an initial parameter set can be found within a close neighborhood of the optimal parameter set (Cooley and Naffi, 1990). Based on this assertion, approximate methods derived from physics consistent with those of the OSU LSM and MM5 are used as initial parameter estimates. Chapter 2 gave a survey of existing parameter aggregation methods that are appropriate for initial parameter estimation. These parameter estimates can be considered as suboptimal parameters from which the optimal parameters can be estimated using the nonlinear parameter estimation tool PEST. A summary of the methods for deriving the initial parameter estimates used in this study is given in Table 2.2 (Chapter 2).

Additional PEST preprocessing routines

PEST requires some special routines to facilitate its communication with the component models coupled to it. Because high precision derivatives of the model output with respect to the parameter set of interest is required by the PEST algorithm for the estimation of the optimal parameter set, PEST has a routine for formatting model output for its internal use. Additionally, PEST communicates with the coupled models through special interfaces that facilitate its operation. These preprocessor routines must be created prior to PEST runs. A detailed description of these preprocessor routines for the 1D SVAT and 3D SVAT experiments can be found in Appendix B. For a detailed general description of the PEST preprocessor routines, see Doherty (2002).

6.2.3 Coupling of models to PEST

The previous sections discussed the preprocessing of the relevant model components of the inverse-SVAT modeling. This section constitutes the second part of the numerical experimentation and focuses on the coupling of the component models discussed in the previous sections, to PEST. Because the exact algebraic solution does not exist, a great deal of innovation is required in providing optimal settings for the parameter estimation process. More importantly, since the estimation of the effective parameters constitutes an enormous computational effort, care must be taken in meeting the necessary conditions of well-posedness (see section 3.3 of chapter 3) so as to facilitate solution convergence and optimization run time.

To couple PEST to the climate models, the interfaces through which PEST communicates with the models must be well designed. Data must be provided with a precision that permits accurate computation of derivatives to aid in the search for the optimal parameter set. Procedures for generating the relevant PEST preprocessor files are described in detail in appendix B. Fig. 6.5 gives a sketch of the coupled PEST-OSU LSM and PEST-MM5.

The handshaking between PEST, OSU LSM, MM5 and the Monte Carlo random number generator is summarized below as follows:

- Random fields are generated using the Monte Carlo random number generator to represent the land surface parameters of interest.
- The synthetic land surface parameters are passed to the SVAT model and observations generate based on the area-weighted average of surface energy fluxes generated by the subgrid cells.
- The same synthetic land surface parameters from the Monte Carlo simulation are used to compute initial parameter estimates based on the existing methods outlined in table 2.2.
- PEST uses the output of the simulation obtained in step 2 and the initial parameter estimates obtained from step 3 to initialize the parameter estimation process.
- PEST uses the initial parameter estimates to run the SVAT model and then compare the output to the observation based on the objective function (e.g. the sum of the mean square error).
- If the difference is within some preset tolerance limit, the effective parameter has been found and the search process is terminated, else PEST updates the parameter based on the search information of the previous iteration (see chapter 3) and then repeats the whole process again until a preset termination criteria is reached.

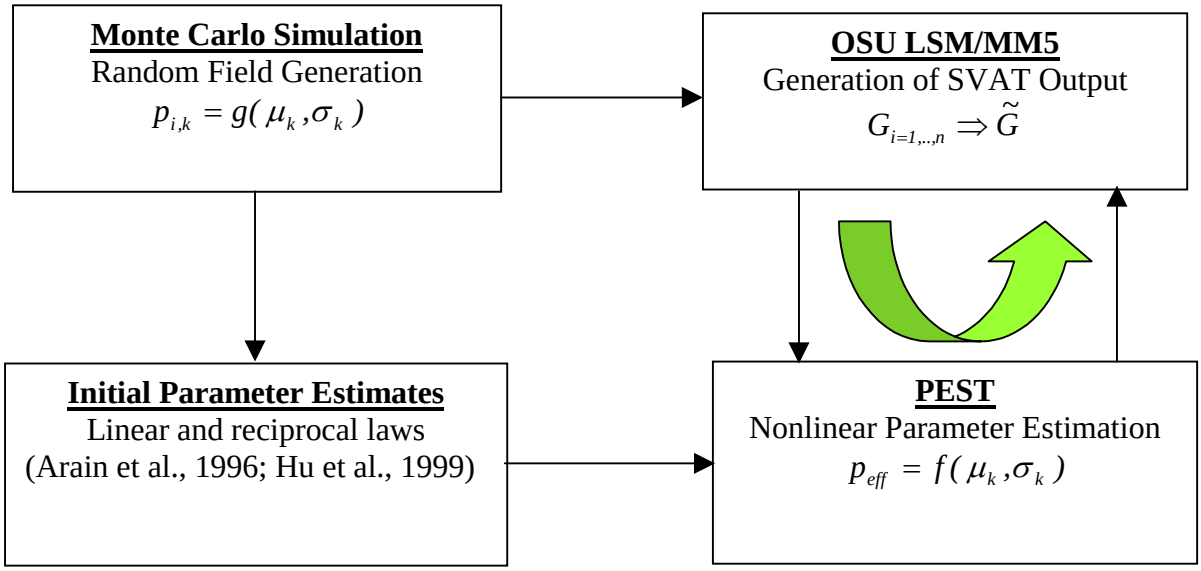

Figure 6.5: Schematic of the numerical experimentation the with Inverse-SVAT Model

A detail description of the internal PEST processes based on the Gauss-Levenberg-Marquardt algorithm (see chapter 3) is summarized in the following steps below:

- The input/output files and system variables are initialized. Additionally, all initial input data are read via the PEST preprocessor files
- The initial parameter estimates are passed to the model input files via the template files and PEST uses these initial parameters to run the SVAT model.
- The instruction files are used to read the output of the SVAT model runs and the initial objective function is computed.
- PEST then starts the parameter estimation process with the optimization iteration.
- After computing the Jacobian matrix, PEST attempts objective function improvement using one or two Marquardt parameters (Lamda).

- If the second Marquardt parameter falls by a factor of 0.03 relative to the first or the factor change in parameter between the previous and current optimization iterations is more than 3, PEST does not test any further lamdas and progresses to the next optimization.
- The optimization process stops after the 3 lowest objective function values are within a relative distance of 0.01.

PEST produces a run record which gives parameter statistics, observation, model output calculated with optimized parameter set, residuals (difference between observation and optimized model output) and other optimization information. A detailed description of the above internal PEST routine can be found in Doherty (2002).

6.3 Concluding remarks

The implementation of the proposed method for upscaling land surface parameters has been presented through numerical experimentation in a coupled SVAT-Parameter estimation environment. The coupling of a nonlinear parameter estimation tool to a 1D SVAT model and its complex 3D extension is a formidable task. Because the inverse problem is ill-posed and has no true solution, the approximate solution demands innovative strategies to constrain the solution to converge to the optimal parameter set. The estimation of each effective parameter constitutes an enormous computational effort, especially, for the 3D SVAT case. The discussion included:

- A description and implementation of the Monte Carlo random number generator.
- A description of the 1D SVAT model setup (OSU LSM) and 3D SVAT model setup (MM5). The one-way nesting approach used to produce initial and boundary conditions for the experimental domain in MM5 was also discussed.
- The preprocessing of the relevant PEST input files with respect to the OSU LSM, MM5, initial parameter estimates and initialization of PEST
- The experimental setup and coupling of PEST to: 1) 1D SVAT and 2) 3D SVAT.

The major challenges to the success of the parameter estimation include:

- **Poor choice of initial parameter estimates**. In general, the closer the initial parameters are to the optimal parameter set, the faster the convergence to the global minimum. Beyond reducing the run time, a good choice of initial parameters make optimization possible, especially for highly nonlinear models or models with local objective function minima in the parameter space at places removed from the global objective minimum.
- **Non-differentiable fitting functions**. If the problem is not continuously differentiable or at least differentiable at points where derivatives are computed, the estimation process would have extreme difficulties in estimating parameters of the model.

The next chapter gives a presentation of the detailed analysis of the results obtained from the numerical experimentation undertaken in this chapter. It also gives a comparison of the results of the proposed method to that of existing methods.

7 ANALYSIS OF RESULTS

7.1 Introduction

In chapters 5 and 6, the conceptual design of the proposed upscaling method and its application in a numerical experiment with 1D SVAT and 3D SVAT models were presented. Several aggregation rules for land surface parameters of varying complexity were surveyed in Chapter 2. The comparison of the results from these studies suggests that simple aggregation rules may have the same order of performance as computationally-intensive schemes (Arain et al., 1996; Hu et al., 1999; Blyth et al., 1993). The proposed methodology is also computationally intensive to the extent that, for the domain setup used in this exercise for the 3D SVAT case, the estimation of an effective land surface parameter requires about 2 days of CPU time. For an upscaling law derived from 100 effective parameter data points, this would be a very expensive venture. Therefore, a prime focus of the analyses in this chapter is to formulate simple aggregation schemes from the trends exhibited by the results obtained from the CPU-intensive experiment applied in this thesis. Procedures required to achieve this objective are presented together with other relevant strategies.

In this chapter, upscaling laws for 1D and 3D SVAT parameters are analyzed to obtain information about subgrid scale processes. Several approaches for comparing the performance of the proposed method and that of existing methods are also presented. The methods that are compared to the proposed method are those of Arain et al. (1996), Blyth (1993) and Hu et al. (1999). In particular, the method of Hu et al. (1999) was chosen for detailed comparison of surface energy fluxes and moisture indicators, because it is a well established theory-based method (i.e. Hu et al. (1999) is derived from relevant planetary boundary layer physics as compared to simple averaging methods that are based on purely statistical arguments). Procedures for enhancing the performance of the parameter estimation process are also discussed. Finally, the uniqueness of the effective roughness length with respect to duration of episodes is analyzed.

7.2 Results for coupled stand-alone SVAT and PEST

7.2.1 Upscaling laws

To account for subgrid scale effects, upscaling laws are derived that map the mean and standard deviation of the distributed land surface parameters at the subgrid scale to their corresponding effective parameter at the grid scale. The potential upscaling laws investigated are: linear, parabolic, polynomial, exponential, logarithmic, Lorentz, logistic and a mixture of different functions. The criteria for selecting the best fitting (regression) models are based on the correlation co-efficient and model complexity (nonlinearity and number of parameters). Generally, the linear and parabolic laws gave the best fits. Upscaling laws were developed for the roughness length, surface albedo, surface emissivity, Clapp-Hornberger soil parameter ***b***, minimal stomatal resistance, vapour pressure deficit factor, leaf area index and plant insolation factor. Details of the best upscaling laws are given in Table 7.1 and discussed below.

Roughness length

Plots for upscaling roughness length using evaporative fraction, sensible and latent heat fluxes as fitting functions are presented in figures 7.1 to 7.3, respectively.

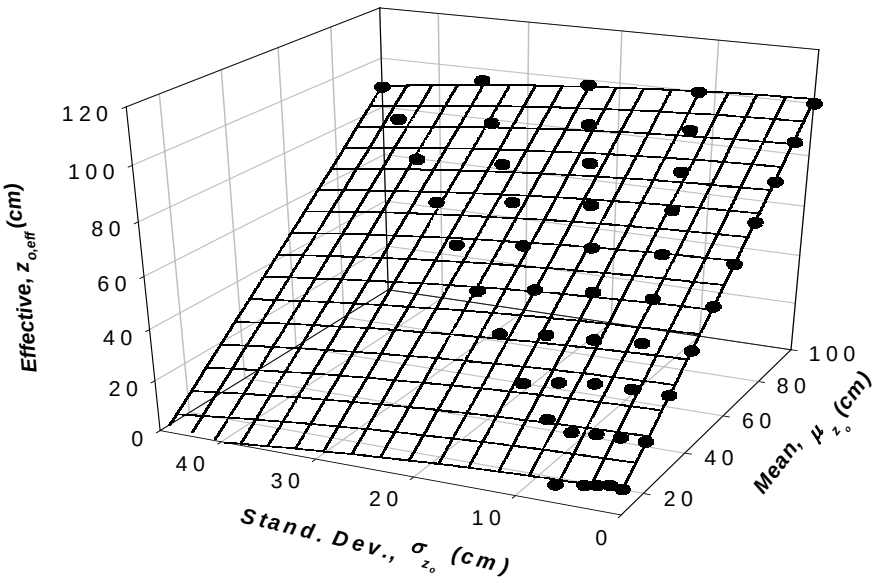

Figure 7.1: Parabolic upscaling plot for roughness length, z_o , R =0.9985. The objective function used in the estimation of z_o is based on the evaporative fraction.

The evaporative fraction and sensible and latent heat fluxes were used in formulating objective functions for the determination of the roughness length because of their dependence on the roughness length. The Bowen ratio was not used, because it is not well-behaved close to zero latent heat fluxes and has been reported to be complicated to analyze (Bastiaanssen, 1995). For the evaporative fraction and latent heat fluxes, the parabolic upscaling law was the best fitting model. For the sensible heat fluxes, the linear law was the best upscaling model. Based on the correlation co-efficients of the various fitting functions, the parabolic upscaling law obtained with the evaporative fraction is the best fitting model for determining the roughness length. The linear upscaling law obtained from the sensible heat fluxes was the second best, while the parabolic plot obtained from the latent heat fluxes was the third.

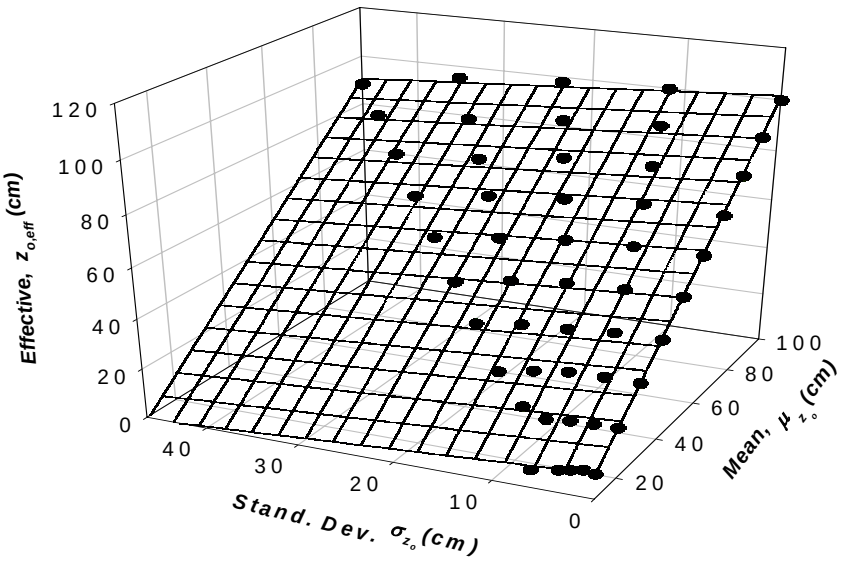

Figure 7.2: Planar upscaling plot for the roughness length, z_o, R =0.9982. The objective function used in the estimation of z_o is based on the sensible heat fluxes.

The evaporative fraction is the most appropriate fitting function for the roughness length because its formulation is based on the sensible and latent heat fluxes (see equation 4.1 in Chapter 4) and hence it properly captures the error associated with estimating roughness length. More importantly, the evaporative fraction is continuous, analytic and bounded between 0 and 1 (an important condition for a successful parameter estimation simulation).

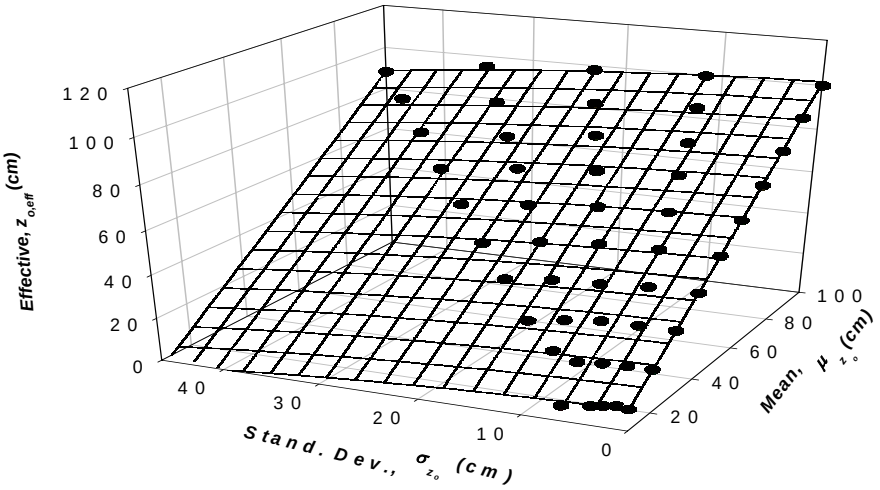

Figure 7.3: Parabolic upscaling plot for roughness length, z_o , R =0.9864. The objective function used in the estimation of z_o is based on the latent heat fluxes.

Surface parameters: Surface albedo and emissivity

Figures 7.4 and 7.5 show the respective upscaling relationships for surface albedo and emissivity. Upscaling laws for these surface parameters are well established (Hu et al., 1999 and 1997). The linear upscaling law was found to best fit the surface parameters, surface albedo and emissivity. The correlation co-efficients were the highest (almost 1). This is because they have linear dependence on the surface radiation functions from which they are computed.

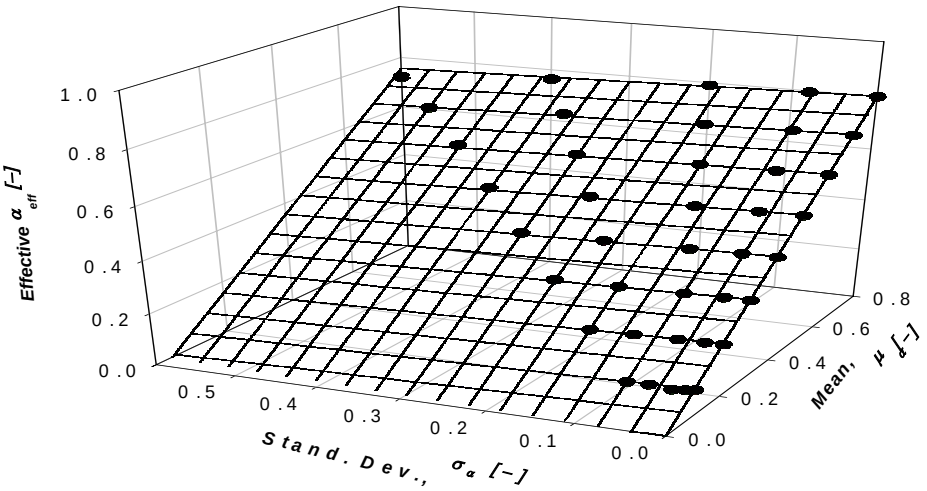

Figure 7.4: Planar upscaling plot for surface albedo, α, R =0.9998. The objective function used in the estimation of α is based on the net shortwave radiation.

The same linear upscaling laws derived for the 1D SVAT case applies in the case of the 3D SVAT case. This is mainly due to the fact that the effective parameter is independent of meteorological forcing. A summary of the upscaling laws and their corresponding measures of fit for the land surface parameters investigated are given in Table 7.1.

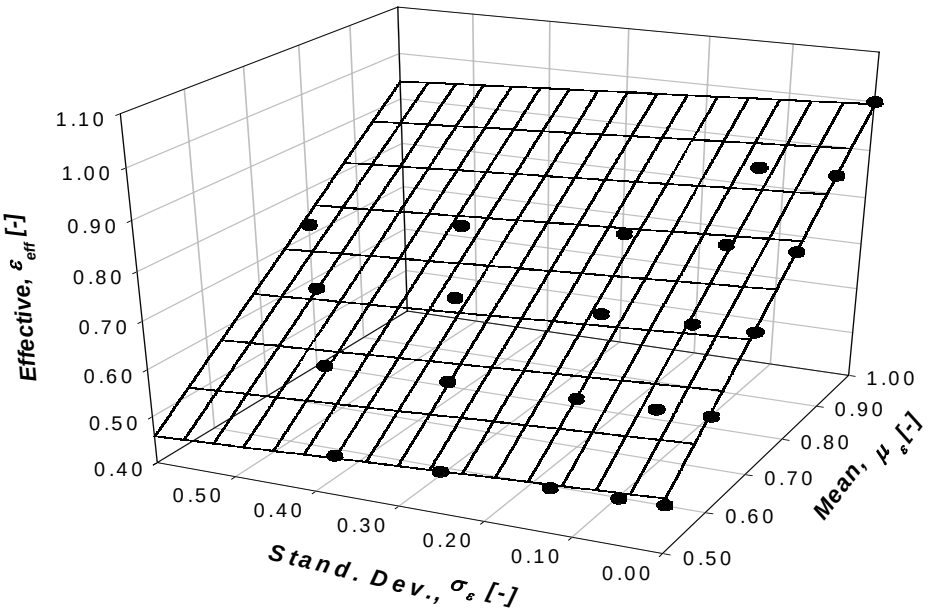

Figure 7.5: Planar upscaling plot for the surface emissivity, ε, R =0.9999. The objective function used in the estimation of ε is based on the outgoing longwave radiation.

The vegetation parameters

Figures 7.6 to 7.9 show the respective upscaling plots for the vegetation parameters: minimal stomatal resistance, vapour pressure deficit factor, leaf area index and plant insolation factor. They depend highly nonlinearly on canopy resistance and hence are difficult to aggregate. The plant insolation factor, solar insolation factor and leaf area index show the highest nonlinearities (Kim and Ek, 1995). Because of their highly nonlinear nature, a good initial parameter set is crucial for their successful estimation. The parabolic upscaling law (with mixed nonlinear terms) was found appropriate for all the vegetation parameters investigated.

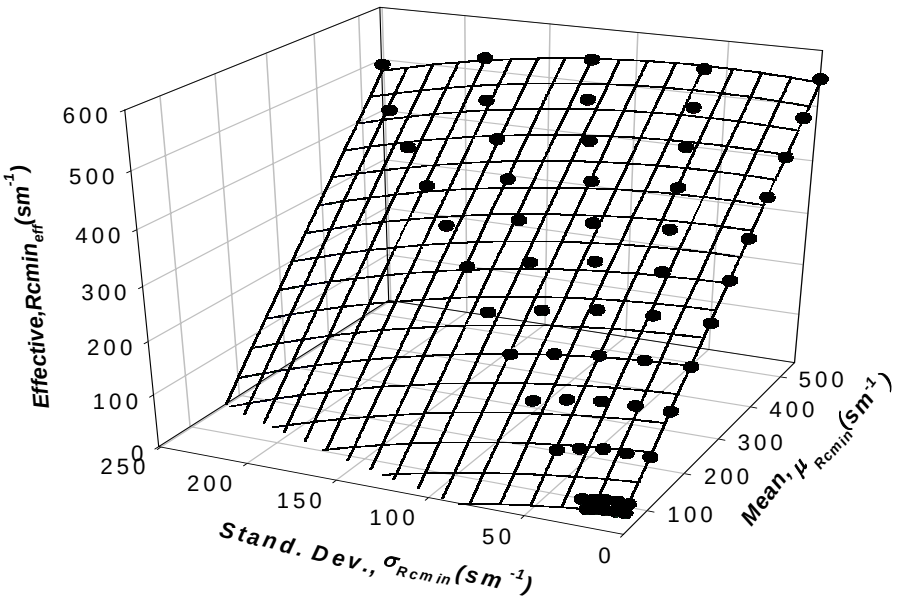

Figure 7.6: Parabolic upscaling plot for the minimum stomatal resistance, ***Rcmin***, R =0.9997. The objective function used in the estimation of ***Rcmin*** is based on transpiration**.**

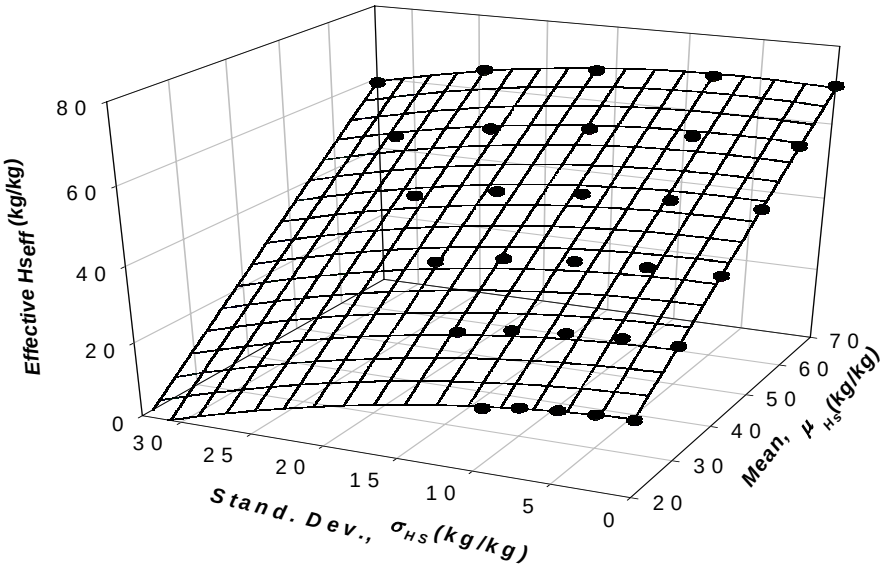

Figure 7.7: Parabolic upscaling plot for the vapour pressure deficit factor, ***Hs,*** R =0.9996. The objective function used in the estimation of ***Hs*** is based on transpiration**.**

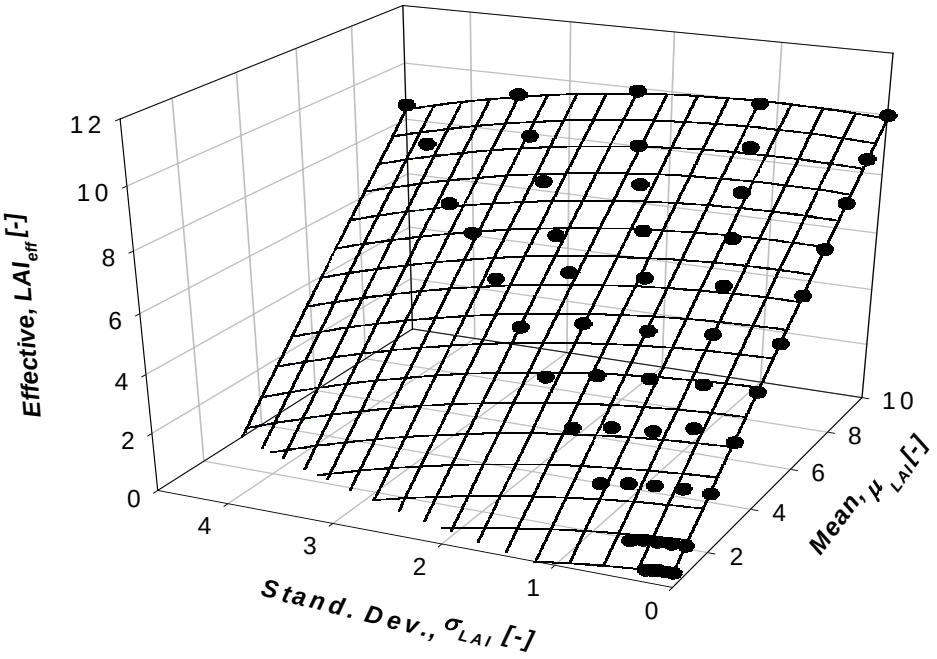

Figure 7.8: Parabolic upscaling plot for the leaf area index, ***LAI,*** *R* =0.9993. The objective function used in the estimation of ***LAI*** is based on transpiration**.**

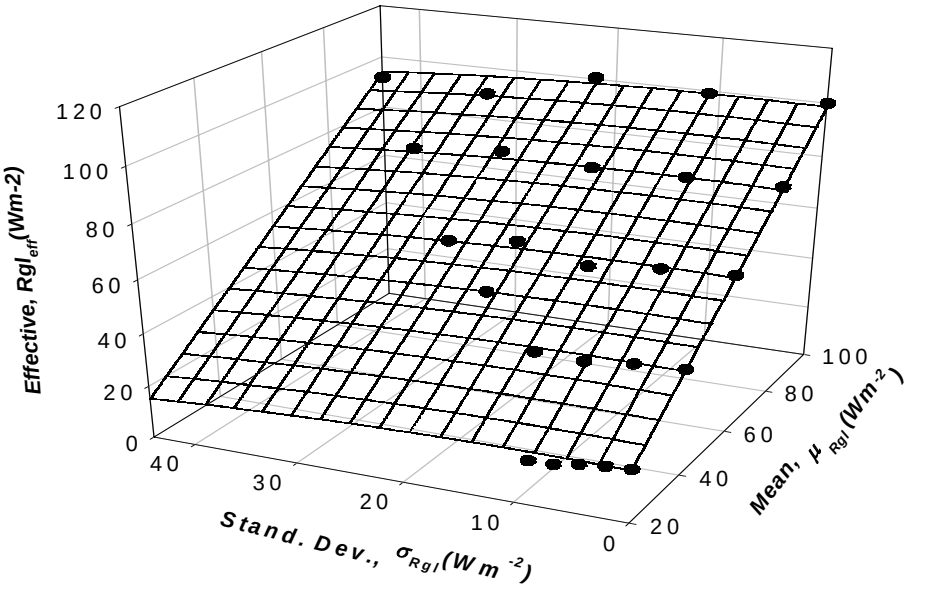

Figure 7.9: Parabolic upscaling plot for the plant insolation factor, ***Rgl,*** *R* =0.9995. The objective function used in the estimation of ***Rgl*** is based on transpiration**.**

The Clapp-Hornberger constant

For the Clapp-Hornberger soil parameter ***b***, the parabolic upscaling law (with no nonlinear mixed terms) was best fitting model. Although the correlation co-efficient was good, it is lesser than those obtained for the vegetation and surface parameters (see Table 7.1). This is due to the highly nonlinear nature of the dependence of the soil hydraulic and thermodynamic properties on ***b*** (see section 3.2.2 of Chapter 3). The upscaling law for ***b*** is shown in figure 7.10.

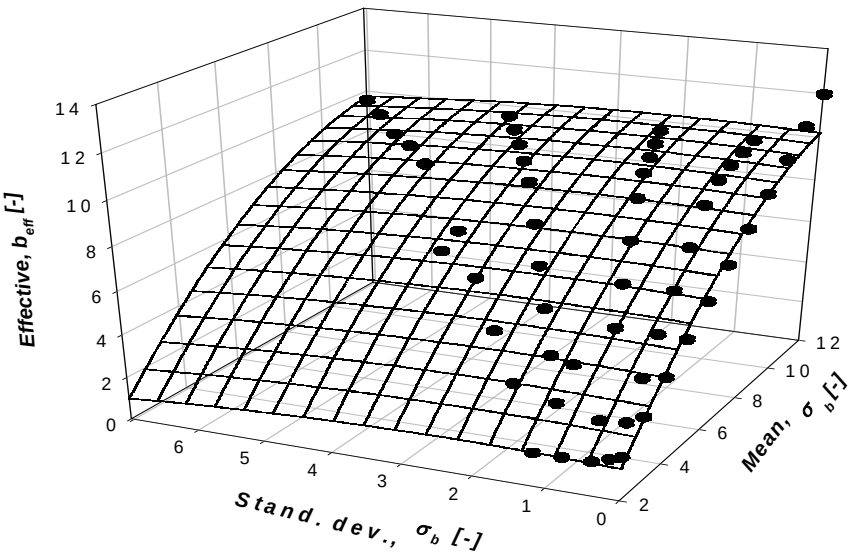

Figure 7.10: Parabolic upscaling law for Clapp-Hornberger parameter, ***b,*** R =0.9583. The objective function used in the estimation of ***b*** is based on soil evaporation.

General observations from the analysis of the upscaling relationships

The general observation from the above upscaling analysis is that when the heterogeneity becomes large, the effective parameter becomes smaller than the mean parameter. However, when the heterogeneity becomes small, the effective parameter approaches the mean parameter (arithmetic mean of the subgrid scale parameters). This is consistent with other related studies (Hu et al., 1997 and 1999). A similar trend was observed with a Monte Carlo simulation of the normally distributed fields. When the standard deviation, which is a measure of heterogeneity becomes large, the sample mean becomes smaller than the population mean. However, when the standard deviation approaches zero, the sample mean approaches the population mean.

Table 7.1: Upscaling laws, objective functions and Goodness-of-Fit for the 1D SVAT parameters. The effective parameters are independent of boundary and meteorological conditions.

Parameter	***Upscaling law***	***Correlation Co-efficient R***
z_o(cm): Λ	$z_{o,eff} = 1.019\mu_{zo} - 0.193\sigma_{zo} - 2.000*10^{-4}\sigma_{zo}^2 + 3.100*10^{-3}\mu_{zo}\sigma_{zo} - 7.700*10^{-3}\sigma_{zo}^2$	*0.9985*
z_o(cm) :H	$z_{oeff} = 1.018\mu_{zo} - 0.2372\sigma_{zo}$	*0.9982*
z_o(cm) :λE	$z_{o,eff} = 1.093\mu_{zo} - 0.232\sigma_{zo} - 1.100*10^{-3}\mu_{zo}^2 + 7.200*10^{-3}\mu_{zo}\sigma_{zo} - 1.360*10^{-2}\sigma_{zo}^2$	*0.9864*
α [-]	$\alpha_{eff} = 0.999\mu_{\alpha} - 4.150*10^{-2}\sigma_{\alpha}$	*0.9998*
ε [-]	$\varepsilon_{eff} = 1.001\mu_{\varepsilon} - 4.410*10^{-2}\sigma_{\varepsilon}$	*0.9999*
Rcmin (sm^{-1})	$Rcmin_{eff} = 1.029\mu_{Rcmin} - 0.333\sigma_{Rcmin} - 1.000*10^{-4}\mu_{Rcmin}^2 + 1.200*10^{-3}\mu_{Rcmin}\sigma_{Rcmin} - 2.400*10^{-3}\sigma_{Rcmin}^2$	*0.9997*
Hs (kg/kg)	$Hs_{eff} = 1.022\mu_{Hs} - 0.293\sigma_{Hs} - 4.000*10^{-4}\mu_{Hs}^2 + 7.500*10^{-3}\mu_{Hs}\sigma_{Hs} - 1.660*10^{-2}\sigma_{Hs}^2$	*0.9996*
LAI [-]	$LAI_{eff} = 1.029\mu_{LAI} - 0.315\sigma_{LAI} - 4.100*10^{-3}\mu_{LAI}^2 + 5.790*10^{-2}\mu_{LAI}\sigma_{LAI} - 0.125\sigma_{LAI}^2$	*0.9993*
Rgl (Wm^{-2})	$Rgl_{eff} = 1.021\mu_{Rgl} - 0.206\sigma_{Rgl} - 3.00*10^{-4}\mu_{Rgl}^2 + 5.3*10^{-2}\mu_{Rgl}\sigma_{Rgl} - 1.180*10^{-2}\sigma_{Rgl}^2$	*0.9995*
Clapp-Hornberger b [-]	$b_{eff} = 1.100\mu_b + 0.1462\sigma_b - 1.680*10^{-2}\mu_b^2 - 2.880*10^{-2}\sigma_b^2$	*0.9583*

More importantly, the upscaling laws summarized in Table 7.1 show that when the standard deviation is zero, the effective parameter is equal to the mean parameter, which is the homogeneous land surface parameter. Hence, the upscaling laws derived from the

experiment give a measure of subgrid scale heterogeneity and are consistent with (both theoretical and experimental) results.

7.2.2 Comparison of proposed method with method of Hu et al. (1999)

To assess the performance of the proposed model, the scale invariance criteria of Hu et al. (1997) was applied. It requires that the percentage change of a grid model output with respect to aggregated output be less than 10% for the change to be negligible. Figures 7.11 to 7.22 show the time series plots for the surface energy fluxes (sensible heat and latent heat fluxes) and the moisture indicators (evaporative fraction and Bowen ratio), respectively for the 1D SVAT investigations. The detailed analysis of model output for the surface energy fluxes and moisture indicators are discussed below. The distribution of the subgrid scale land surface parameters used in this investigations have a sample mean of 100 and sample standard deviation of 46.69.

Sensible heat fluxes

The time evolution of the sensible heat fluxes is given in figure 7.11 for the observed, proposed method and that of Hu et al. (1999). Figures 7.12 and 7.13 give the corresponding percentage difference and residual sensible heat fluxes. The maximum residual sensible heat flux as can be seen from figure 7.13 is 1.48 Wm^{-2}, which is small (< 5 Wm^{-2}) compared to that obtained from the method of Hu et al. (1999), which is 6.97 Wm^{-2}.

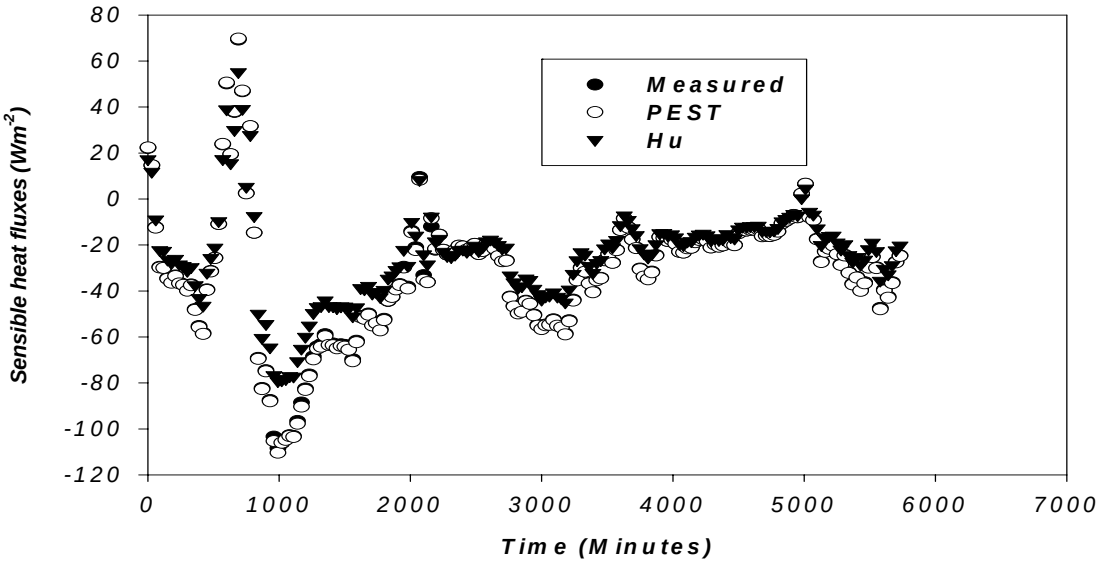

Figure 7.11: Time evolution of the sensible heat fluxes for the measured and methods based on the proposed and Hu et al. (1999).

The time evolution of the residual sensible heat fluxes tends to increase with increasing sensible heat fluxes. Similar results have been reported in related literature (Moran et al., 1997). However, percentage differences are high at night time, where the residual sensible heat fluxes are far below 5 Wm^{-2} as compared to the low percentage differences observed during the day where the residual sensible heat fluxes are sometimes greater than 5 Wm^{-2}.

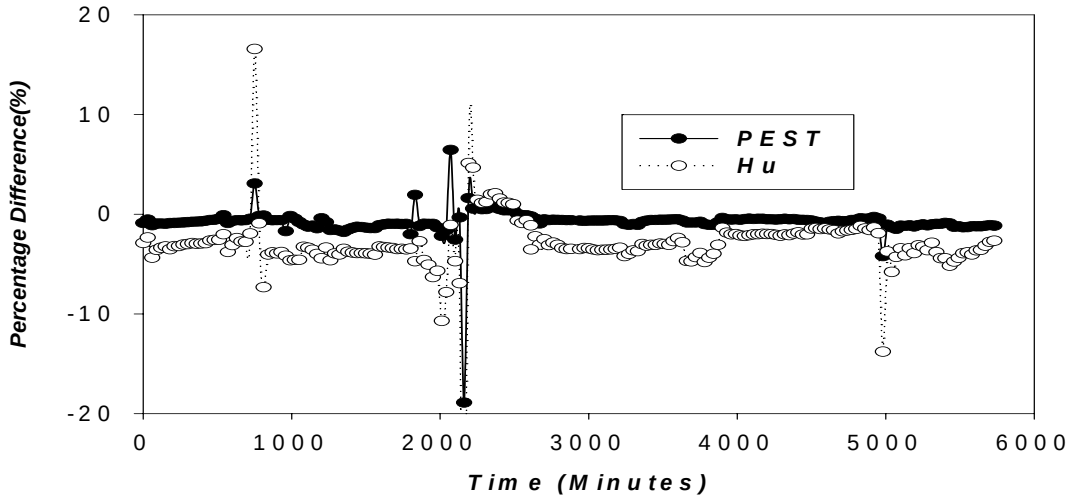

Figure 7.12: Percentage difference in sensible heat fluxes.

Although appreciable differences exist between values of effective roughness lengths for both methods at higher degrees of heterogeneity, the observed sensible heat fluxes were quite close. The method of Hu et al. (1999) overestimates the sensible heat flux, whereas the proposed method consistently reduces the error to zero.

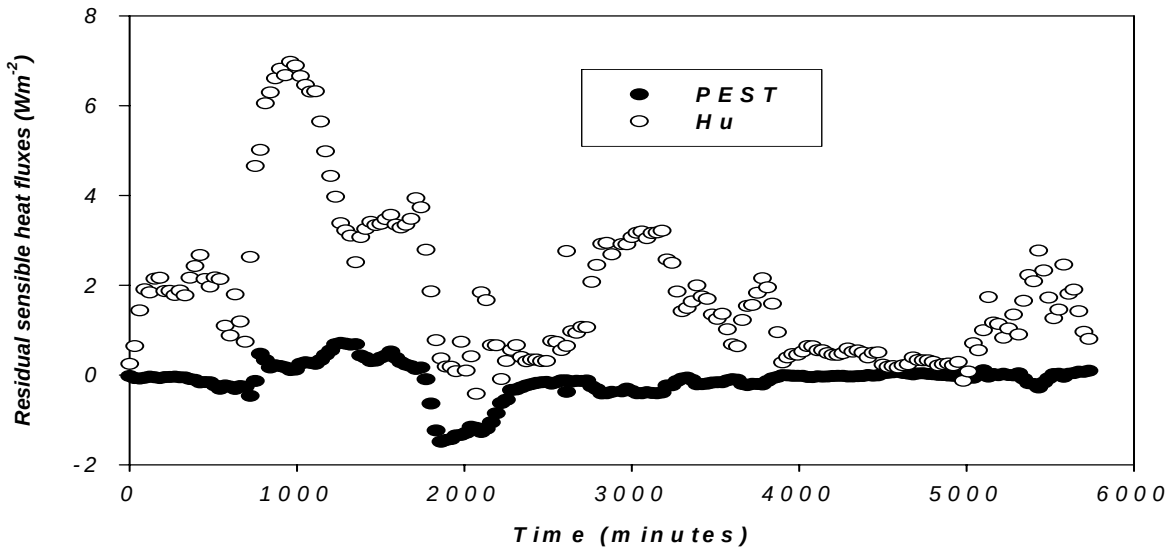

Figure 7.13: Time evolution of the residual sensible heat fluxes for the proposed method and Hu et al. (1999).

Latent heat fluxes

The time evolution of the latent heat fluxes and the corresponding percentage difference and residual latent heat fluxes are respectively given in figures 7.14 to 7.16. A similar trend to that of the sensible heat fluxes was also observed in the case of the latent heat fluxes in that residual fluxes increase for daytime fluxes and decreases for nighttime fluxes. More importantly, maximum residual latent heat fluxes are much larger than that of the residual sensible heat fluxes.

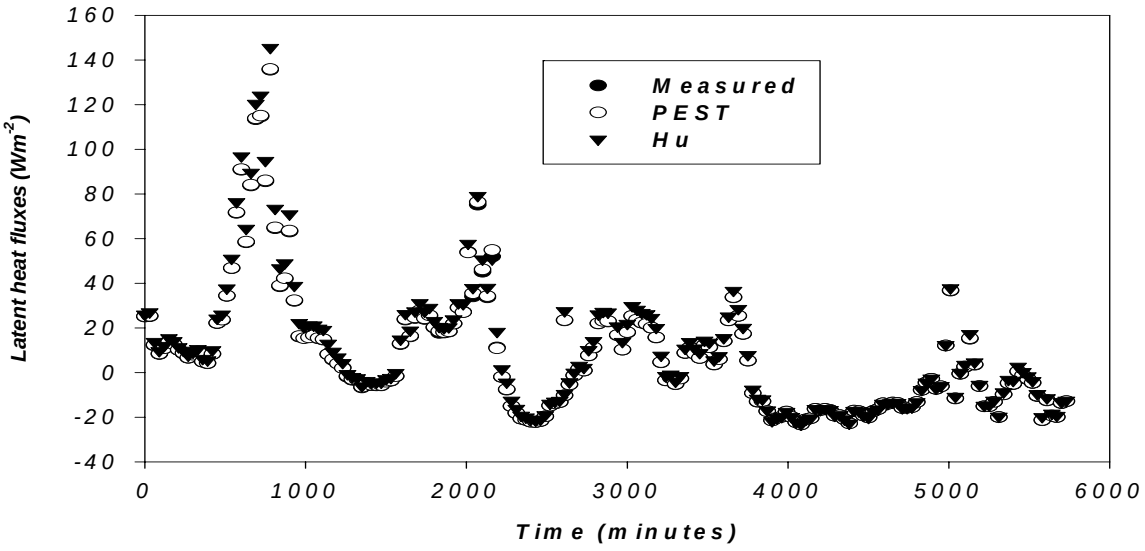

Figure 7.14: Time evolution of the latent heat fluxes for the measured and methods based on the proposed and Hu et al. (1999).

The plots show significant deviations from the observed for the method based on Hu et al. (1999) than that of the proposed method. Whereas quite a large number of points exceed 5 Wm^{-2} in residual latent heat fluxes for the method based on Hu et al. (1999), no point exceeded 5 Wm^{-2} in the case of the proposed method.

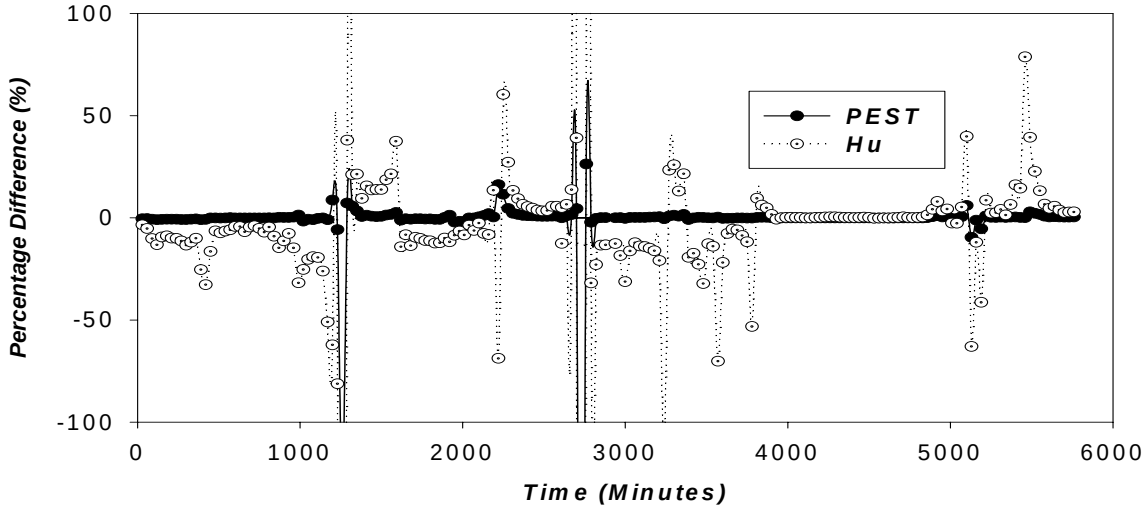

Figure 7.15: Percentage difference in latent heat fluxes.

The latent heat fluxes show large percentage differences for the method of Hu et al. (1999), whereas the proposed method consistently reduces it to zero. For the proposed method, 7 out of 192 points violated the scale invariance criteria as against 112 out of 192 points for method of Hu et al. (1999).

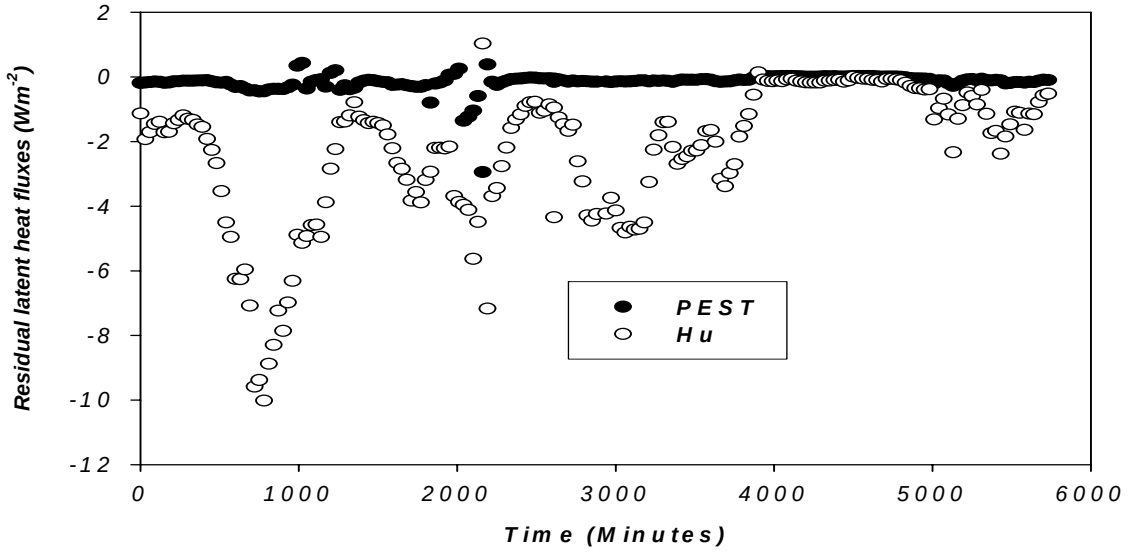

Figure 7.16: Time evolution of the residual latent heat fluxes for the proposed method and Hu et al. (1999).

Evaporative fraction

Figures 7.17 to 7.19 show respectively, the time evolution of the evaporative fraction and the corresponding percentage difference and residuals for proposed method and that of Hu et al. (1999). The observed trend for the residual evaporative fraction is quite different from the sensible and latent heat fluxes in that the residual evaporative fraction closely matches that of the corresponding percentage differences.

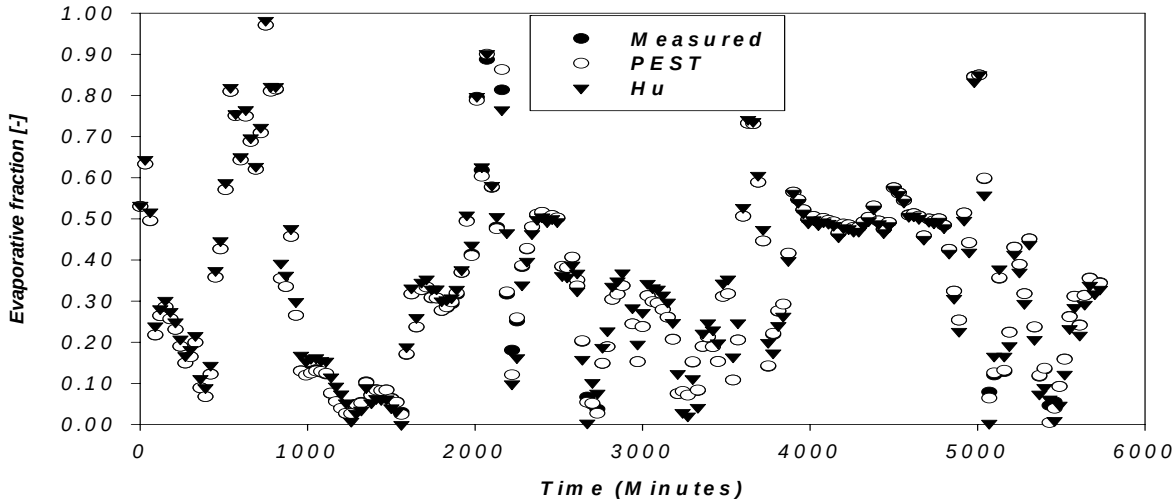

Figure 7.17: Time evolution of the evaporative fraction for the measured and methods based proposed and Hu et al. (1999).

For the proposed method, only 2 points have residuals greater than 0.05, whereas for the method of Hu et al. (1999), quite a number of points (about 20%) have residual evaporative fraction exceeding 0.05. However, the percentage differences in evaporative fraction (Figure 7.18) show a similar trend to those of the latent heat flux (Figure 7.15). For methods based on PEST, 7 out of 192 points violated the scale invariance condition as against 54 out 192 for those based on Hu et al. (1999).

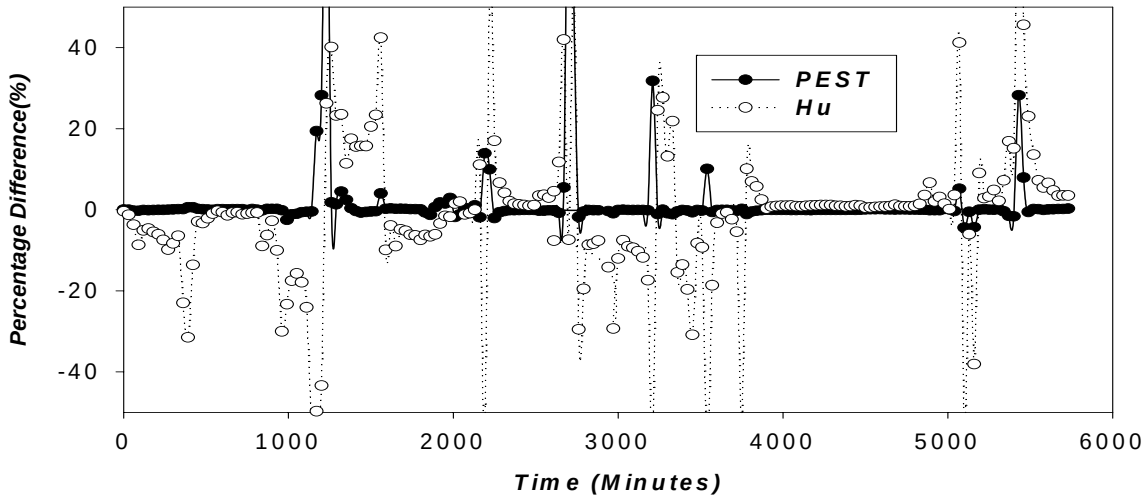

Figure 7.18: Percentage difference in evaporative fraction.

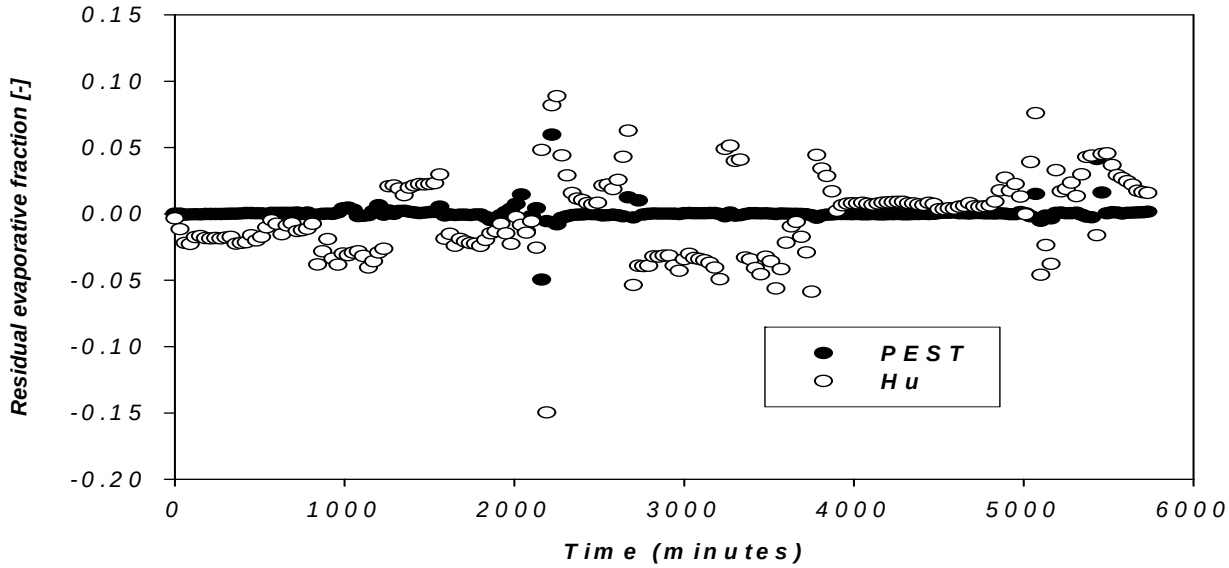

Figure 7.19: Time evolution of the residual evaporative fraction for the proposed method and Hu et al. (1999).

Bowen ratio

The Bowen ratio does not follow any specific trend, and the fluctuations/errors are very erratic and large. A few points were in excess of 100,000 and hence were eliminated to enable the detailed display of the time evolution of the Bowen ratio and the corresponding residual Bowen ratio. Figures 7.20 to 7.22 give the respective time evolution of the Bowen ratio and the corresponding percentage difference and residuals. The higher residuals correspond at the same points in both the time evolution plots of

the Bowen ratio and the corresponding residual Bowen ratio. The high values occur mostly at night, when low values of the latent heat fluxes are observed. The plots show that the proposed method and that of Hu et al. (1999) have similar performance with respect to the Bowen ratio. Because the Bowen ratio function is not analytic, it is not suiTable for use as objective function in a parameter estimation process.

The Bowen ratio is inappropriate for scale invariance analysis, because it is not well defined at vanishing latent heat fluxes as illustrated in figure 7.21. In this case, over 112 out of 192 points violated the scale-invariant criteria for both the proposed method and that of Hu et al. (1999).

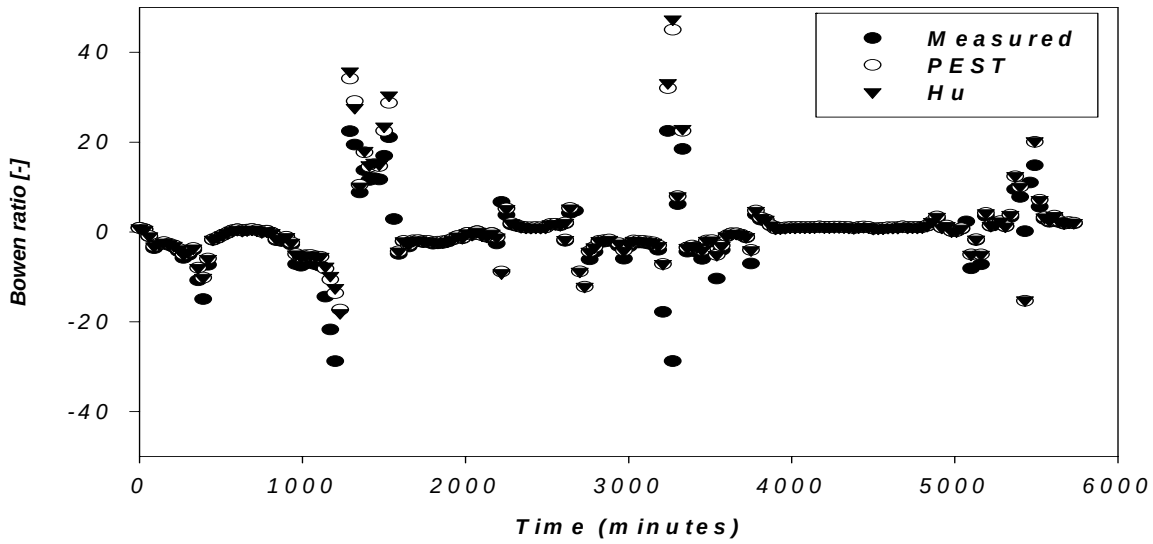

Figure 7.20: Time evolution of the Bowen ratio for the measured and methods based proposed and Hu et al. (1999).

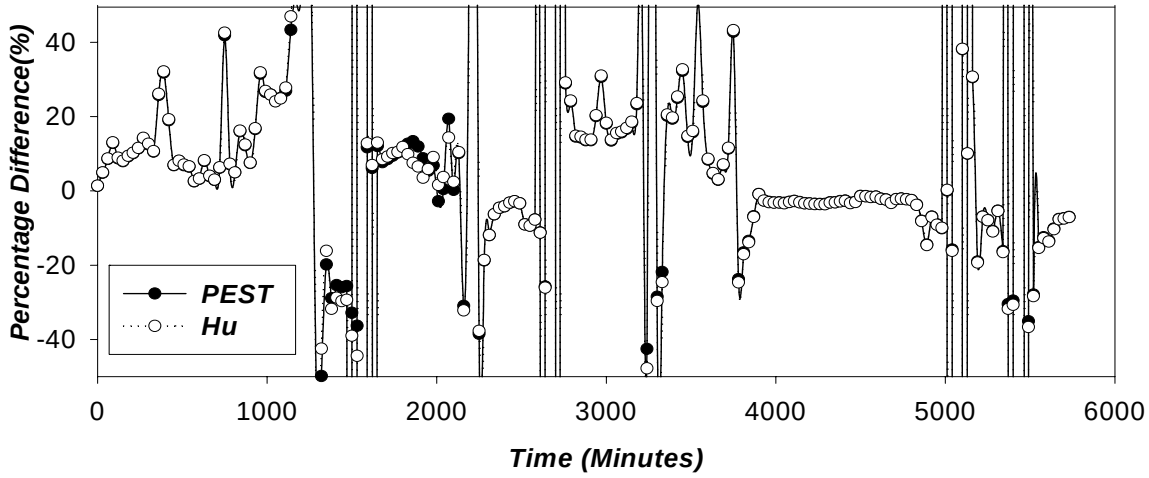

Figure 7.21: Percentage difference in Bowen ratio.

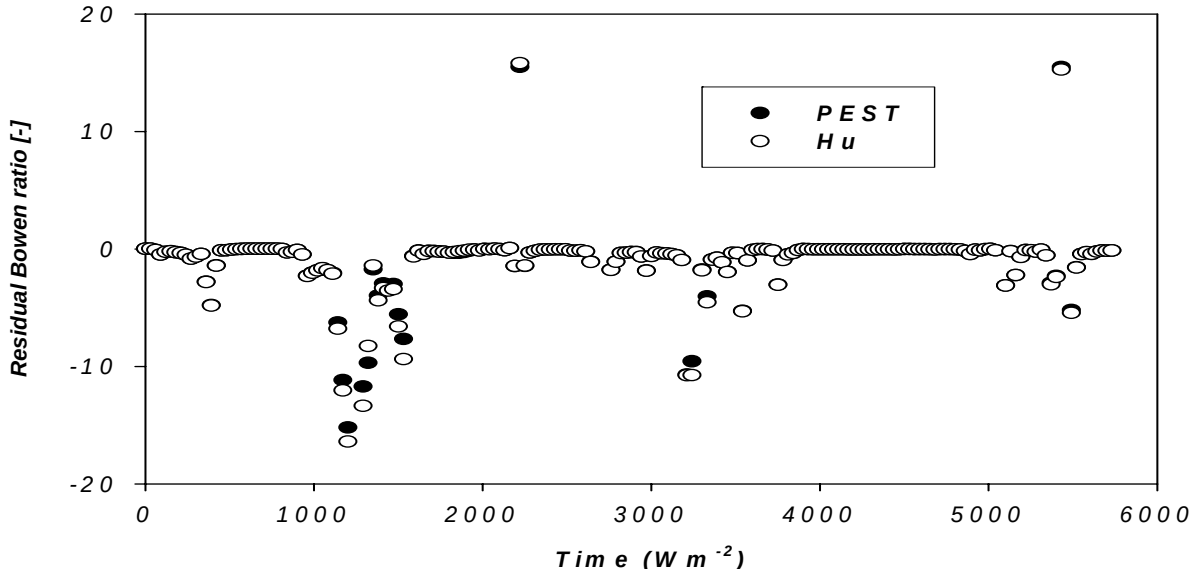

Figure 7.22: Time evolution of the residual Bowen ratio for the proposed method and Hu et al. (1999).

Additional validation of the proposed method: Comparison with method of Blyth et al. (1993)

Most of the results obtained in this experiment are closer to the geometric mean of the subgrid scale parameters, which is also bounded by the harmonic and arithmetic means. More importantly, Blyth et al. (1993) used observation data to show that effective parameter estimates obtained as the average of the harmonic and arithmetic means give better results than either the harmonic or arithmetic means. These effective parameters are often very close to the geometric mean as shown in figures 7.26 to 7.28 for the 3D SVAT case (will be discussed later in this section). A similar trend was observed in the 1D SVAT case. A comparison of the method of Blyth (1993) with the proposed method and the geometric mean is given in Tables 7.2 to 7.5. The conclusion drawn from this analysis is that the geometric mean is a better aggregation scheme than the other simple averaging methods, as its values are the closest to the PEST estimated or optimal parameter estimates.

A detailed comparison of the proposed method with other existing simple averaging methods will be given for the 1D SVAT case later in section 7.5 of this chapter. For the analysis, a similar Chi square versus parameter plots will be used to assess the performance of the various models. The 3D SVAT case was omitted because it will have been computationally very expensive to undertake as discussed in the introduction to this chapter.

Table 7.2: Plant insolation factor, RGL (μ_{RGL} =70 Wm^{-2}, σ_{RGL} =32.83 Wm^{-2})

Method	Parameter value	Chi square value
PEST	59.74	214510
Geometric mean (GM)	59.74	214510
Mean of HM and AM (BM)	56.92	283947

Table 7.3: Leaf area index, LAI (μ_{LAI} =10, σ_{LAI} =4.69)

Method	Parameter value	Chi square value
PEST	8.53	229941
Geometric mean (GM)	8.53	229941
Mean of HM and AM (BM)	8.13	285494

Table 7.4: Roughness length, zo (μzo =100cm, =σzo 46.69 cm)

Method	Parameter value	Chi square value
PEST	88.53	15.65
Geometric mean (GM)	85.34	39.45
Mean of HM and AM (BM)	81.30	75.18

Table 7.5: Plant Insolation factor, Rgl (μRgl=500 sm-1, σRgl=234.5 sm-1)

Method	Parameter value	Chi square value
PEST	426.70	114969
Geometric mean (GM)	426.70	114969
Mean of HM and AM (BM)	406.47	114969

7.3 Results for coupled Mesoscale Climate Model MM5-PEST (3D SVAT)

7.3.1 Upscaling laws

The analysis in this section focuses on upscaling laws for the 3D SVAT case. To account for subgrid scale effects, upscaling laws are derived that map the mean and standard deviation of the distributed land surface parameters at the subgrid scale to their corresponding effective parameter at the grid scale for the coupled MM5-PEST case. Due to constraints on computing resources and experience gained from the 1D SVAT and preliminary 3D SVAT experiments, the evaporative fraction was used in formulating the objective functions for all the 3D SVAT land parameters. Details on the efficiency of the evaporative fraction as an objective function will be discussed in section 7.4. Figures 7.23 to 7.25 show the respective plots of the upscaling law for the roughness length, minimal stomatal resistance and solar insolation factor. Table 7.6 gives their upscaling laws and the measure of Goodness-of-Fit.

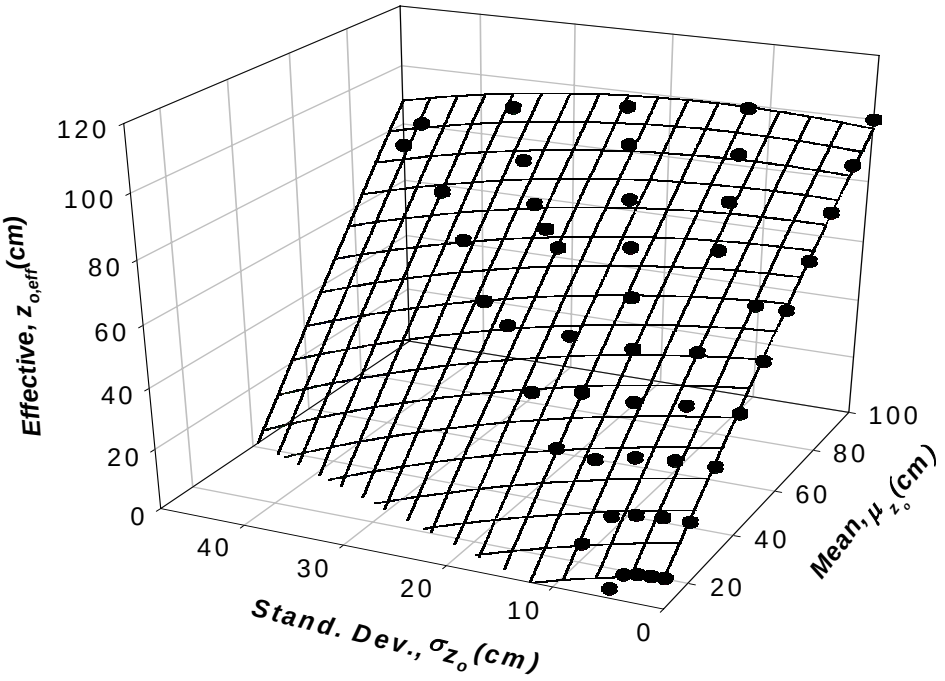

Figure 7.23: Parabolic upscaling plot for the roughness length, z_o, R =0.9762**.** The objective function used in the estimation of z_o is based on the evaporative fraction.

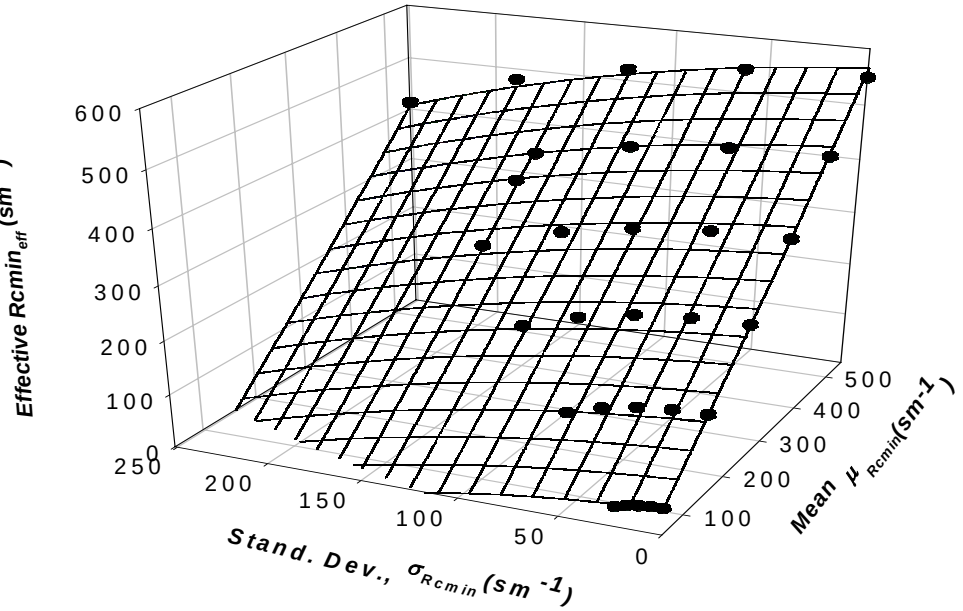

Figure 7.24: Parabolic upscaling plot for the minimum stomatal resistance, ***Rcmin,*** R =0.9987**.** The objective function used in the estimation of ***Rcmin*** is based on the evaporative fraction.

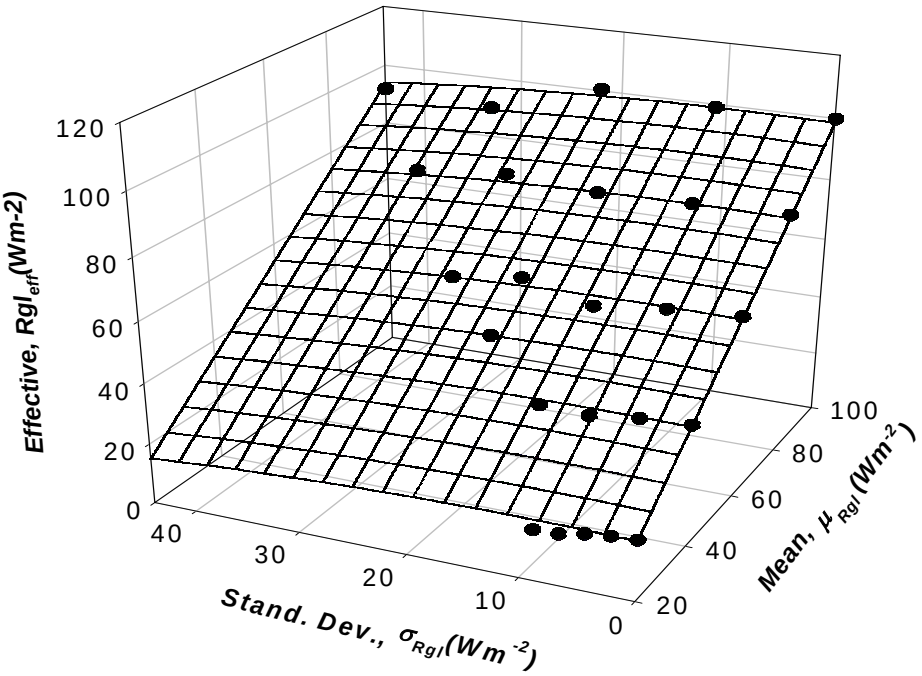

Figure 7.25: Parabolic upscaling plot for the solar insolation factor, *Rgl, R* =0.9872. The objective function used in the estimation of *Rgl* is based on the evaporative fraction.

In the case of the surface emissivity and albedo, it was found that a planar fit is best suited for interpolation between mean, standard deviation and effective values of emissivity and albedo. Their upscaling laws were given in Table 7.1. It was observed that parabolic fits are best suited for interpolation between the mean, standard deviation and effective values of the roughness length, minimum stomatal resistance and solar insolation factor. These results follow a similar trend observed in the 1D SVAT case discussed in section 7.2.1.

Table 7.6: Upscaling laws and Goodness-of-Fit measures for the 3D SVAT parameters. The effective parameters are independent of boundary and meteorological conditions.

Parameter	Upscaling Law	Correlation Co-efficient R
z_o (cm)	$z_{oeff}=1.095\mu_{zo}-1.092\sigma_{zo}-1.200*10^{-3}\mu_{zo}^2+1.480*10^{-2}\mu_{zo}\sigma_{zo} - 1.530*\sigma_{zo}^2$	0.9762
Rcmin (sm^{-1})	$Rcmin_{eff}=1.019\mu_{Rcmin}-0.375\sigma_{Rcmin} - 3.001\mu_{Rcmin}^2 + 6.000*10^{-4}\mu_{Rcmin}\sigma_{Rcmin} - 2.000*10^{-3}\sigma_{Rcmin}^2$	0.9987
Rgl (Wm^{-2})	$Rgl_{eff}=0.939\mu_{Rgl}+0.165\sigma_{Rgl}+6.000*10^{-4}\mu_{Rgl}^2 - 2.400*10^{-3}\mu_{Rgl}\sigma_{Rgl} - 3.000*10^{-4}\sigma_{Rgl}^2$	0.9872

Comparison of the upscaling relationship for the 1D and 3D SVAT

Tables 7.1 and 7.6 show that the derived upscaling relationships for the 1D SVAT and 3D SVAT have the same functional forms (but different coefficients) for each land surface parameter investigated. Additionally, the derived upscaling laws are independent of meteorological conditions because the 1D SVAT and 3D SVAT experiments were forced (run) with different meteorological and terrain information and during different periods of investigation. Hence the upscaling relationships derived for the 1D SVAT case are applicable to the 3D SVAT case within the limits of the assumptions and conditions under which the experiments were undertaken. More importantly, these results are consistent with other related research (Arain et al., 1996; Blyth et al., 1993; Hu et al., 1999).

Variation of the effective parameter with degree of heterogeneity

In section 7.2.1, a discussion on the behavior of the effective parameter with surface heterogeneity was discussed. A similar trend was observed with the 3D SVAT case. The variation of the effective parameter with heterogeneity is shown in figures 7.26 to 7.28 for z_o, ***Rcmin*** and ***Rgl,*** respectively. Four aggregation schemes: PEST, geometric mean (GM), harmonic mean (HM) and the average of the harmonic and arithmetic means (BM) are compared. The plots show that as heterogeneity increases, the effective parameter becomes smaller than the mean of the subgrid scale parameters. However,

when the heterogeneity approaches zero, the effective parameter approaches the mean parameter, which is the case for the homogeneous land surface. More importantly, it can be observed that at low heterogeneity, the effective parameter estimated from the various schemes converges to the same value. Additionally, it was observed that the plot for the effective parameter estimated from PEST is oscillatory for ***Rgl***. This may be due to irregularities in the parameter search space and depends much on the initial parameter estimate used to drive the estimation process. In this experiment, the harmonic mean was used to compute the initial parameters.

The effective parameter estimates obtained by the proposed method (PEST) are based on 95 % confidence interval statistics. The parameter estimates obtained from simple averaging formulations (GM, HM, BM) are given as point estimates. The overlapping of the error bars on the PEST estimates by estimates obtained from the simple average methods implies that the effective parameter estimates are significantly not different from the PEST estimates. The detailed discussion on specific land surface parameters is given below.

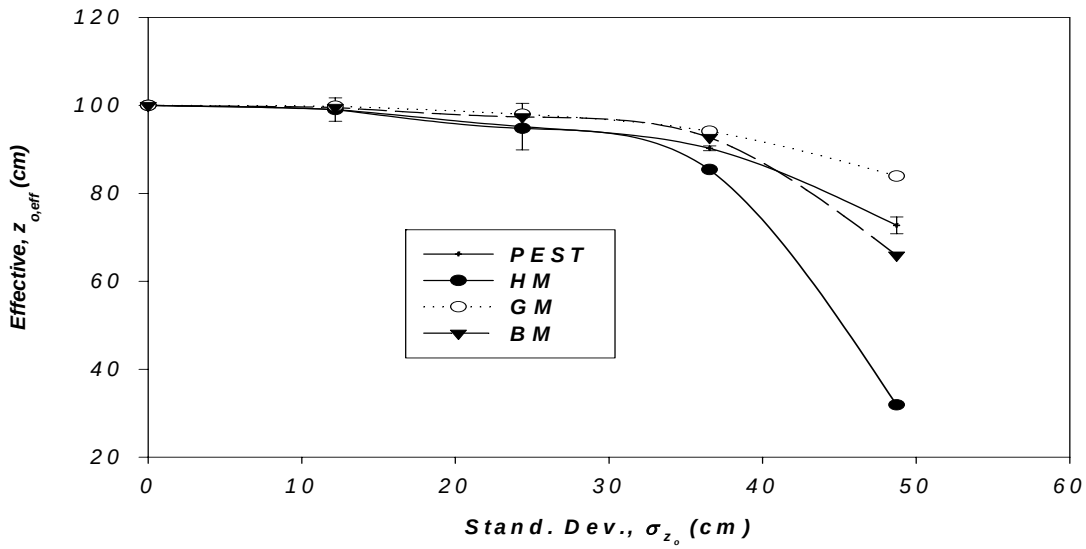

Figure 7.26: Variation of effective z_o with heterogeneity. (Parameters are distributed with: μ_{zo} =100 cm, σ_{zo} =44.69 cm).

In the case of the roughness length, z_o, all the methods are not significantly different from the PEST estimates at low to medium degree of heterogeneity. The HM

estimates are the most farthest from the PEST estimates at high degree of heterogeneity. This is also consistent with results obtained in the 1D SVAT case, and are shown in a chi square analysis in section 7.5.

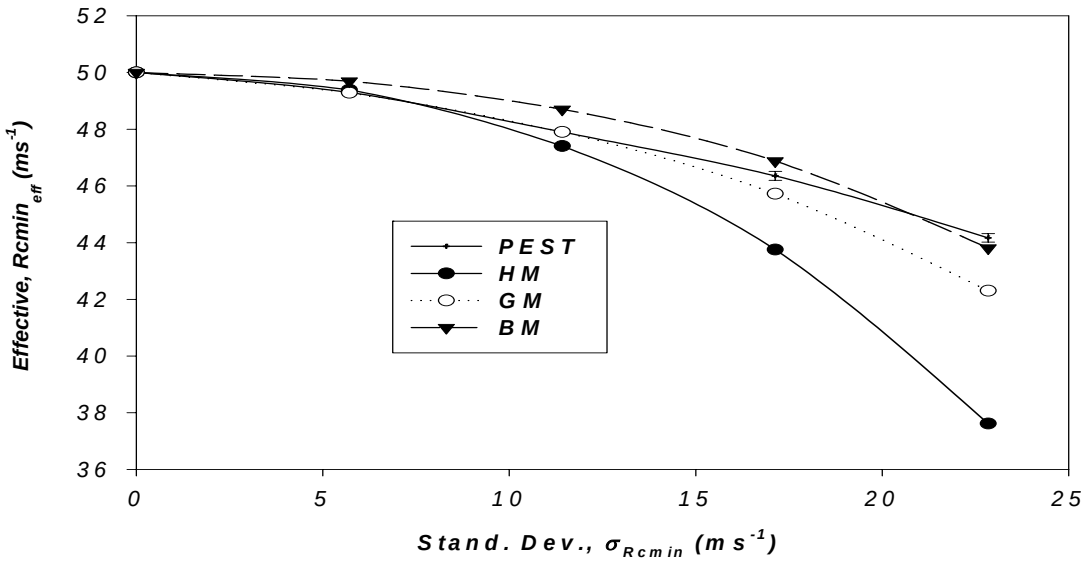

Figure 7.27**:** Variation of effective ***Rcmin*** with heterogeneity. (Parameters are distributed with: μ_{Rcmin} =50 sm^{-1}, σ_{Rcmin} =22.84 sm^{-1}).

For the ***Rcmin***, the BM is fairly close to both the PEST and GM values at low degrees of heterogeneity. However, at high degrees of heterogeneity, BM is closer to the PEST estimates than GM. In general, HM is the farthest from the PEST estimates, indicating it is the least accurate of the various methods. Similar results have been observed in the 1D SVAT case and are shown in a number of Chi square vs parameter space plots for the land surface parameters investigated in this research.

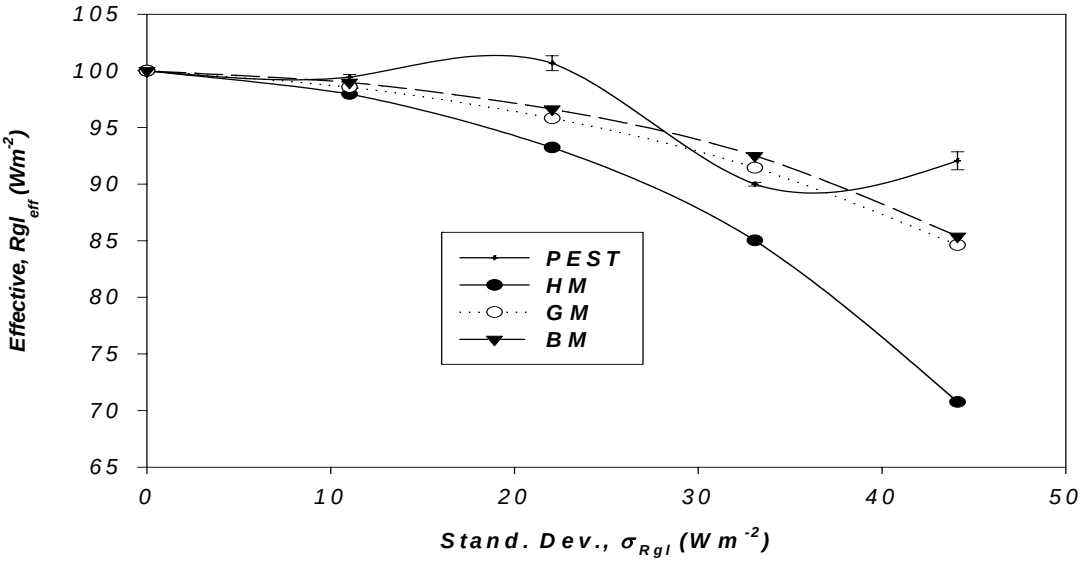

Figure 7.28: Variation of effective ***Rgl*** with heterogeneity. (Parameters are distributed with: μ_{Rgl} =100 Wm^{-2}, σ_{Rgl} =44.69 Wm^{-2}).

The parameter space for ***Rgl*** is very rough, therefore the choice of a good initial parameter set is crucial for the location of the global minimum. This is evidenced by the oscillatory nature of the line linking the PEST estimates. In general, the global minimum/optimal parameter is within the neighborhood of GM, because although the initial parameter estimates used in the optimal parameter search process was HM, the resulting optimal/PEST effective parameters are within a close neighborhood of GM. This is also consistent with results obtained from the chi square analysis with the 1D SVAT in section 7.5.

7.3.2 Comparison of the proposed method to method of Hu et al. (1999): The 3D SVAT case

The comparison made in this section is analogous to that of the 1D SVAT case presented in section 7.2.2. The distribution of the subgrid scale land surface parameters used in this investigations have a sample mean of 100 and sample standard deviation of 46.69.

Sensible heat fluxes

For the coupled 3D SVAT (MM5-PEST) runs, the results generally show similar trends to those of the 1D SVAT case discussed in section 7.3.1. However, marked differences exist for the sensible heat flux where the relative changes during the night violate the scale invariance criteria due to sign changes and very low values of the sensible heat fluxes as illustrated in Figures 7.29 to 7.31.

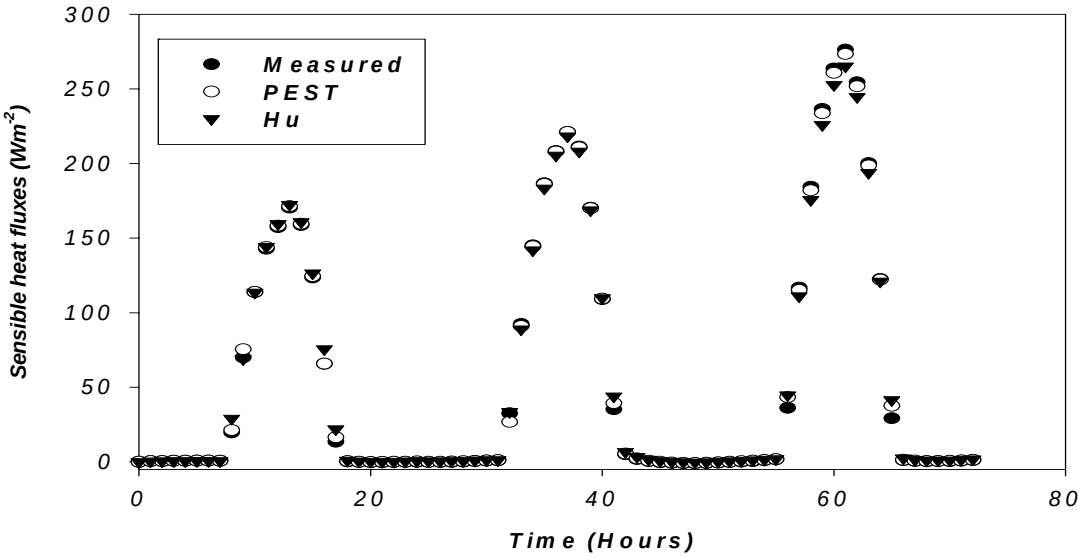

Figure 7.29: Time evolution of the sensible heat fluxes for the measured and methods based proposed and Hu et al. (1999).

A careful examination of the plots shows that generally both methods perform very well, because the regions with very high percentage differences occur at low incident solar radiation (mostly at night; around hours 18 - 36, 42 - 50 and 65 –75).

The residual fluxes at these times are insignificant (almost zero) to affect the energy dynamics appreciably (Moran et al., 1997; Nakaegawa et al., 2001).

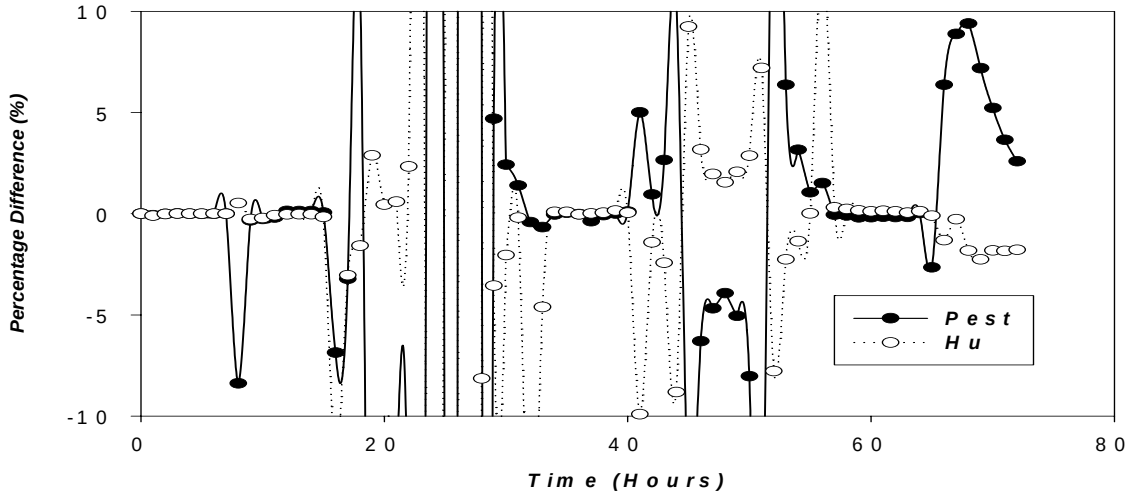

Figure 7.30: Percentage difference in sensible heat fluxes.

Generally, there are no significant differences between the observed sensible heat fluxes and those of the proposed method and Hu et al. (1999) at low sensible heat fluxes, which occur mostly at night and in the early morning. However, at high values of the sensible heat fluxes, mostly during daytime (between 9 – 16 hours GMT), significant differences exist between the two methods as evidenced in the residual plots. A maximum residual sensible heat flux of 11.90 Wm^{-2} was observed for the proposed method as against 12.26 Wm^{-2} obtained for the method of Hu et al. (1999). Also, 9 out of 72 points have residual sensible heat fluxes in excess of 5 Wm^{-2} as against 13 out of 72 for the method of Hu et al. (1999). Hence, the two methods show comparable performance with respect to the sensible heat fluxes, as in the 1D SVAT case.

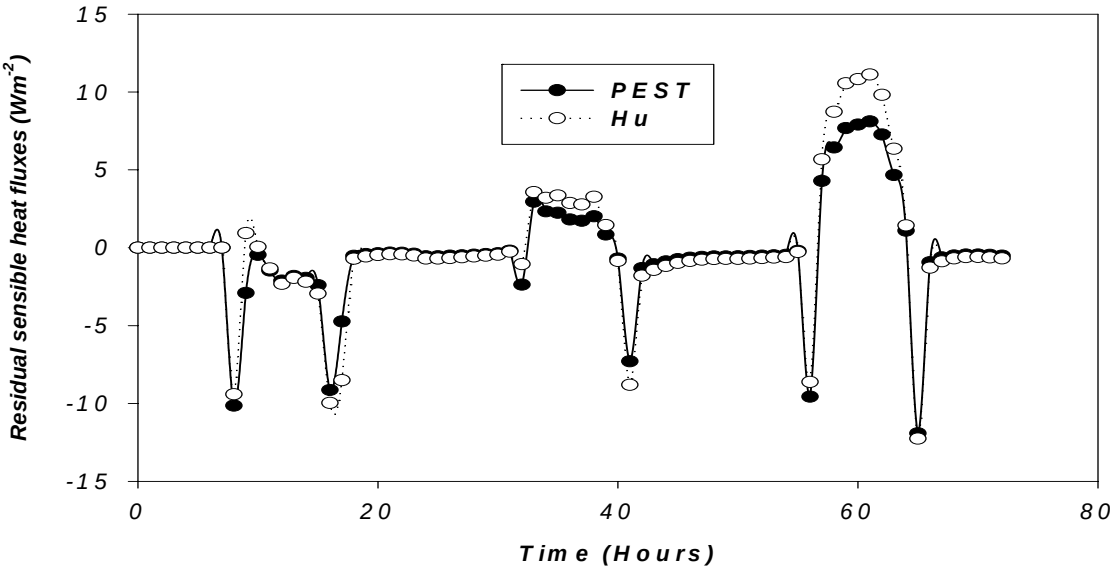

Figure 7.31: Time evolution of the residual evaporative fraction for the proposed method and Hu et al. (1999).

Latent heat fluxes

A similar trend as observed for the sensible heat fluxes was also observed for the latent heat fluxes. Figures 7.32 to 7.34 show the time courses for the latent heat fluxes and the associated percentage difference and residuals. The magnitudes of the latent heat fluxes and their corresponding residual latent heat fluxes are higher than those of the sensible heat fluxes. However, the percentage differences are within the scale-invariance criteria of less than 10% (Hu et al., 1999) as shown in figure 7.33. Residual latent heat fluxes in excess of 30 Wm^{-2} have been observed for the method of Hu et al. (1999) as compared to a maximum of 14.26 Wm^{-2} for the proposed method. More importantly, the number of points with residual sensible heat fluxes greater than 5 Wm^{-2} is small (11 out of 72) for the proposed method compared to that of Hu et al. (1999) (26 out of 72). This shows improved performance of the proposed method compared to that of Hu et al. (1999). A similar observation was realized with respect to the 1 D SVAT case.

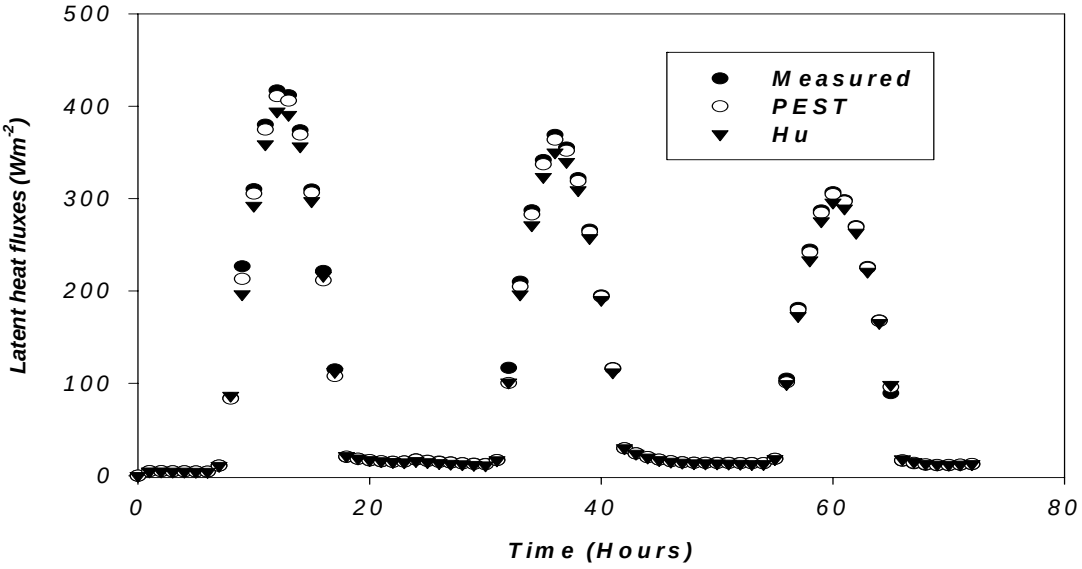

Figure 7.32: Time evolution of the latent heat fluxes for the measured and methods based proposed and Hu et al. (1999).

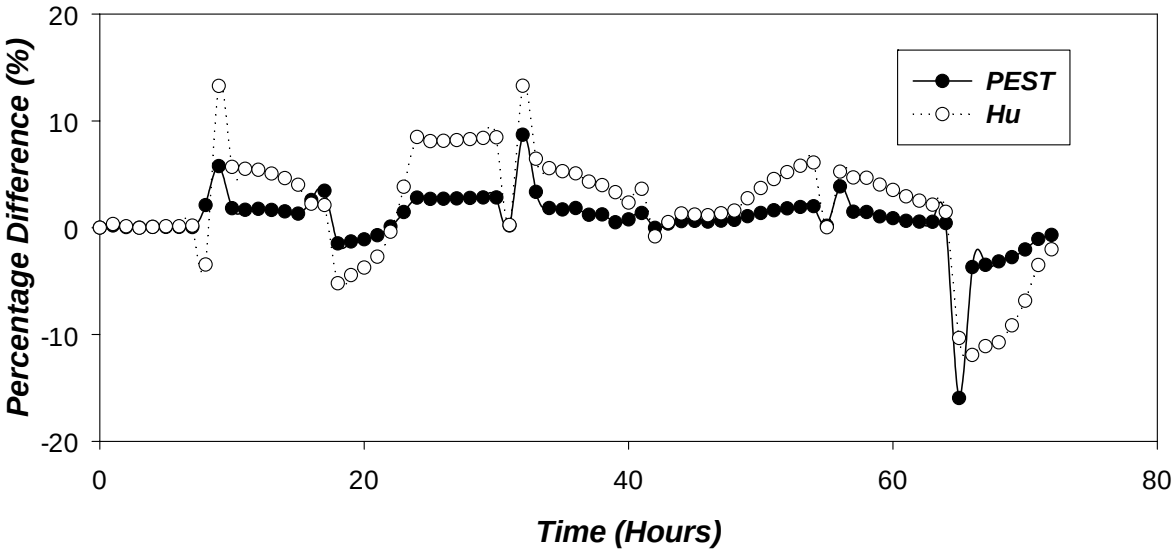

Figure 7.33: Percentage difference in latent heat fluxes.

More importantly, the low percentage differences in latent heat fluxes (Figure 7.33) for both methods compared to the 1D SVAT case (7.15) indicate that the subgrid scale effects are better resolved in the 3D SVAT case under the prevailing conditions. This further suggests that the lateral interactions between adjacent cells tend to

minimize the observed errors quite well compared to the stand-alone version (1D SVAT) where these interactions are assumed negligible. For lower degrees of subgrid scale variability, the two methods give the same parameter estimates for roughness length as shown in figure 7.28.

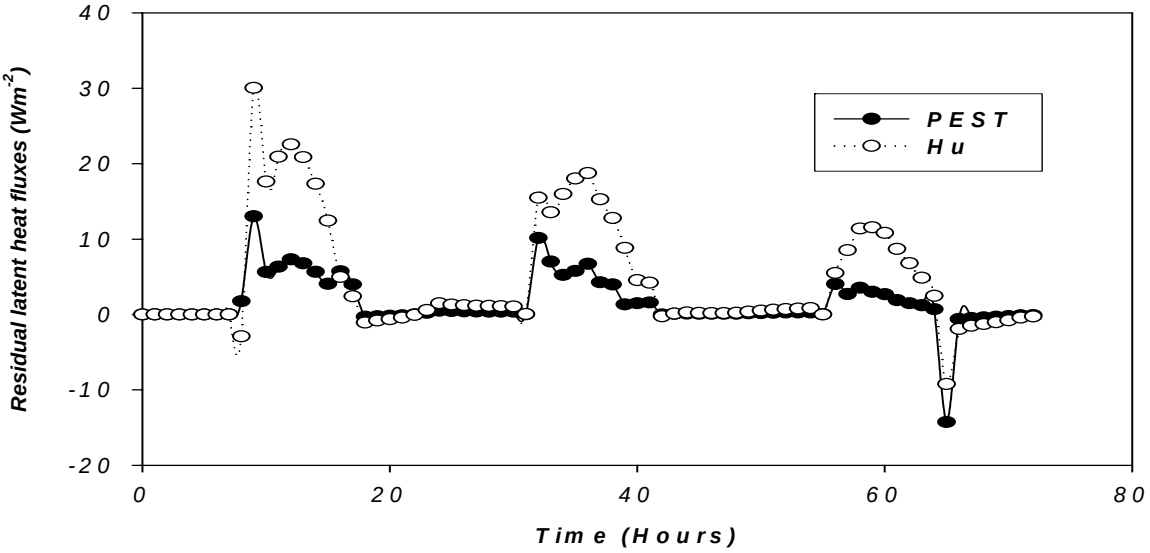

Figure 7.34: Time evolution of the residual latent heat fluxes for the proposed method and Hu et al. (1999).

Evaporative fraction

Figures 7.35 and 7.36 show the respective time courses for the percentage difference and the corresponding residual evaporative fraction for the proposed method and that of Hu et al. (1999). The plots show a strong correlation between the residual and percentage differences in the time evolution of the evaporative fraction. More importantly, a similar but weaker trend was observed in the 1D SVAT case than depicted in figures 7.35 and 7.36.

For the latent heat fluxes and evaporative fraction both methods satisfy the scale invariance condition very well, while the proposed method performs much better than that of Hu et al. (1999).

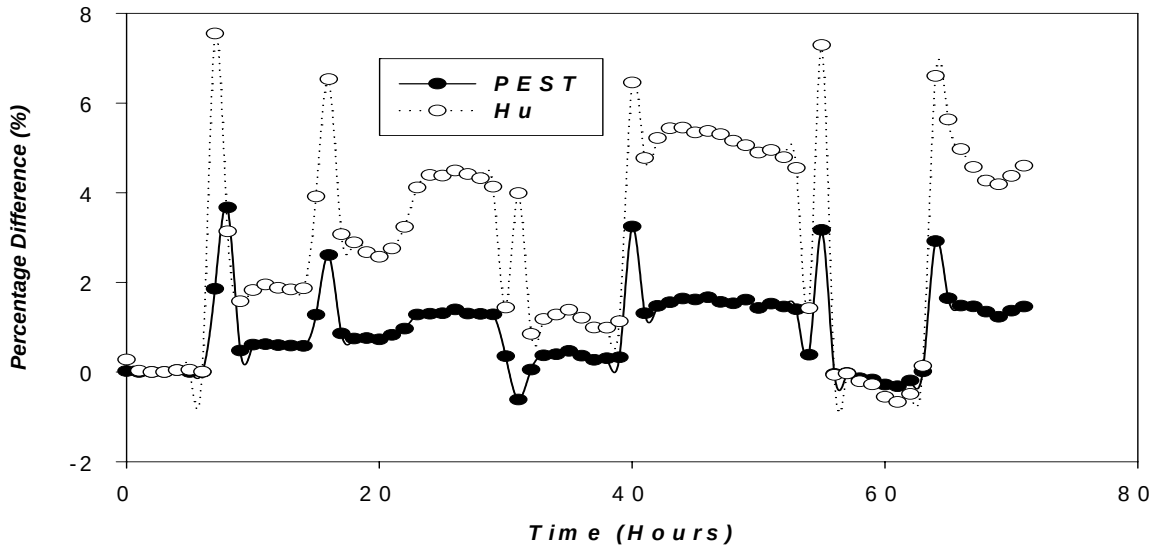

Figure 7.35: Percentage difference in evaporative fraction.

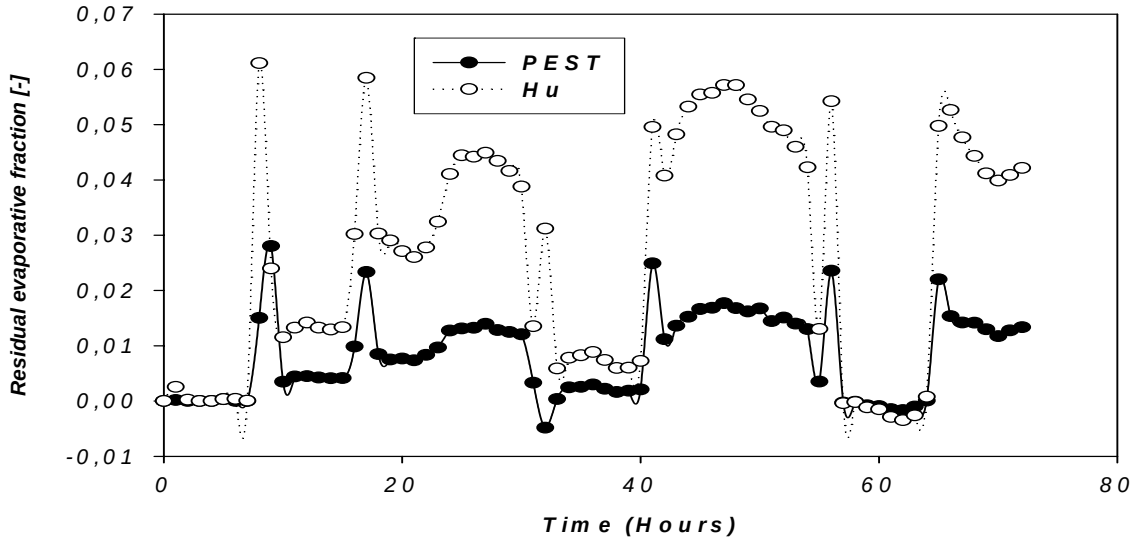

Figure 7.36: Time evolution of the residual evaporative fraction for the proposed method and Hu et al. (1999).

Surface parameters

For the derivation of effective albedo, reflected shortwave radiation was used as the fitting function. In the case of emissivity, surface temperature was applied. Here, Hu et al. (1999) and the proposed method yield nearly identical results. The associated errors

are negligible, confirming results from related studies (Chehbouni et al., 1995; Hu et al., 1997; Hu et al., 1999; Li et al., 1994).

7.4 Effect of choice of objective functions, initial parameters and parameter bounds on results of the parameter estimation process

Each point in the 3D upscaling plane presented in sections 7.2 and 7.3 constitutes a great deal of computational effort. For example, it takes on average about 45 MM5 model calls (runs) to obtain a point in the upscaling relation using latent heat fluxes as fitting functions for the objective function. With each MM5 model call of about one hour duration, this translates to at least 6 months of computer time per upscaling law of 100 points. The computational effort required for even three land surface parameters using this setting would be prohibitively expensive in terms of computing resources (e.g., CPU time and storage).

Therefore, an important component of the research was to find effective ways of saving computing resources during the parameter estimation process by reducing the duration of model runs while ensuring accurate results. One approach was to formulate the solution strategy to meet the key requirements of well-posedness discussed in Chapter 3 as close as possible. The main requirements for achieving a feasible solution and faster convergence to the true solution are: 1) the initial parameter set must lie within a region R, bounded by the parameter set containing the global minimum, 2) the fitting function must be continuously differentiable for the range of parameters bounded by the region R, and 3) the covariance matrix for the parameters bounded by the region R must be a nonsingular and continuous function for the range of parameters bounded by the region R (Cooley et al.,1990; Doherty, 2002, and Sun 1994).

To realize these objectives, transformation of the functions of interest (latent and sensible heat fluxes) to a form (e.g. evaporative fraction) that guarantees a feasible solution and faster convergence was made. Similarly, much effort was made to obtain good initial parameters that were within the close neighborhood of the true solution (condition 1 above) using limiting cases of the transformed functions and other well-known methods (Arain et al., 1996; Hu et al., 1999; Noilhan et al., 1996;Shuttleworth et al., 1999). Additionally, a criterion for parameter bounds was developed to restrain the solution from wandering in the non-feasible region of the parameter search space, hence

saving computing resources and CPU time. The lower and upper bounds were respectively obtained as the harmonic and arithmetic means of the subgrid scale parameters.

Objective functions

Verification and implementation of the above assumptions were made for the estimation of roughness length by undertaking model runs for fitting functions of evaporative fraction, latent and sensible heat fluxes using the same initial parameter of 31.8 cm obtained by the method of Hu et al. (1999). The result for each fitting function was fed to MM5 and the results compared to the aggregated sensible heat fluxes (observation). Model calls for evaporative fraction, latent and sensible heat fluxes were 26, 20 and 45, and corresponding parameter estimates 72.42 cm, 42.84 cm and 69.99 cm respectively. Although the number of model calls for sensible heat flux was the least, this had the poorest fit as it was trapped in a local minimum. Evaporative fraction has the best fit and second least model calls. These results are shown in Table 7.7 and illustrated in figures 7.37 and 7.38. Additionally, these values were used to generate latent heat fluxes. The roughness lengths obtained from using evaporative fraction and latent heat fluxes gave (almost) the same deviations, whereas those for the sensible heat fluxes gave the highest deviations from the observation. This scenario is illustrated in figure 7.39.

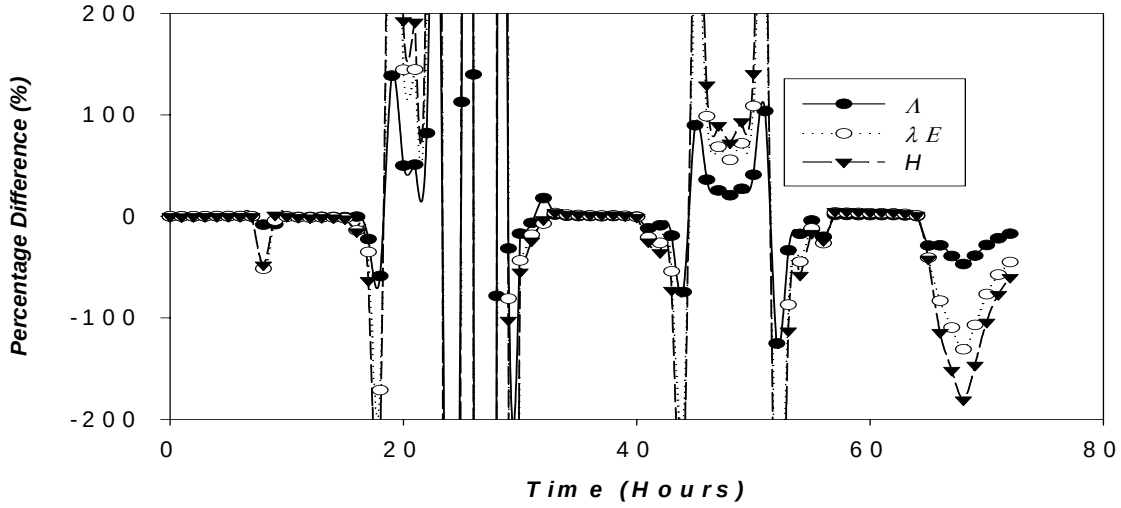

Figure 7.37: Sensible heat fluxes based on z_o estimates for different fitting functions.

Table 7.7: Comparison of objective functions based on the evaporative fraction, sensible heat latent and fluxes.

Fitting function	Number of model calls	Roughness length (cm)
Λ[-]	26	72.72
λE(Wm^{-2})	45	69.99
H (Wm^{-2})	20	42.84

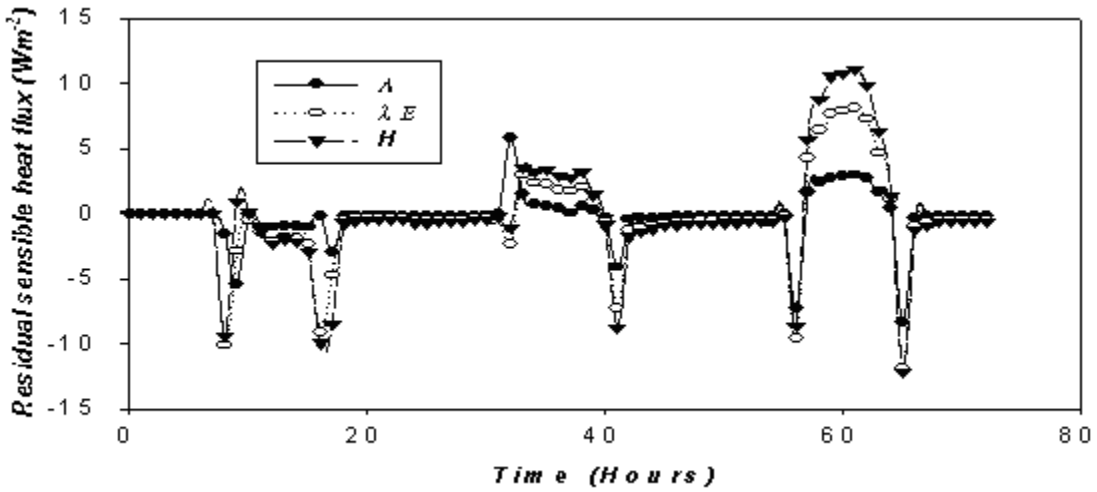

Figure 7.38: Residual sensible heat fluxes based on z_o estimates for different objective functions.

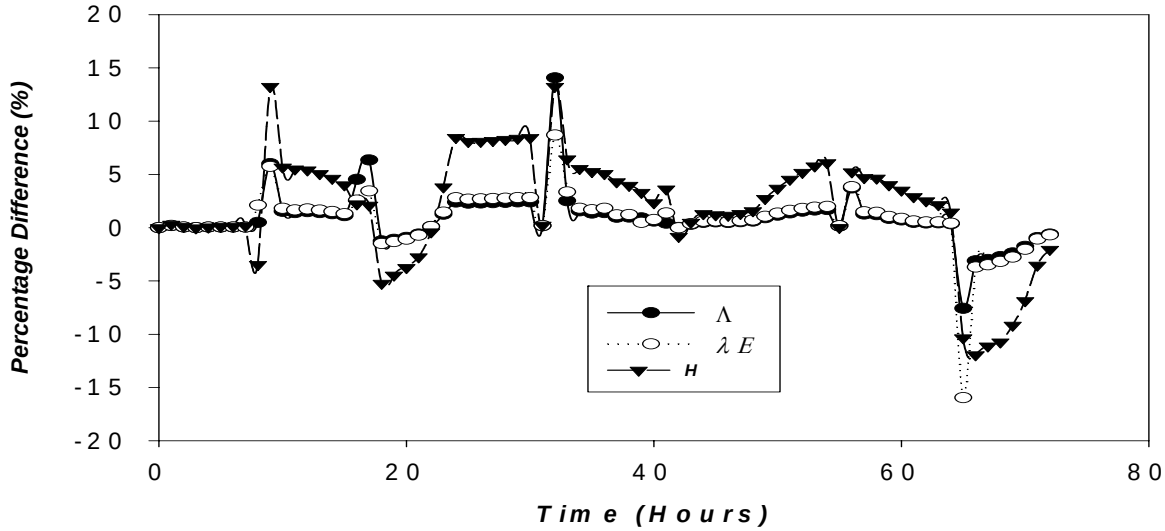

Figure 7.39: Percentage difference in latent fluxes based on z_o based on different objective functions.

Initial parameter estimates

The effect of the choice of initial parameters on the result of the parameter estimation process was further investigated. Initial values based on the arithmetic mean, harmonic mean (Hu et al., 1999) and an arbitrary value of half the mean were chosen to drive the parameter estimation process. The results show that parameter estimates obtained using initial values based on harmonic mean (Hu et al., 1999) give the best results as shown in figure 7.40.

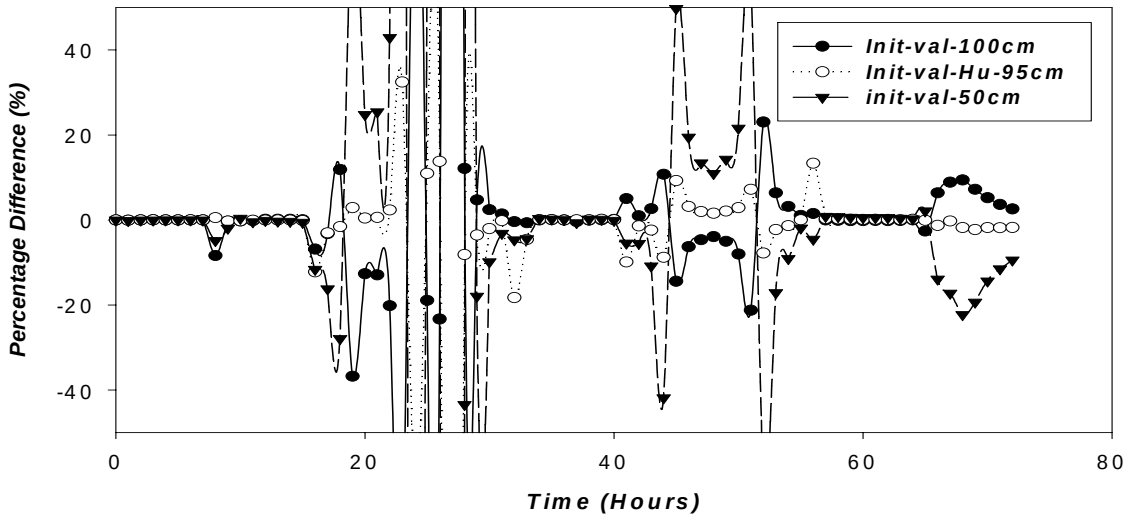

Figure 7.40: Sensible heat fluxes based on different initial z_o estimates.

Transformation of fitting functions from sensible and latent heat to evaporative fraction and use of appropriate initial parameter estimates had the following advantages:

- Better measures of fit observed with correlation coefficients and chi square minimum.
- Reduced total number of model calls leading to reduction in simulation time per parameter estimation process. On the average, over 50% reduction in simulation time was realized. This reduces the required effort on the average from about 2-3 days to about 1 day per parameter estimation process.

These achievements constitute a great step towards the realization of the objective of the thesis in that upscaling laws that require over 60 parameters could be obtained within 2-3 weeks instead of about 3 months observed in previous experiments.

More importantly, better parameter estimates were obtained at greatly reduced model simulation times.

7.5 Chi square analysis: 1D SVAT case

To undertake the parameter estimation process, PEST must be initialized with good initial parameter estimates so as to increase the chances of locating the optimal parameter set. More importantly, there is the need for an appropriate framework upon which the performance of the different aggregation schemes discussed in this chapter can be compared. For this reason, one seeks for appropriate initial parameters or approximate aggregation schemes based on physics compatible with that of the SVAT models used in this research.

To this end, the PEST's PARREP facility (Doherty, 2002), which is used to generate chi square values for given parameters, was coupled to the OSU LSM and used to produce chi square values for some selected parameter values that scan the parameter spaces of the land surface parameters of interest. Plots of chi square versus land surface parameters were produced to provide a medium for comparing results of the proposed method and the existing parameter aggregation methods. The chi squared plots for the various effective land surface parameters are given in figures 7.41 to 7.50. Additionally, sets of chi square values and their corresponding parameter values are given in Tables 7.8 and 7.9 for comparison. The investigation was done for both 9 and 81 subgrids to investigate the impact of the number of subgrids on the estimation of the effective parameter.

These results show that the choice of initial parameter estimates based on the harmonic and geometric means of subgrid scale parameters is justified, as the initial parameter sets lie within reasonable ranges (close neighborhood) of the chi squared minima. It was also observed that the optimal parameter sets are very close to the geometric means of the distributed land surface parameters as discussed previously. More importantly, the results for the 9 subgrids are consistent with those of the 81 subgrids. The method of Hu et al. (1999), which is a theory-based method, gives effective roughness length and canopy resistance as the harmonic mean of the distributed land surface parameters and serves as an appropriate initial parameter estimate method. In this scheme, corrections for errors associated with the

approximations made in formulating the effective parameters are difficult to quantify and hence omitted in the formulation. This leads to underestimation of the roughness length. The geometric mean and method of Blyth et al. (1993), which are upper bounds for the harmonic mean, seem to capture these errors quite well. Similar arguments can be made for the method of Arain et al. (1996), whose parameter estimates for minimum stomatal resistance is based on the harmonic mean. Also, the aggregation scheme proposed by Arain et al. (1996) for estimating the effective leaf area index (which is based on the arithmetic mean) overestimates the leaf area index. The geometric mean and method of Blyth et al. (1993), which are lower bounds to the arithmetic mean, approximate the optimal parameter set very well.

Parameter bounds for the effective parameter

Based on the observations derived from the chi square analysis and other upscaling analysis presented so far, the criteria for the parameter bounds derived from the analyses of this research formulated by the relation

$$HM \leq p_{eff} \leq AM \qquad 7.1$$

where HM and AM are the respective harmonic and arithmetic means of the subgrid scale parameters. Additionally, the arithmetic, harmonic and geometric means are known to be related by the inequality

$$HM \leq GM \leq AM \qquad 7.2$$

This is consistent with the results obtained from the 3D SVAT analysis in section 7.3.1.

7.5.1 Dependence of number of subgrids on estimation of effective parameters: The case of 9 and 81 subgrid parameter distributions with the same means

The effect of increasing the number of subgrids on the estimation of the effective parameters was investigated for the 1D SVAT case. For this experiment, the coupled 1D SVAT-PEST was applied to two configurations with 9 and 81 subgrids, respectively. The objective functions used in the investigation for each land surface parameter can be found in Table 7.1. The chi squared plots for the various effective land surface parameters are shown in figures 7.41 to 7.50. Additionally, sets of chi square values and

their corresponding parameter values are given in Tables 7.8 and 7.9 for comparison. The detailed analysis of the results is given in the ensuing discussion.

Roughness length

Figures 7.41 and 7.42 give the respective chi square plots for the 9 and 81 subgrid cases. Generally, no significant differences were observed between the 9 and 81 subgrid cases. The shape of the parameter spaces and key features are preserved in both cases. The roughness length has a relatively smooth parameter space compared to the other parameters investigated in this research. There is an initial increase in the chi square value up to about 10 cm and then decreases towards the global minimum, with some undulations at specific regions.

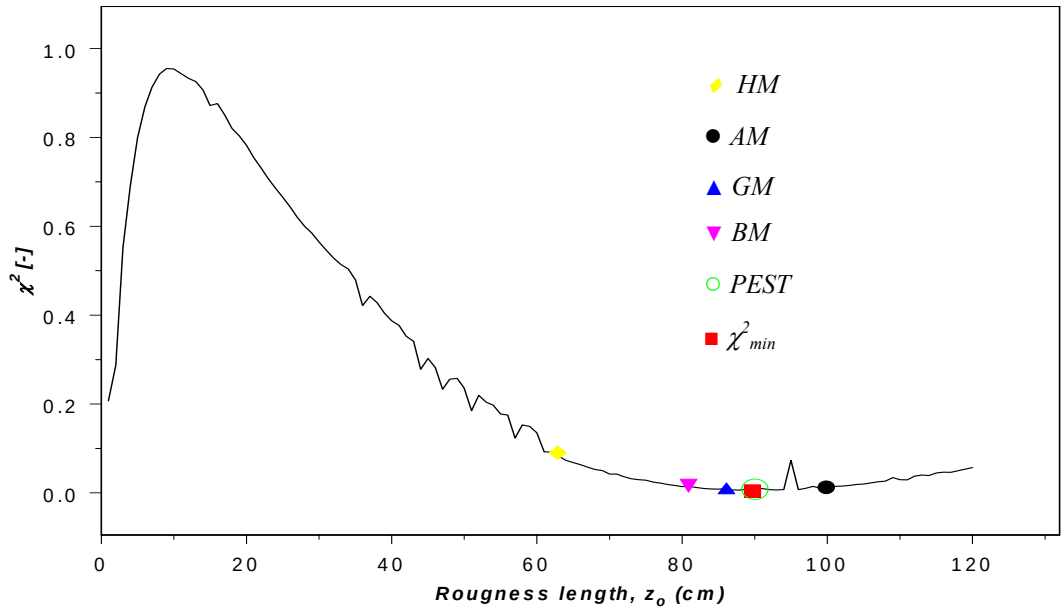

Figure 7.41: Chi squared plot for roughness length, z_o (9 subgrids).

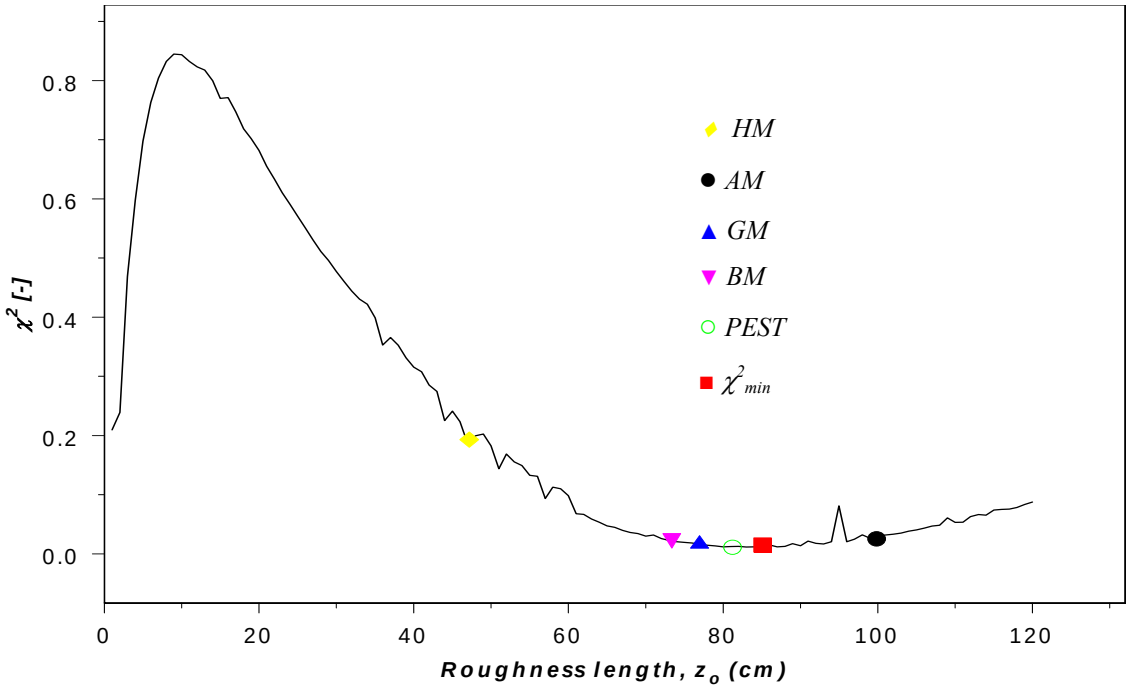

Figure 7.42: Chi squared plot for roughness length, z_o (81 subgrids).

The chi square minima are located at different parameter values (85.01 cm for the 81 subgrid case and 90.00 cm for the 9 subgrid case) and are close to GM, BM and PEST estimates. The parameter space is particularly rough in the region below 60 cm in both cases and hence the search for the optimal parameter with initial parameters less than 60 cm will most probably end up in a local minimum. Additionally, the location of the peak between 90 cm and 100 cm would make the search for the optimal parameter difficult with an initial estimate of about 100 cm.

Minimum stomatal resistance

The minimum stomatal resistance is the plant resistance to flow of water under optimal conditions where the environmental factors regulating transpiration are not limiting. Its nonlinear dependence on the canopy resistance implies that it has a rough parameter space where the search for the optimal parameter can be a formidable task. Figures 7.43 and 7.44 show the respective chi square plots of the minimum stomatal resistance for the 9 and 81 subgrid cases.

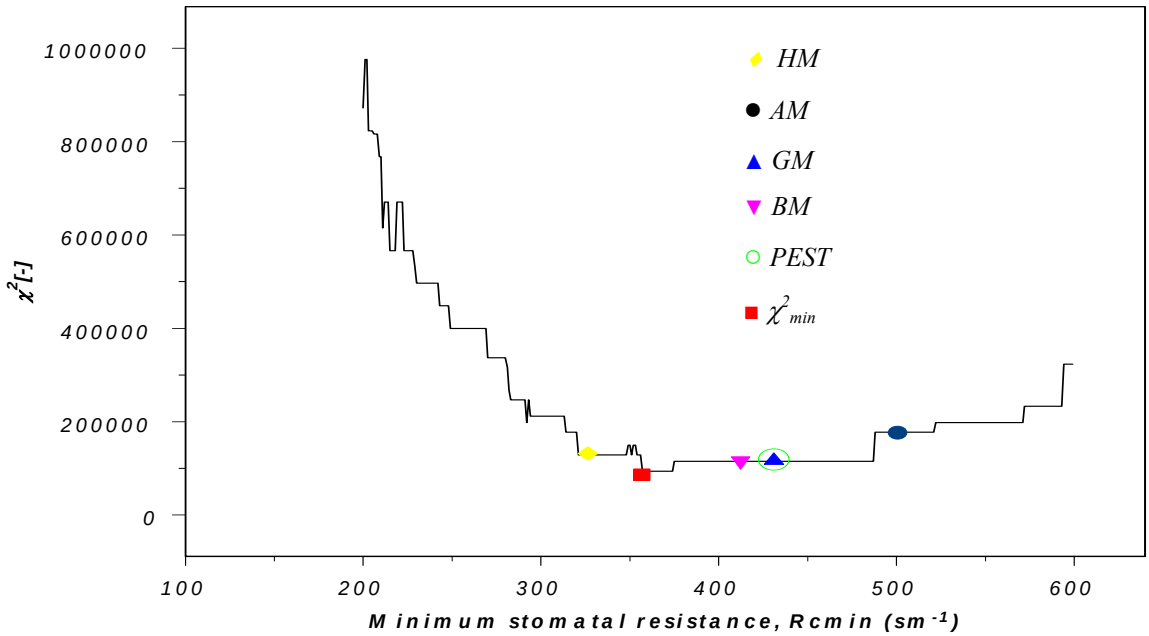

Figure 7.43: Chi square plot for minimum stomatal resistance, ***Rcmin*** (9 subgrids).

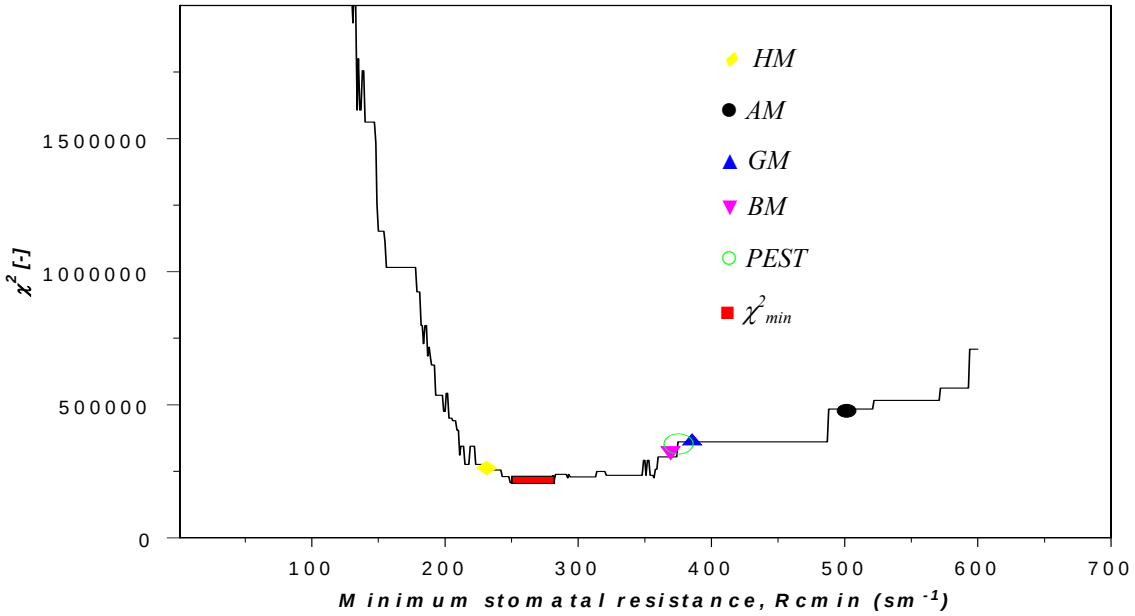

Figure 7.44: Chi square plot for minimum stomatal resistance, ***Rcmin*** (81 subgrids).

Distinct differences exist between the parameter spaces for the 9 and 81 subgrid cases. The chi square minimum occur over a range of parameter values in both cases, but are wider in the 81 subgrid case with a range of 249 – 280 at chi square minimum value of 205,895 as compared to a parameter range of 357 – 374 at a chi square value of 94,136. Additionally, these ranges occur at larger values in the 9 subgrid

case compared to the 81 subgrid case. This is possibly due to the fact that the GM, which is consistently close to the optimal parameter/chi square minimum, is larger in the 9 subgrid case than in the 81 subgrid case.

The location of GM, BM and PEST estimates are closer to the chi square minimum than the HM estimates in the 9 subgrid case; the reverse is true for the 81 subgrid case. The general observation with respect to the effective Rcmin is that, for large values, HM, GM and BM have comparable performances as the parameter space seems to have a flat/ large range of values for the chi square minimum.

Vapor pressure deficit factor

The respective chi square plots for the vapor pressure deficit factor for the 9 and 81 subgrids are given by figures 7.45 and 7.46. The parameter space for the vapor pressure deficit factor is the roughest among the parameters investigated. The distinct flat regions in the parameter space are possibly due to the fact that the response of the vapor pressure deficit function performs poorly during the winter period when the experiment was undertaken. Several contrasting views exist on the parameterization of the vapor pressure deficit on transpiration (Lynn and Carlson, 1990; Lhomme et al., 1998). Lynn and Carlson (1990) argue that the effect is not direct. Lhomme et al. (1998) suggest an average value of 24 kg/kg for ***Hs*** and recommend that the vapor pressure deficit function be put to 1. Also, there are reports that the vapor pressure deficit parameterization works for forests and other large trees, and hence is not appropriate for the land cover type used in this investigation. These arguments show that the complexity of the formulation of vapor pressure depends of transpiration and hence on ***Hs***.

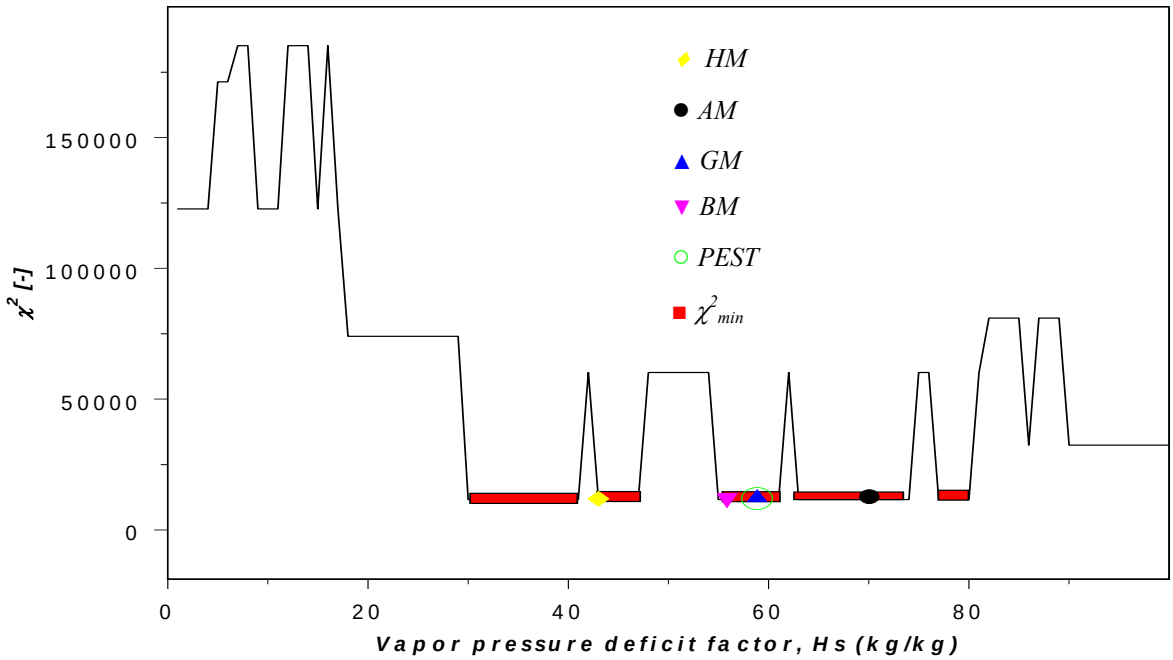

Figure 7.45: Chi square plot for vapor pressure deficit factor, ***Hs*** (9 subgrids).

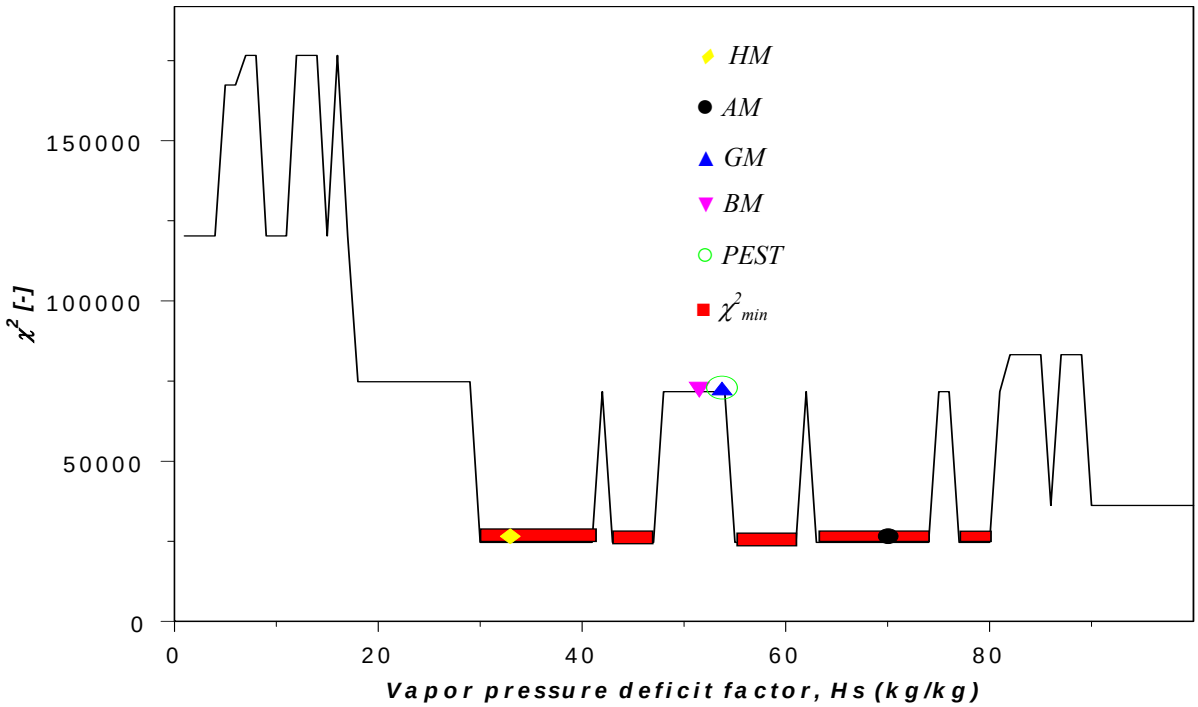

Figure 7.46: Chi square plot for vapor pressure deficit factor, ***Hs*** (81 subgrids).

The distinct flat regions in the parameter space imply that the search process would be easily trapped in these range of parameters. The choice of the initial parameter is therefore crucial. There was no change in the shape of the parameter space for both

the 9 and 81 subgrids scenarios. The chi square minimum is located exactly at the same parameter ranges in both 9 and 81 subgrids scenarios at ***Hs*** values in the ranges of 30-41, 43-47, 55-61, 63-74 and 77-80. However, the chi square minimum values are different for both cases. For the 9 subgrids case, the chi square minimum occurs at 1157, whereas in the case of the 81 subgrids, the value is 24,634.

The chi square minimum for the 81 subgrids case is larger than that of the 9 subgrids case because the sum of square error objective function is computed over 81 subgrid points and also for the case of the 9 subgrids scenario. Additionally, the GM, BM and PEST estimates are the chi square minimum values for the 9 subgrid case whereas in the 81 subgrids case they lie in a flat local minimum.

Leaf area index

The chi square plots for the leaf area index for both the 9 and 81 subgrids are given respectively in figures 7.47 and 7.48. Generally, there are no significant differences in the parameter spaces between the 9 and 81 subgrid cases for the leaf area index. The parameter space for the leaf area index is relatively less rough compared to the other vegetation parameters investigated. The chi square function decreases steeply from low values towards the global minimum and thereafter increases gradually with increasing parameter values.

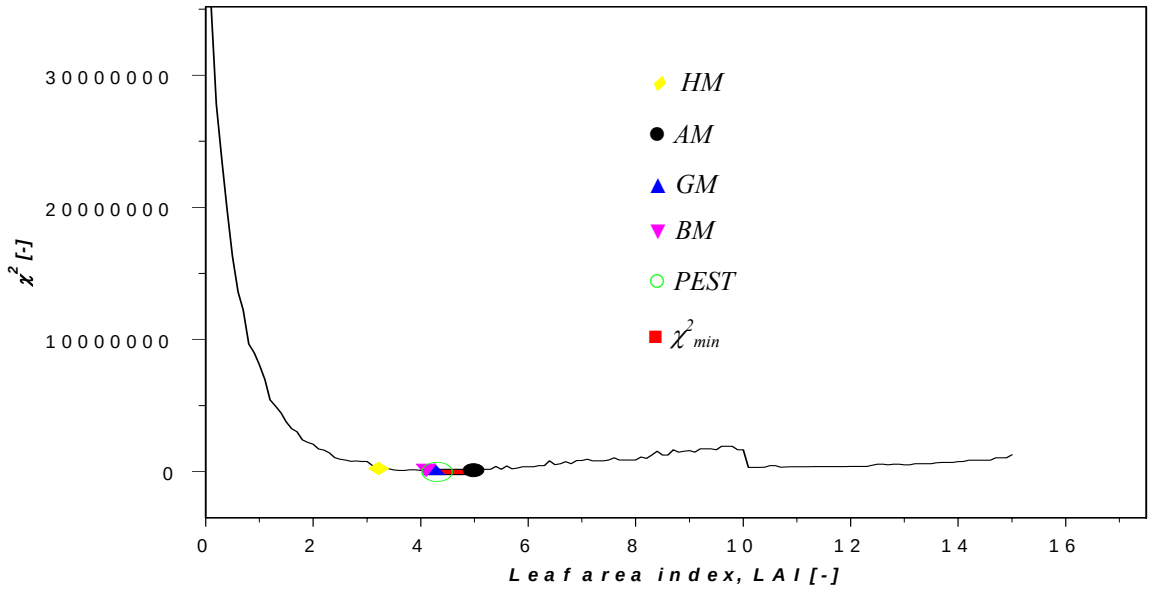

Figure 7.47: Chi square plot for leaf area index, ***LAI*** (9 subgrids).

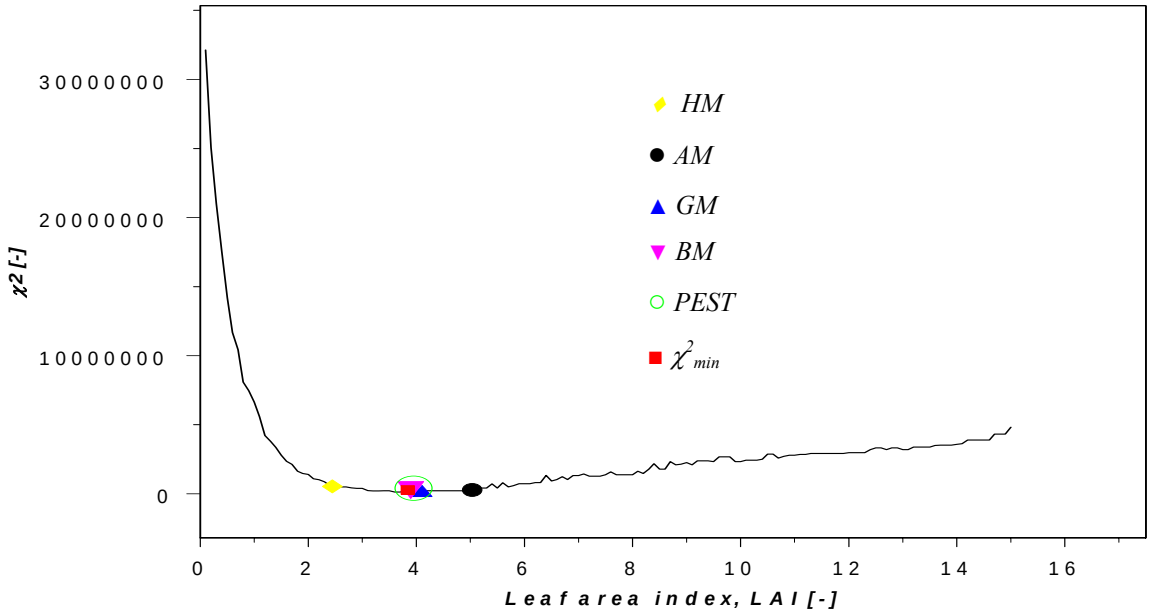

Figure 7.48: Chi square plot for leaf area index, ***LAI*** (81 subgrids).

The striking difference between the two cases can be seen around the neighborhood of 10, where there is a sudden drop in the chi square value of the 9 subgrid case. However, the chi square minimum occurs at 66,360 within a wider range/flat range (4.1 – 4.9) for the 9 subgrid case than the 81 subgrid case (3.6 – 3.7) where it occurs at 125,105. More importantly, GM, BM and PEST estimates have the same values as the chi square minimum in both 9 and 81 subgrid cases. In the 9 subgrid case, AM has the same value as the chi square value, whereas, in the 81 subgrid case,

the AM value is quite close to the chi square minimum estimate. The parameter space is rougher after AM, and hence a search process for the optimal parameter set starting above AM would have great difficulty in locating the global minimum.

Plant insolation factor

Figures 7.49 and 7.50 show the chi square plots of the plant insolation factor for both the 9 and 81 subgrids, respectively. There are no significant differences in the shape of the parameter spaces for both the 9 and 81 subgrid cases, except that the chi square minimum is closer to AM in the 81 subgrid case than in the 9 subgrid case. Additionally, the chi square minimum (241,773) occurs in the parameter range 89 – 91 for the 81 subgrid case where as in the 9 subgrid case (183,643) it occurs at a parameter value of 96. The parameter space of the plant insolation factor is very rough, and hence the estimation of the effective parameter is a formidable task. Each of the minor peaks/spikes in the parameter space constitutes a computational barrier for the parameter search process as it serves as a trap of a local minimum. The choice of appropriate initial parameter estimates for driving the parameter search process is therefore crucial for the location of the chi square minimum. More importantly, any search process starting before BM would have difficulty in locating the chi square minimum. In this experimentation, two initial parameter estimates computed as GM and HM were tested based on experience from preliminary studies and related literature (Arain et al., 1996). Each search process got trapped around the respective initial parameter estimates. For the case of HM, this is most likely due to the rough edges of a local minimum. For the case of GM, it may be either due to the fact that the termination condition for the optimal parameter was met or also to a local minimum problem. An initial parameter estimate based on AM would be a good choice as it is close to the chi square minimum in both 9 and 81 subgrids cases. Also, there are less rough surfaces to impede the search for the optimal parameter set.

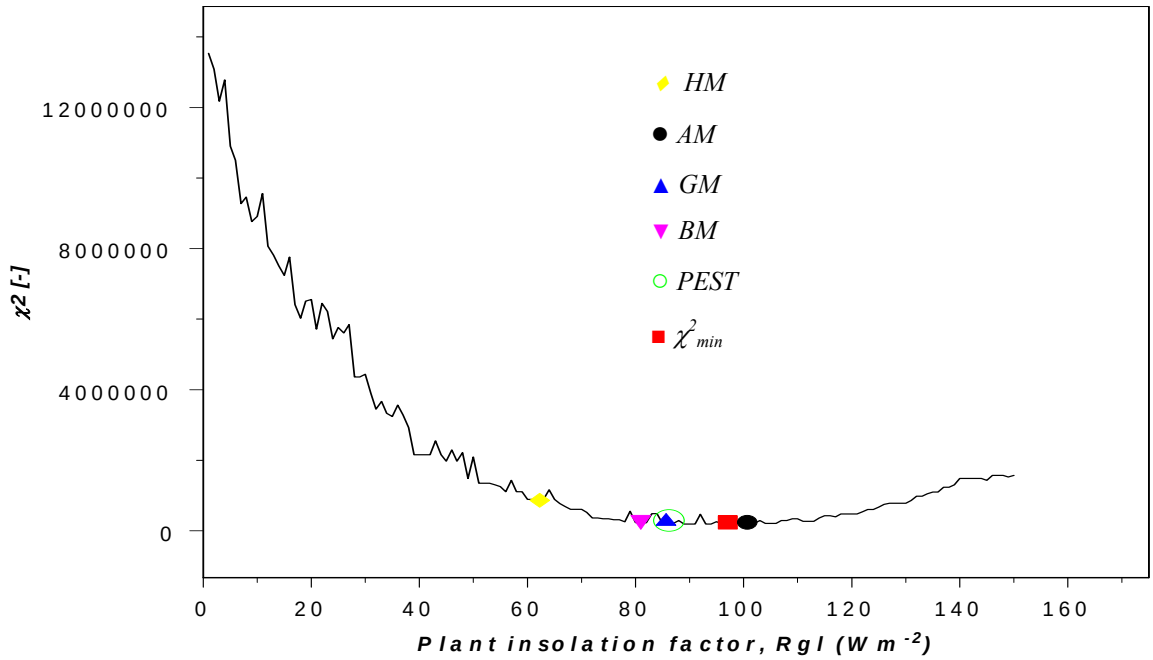

Figure 7.49: Chi square plot for plant insolation factor, ***Rgl*** (9 subgrids).

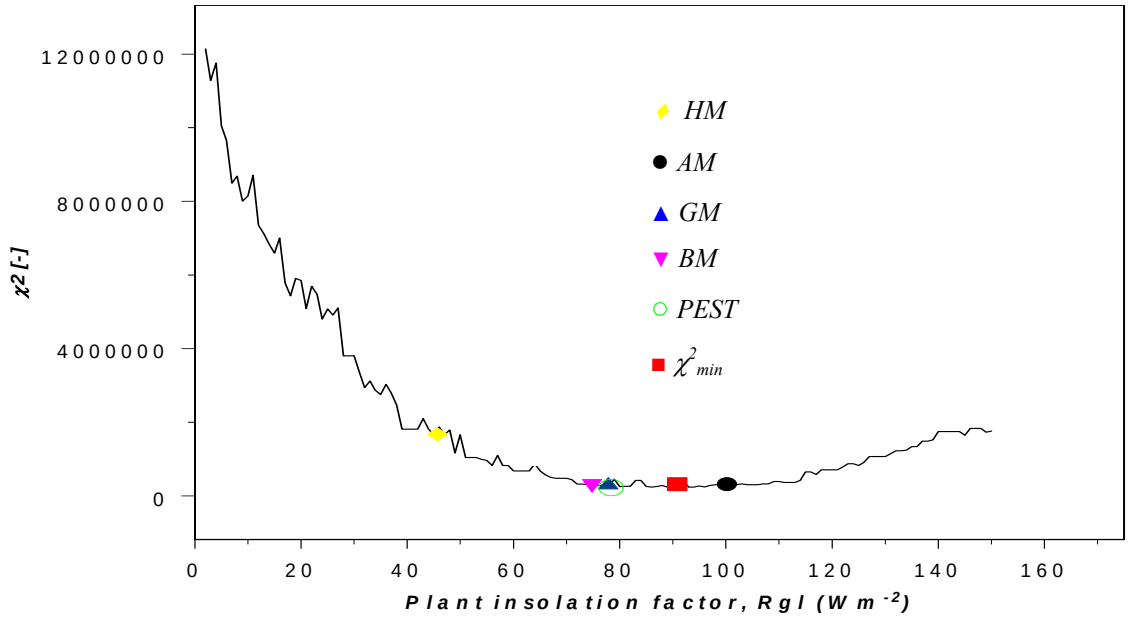

Figure 7.50: Chi square plot for plant insolation factor, ***Rgl*** (81 subgrids).

7.5.2 General remarks on the chi square analysis

The general observation from this analysis is that there is no significant difference in the shape and key features of the parameter spaces for the land surface parameters investigated for both 9 and 81 subgrid cases. Increasing the number of subgrids did not influence the spikes/peaks in the parameter space. These spikes may be due to an

intrinsic property of the parameter space. Additionally, the location of the chi square minimum is within the close neighborhood of the GM in both cases. The main differences are in the location of the GM, BM, HM and optimal parameter sets. In effect, since the mean of the distributions of the land surface parameters used for the chi square experiments in the 9 and 81 subgrid cases are the same while their corresponding standard deviations are different, the estimation of the effective parameters can be analyzed on mainly statistical bases. Based on these findings, simple statistical experiments can be designed to investigate some key properties of the effective parameters before selected detailed SVAT experiments that require computationally expensive runs are undertaken. This would constitute a significant step towards reducing the computational effort required in such investigations.

Table 7.8: Chi squared analysis of parameter space for the 1D SVAT (9 subgrids)

Parameter	***Parameter space value at χ^2_{min}***	***Parameter space χ^2_{min}***	***PEST value***	***PEST χ^2_{min}***	***Geometric Mean of parameters***	***Geometric Mean χ^2_{min}***	***Harmonic Mean of parameters***	***Harmonic Mean χ^2_{min}***	***Arithmetic Mean of parameters***	***Arithmetic Mean χ^2_{min}***
Rgl (Wm^{-2})	86.00/93.00	183643.00	85.34	183643.00	85.34	183643.00	62.59	891980.00	100.00	211421.00
LAI (.)	4.10-4.90	66360.00	4.27	66360.00	4.27	66360.00	3.13	358020.00	5.00	114970.00
Rcmin (sm^{-1})	358.00 359.00	87191.00	426.70	114970.00	426.70	114970.00	312.94	212191.00	500.00	177469.00
Hs (kg/kg)	30.00-47.00 55.00-73.00 77.00-80.00	11574.00	59.00	11574.00	59.00	11574.00	43.83	11574.00	70.00	11574.00
z_o-Λ (cm)	90.00	6.16e-3	86.80	7.03e-3	85.34	8.78e-3	62.59	8.27e-2	100.00	1.25e-2

Parameter	***Arithmetic Mean of parameters***	***Arithmetic Mean χ^2_{min}***	***Blyth Mean parameters***	***Blyth Mean χ^2_{min}***
Rgl (Wm^{-2})	100.00	211421.00	81.30	218360.00
LAI (.)	5.00	114970.00	4.06	66360.00
Rcmin (sm^{-1})	500.00	177469.00	406.50	114970.00
Hs (kg/kg)	70.00	11574.00	56.92	11574.00
z_o-Λ (cm)	100.00	1.25e-2	81.30	1.45e-2

Table 7.9: Chi squared analysis of parameter space for the 1D SVAT (81 subgrids)

Parameter	***Parameter space value at χ^2_{min}***	***Parameter space χ^2_{min}***	***PEST value***	***PEST χ^2_{min}***	***Geometric Mean of parameters***	***Geometric Mean χ^2_{min}***	***Harmonic Mean of parameters***	***Harmonic Mean χ^2_{min}***	***Arithmetic Mean of parameters***	***Arithmetic Mean χ^2_{min}***
Rgl (Wm^{-2})	89.00-91.00	241773.00	76.11	284978.00	76.11	284978.00	46.74.00	1662290.00	100.00	302727.00
LAI (.)	3.60-3.70	125105.00	3.6-3.7	125105.00	3.81	215385.00	2.34	865839.00	5.00	321093.00
Rcmin (sm^{-1})	249.00 - 280.00	205895.00	380.54	360215.00	380.54	360215.00	233.68	254506.00	500.00	484444.00
Hs (kg/kg)	30.00-47.00 55.00-73.00 77.00-80.00	71704.00	53.28	71704.00	53.28	71704.00	32.72	24634.00	70.00	24634.00
z_o-Λ (cm)	81.59	1.26e-2	85.00	1.13e-2	76.11	1.83e-2	46.74	2.23e-1	100.00	2.86e-2

Parameter	***Arithmetic Mean of parameters***	***Arithmetic Mean χ^2_{min}***	***Blyth Mean parameters***	***Blyth Mean χ^2_{min}***
Rgl (Wm^{-2})	100.00	302727.00	73.37	321243.00
LAI (.)	5.00	321093.00	3.67	125105.00
Rcmin (sm^{-1})	500.00	484444.00	366.84	303888.00
Hs (kg/kg)	70.00	24634.00	51.39	71704.00
z_o-Λ (cm)	100.00	2.86e-2	73.37	2.29e-2

7.6 Dependence of effective roughness length on the duration of episode.

To check the uniqueness of the parameter estimation process for the duration of model runs, the estimation process was done for roughness length for periods ranging from 1 day to 30 days using the coupled 1D SVAT-PEST model. Figures 7.51 to 7.53 show the plots of the roughness length obtained for different duration of episodes. Figures 7.51 and 7.52 give regression plots of the roughness length with respect to duration of episodes; error bars are based on the standard deviation and residuals, respectively. The effective roughness length values ranges from 85.33 cm to 93.04 cm. It has an average of 88.67 cm, a standard deviation of 2.62 cm and a co-efficient of variation of 0.0295. A linear regression analysis of the effective roughness lengths for the episodes gives a gradient of –0.1460 cm per day (for the duration considered). This shows a relatively low variation in the effective roughness length and hence uniqueness of the parameter estimation process with respect to duration of episodes. Details of the analysis are given in Tables 7.9 and 7.10.

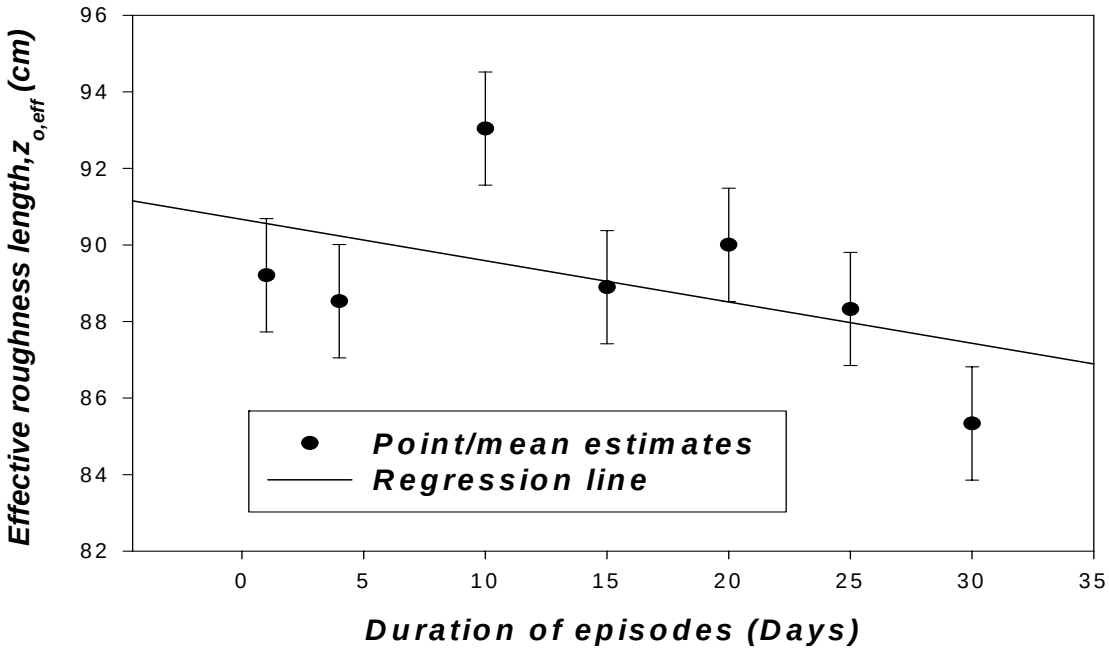

Figure 7.51: Linear regression plot for different duration episodes for investigating the uniqueness of the effective roughness length obtained from the sensible heat fluxes. Error bars are based on the standard deviation.

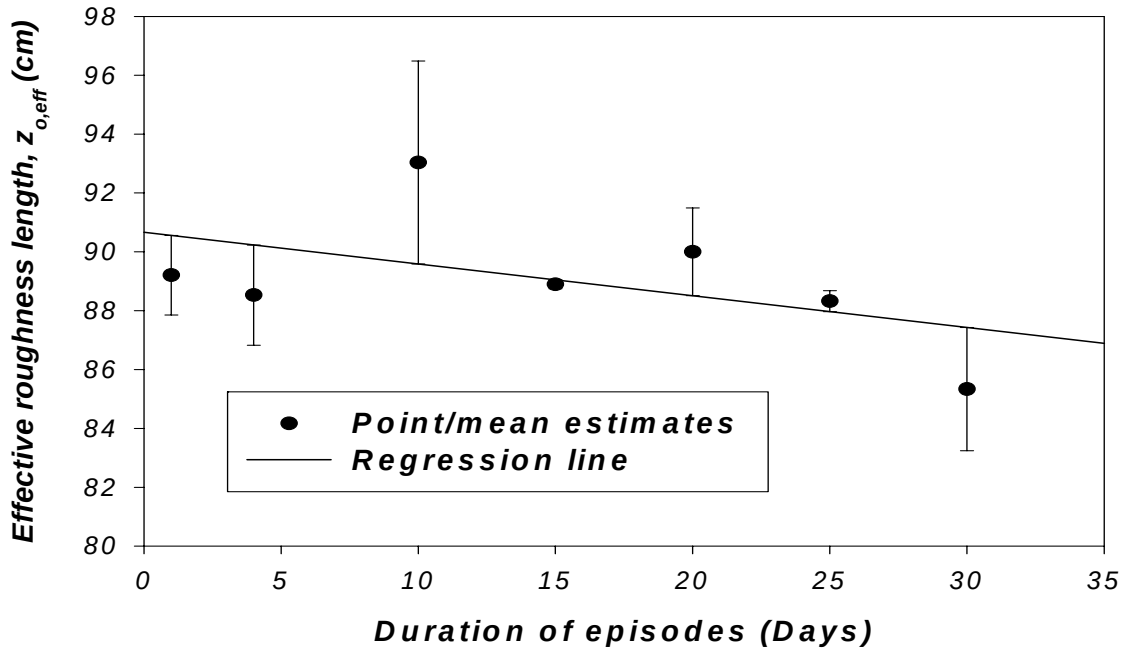

Figure 7.52: Plot showing the linear regression of effective roughness lengths obtained for different duration of episodes. Error bars are based on residuals of points from the regression line.

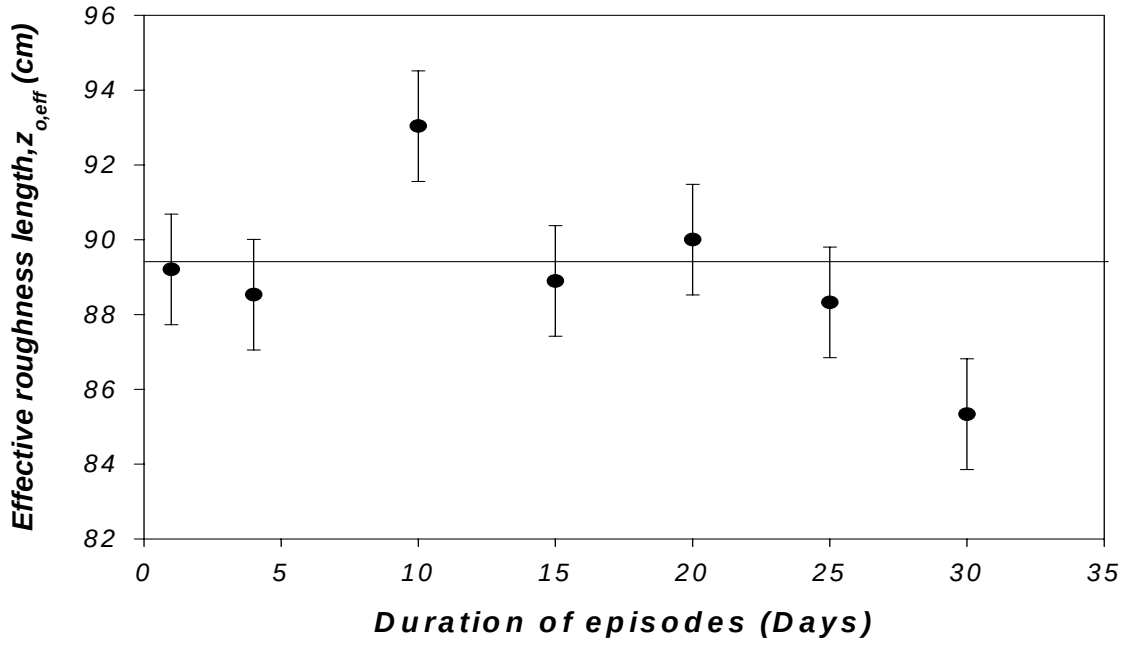

Figure 7.53: Plot showing significant differences between effective roughness lengths obtained for different duration of episodes.

Figure 7.53 shows the range of possible values of the effective roughness length that overlap for episodes of specific durations. It can therefore be deduced from figure 7.53 that:

- The effective roughness lengths obtained for episodes of duration 10 and 30 days are significantly different from those of 1, 5, 15, 20 and 25 days.
- There is no significant difference between roughness lengths obtained for episodes of duration 1, 5, 15, 20 and 30 days.

The detailed information for the regression analysis of the dependence of the duration of episodes on the effective roughness length is given in Tables 7.9 and 7.10. The high t-statistics (> 50) value for the intercept coupled with the low P value (< 0.05) implies there is a very high probability that the intercept is 90.86 cm. By similar arguments, the low t-statistics (< 2.5) value for the slope of the regression line coupled with its high P value (> 0.05) indicates that the duration of the episodes does not contribute much to the estimation of the effective roughness length.

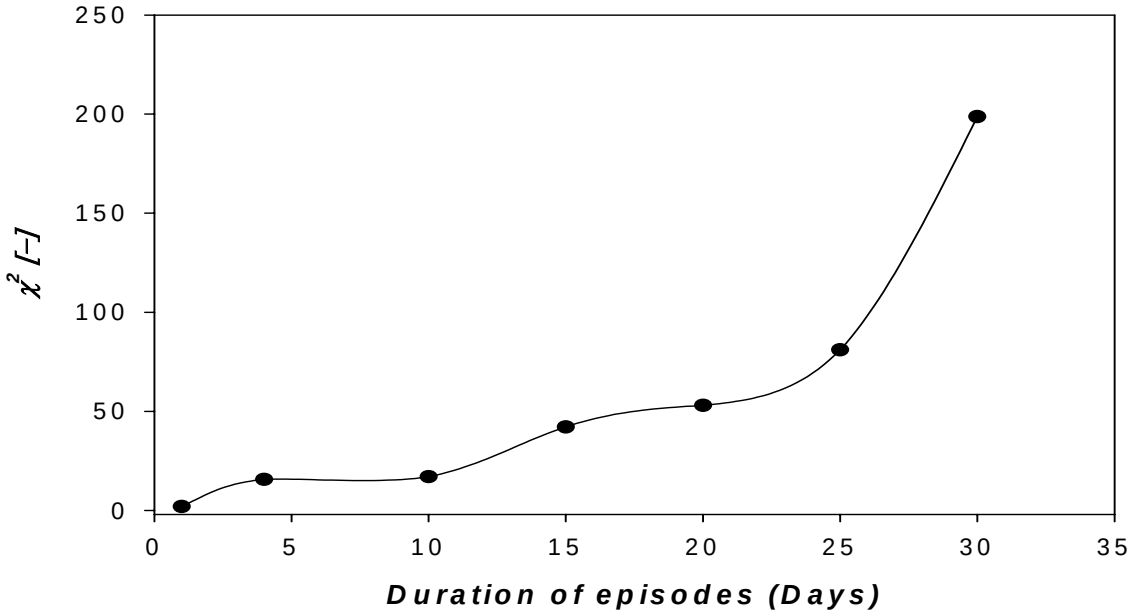

Figure7.54: Plot showing relation between chi square minimum corresponding to the effective roughness lengths obtained for different duration of episodes.

The time course of the chi square minimum for the different duration of episodes is given in figure 7.54. The plot shows an increase in chi square minimum with the duration of episodes as expected (proportional to sum of residuals for the number of data points; Doherty, 2002). However, the increase is not linear but follows a multiple sigmoidal trend where it rises and flattens in some ranges of duration of episodes. The plot/chi square value increases slowly in the ranges 5 – 10, 15 – 20 and increases exponentially in the ranges 1 - 4, 10 - 15, 20-25 and 25 - 30. The regions/points where the plot is steep may indicate the presence of outliers or bifurcations in the inverse solution that tend to increase the chi square values exponentially. Comparison of figures 7.53 and 7.54 suggests that the effective roughness length for episodes with durations of 10 and 30 days may be outliers.

Table 7.8: Regression statistics

Multiple R	0.60
R Square	0.36
Adjusted R quare	0.23
Standard Error	2.30
Observations	7

Table 7.9: Further regression statistics

	Coefficients	***Standard Error***	***t- Stat***	***P-value***	***Lower 95%***	***Upper 95%***
Intercept (cm)	90.86	1.57	57.73	2.95E-08	86.81	94.91
Duration (cm/day)	-0.15	0.09	-1.67	0.12	-0.37	0.08

Table 7.10: Predicted, residual and chi square minimum values

Duration of episodes (Days)	***PEST*** z_o ***(cm)***	***Predicted,*** z_o***(cm)***	***Residuals*** z_o***(cm)***	***Chi square minimum*** χ^2_{min} ***[-]***
30	85.33	86.48	-1.15	198.70
25	85.69	87.21	-1.52	81.02
20	90.00	87.94	2.01	53.01
15	88.90	88.67	0.23	42.11
10	93.04	89.40	3.64	17.02
4	88.53	90.28	-1.74	15.65
1	89.21	90.71	-1.51	2.01

7.7 Concluding Remarks

The detailed analysis of the results obtained from the numerical experimentation on the proposed upscaling law described in Chapter 6 was presented in this chapter. The comparison with other methods using the chi square analysis and other methods of relevance to this thesis was also presented, with particular emphasis on the strengths and weaknesses of each methodology. The analogy drawn between the Monte Carlo random number experiment and the results of this research suggests that effective parameter estimates can be obtained from purely statistical experiments subject to the physical constraints (e.g. prior information) of the physical problem under investigation. More importantly, the investigation suggests that simple averaging techniques have comparable performance to complex time and resource intensive techniques. Additionally, the investigations show that with the appropriate choice of initial parameter set and objective function, the computational effort required in the complex resource-intensive methods can be significantly reduced.

The findings obtained from this research are consistent with related literature. For instance, Noilhan et al. (1997) developed methodologies for areally-averaging land surface parameters over large areas with mesoscale heterogeneity within the framework of the Hapex-Mobilhy and EFEDA experiments. They computed the effective albedo, leaf area index and vegetation cover to be the arithmetic mean of the subgrid scale parameters. Roughness length was averaged logarithmically and the stomatal resistances as harmonic or inversely-averaged values. These aggregation schemes were tested by comparing a 1D SVAT model result with that of the 3D SVAT model results and it was observed that the effective average fluxes obtained with the 1D SVAT model match those of the 3D SVAT with a small relative error. They also observed that for dry vegetated surfaces the variability of the stomatal resistance is relatively small compared to that of the extremely variability observed for partially wet mesoscale canopies. Also, Kabat et al. (1997) investigated the possibility of using a scale-invariant parameterization for scaling soil parameters. They observed that the parameterization of the dynamical relations (Darcy-Richards) governing soil water transport is generally not scale-invariant, therefore, the parameters describing the nonlinear, area-average soil hydraulic functions should be treated as calibration parameters, which do not necessary have any physical meaning. They argued that with specific assumptions, techniques

such as inverse modeling can give effective parameters that can be implemented in large -scale models. They further concluded that the method of using the dominant soil type to represent the whole grid can result in a severe underestimation of evaporation.

The next chapter gives a summary discussion and conclusion for the work undertaken in this thesis. The outlook for future research is also discussed.

8 SUMMARY AND CONCLUSION

8.1 Achievements

The general objective of the thesis was to develop a methodology for upscaling land surface parameters to address the problem of parameterizing subgrid scale heterogeneity effects. To this end, an inverse-SVAT method was developed and applied to both 1D and 3D SVAT models through numerical experimentation.

Specific objectives that were realized include:

- Development of an inverse-SVAT modeling algorithm for estimating effective land surface parameters.
- Derivation of upscaling laws, allowing one to scale distributed land surface parameters from the subgrid scale to the gridscale: 1) roughness length, 2) albedo, 3) emissivity, 4) minimum stomatal resistance, 5) plant insolation factor, 6) vapor pressure deficit factor, 7) leaf area index and 8) Clapp-Hornberger soil parameter ***b***.
- Identification of computationally efficient parameter aggregation rules using simple averaging methods.
- Development of a unified framework for model comparison, enabling comparison of the developed aggregation scheme to existing methods (Arain et al., 1996; Chehbouni et al., 1995, Hu et al. 1999; Noilhan et al., 1996; Shutleworth et al., 1997).
- Development of an experimental environment that allows the coupling of models of different complexity. Ideal for automatic calibration of complex models.
- Establishing the differences in the upscaling laws between stand-alone and 3D versions.
- Identification of optimal objective functions and parameter bounds for enhancing parameter estimation process (general application to inverse problems).
- Identification of indeterminate states of solution; recommendation for selection of initial parameter guesses.

- Sensitivity analysis of surface energy fluxes and moisture indicators to perturbations in vegetation parameters in the Volta Basin.

8.2 Method

This work has demonstrated how inverse modeling can be used to obtain effective land surface parameters and establish scale invariance for the surface energy fluxes (latent and sensible heat fluxes), moisture indicators (Bowen ratio and evaporative fraction), surface temperature, and reflected shortwave radiation.

To justify the choice of initial parameter estimates and also validate the performance the proposed scheme, the PEST's PARREP facility (Doherty, 2000) was coupled to the OSU LSM to produce Chi Square values for some selected parameter values that scan the parameter spaces of the land surface parameters of interest. Plots of Chi Square versus land surface parameters were developed and the results of the proposed method compared to the existing methods surveyed in chapter 2. This provided a tool upon which performances of the various methods were assessed. The results show that the proposed method performs very well, and more importantly, the methods adopted for estimating the initial parameters are appropriate. That is, they guarantee that the initial parameter sets are within a close neighborhood of the optimal solution. This is a major requirement for a successful parameter estimation process.

The thesis also outlined the limitations involved in implementing inverse modeling when the function of interest is not well defined as illustrated in chapter 7 with the example on the Bowen ratio in section 7.2.2 and the analysis in section 7.4. Information obtained from these plots enables one to develop better strategies for analyzing residual errors to improve the parameter estimation process. For example, we know from this study that in the stand alone coupled SVAT-PEST runs, the residual error distribution for parameter estimates based on Hu et al. (1999) is Gaussian for latent heat fluxes and evaporative fraction, hence we can use the relevant parameter transformation to improve the parameter estimates. Similarly, an appropriate parameter transformation can be made in the case of the sensible heat flux estimates based on Hu et al. (1999) which consistently overestimates the observed sensible heat fluxes.

On the other hand, the plots for the evaporative fraction are well within the scale invariant condition for both methods in the coupled MM5-PEST runs. This is due

to the fact that the evaporative fraction is well defined (bounded between 0 and 1) and stable. This is a requirement for parameter convergence and hence makes the evaporative fraction a natural choice for the parameter estimation formulation for roughness length and other land surface parameters. As there exist a strong mutual dependence of the latent and sensible heat fluxes on roughness length, using evaporative fraction as model output response in estimating the roughness length captures parameter sensitivities that properly reflect their interdependencies. This was discussed in section 7.4 of chapter 7.

A criterion for determining effective parameter bounds was developed to restrain the search process from wandering in the non-feasible region of the parameter space and hence reducing model run time considerably. The lower and upper limits of the effective parameter bounds were found to be the harmonic and arithmetic means of the subgrid scale parameters respectively.

Moreover, it is important to note that the proposed method provides effective parameters that are independent of the length of the forcing episode as discussed in chapter 7 (section 7.3.1); in case of other methods (Arain et al., 1996; Chehbouni et al., 1995) this is not the case; Hu et al. (1999) require an approximation on the temperature difference between subgrid and grid to achieve this goal.

8.3 Results

Several aggregation rules for upscaling land surface parameters and aggregating surface energy fluxes were surveyed in chapter 2. The use of simple averaging rules has been reported in several studies (Arain et al., 1996; Blyth et al., 1993) to offer comparable performance to complex and computationally expensive schemes. Chapter 7 gave a detailed analysis of the results of the thesis. More importantly, a simple aggregation scheme based on the geometric mean of distributed land surface parameters was found to be the most appropriate among the simple aggregation rules. A summary of comparison of the proposed method with other methods and the results of the upscaling laws for the 3D and 1D SVAT land surface parameters are given in tables 8.1 and 8.2 respectively.

Table 8.1: Coupled MM5-PEST parameter upscaling laws (3D SVAT).

Parameter	Objective function	Upscaling law	General Comparison to existing methods
Roughness length (z_o)	Evaporative fraction	Parabolic	Represents surface energy fluxes better than Hu et al., (1999).
Surface albedo (α)	Reflected shortwave	Planar	Same as Hu et al. (1997 and 1999), Chehbouni et al. (1995).
Surface emissivity (ε)	Surface temperature	Planar	Same as Hu et al. (1997 and 1999), Chehbouni et al. (1995).
Insolation factor (*Rgl*)	Evaporative fraction	Parabolic	Represents surface energy fluxes better than Arain et al. (1996) and Blyth et al. (1993). Same values as the geometric mean.

Table 8.2: Coupled 1D SVAT-PEST parameter upscaling laws.

Parameter	**Objective function**	**Upscaling law**	**Comparison**
Roughness length (z_o)	Evaporative fraction	Planar or weak Parabolic	Represents surface energy fluxes better than Hu et al., (1999) and geometric mean.
Surface Albedo (α)	Reflected shortwave	Planar	Same as existing methods.
Surface emissivity (ε)	Surface temperature	Planar	Same as existing methods.
Minimum stomatal resistance (***Rcmin***)	Evaporative fraction	Parabolic	Represents surface energy fluxes better than Arain et al. (1996) and Blyth et al. (1993). Same as the geometric mean.
Insolation factor (***Rgl***)	Transpiration	Parabolic	Represents surface energy fluxes better than Arain et al. (1996) and Blyth et al. (1993). Same as the geometric mean.
Leaf area index (***LAI***)	Transpiration	Parabolic	Represents surface energy fluxes better than Arain et al. (1996) and Blyth et al. (1993). Same as the geometric mean.
Vapour pressure deficit factor (***Hs***)	Transpiration	Parabolic	Represents surface energy equally as existing schemes. Same as the geometric mean.
Clapp-Hornberger parameter (***b)***	Soil evaporation	Parabolic	N/A

8.4 Conclusion

In conclusion, the proposed method provides a convenient framework for upscaling land-surface parameters such that surface energy fluxes and moisture indicators in complex terrains become scale invariant. To extend the applicability of the proposed method, an investigation of its implementation in a full mesoscale climate model (MM5) was undertaken to account for the lateral interactions between atmospheric state variables of adjacent grids and the result was very promising. It was observed that the overall upscaling laws (planar, parabolic) themselves do not differ between the full 3D version and the stand alone version. However, the parameters appearing in the regression function differ: in general, the curvature show higher slopes in the fully 3D mode.

8.5 Outlook

Outlook for future work would include the implementation of the derived scaling laws in a mesoscale meteorological model to account for subgrid scale effects of the heat fluxes and apply it for global and regional climate simulations. In particular, the influence of cluster effects in subgrid scale variability must be investigated. Extended runs are also needed to investigate in detail, the influence of seasonal variability of land surface parameters on scale invariance and how to properly represent spatio-temporal variability of land surface processes at different scales of RCMs and GCMs.

The impact of different statistical distributions of land surface parameters on aggregation schemes for land surface parameters and surface energy fluxes must also be investigated in detail. In particular, cluster effects and the influence of parameter correlations needs to be investigated and incorporate the assumption of distinct variability of land surface parameters. Also, detail statistical experiments that would include higher moments and related statistical parameter distributions of subgrid scale effects (instead of only mean and standard deviation used in this research) needs to be investigated.

9 REFERENCES

André, J.-C., Bougeault, P., and Goutorbe, J.-P., (1990): Regional estimates of heat and evaporation fluxes over non-homogeneous terrain. Examples from the HAPEX-MOBILHY Programme. *Boundary Layer Meteorol.*, ***50***, 77 – 108.

Anji S., Giorgi, F., and Dickinson, R. E. (1994): Simulating fluxes from heterogeneous land surfaces: Explicit subgrid method employing the Biosphere-Atmosphere transfer scheme (BATS). *J. Geophys. Res*., **99(D9**), 18,651-18,667.

Arain, M. A., Michaud, J., Shuttleworth, W. J. and A. J. Dolman (1996): Testing of Vegetation parameter Aggregation Rules applicable to the Biosphere-Atmosphere Transfer Scheme (BATS) and the FIFE site. *J. Hydrology*, **177**, 1-22.

Arain, M. A., Burke, E. J., Yang, Z.-L. and Shuttlewoth, W. J. (1999): implementing surface parameter aggregation rules in the CCM3 global climate model: regional responses at the land surface. *Hydrol. Earth Sys. Sci.*, **3(4)**, 463 – 476.

Avissar, R., and Pielke, R. (1989): A parameterization of heterogeneous land surfaces for atmospheric numerical models and its impact on regional meteorology. *Mon. Wea. Rev.*, **117**, 2113 – 2136.

Bastiaanssen, W. G. (1995): Regionalisation of surface flux densities and moisture indicators in composite terrain. *PhD thesis, Wageningen Agricultural University*.

Bates, M. and D. G. Watts, (1988): Nonlinear Regression Analysis and its Applications. *John Wiley and Sons, New York*. 32 - 66.

Beljaars, A. C., and Tiedkte, (2001): Meteorological training course lecture notes, ECMWF.

Betts, A. K., and Ball, J. H. (1998): FIFE surface climate and site-average dataset 1987 – 89. *J. Atmos. Sci.*, **55**, 1091 – 1108.

Blyth, E.M., Dolman, A. J., and Wood N. (1993): Effective resistance to sensible and latent heat flux in heterogeneous terrain. *Quart. J. Roy. Soc*. **119**, 423 – 442.

Bonan, G. B., Pollard, D., and Thompson, S. L. (1993): Influence of subgrid-scale heterogeneity in leaf area index, stomatal resistance, and soil moisture on grid-scale land-atmosphere interactions *J. Climate*, **6**, 1882 -1897.

Brubaker, K. L., D. Entekhabi, and P.S. Eagleson (1993). Estimation of continental precipitation recycling. *J. Climate*, **6**, 1077 – 1089.

Brutsaert, W. (1982): Evaporation into the atmosphere: Theory, history and applications, *Kluwer Academic Press*.

Carlson, T. N., and Boland, F. E. (1978): Analysis of urban-rural canopy using a surface heat flux/temperature model. *J. Appl. Meteorol*., **17**, 998 – 1013.

Chehbouni, A., Njoku, E. G., Lhomme, J. P., and Kerr, Y. H. (1995): Approaches for averaging surface parameters and fluxes over heterogeneous terrains. *J. climate*, **8**, 1386-1393.

Chen, F. and Dudhia J. (2001): Coupling an Advanced Land-Surface/Hydrology Model with the Penn State/NCAR MM5 Modeling System, Part I: Model Implementation and Sensitivity. *Mon. Weath. Rev,*. **129**, 569 –585.

Chen, F., and Avissar, R. (1994a): The impact of land-surface wetness on mesoscale heat fluxes. *J. Appl. Meteorol*., **33**, 1324 – 1340.

Claussen M. (1995): Flux aggregation at large scales: on the limits of validity of the concept of blending height. *J. Hydrology*, **166**, 371 – 382.

Claussen, M. (1989): Subgrid-scale fluxes and flux divergence in a neutrally stratified, horizontally inhomogeneous surface-layer, *Beitr. Phys. Atmos.* **62**, 235 – 246.

Claussen, M. (1990): Area –averaging of surface fluxes in a neutrally stratified, horizontally inhomogeneous atmospheric boundary layer. *Atmos. Environ*. **24a**, 1349 – 1360.

Claussen, M. (1991): estimating of areally-averaged surface fluxes, *Boundary-Layer Meteorol*. **54**, 387 – 410.

Claussen, M. (1995a): Estimation of regional heat and moisture fluxes in homogeneous terrain with bluff roughness elements, *J. Hydrol*ogy, **166**, 353 – 369.

Claussen, M. (1995b): Flux aggregation at large scales: on the limits of the concept of the blending heights. *J. Hydrology*. **166**, 371 – 382.

Cooley R. L. and R.L. Naff, (1990): Techniques of Water-Resources Investigations of the United States Geological Survey-Regression Modeling of Groundwater Flow (Chapter 4), *USGS Publication Series*, 50 – 74.

Cosby, B. J., Hornberger G. M., Clapp, R. B. and Ginn, T. R. (1984): A statistical exploration of the relationships of soil moisture characteristics to the physical properties of soils. *Water Resour. Res.*, **20**, 682 – 690.

Cuenca, R. H., Ek, M. and Mahrt, L. (1996): impact of soil water property parameterization on atmospheric boundary-layer simulation. *J. Geophys. Res.*, **101**, 7269 -277.

Deardoff, J. W. (1978): Efficient prediction of ground surface temperature and moisture, with inclusion of a layer of vegetation. *J. Geophys. Res.*, **83**, **(C4)**, 1889 -1903.

Dickinson, R. E. (1984): modeling evapotranspiration for three-dimensional global climate models. *Climate Processes and Climate sensitivity: Maurice Ewing vol. 5, Geophys. Monogr.*, No.**29**, *Amer. Geophys. Union*, 58 – 72.

Dickinson, R.E., Errico, R. M., Giorgi, F., and Bates, G. T. (1989): A regional climate model for the Western U.S., Clim. Change, 15, 383 – 422.

Diekkrüger, B., D. Söndgerath, K.C. Kersebaum and McVoy, C.W. (1995): Validity of agroecosystem models - A comparison of the results of different models applied to the same data set. Ecological Modelling, 81(1-3):3-29.

Diekkrüger, B. (2003): Upscaling of hydrological models by means of parameter aggregation techniques. In: Neugebauer, H.J. and Simmer C. (Eds.): Dynamics of earth systems. Lecture Notes in Earth Sciences, Springer Verlag, 97, 145-165.

Diekkrüger, B. (2003): Models - calibration, validation, sensitivity analysis (I and II). Presentation at Bonn (http://www.giub.uni-bonn.de/hrg/Poster.htm).

Doherty J., (2002): Model-Independent Parameter Estimation (PEST), Watermark Numerical Computing, 2-1 – 2-19.

Dolman, A. J. (1992): A note on areally-averaged evaporation and the value of the effective surface conductance. J. Hydrology, 138, 583 – 589.

Ek, M., and Mahrt, L. (1991): OSU 1-D PBL Model User's Guide version 1.0.4, Department of Atmospheric Sciences, Oregon State University, 3 - 12.

Entekhabi, D. and Eagleson, P. S. (1989): Land surface hydrology parameterization for atmospheric General Circulation Models including subgrid scale spatial variability. *J. climate*, **2**, 816 – 813.

Famiaglietti, J. and Wood, E. F.: Evapotranspiration and runoff from Large areas: Land surface hydrology for atmospheric General Circulation Models, in E. F. Wood (ed), Land surface atmospheric interactions for climate models: Observations, Models and Analysis. *Kluwer Academic Publishers*, 179 – 204.

Friedrich, K., and Mölders, N. (2000): On the influence of surface heterogeneity on latent heat fluxes and stratus properties. *Atmos. Res*., 54, 59 -85.

Gao, X. and Sorooshian, S. (1994): A stochastic precipitation disaggregation scheme for GCM applications. *J. Climate,* **7**, 238 - 247.

Garratt, J. R., and Prata, A. J. (1996): Surface radiation budget: Scaling up from local observations, in J. B. Steward, E. T. Engman, R. A. Feddes, and Y. Kerr (eds), Scaling up in Hydrology using remote sensing, (Chap. 5). *John Wiley and Sons, N.Y.,* 77 – 91.

Garratt, J. R., Pielke, R. A., Miller, W. F., and Lee, T.J. (1990): Mesoscale model response to random, surface-based perturbations – A sea breeze experiment. *Boundary-Layer Meteorol*., **52**, 313 – 334.

Hall, F. G., Huemmrich, K. F., Goetz, S. J., Sellers, P. J., and Nickeson, J. E. (1992): Satellite remote sensing of surface energy balance: Success, failures, and unresolved issues in FIFE. *J. Geophys. Res.***, 97 (D17)**, 19,061 – 19,089.

Hanks, R.J., and Aschroft, G. L. (1986): Applied soil physics. *Springer-Verlag*, 159.

Jacquemin, B., and Noilhan, J. (1990): Sensitivity study and validation of a land surface parameterization using the HAPEX-MOBILHY data set. *Boundary layer Meteorol.,* **52**, 93 – 134.

Jhorar R.K., Bastiaanssen W.G.M., Feddes R.A., and Van Dam J.C. (2002): Inversely estimating soil hydraulic functions using evapotranspiration fluxes. *J. Hydrology*, **258**, 198 – 213.

Kim, J., and Ek, M. (1995): A simulation of the surface energy budget and soil water content over the Hydrologic Atmospheric Pilot Experiments-Modélisation du Bilan Hydrique forest site. *J. Geophys. Res.*, **100(D10)**, 20, 845 – 20, 854.

Koren, V., Schaake, J., Mitchell, K., Duan Q.-Y. and Chen, F. (1999): A parameterization of snowpack and frozen ground intended for NCEP weather and climate models. J. Geophys. Res., **104**, 19,569 – 19,585.

Koster, R. D. and Suarez, M. J. (1992): A comparative analysis of two land surface heterogeneity representations. *J. Climate,* **5,** 1379 – 1390.

Koster, R., and Milly, C. P. (1997): The interplay between transpiration and runoff formulations in land surface schemes used with atmospheric models. *J. Climate*, **10**, 1578 – 1591.

Kunstmann, H. and Jung, G. (2003): Water Resources Systems-Water Availability and Global Climate Change. *Proceedings of Symposium HS02a, IUGG2003, IAHS Publication No. 280,* Sapporo, July 2003.

Lhomme, J. P., Chehbouni, A., and Monteny, B. (1994): Effective parameters for surface energy balance in heterogeneous landscape. *Boundary-Layer Meterol*. **71**, 297 – 309.

Li, B. and Avissar, R. (1994): The impact of spatial variability of land surface characteristics on land surface heat fluxes. *J. Climate*, **7**, 527 – 537.

Louis, J. F. (1979): A parametric model of vertical eddy fluxes in the atmosphere. *Boundary-Layer Meteorol*., **17,** 187 – 202.

Louis, J. F., Tiedkte, M., and Geleyen, J. F. (1982): A short History of the operational PBL - Parameterization of ECMWF, Workshop on planetary boundary layer parameterization. *European Centre for Medium Range Weather Forecast, U.K*., pp 59 – 79.

Mahrt, L. (1987): Grid-averaged surface fluxes. *Mon. Wea. Rev.*, 115, 1550 – 1560.

Mahrt, L. and Ek, M. (1984): The influence of Atmospheric stability on potential evaporation. *J. Clim. Appl. Meteorol*., **23**, 222 – 234.

Mahrt, L. and Sun, J. L. (1995): Dependence of surface exchange co-efficients on averaging scale and grid size. *Quart. J. Roy. Meteorol. Soc*., **121**, 1835 – 1852.

Mahrt, L. (2000): Surface heterogeneity and vertical structure of the boundary layer. *Boundary-Layer Meteorol.,* **96**, 33-62.

Manabe, S. (1969). Climate and the ocean circulation 1. the atmospheric circulation and the hydrology of the earth's surface. *Mon. Weather. Rev.,* **97(11)**:739-774.

Mason, P. J. (1988): The formation of areally-averaged roughness lengths. *Quart. J. Roy. Meteorol. Soc*., **144**, 399 - 420.

McCumber, M. C., and Pielke, R. A. (1981): Simulation of the effects of surface fluxes of heat and moisture in a mesoscale numerical model soil layer. *J. Geophys. Res.,* **86**, 9929 – 9938.

Moran M. S., Humes K. S., and Pinter P. J. (1997): The scaling characteristics of remotely-sensed variables for sparsely-vegetated heterogeneous landscapes. *J. Hydrology*, **190**, 337 – 362.

Nakaegawa T., Oki T., and Musiake K. (2001): Aggregation criteria for surface heat balances in a heterogeneous area based on a linear model. *Adv. Water Res.,* **24**, 1159 – 1171.

Nicholson, S.E., C. J. Tucker, and M. B. Ba, (1998): Desertification, drought, and surface vegetation: An example from the West African Sahel. *Bull. Amer. Meteor. Soc.,* **79**, 815 – 829.

Noilhan, J. and Planton, S. 1989): A simple Parameterization of Land Surface Processes for Meteorological Models. *Mon. Wea. Rev.*, **117**, 536-549.

Pan, H.-L., and Mahrt, L. (1987): Interaction between soil hydrology and boundary-layer development. *Boundary Layer Meteorol*., **38**,185 – 202.

Peters-Lidard, C. D., Blackburn, E., Liang X., and Wood, E. F. (1998): The effect of soil thermal conductivity parameterization on surface energy fluxes and temperatures. *J. Atmos. Sci.*, **55**, 1209 – 1224.

Pielke, R. A., Zeng, X., Lee T. S, Dalu, G. A. (1997): Mesoscale fluxes over heterogeneous flat landscapes for use in larger scale models. *J. Hydrology*, **190**, 317 – 336.

Press, W. H., Teukolsky, S. A., Vetterling, W. T., and Flannery B. P. (1992): Numerical Recipes in FORTRAN: the art of scientific computing, Second Edition. *Cambridge University Press*, (Chap. 7).

Raupach, M. R. and Finnigan, J. J. (1995): Scale issues in boundary layer meteorology: Surface energy balances in heterogeneous terrain. *Hydrol. Processes***, 9**, 589 – 612.

Raupach, M. R., (1991): Vegetation-Atmosphere interaction in homogeneous and heterogeneous terrain: Some implications of mixed-layer dynamics. *Vegetatio.*, **91**, pp 105 – 120.

Raupach, M. R.: Vegetation-Atmosphere interaction and surface conductance at leaf, canopy and regional scales. *Agric. For. Meteorol*., 73, 151 – 179.

Rodgers C. D., (2000): Inverse methods for atmospheric sounding-Theory and Practice. *World Scientific Publishing*, 81-100.

Sambridge M. and K. Mosegaard (2002): Monte Carlo Methods in Geophysical Inverse Problems. *Rev. Geophysics*, **40**, 3, 1 – 25.

Schaake, J. C., Koren, V. I., Duan, Q. Y., Mitchell, K., and Chen F. (1996): A simple water balance model (SWB) for estimating runoff at different spatial and temporal scales. *J. Geophys. Res*., **101**, 7461 – 7475.

Sellers, P. J., Heiser, M., and Hall, F.G. (1992): Relations between surface conductance and spectral vegetation indices and intermediate (100^2 m to $15km^2$) length scales. *J. Geophys. Res.*, **97(D17)**, 19,033 – 19,059.

Schaake, J. C. Jr. (1994): Science strategy of GEWEX Continental-Scale International Project (GCIP). *Adv. Water Resour.*, **17**, 117 – 127.

Shuttleworth, W. J. (1991): The modellion concept. *Rev. Geophys*., **29**, 585 – 606.

Shuttleworth, W. J. (1997): Combining remotely-sensed data using aggregation rules for surface parameters in global models. *Hydrol. Earth Sys. Sci.*, **2**, 149 – 158.

Shuttleworth, W. J., Yang, Z.-L., and Arain, M. A. (1997): Aggregation rules for surface parameters in global models. *Hydrol. Earth Sys. Sci.*, **2**, 217 – 226.

Sun N. (1994): Inverse Problems in Groundwater Modeling. *Kluwer Academic Publishers*, 39-51.

Tarantola, A. (1987): Inverse Problem Theory. *Elsevier*, pp 613.

Taylor C. M. Harding R. J. and Thorpe A. J. (1997): A mesoscale simulation of land surface heterogeneity from HAPEX-Sahel. *J. Hydrology*, **188 -189**, 1040 – 1066.

Tian, H., Melillo J.M., Kicklighter, D. W., McGuire, A.D., and Helfrich, J. (1999): The sensitivity of terrestrial carbon storage to historical climate variability and atmospheric CO_2 in the United States. *Tellus*, **51B,** 414-452.

Tikhonov, A. N. (1963): Solution of incorrectly formulated problems and the regularization method. *Soviet Math. Dokl.*, **4**,1035-1038.

van de Giesen, N., Andreini, M., van Edig, A., and Vlek, P. (2001): Competition for water resources of the Volta Basin. IAHS Publication, **268**, 99-205, IAHS Press.

Viterbo, P. (1996): The representation of surface processes in General Circulation Models, (PhD Thesis), *ECMWF*.

Viterbo, P. and Beljaars, A. C. (1995): An improved land surface parameterization scheme in the ECMWF model and its validation. *J. Climate*, 8, 2716 – 2748.

Walker, J. and Rowntree, P. R. (1977): The effect of soil moisture on circulation and rainfall in a tropical model. *Quart. J. Roy. Meteorol. Soc.*, **103**, 29 – 46.

Weisstein E.W.,(1999): Box-Muller Transformation. *MathWorld, Wolfram Research Inc.*,

Wetzel, P., and Chang, J. T. (1987): Concerning the relationship between evapotranspiration and soil moisture. *J. Climate Appl. Meteor.*, **26**, 18 – 27.

Wieringa, J. (1986): Roughness dependent geographic interpolation of surface wind speed average. *Quart. J. Roy. Meteorol. Soc.*, **112**, 867 -889.

Wood, E. F. (1994): Scaling soil moisture and evapotranspiration in runoff models. *Adv. Water Resour.*, **17**, 25 – 34.

Wood, E. F. and Lakshmi, E. (1993): Scaling water and energy fluxes in climate systems: Three land-atmospheric modeling experiments. *J. Climate***, 6**, 839 – 857.

Wood, N. and Mason, P. J. (1990): The influence of stability on effective roughness lengths, *in Proc. of the 9th Symposium on Turbulence and Diffusion*, (Roskilde, April 30 - May 3, 1990), 247 – 249.

Xiao, X., Melillo, J. M., Kicklighter, D. W., Pan, Y., McGuire, A. D., and Helfrich, J. (1998): Net primary production of terrestrial ecosystems in China and its equilibrium responses to changes in climate and atmospheric CO_2 concentration. *Acta Phytoecologica Sinica* **22(2),** 97-118.

Appendix A: Model Description

1 OSU LSM (1D SVAT Model)

The OSU LSM is a stand-alone, uncoupled, 1D column version used to execute single-site land-surface simulations. It was developed by the climate group of Oregon State University and has been widely used in various studies on climate and environment.

It is capable of predicting single site-specific thermodynamical and hydrological state variables of the land, vegetation and atmosphere components of the earth's climate system (Mitchell, 2000). It is based on the coupling of the diurnally-dependent potential evaporation approach of Ek and Mahrt (1984), the multi-layer soil model of Mahrt and Pan (1984), and the primitive canopy model of Pan and Mahrt (1987). Several modifications have been made over the past 20 years. It was extended by Chen et al. (1996) to include the canopy resistance formulation of Noilhan and Planton (1989) and Jacquemin and Noilhan (1990). It has a single-layer canopy and multi-layer soil geometry of up to 20 layers. It simulates the following prognostic variables: soil moisture and temperature in each soil layer, and snow cover.

In this traditional 1D uncoupled mode, near-surface atmospheric forcing data is required as input. The observation data is available at 30 minutes interval (or interpolated to 30-minute time intervals from about 1-6 hour interval observations). For observation intervals longer than 1-hour, the incoming surface solar insolation are interpolated with a solar zenith angle weighting, in order to capture the full amplitude of the diurnal solar insolation. The required forcing data are 1) air temperature at 3m above ground, 2) air humidity at 3m above ground, 3) surface pressure 4) wind speed at 10m above ground, 5) surface downward longwave radiation, 6) surface downward solar radiation and 7) precipitation.

A significant extension to OSU LSM code is the inclusion of the Fortran "NAMELIST" construct which provides an alternative parameter input facility for external models (e.g. random number generator and PEST input/output communication files) without the need for recompilation of the whole code.

The main steps involved in the computation of SVAT state variables are summarized as follows:

- The input/output files are initialized with data from the control file (model configuration, site characteristics, and initial conditions).
- The time-step loop (including optional spin-up loop as indicated by control file) is invoked to enable the reading of atmospheric forcing data and conversion of signs and units to forms consistent with the model physics.
- The monthly-mean surface greenness and surface albedo are interpolated to Julian day of the model time step.
- The downward solar, longwave radiation and wind speed from input forcing are assigned to appropriate model variables and the intermediate model variables (e.g. actual and saturated specific humidity from input atmospheric forcing) are computation.
- The model physics are invoked to numerically solve the governing equations of the soil, vegetation and atmospheric interactions. The state variables and surface energy fluxes over each time step are continually updated.
- The output data from the simulation is written to the appropriate output files for each time step.

A schematic for the OSU LSM model routine is given in figure A.1. The thermodynamic and energy related variables computed include the sensible heat fluxes, temperature (soil, air and surface), short and long wave radiations (incoming and outgoing) soil heat flux and other intermediate energy terms. The hydrological variables produced include latent heat fluxes, humidity, soil moisture (for each layer), transpiration, direct soil evaporation, evapotranspiration and other water related variables.

It is currently been developed by the NOAH group (**N**ational Centers for Environmental Prediction, **O**regon State University, **A**ir Force and the **H**ydrologic Research Laboratory) and hence its new name NOAH LSM. The detailed model physics and parameters can be found in chapter 3. Additional information can be found in Chen and Dudhia (2001), Ek and Mahrt (1991) and Mitchell (2000).

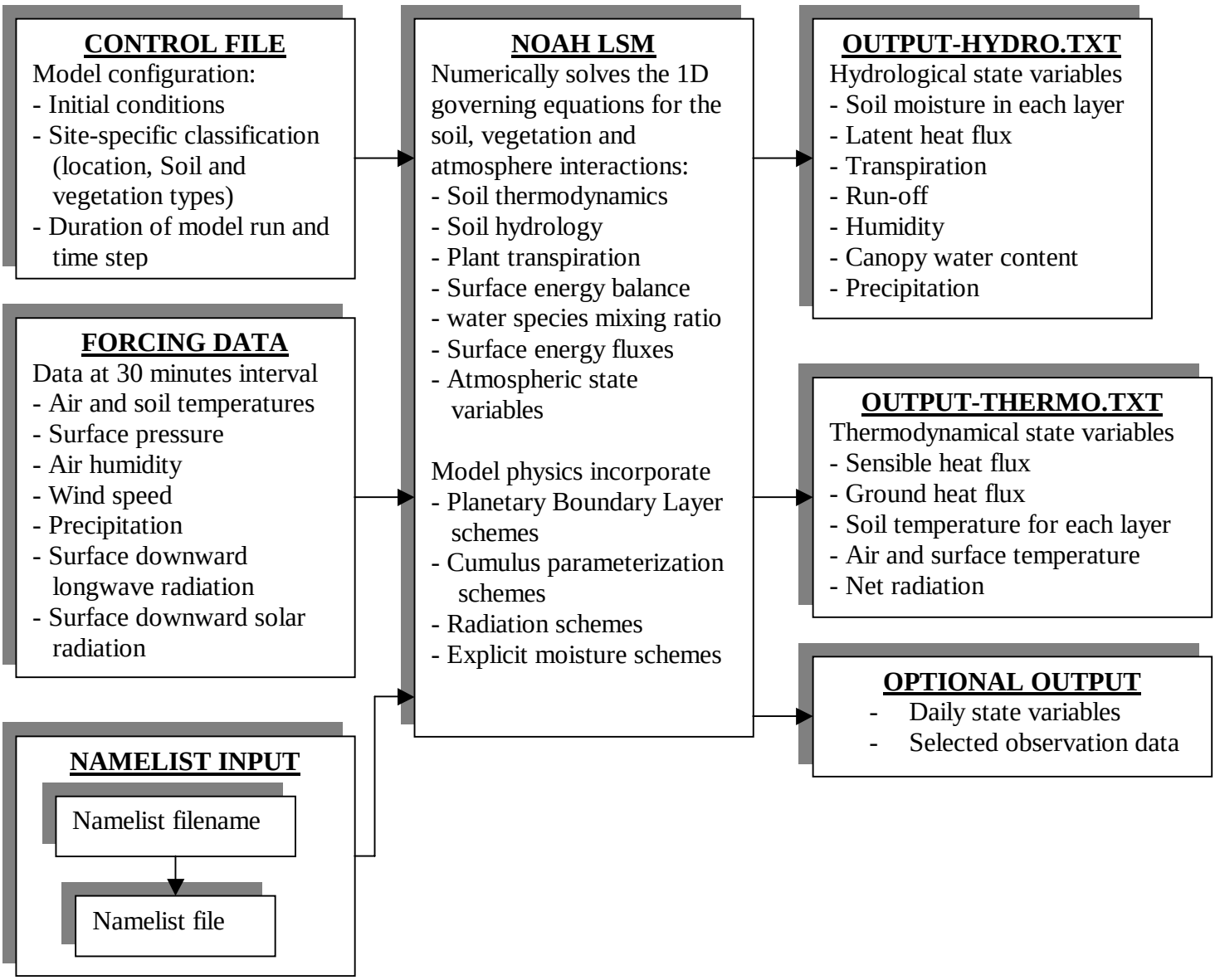

Figure A. 1: Schematic of the OSU LSM model.

2 Mesoscale Model (3D SVAT Model): Coupled MM5-OSU LSM

The Penn State University (PSU)/National Centre for Atmospheric Research (NCAR) mesoscale model (MM5) was used in the fully coupled 3D SVAT-PEST experiment. MM5 is a limited area, nonhydrostatic, terrain following sigma-coordinate model. It consists of a collection of climate physics algorithms for predicting mesoscale atmospheric phenomena. It has been developed as a community mesoscale model and has been continuously improved over the years by a wide group of international developers/users. The model improvements implemented over the years include:

- Multiple nesting capability and nonhydrostatic dynamics, which allows for its application in at scales of very high resolution.
- Multi-tasking capabilities on shared and distributed memory machines, and Four dimensional data assimilation capability.

Included in the model are a number of variable resolution terrain and landuse data schemes. The data information include: landcover type, soil type, deep soil properties, vegetation fraction, and land-water mask data set. Additionally, the model allows for much flexibility in multi-nesting applications. This multi-nesting facility permits the model runs from global or synoptic scale down to cloud resolving scale in a single model run. The model can be run in both 2-way and 1-way nesting modes. For the 2-way nesting mode, the nest's input from the coarse domain comes via its boundaries, while the feedback to the coarser domain occurs over the nest interior. Multiple nests and moving nests are possible and the nesting ratio is always 3:1. For the 1-way nesting mode, feedback from the nest domain to the mother domain is not permitted. The fine model domain is driven by the coarse model domain with no restriction on the nesting ratio. In the 1-way mode, the model is first run with the coarse domain to create output information that is time-interpolated to provide initial and boundary conditions for the nest domain. Because it is vital that the terrain information of the nest domain is consistent with the coarser domain in the boundary zone, the terrain preprocessor is run with both domains. Fig A.3 shows the schematic for the one-way nesting approach. A detail model description of MM5 can be found in Dudhia et al., (2000).

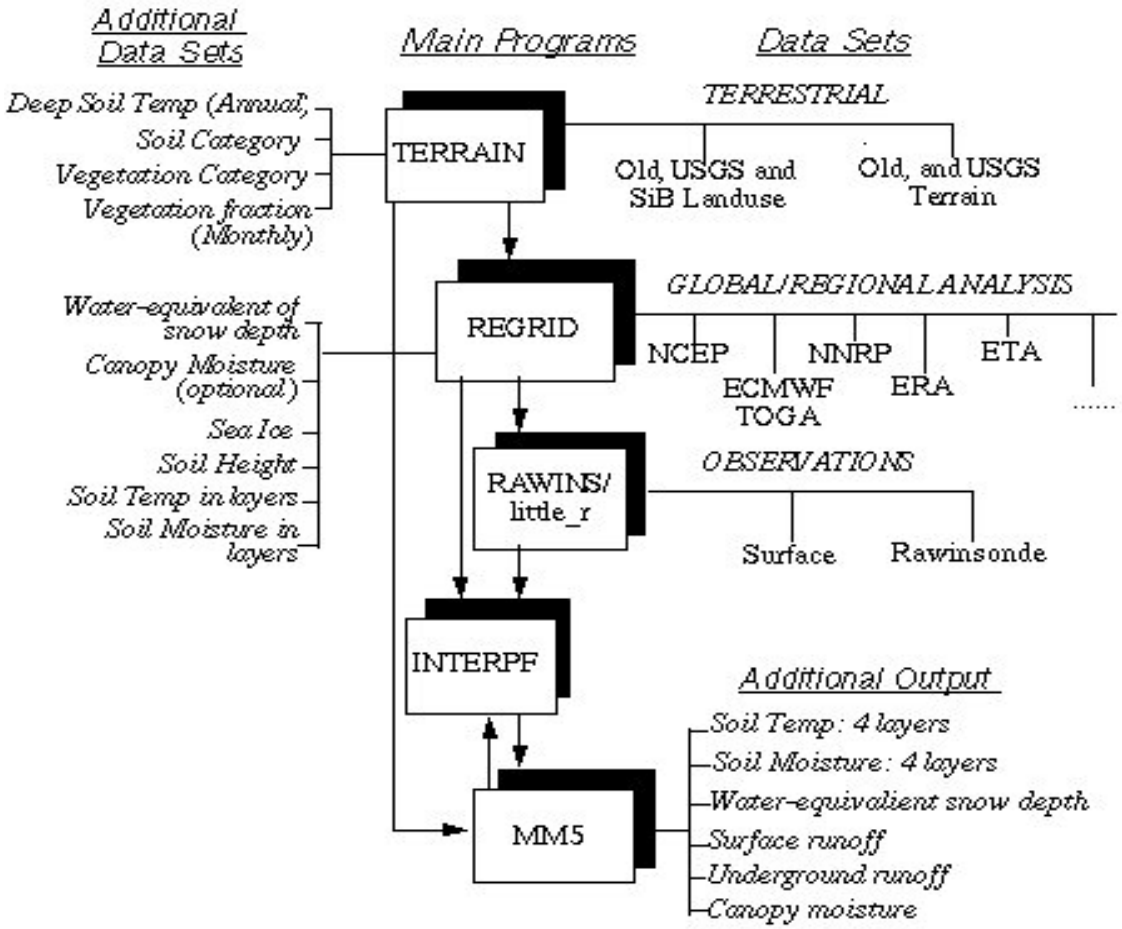

Figure A. 2: Schematic for MM5 modeling system. Source: MM5 Homepage (www.mmm.ucar.edu /mm5/lsm /lsm-docs.html).

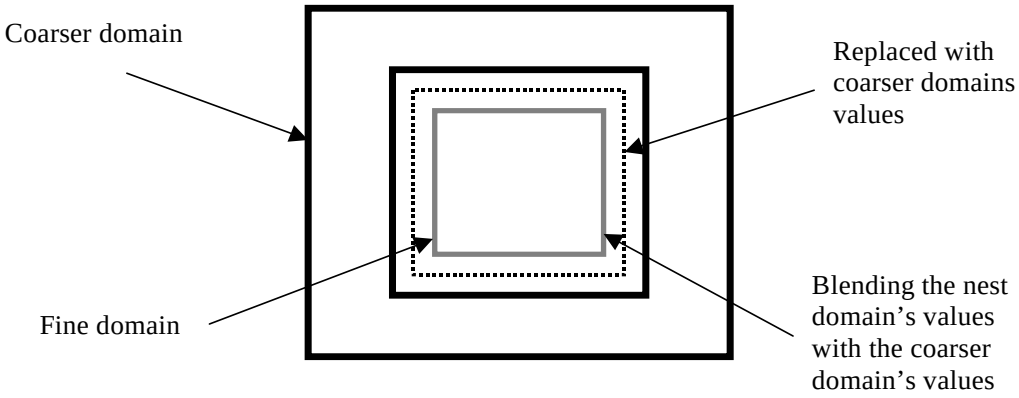

Figure A. 3: Schematic of one-way nesting showing blending of a nest domain's boundary and initial conditions with that of a mother domain. Source: (Dudhia et al., 2000)

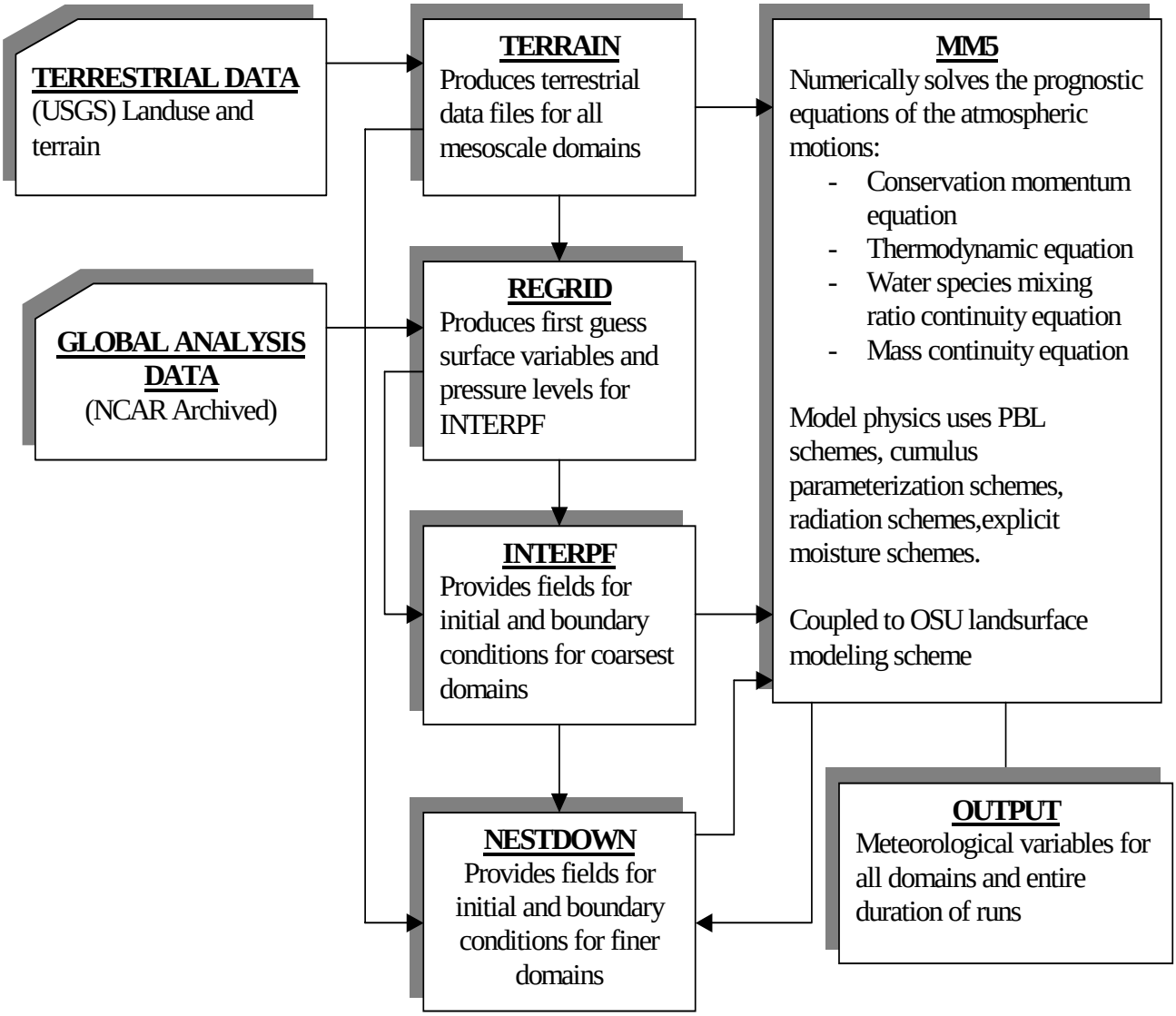

Figure A. 4: Schematic of the one-way nesting approach.

3. The Nonlinear Optimal Parameter Estimation Tool (PEST)

Parameter optimization is achieved using the highly efficient Gauss-Marquardt-Levenberg method for which the discrepancies between model-generated variables and corresponding observation is reduced to a minimum in the least square sense. While requiring that the model output be differentiable with respect to the adjustable parameters, this method normally requires fewer model runs to achieve convergence to the optimal set than existing parameter estimation methods. Figure 5.10 shows the structure of the PEST scheme.

PEST requires three input files:

- Template files, one for each model input file on which model parameters needed for optimization are identified
- Instruction files, one for each model output file on which model generated observations required for the objective function are identified, and
- An input control file, which provides PEST with the names of all template and instruction files, the names of the corresponding model input and output files, the problem size, control variables, initial parameter values and bounds, observation data and related settings necessary for the parameter estimation process.

The template file provides a medium through which PEST reads model input parameters and transform these parameters to the appropriate precision and format for the parameter estimation process. The instruction files provides an interface by which PEST reads model generated output and transform them to the required precision and form for the computation of the objective functions and derivatives required for the parameter estimation process. Unlike parameter values for which precision is important but not a strict requirement, precision in the representation of model-generated output is critical for the success of the parameter estimation process. The Gauss-Levenberg-Marquardt method of nonlinear parameter estimation upon which the PEST algorithm is based, requires that the derivative of each model-generated output with respect to each parameter be computed for every optimization iteration. PEST computes these derivatives using the finite difference technique or one of its three-point variants

(Doherty, 2002). In all cases, the derivative depends on the difference between two or three model-generated output on the basis of incrementally-varied parameter values.

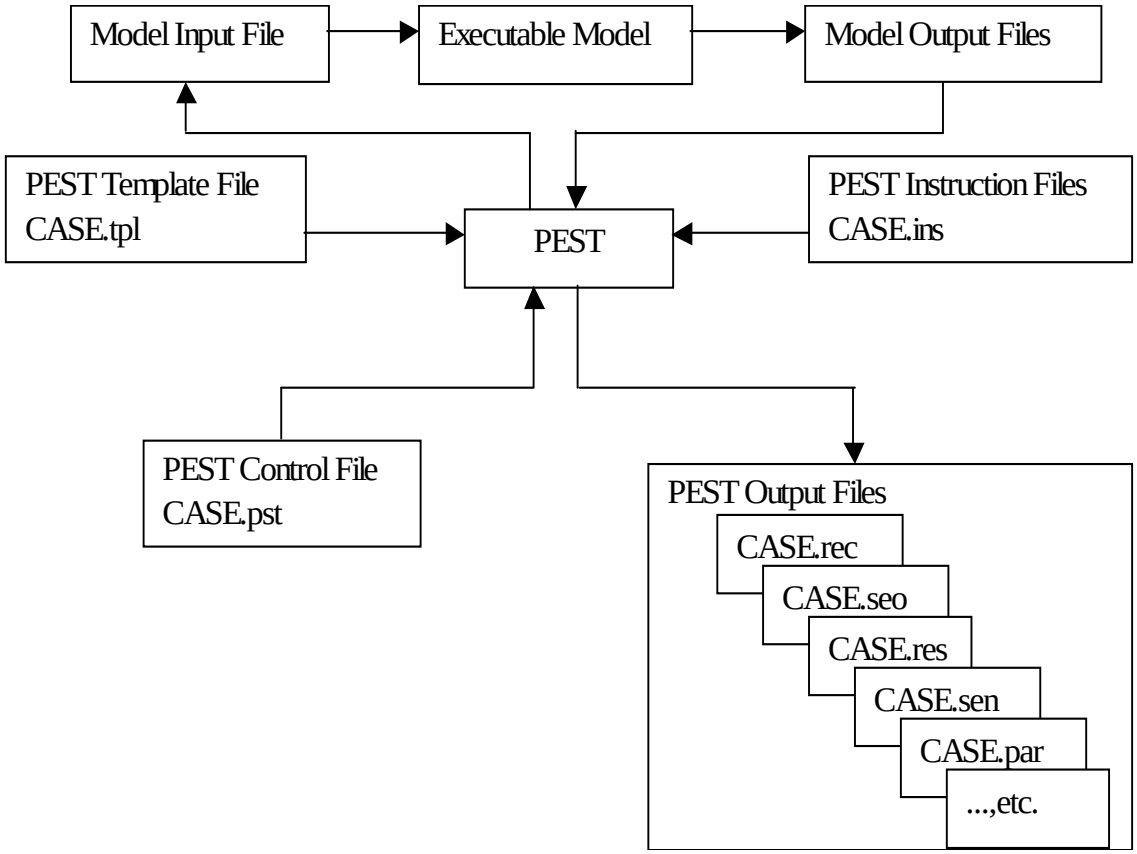

Figure A. 5: Schematic of the PEST model.

The control file is the control center of parameter estimation process as it provides the platform for coupling the model to PEST. It uses the template and instruction files as interfaces through which effective handshaking between PEST and the model is achieved. The relevant settings required by the Gauss-Levenberg-Marquardt algorithm to drive the parameter estimation process are specified in the control file. These include the names of all template and instruction files, the names of the corresponding model input and output files, the problem size, control variables, initial parameter values and bounds, measurements and related settings necessary for the parameter estimation process. Additionally, executable commands needed to run the model to produce the information required by PEST are supplied in a batch file.

PEST works by taking control of the model and running it as many times as it needs to achieve the required parameter optimization. Each time PEST runs the model, it first writes the normal input files containing the parameters used by the model. After each model run, PEST reads the normal output files, locating those files with corresponding PEST formatted observation files. Settings are adjusted so that the method is tailored to best suit the problem under investigation. An efficient technique is used to compute accurate model output derivatives even when the model output is granular due to the limitation in the model numerical solution.

Prior information on parameters and relationships between parameters are incorporated into the parameter estimation process. Parameters are transformed to appropriate forms by power laws to accelerate the convergence of the solution to the optimal parameter set. Upper and lower bounds on parameters are imposed on parameters to constrain the parameter estimation process within the feasible region of the parameter space. Objective functions that are analytic (well behaved) greatly enhance solution convergence and drastically reduces the time for optimization runs. For this exercise, the combination of factors outlined above greatly improved the parameter estimation process, in particular, with the 3D climate mode where CPU time and computing resources were critical for the success of solution convergence. At the end of a successful optimization process, several output files are generated. The relevant output files for this thesis are the run record file (CASE.rec), the optimal parameter values file (CASE.par), the parameter sensitivity file (CASE.sen) and the residual file (CASE.res).

Appendix B: Preprocessing of relevant PEST files

1 OSU LSM

The OSU LSM is run with the model configuration outlined in appendix A.1. The relevant OSU LSM files that supply the land surface parameters to the physics routine are modified to include the random number generator that provides the synthetic land surface parameters for the model computations.

The PEST procedure for creating the instruction, template, parameter and control files for OSU LSM can be found in Doherty (2002). For albedo, the control file is modified to incorporate the random number generator. For the plant insolation factor, leaf area index, vapor pressure deficit factor and minimum stomatal resistance, the namelist file (namelist_chg_example) file is modified accordingly. The observation or fitting functions are transpiration, surface temperature, net radiation, and latent and sensible heat fluxes. A routine is coupled to the OSUL LSM to extract the relevant output after each run for each parameter of interest.

The observation data for the parameter estimation process is obtained by running the OSU LSM with the appropriate modified routine where the parameter of interest is passed to the OSU LSM system via the namelist facility. The PEST instruction file is used to extract the observation data produced from the OSU LSM runs and then converted to PEST precision format. The PEST control file contains the PEST formatted observation, instruction and template for the corresponding model input/output files. The control file is modified to include the appropriate settings required by the Gauss-Levenberg-Marquardt algorithm and the executable (batch) files. A schematic showing the detailed handshaking between PEST, OSU LSM and the random number generator is shown in figure B.1.

2 MM5

The finest MM5 domain (domain 5) prepared from the one-way nesting approach (see appendix A.2) is used for the coupled MM5-PEST simulations. The relevant MM5 files that supply the land surface parameters to the system are modified to include the random number generator that provides the synthetic land surface parameters for the model computations. This constitute the parameter initialization file (init.F) and the surface flux routine (sflx.F). For roughness length, emissivity and albedo, the init.F subroutine is modified. For the plant insolation factor and minimum stomatal resistance, the sflx.F file is modified. An extraction routine is incorporated in the MM5 output routine to write out the required observation (fitting function) for each parameter. The observation data (fitting functions) are the surface temperature, net radiation, and latent and sensible heat fluxes.

The PEST procedure for creating the template, instruction, parameter and control files for MM5 can be found in Doherty (2002). Template and parameter files are produced for each of the modified files. Additionally, corresponding instruction files are produced for the observation.

To prepare observation data for the parameter estimation process, MM5 is run with the appropriate modified routine where the parameter of interest is passed to the MM5 system. The relevant output (observation or fitting function) is written out in a PEST compatible format (ASCII). The PEST instruction file extracts the observation data produced by the MM5 run and then converts it to the PEST precision format. Similarly, corresponding template and parameter files are produced.

Finally, a PEST control file is produced from the PEST formatted observation, parameter and template files. The control file is modified to include the appropriate settings required by the Gauss-Levenberg-Marquardt algorithm and the executable (batch) files. Figure B.1 shows the coupling of MM5 and PEST and the relevant handshaking between the various components of the coupled system.

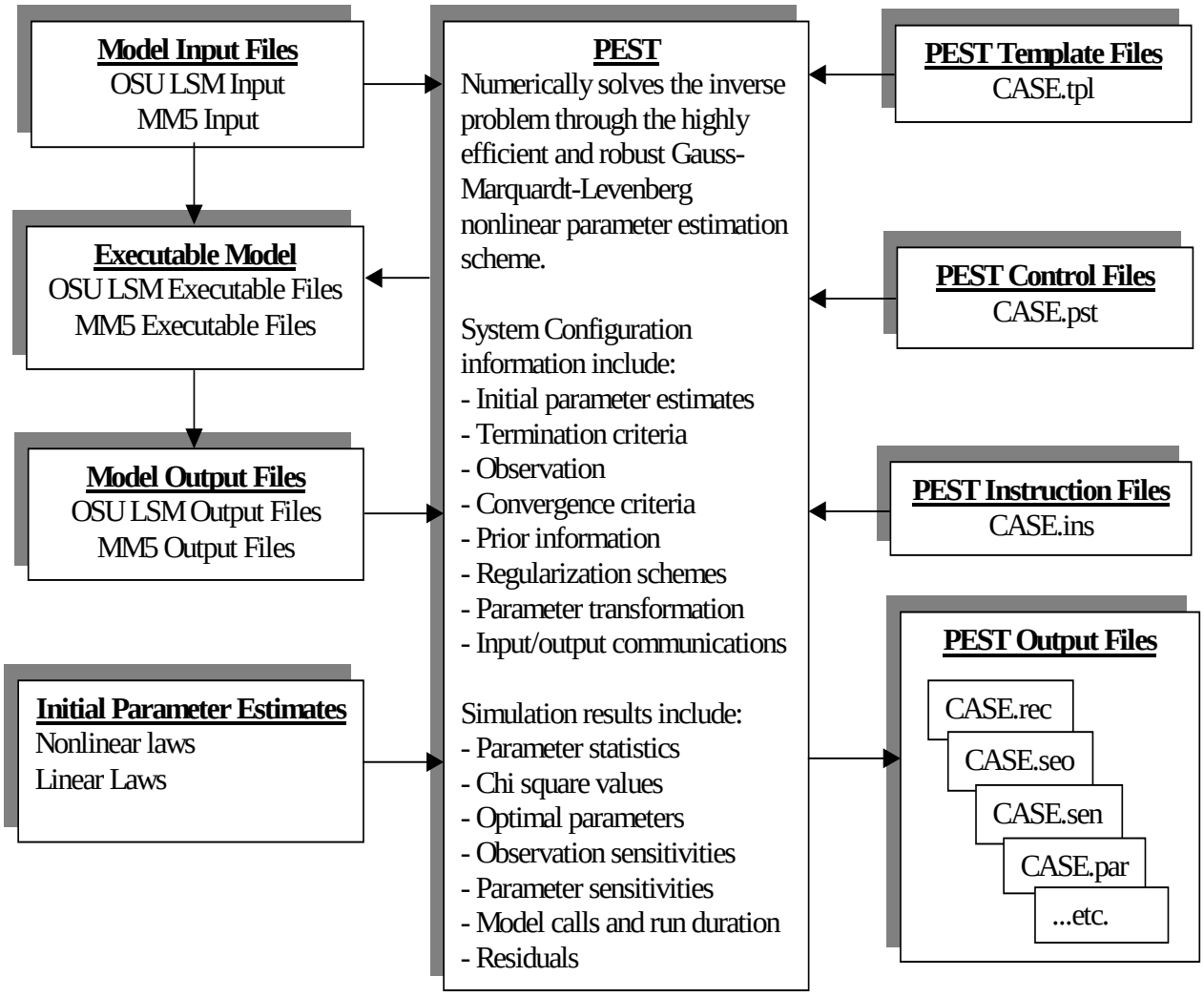

Figure B 1: Setup of the numerical experiment for coupling PEST to OSU LSM and MM5.

ACKNOWLEDGEMENT

My heartfelt gratitude to Professor P. Vlek (Director, Centre for Development Research, ZEF, University of Bonn) and Professor B. Diekkrüger (Geography Institute, University of Bonn) for supervising my research. I also gratefully acknowledge the enormous support given by Professor F. K. Allotey (Institute of Mathematical Sciences, Ghana), Dr. Nick van de Giesen (Coordinator, GLOWA-Volta project) and Professor A. Kunoth (Institute of Advanced Mathematics, University of Bonn) towards the success of this research. Special thanks to Dr. Manske (Coordinator, PhD program) and administration of the PhD Program of the Center for Development Research (ZEF), University of Bonn and also to the sponsors of this research (NRW and BMBF).

I most gratefully acknowledge the immense contribution of Dr. H. Kunstmann (Institute of Meteorology and Climate Research) for the time and mentoring he provided during the entire period of this research. I greatly acknowledge the support of Professor W. Seiler (Director, Fraunhofer Institute for Climate and Environmental Research/ Institute of Meteorology and Climate Research (IFU-IMK), Garmisch) and his administration for providing the necessary resources for this research. Special thanks to the Climate Modeling Group of Institute of Meteorology and Climate Research, Garmisch, in particular, Dr. R. Knoche, Dr. R. Forkel, Frau G. Jung, Herr A. Marx, Herr J. Wilhelm and all those who contributed in several ways to make my research in IFU-IMK successful. Special thanks also to the administration of the International Centre for Theoretical Physics (Trieste) and the climate modeling team (AIACC 070) at the University of Cape Town for their contribution to this work.

I would also like to express my sincere gratitude to my family who provided much support towards my stay in Germany. My special thanks go to my “German parents” Herr and Frau Fuchs (Garmisch), Dr. and Dr. Mrs. Wassmann (Garmisch), Dr. P. Okyere (Siemens, Munich) and Frau Monika Pauli (ALDI, Weiden) for making my stay in Bayern very pleasant.

Finally, I would like to acknowledge all those who contributed in diverse ways towards the success of this research.